DOCTOR OF PHILOSOPHY

Development of PCM-gypsum plasterboard integrated transpired solar collector for building envelopes

Bake, Maitiniyazi

Award date:
2021

Awarding institution:
Coventry University

Development of PCM-Gypsum Plasterboard Integrated Transpired Solar Collector for Building Envelopes

By

Maitiniyazi Bake

September 2020

Development of PCM-Gypsum Plasterboard Integrated Transpired Solar Collector for Building Envelopes

By

Maitiniyazi Bake

September 2020

A thesis submitted in partial fulfilment of the University's requirements for the Degree of Doctor of Philosophy

Certificate of Ethical Approval

Applicant:

Maitiniyazi Bake

Project Title:

Investigating the performance of Climate Responsive Building Envelope

This is to certify that the above named applicant has completed the Coventry University Ethical Approval process and their project has been confirmed and approved as Low Risk

Date of approval:

10 April 2019

Project Reference Number:

P89902

Content redacted on data protection grounds

Content redacted on data protection grounds

Abstract

It has been reported that over a third of anthropogenic greenhouse gas emissions stem from the operation of buildings (energy production and use; heat and air conditioners). One of the key challenges identified by the UK government is to halve the lifetime carbon emissions of buildings. This can only be done by designing energy efficient buildings where the envelope plays an active role.

The research has developed a methodology to integrate thermal energy storage along with a transpired solar collector for efficient envelope design. The energy storage part was developed by incorporating micro-encapsulated Phase Change Material (MPCM) into gypsum plasterboard in the back wall of a transpired solar collector (TSC). In this thesis, the works conducted (i) an extensive literature review on the classification/importance of building envelopes, energy storage technology, TSC technology, the integration of PCMs into building envelope components and TSCs; (ii) the design/fabrication of absorber plates and PCM-gypsum plasterboard, including examining the physical/thermal properties of such a plasterboard; (iii) an in-lab experimental investigation of key parameters influencing building envelope performance and the charging/discharging of PCM-gypsum plasterboard; and (iv) validation of the numerical model and parametric study investigating the impact of key parameters on building envelope performance to highlight the benefits of using PCM-gypsum plasterboard as part of a building envelope.

The characterisation results showed that increasing the PCM proportion reduced the bulk density and compressive strength and increased the thermal conductivity of the PCM-gypsum plasterboard. The experimental study presented that the airflow rate had the most significant influence on building envelope performance and increasing the airflow rate reduced the outlet temperature. The parametric study presented that the highest airflow rate ($50 m^3/hr$) had the lowest outlet temperature of 35°C during PCM charging and the highest heat releasing rate during the discharging process. The building envelope with PCM-gypsum plasterboard delivered an outlet temperature of 18°C, that was 6°C higher than the one provided by the building envelope with gypsum plasterboard. Therefore, it is recommended that integrating TSC with PCM-gypsum plasterboard to be used in building envelope design is a potential approach to deliver energy savings.

Acknowledgements

I would like to express my sincere gratitude to Dr. Ashish Shukla, my director of studies, for his direction, supervision, motivation and sharing of knowledge and expertise, which guided and supported me not only in my research study, but also in my life throughout this PhD study. I am also greatly thankful to my second supervisor Prof. Shuli Liu for her unlimited motivation, support and supervision during this research project.

I have been blessed and delighted to have had enormous assistance and advice relating to research from my colleagues and friends who helped and encouraged me during my study.

My special thanks go to all the technicians of the John Lang Building at Coventry University. One of them, the special one, is Ian Breakwell. I owe great appreciation to Mr. Ian Breakwell, who has provided me with great help in my experimental work.

Most importantly, I would like to express my deepest gratitude to all my family members: my parents, brothers and sisters, who continuously provided me with enormous emotional support, caring/love and encouragement during my research years. Nobody knows how much I owe my family, who deserve special and sincere thanks for their care and encouragement during my research study, especially at difficult times.

CONTENTS

Abbreviations

ANFIS	Adaptive network based fuzzy inference system
BITSC	Building integrated with transpired solar collectors
BIPV/Ts	Buildings integrated with photovoltaic/transpired solar collector system
CHTC	Convective heat transfer coefficient
BEIS	Department for Business, Energy & Industrial Strategy
CFD	Computational Fluid Dynamics
CGS	Clean growth strategy
DEID	Department for International Development
Defra	Department for Environment, Food & Rural Areas
DfT	Department for transport
DSF	Double skin façade
EPSRC	Engineering and Physical Sciences Research Council
HVAC	Heating, ventilation and air-conditioning
HP	Heat pump
IEA	The International Energy Agency
GTC	Glazed transpired solar collector
MPCM	Microencapsulated phase change material
PCM	Phase change material
PCM-G	Phase change material enhanced gypsum plasterboard
PV	Photovoltaic
PVTW	Photovoltaic Trombe wall
PS	Pitch size
RIUTC	Roof-integrated unglazed transpired solar collector
RNG	Re-Normalization Group Theory
SBEC	Sustainable Building Envelope Centre
SEM	Scanning Electron Microscope
SST	The Shear Stress Transport Theory
SUT	Solar updraft tower
TES	Thermal energy storage

TSC	Transpired solar collector system
TSCUT	Transpired solar collector updraft tower
TSC-TES	Transpired solar collector combined with thermal energy storage
TTC	Transparent transpired collector
UTC(s)	Unglazed transpired solar collector (system)
UTSAH	Unglazed transpired solar air heater
VDSF	Ventilated double skin façade

Nomenclature

A	Total collector area (m^2)
A_s	Collector surface area (m^2)
$C_{p.air}$	Specific heat capacity of air (J/kg.K)
$C_{p.gypsum}$	Specific heat capacity of gypsum (J/kg.K)
$C_{p.PCM}$	Specific heat capacity of phase change material (J/kg.K)
$C_{p.p}$	Specific heat of absorber plate material (J/kgK)
D	Perforation hole diameter (mm)
h_{conv}	Convective heat transfer coefficient (W/m^2K)
H	Enthalpy (J/kg)
ΔH	Latent heat (kJ)
I_T	Solar radiation incident on the collector (W/m^2)
L	Latent heat of PCM (kJ)
m_{PCM}	Mass of phase change material (kg)
$\dot{m}_{air}$	Mass flow rate through the collector (kg/s)
m_p	Mass of the absorber plate (kg)
Nu	Nusselt number
P	Pith of perforation (mm)
Pr	Prandtl number
ΔP	Total pressure drop across the collector
ΔP_p	Pressure drop across the absorber plate
ΔP_{fric}	Frictional pressure drop

ΔP_{buoy}	Buoyancy pressure drop
ΔP_{acc}	Acceleration pressure drop
$Q_{abs,p}$	Solar energy absorption (W)
$Q_{conv,\mathrm{p}\rightarrow\mathrm{plen}}$	Convection heat transfer from absorber plate to plenum air (W)
$Q_{conv.p\rightarrow\mathrm{sur/inlab}}$	Convection heat transfer from absorber plate to surrounding ambient air (W)
$Q_{conv,plen\rightarrow\mathrm{PCM-G}}$	Convection heat transfer from plenum air to PCM gypsum plasterboard (W)
$Q_{rad.col\rightarrow bw}$	Radiation heat transfer from absorber to back wall (W)
$Q_{rad.\mathrm{p}\rightarrow sur}$	Radiation heat transfer from absorber plate to surrounding ambient air (W)
$Q_{rad,p\rightarrow\mathrm{PCM-G}}$	Radiation heat transfer from absorber plate to PCM-gypsum plasterboard (W)
Q_u	Useful energy to heat the air and deliver to building inside (W)
Q_{out}	Delivered energy (W)
Q_{loss}	Heat loss (W)
Q_{stored}	Heat stored in PCM-gypsum plasterboard (W)
$Q_{sensible\ heat}$	Sensible heat (kJ)
$Q_{latent\ heat}$	Latent heat (kJ)
Re	Reynolds number
$T_{air.plen}$	Plenum air temperature (K)
T_f/T_{gypsum}	Final temperature of PCM-gypsum plasterboard (K)
T_{inlab}	In-lab air temperature (K)
T_{out}	Outlet air temperature (K)
T_p	Average absorber plate temperature (K)
T_m	Melting temperature (K)
T_s	Solidus temperature (K)
T_l	Liquidus temperature (K)
ΔT	Air temperature rise (K)
ρ_{air}	Density of air (kg/m^3)
μ_{air}	Viscosity of ambient air ($kg/m \cdot s$)
ρ_p	Density of absorber profile material (kg/m^3)
ρ_{PCM-G}	Density of PCM-gypsum plasterboard (kg/m^3)
W	Plenum width (mm)

$\dot{V}$	Airflow rate (m^3/hr)
v_{app}	Approach velocity (m/s)
$v_{air.plen}$	Plenum air speed (m/s)
v_{hole}	Air speed across hole (m/s)
η	Collector efficiency
ε_{HX}	Heat exchange effectiveness
σ_{sb}	Stefan Boltzmann Constant ($5.6 \times 10^{-8} W/m^2K^4$)
$\propto_p$	Solar absorptance of the collector surface
σ	Absorber porosity
$\varepsilon_{PCM.g}$	Thermal emissivity of PCM-gypsum plasterboard
ε_p	Thermal emissivity of absorber plate facing back wall
β	Liquid fraction

Subscripts

app	Approach velocity
inlab	In-lab air temperature
rad	Radiation, convective
conv	Convection, convective
P	Absorber plate
plen	Plenum/plenum air
in	Inlet
out	Outlet
loss	Loss
sur	Surroundings

List of Figures

List of Tables

Chapter 1. **Introduction**

1.1 Research background

The building sector covers 44% of total energy usage as one of the highest energy-consuming sectors in the UK, making it more important if greenhouse gas (GHG) emissions need to be reduced (Pérez-Lombard, Ortiz and Pout 2008). A similar trend of highest percentage share of energy consumption from the building sector is also observed across the world (Uqaili and Harijan 2012).

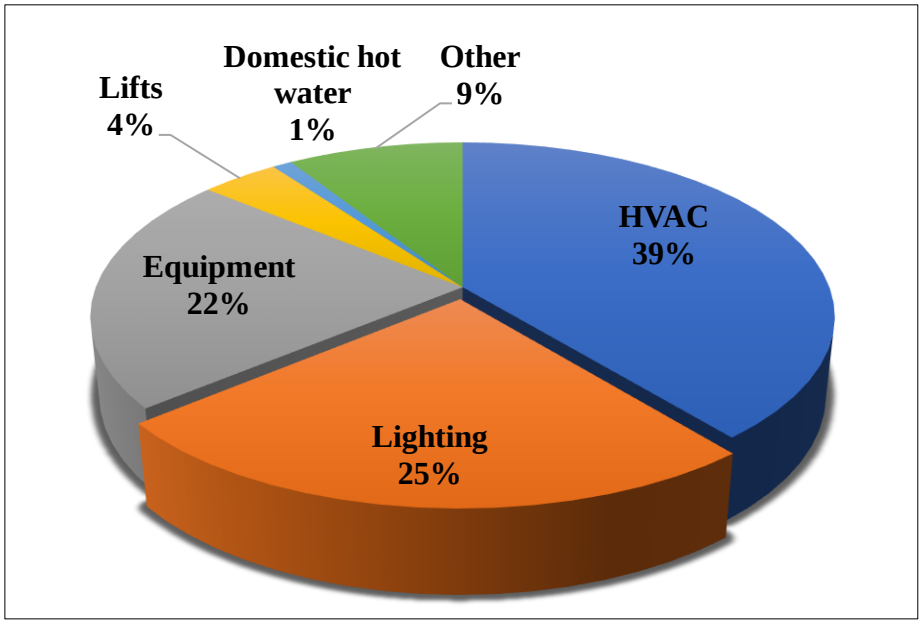

Figure 1-1. Distribution of energy use in commercial buildings (Residovic 2017)

Figure 1-1 shows that building energy consumption mainly includes equipment, lighting and heating/cooling. Heating/cooling is responsible for approximately 39% of the total energy usage (Programme 2007). Multiple researches have pointed out that the biggest proportion of energy usage in commercial buildings come from heating, ventilation and air conditioning (HVAC) services (Kant, Shukla and Sharma 2018). There are around 1.8 million commercial buildings accounting for 12% of greenhouse gas emissions around the UK (Aldersgate Group 2018). Hence, reducing a building's energy use and its greenhouse gas emissions is one of the major issues demanding solutions and increasing amounts of investment from the government. Reducing building energy consumption through greater energy efficiency and using advanced technologies like energy storage and solar technology have been a promising approach. According to the Clean Growth

Strategy (CGS), the UK government invested on a massive scale between 2015 and 2021 (Department for Business 2018). Figure 1-2 displays that £184 million in public funds has been applied to improve energy efficiency in UK industry (UK government 2018). In particular, research on energy storage technology has claimed the highest public funds at £265 million.

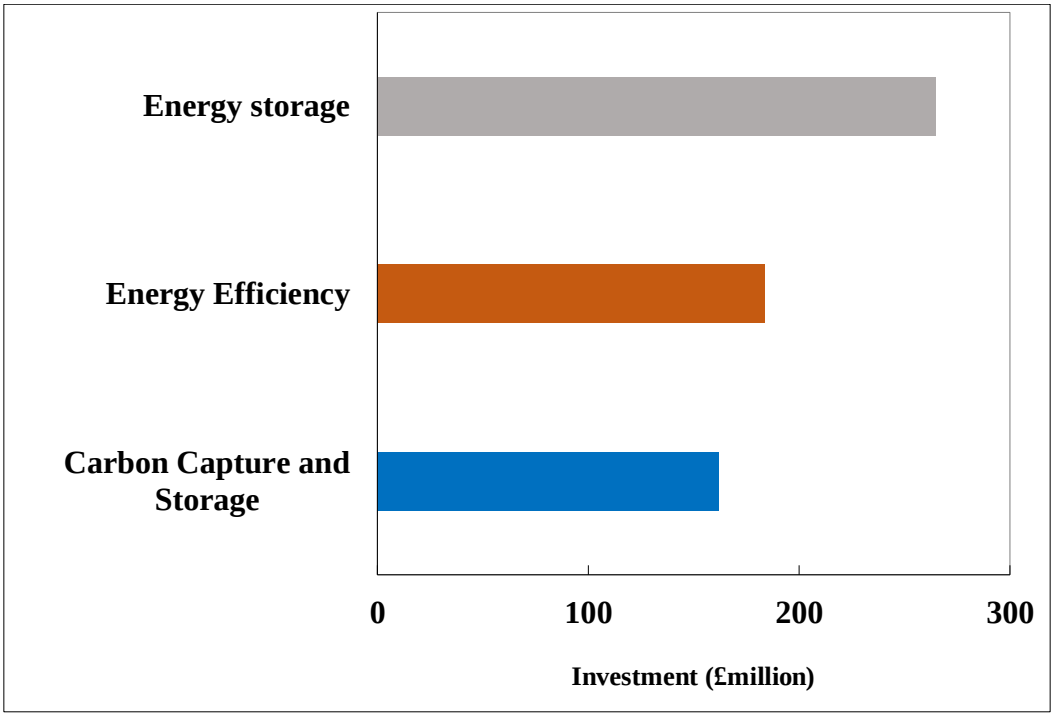

Figure 1-2. UK government investment in clean growth technology (2015-2021) (Innovate UK, Research Council, BEIS, DfT, DFlD, Defra)

Across the UK government, EPSRC funds have mainly been offered to research on energy storage and energy efficiency over the past 5 years (EPSRC 2019). Figure 1-3 shows that funds for energy efficiency have been the greatest in each year during the past 5 years, especially in 2018, at £34 million.

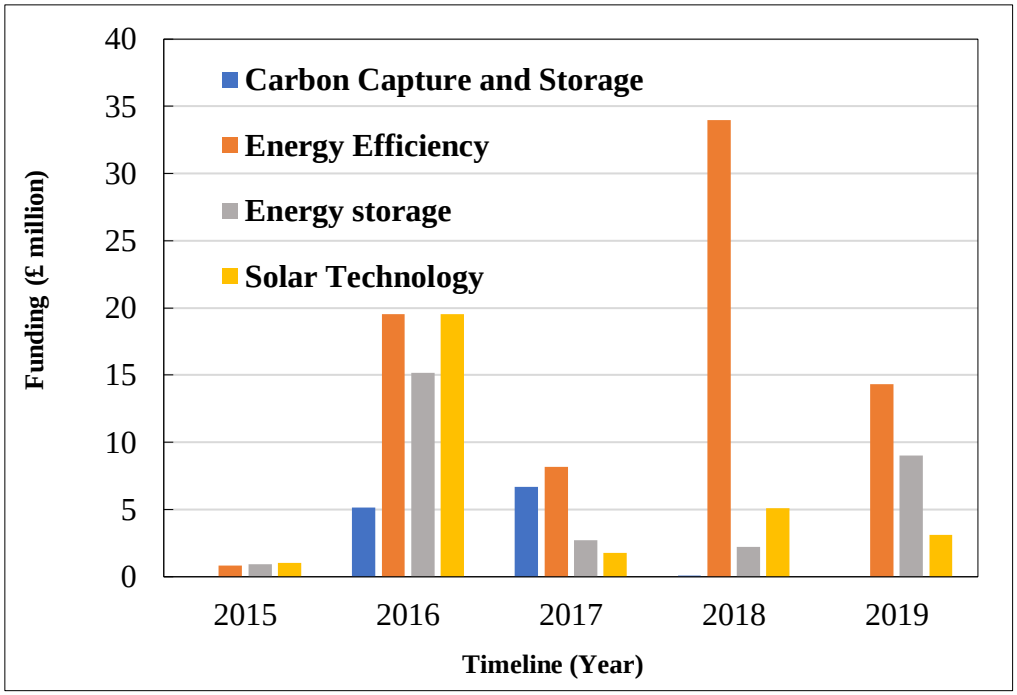

Figure 1-3. Distribution of EPSRC funds between 2015 and 2019 (EPSRC 2019)

Figure 1-3 indicates that improving energy efficiency is significantly important in order to reduce building energy consumption and limit GHG emissions so as to achieve a 20% reduction in energy use by 2030 (EPSRC 2019). In order to improve building energy efficiency and reduce energy consumption, various strategies have been proposed by researchers, e.g. energy efficiency including improvements in building design (Asman et al. 2019), the use of renewable energy (Leal Filho et al. 2019), the use of the novel materials like phase change materials (Mija et al. 2017; Li et al. 2019), building operation strategies (Tettey, Dodoo, and Gustavsson 2016; Sayadi et al. 2019), efficient HVAC design (Lathia and Mistry 2016; Gärtner, Massa Gray, and Auer 2020), end-user engagement (Hafer et al. 2018; Jenkins et al. 2019), building retrofitting (Ascione et al. 2019) and so on. Meanwhile, several possible solutions have been investigated to minimise the energy consumption of buildings, for example passive energy-saving technologies, e.g. heat pumps (Wu et al. 2018), energy storage systems (Comodi et al.,2017) and the application of renewable or sustainable energy sources including solar energy or wind energy into a building's energy systems (Panwar, Kaushik, and Kothari 2011). In particular, one method of reducing building energy consumption and limiting

CO_2 emissions can be completed via solar technology, where solar energy is transformed into thermal energy (Li et al. 2020; Peci et al. 2020).

However, an efficient envelope is one of the key factors in improving building energy efficiency and reducing GHG emissions, as the effectiveness of all the above-mentioned technologies depends on the quality of the building envelope. Furthermore, Figure 1-4 displays that there have been many envelope types used in building construction throughout history (Straube 2006; Designing Buildings Wiki 2019).

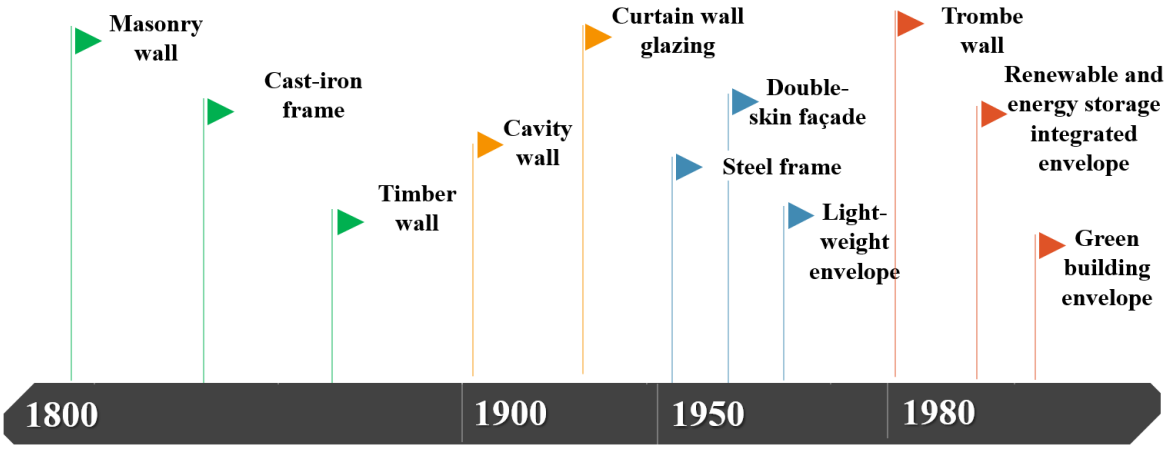

Figure 1-4. Timeline of the main envelopes in buildings since 1800

Figure 1-4 demonstrates that there have been many different types of building envelope used in construction. Recently, renewables and energy storage integrated building envelopes have been attracting increasing awareness within building science. It is believed that the implementation of thermal energy storage in building envelope design can reduce heating and cooling requirements. Introducing renewables, like a solar thermal system, is also likely to produce greater energy from solar resources (Lizana et al. 2017). Such a method can be achieved by an integrated building envelope, where energy-generating technology can be introduced at an early design stage (Agathokleous et al. 2019), although there are some issues in terms of cost, aesthetics, payback and maintenance. This has made it difficult to increase the use of such systems. However, the proposed system will overcome these shortcomings and will use a transpired solar collector (TSC), where efficiency can be up to 80%, as part of the building envelope incorporated with thermal energy storage (e.g. phase change material).

According to Table 1-1, Scholars have also described that one of the more advanced methods is to introduce a phase change material (PCM) into the design of the building envelope. PCMs have been widely used in building envelopes. Previous studies examining the advantages and limitations of introducing PCMs into building envelopes are shown in Table 1-1 (Bajare, Kazjonovs, and Korjakins 2011; Kośny 2015; Jingchao Xie et al. 2018; Frigione, Lettieri, and Sarcinella 2019).

Table 1-1. Summary of the advantages and limitations of introducing PCMs into building envelopes

Advantages
a) Increasing the thermal mass of the building envelope; b) Maintaining the room temperature for longer period by reducing the internal temperature swings; c) Reducing the solar gain and preventing the overheating problem; d) Improving the utilisation of the heat produced via absorbing external solar energy and thermal energy generated by the mechanical system of a building; e) Increasing the thermal energy storage capacity of the building envelope without changing the building fabric's temperature;
Limitations
a) Thermal instability; b) Flammability of paraffin based PCMs; c) PCM changes in volume during charging and discharging periods; d) Non-uniform appearance during phase changes; e) Leakage during the melting process; f) Higher cost of implementing PCMs by using aluminium containers; g) Hard to replace when not working if using paraffin within the building envelope structure.

Even though there are some limitations mentioned above in Table 1-1, PCM incorporated with gypsum is one of the most common and popular methods to use as part of a building envelope, due to the advantages of low gypsum prices, fire resistance, aesthetics and being environmentally-friendly (Lushnikova and Dvorkin 2016). In addition, gypsum

material can easily be used for internal/external walls and ceilings (Borreguero, Garrido et al. 2014). Consequently, integrating a PCM into a building envelope is one of the most promising methods to reduce a building's energy consumption and thereby increase its efficiency (Biswas et al. 2014).

There have been a large number of studies on the performance of transient solar collectors, including the effects of various parameters and external environmental factors (Wang, Shukla, and Liu 2017). Researchers have also studied the advantages of combining TSCs with other technologies, for instance energy storage (PCM) (Poole et al. 2018; Badescu et al. 2019a), PV panels (Athienitis et al. 2011; Tian et al. 2018) and heat pumps (Safijahanshahi and Salmanzadeh 2019a). Due to the application of a TSC, the power consumption of a heat pump may drop by up to 10% (Safijahanshahi and Salmanzadeh 2019a). A study has shown that the combined techniques of TSCs and PCMs can store 34% of all useful energy required for night-time operations (Poole et al. 2018). Rising air temperature changes alongside TSCs are reduced due to the implementation of PCMs (Badescu et al. 2019a). Meanwhile, it brings some possible problems such as (i) thermal instability; (ii) the higher cost of implementing PCMs by using aluminum containers; (iii) leakage during the melting process. These problems may affect the thermal performance of a TSC integrated with PCM-gypsum plasterboard, where the microencapsulated PCM is directly mixed with gypsum homogenously.

Furthermore, there has been no or only limited research into the potential benefits of introducing TSCs and PCMs into building envelope design. This study proposes a new approach to applying TSCs and PCMs into a building envelope to address the above-mentioned problems that may arise during integrating both TSCs and PCMs. In addition, this study has also experimentally and numerically studied the performance of such building envelopes to establish which parameters have the greatest impact on the performance of the building envelope.

1.2 **Research Aim and Objectives**

This PhD research aims to investigate an integrated building envelope design incorporating TSCs and energy storage technology. The aim will be accomplished through the following objectives:

a) To establish a comprehensive literature review on building envelopes, the implementation of PCMs into building envelopes, TSC technology, and especially, TSCs incorporated with phase change materials (PCMs);
b) To design a gypsum plasterboard introducing microencapsulated PCM;
c) To examine the physical/thermal properties of the PCM-gypsum plasterboard;
d) To design a building envelope incorporating the PCM-gypsum plasterboard and TSC technology;
e) To study the building envelope's performance and identify the key performance indicators.

1.3 **Research design**

This thesis was divided in three stages including the initial identification of key performance indicators for the proposed design through simple mathematical modelling, followed by experimental work. The third stage was numerical simulation and model validation following the parametric study.

In the first part, the literature review considered the existing knowledge of integrated building envelope design. The application of TSCs and PCMs in building envelope/components, especially using with gypsum plasterboard, was reviewed. TSCs incorporated with PCMs in terms of approach and advantages based on previous researches were reviewed.

In the second part, the experimental work investigated the in-lab performance of the building envelope that introduced the TSC and PCM enhanced gypsum plasterboard. Firstly, characterisation testing was conducted on PCM-gypsum plasterboard to examine the physical and thermal property changes of PCM-gypsum plasterboard due to the addition of a PCM. Afterwards, the in-lab thermal performance was investigated through studying the impact of the three main parameters such as airflow rate, plenum size and pitch size on the building envelope's performance. In addition, the advantage of applying PCM-gypsum plasterboard into the building envelope was examined. The effect of these parameters on the melting and solidification processes of PCM-gypsum plasterboard were also studied experimentally.

In the third stage, a numerical model using ANSYS Fluent Software numerical modelling studied the building envelope's performance through investigating the impact of various parameters such as approach velocity, plate temperature and inlet temperature on the building envelope's performance. Numerical modelling was used to verify and validate the numerical model through comparing the outcomes of the experimental results. Furthermore, a parametric study was carried out to find out the optimal design option by investigating several key parameters such as airflow rate, inlet temperature, plenum size, pitch dimension, hole diameter and the thermal conductivity of PCMs on building envelope performance and the charging/discharging behaviour of the PCM-gypsum plasterboard. The simple case was also investigated by using optimal design to highlight the importance of using PCM-gypsum plasterboard rather than gypsum plasterboard as part of the building envelope.

1.4 **Research innovations**

The proposed building envelope has the following innovative features:

1.4.1 ***Design advantages of the building envelope***

a) The proposed building envelope structure includes a transpired solar collector and a PCM-reinforced gypsum plasterboard as part of the enclosure to store additional energy from the ventilation system and capture the built environment's heat loss. This building envelope increases the heat transfer between the intake and the form through well-designed perforations and prevents the influx of rainy or snowy weather into the plenum;
b) PCM-gypsum plasterboard was made through mixing the gypsum and microencapsulated PCM directly with any containment measures;
c) This building envelope enables a significant reduction in building material costs compared to conventional building envelopes;
d) Such a building envelope would be active and alive as it would preheat the air using free solar energy and also prevent overheating problems during hot temperature periods. especially in summer;
e) This building envelope will improve building energy efficiency and make buildings more sustainable and energy efficient.

1.4.2 *A new intergradation approach*

During the production of the PCM-gypsum plasterboard, the microencapsulated PCM and gypsum were mixed homogenously and directly without containing measures, like using aluminum or metal. This enables not only a reduction in the material costs but also a promising thermal performance. In addition, it would be new to use PCM-gypsum plasterboard and TSC collectively as part of a building envelope.

1.5 **Structure of this PhD Thesis**

The following PhD thesis is organised into eight chapters regarding a developed approach/method to study the performance of a building envelope that integrates a TSC with a PCM. The first chapter introduces the research background, the aim and objectives, the research design, the research innovations with contributions to the knowledge and the outline of the thesis.

Chapter 2 gives the literature review on the classification/importance of building envelopes and the theory of energy storage technologies. It also demonstrates the development of building envelopes and PCM implantation on building envelope components, alongside demonstrating several case studies. It will also state the researches done on the integration of PCM with gypsum plasterboard. This chapter also states the brief concept, the working principle, the construction of TSCs, a parametric study on TSCs and numerous forms of TSCs, followed by several of their implementations in the building industry as case studies.

Chapter 3 describes a detailed explanation of the method used and the hypothesis for this research study. The research approach includes a literature review, an experimental investigation and numerical modelling. Also, the basic mathematical modelling for this study is also established, especially for analysing the building envelope's performance in terms of air temperature rise, heat exchange effectiveness, collector efficiency, and heat stored/released during charging and discharging duration.

Chapter 4 describes the conceptual design and potential benefits of the building envelope and the PCM-gypsum plasterboard. The PCM enhanced gypsum plasterboard is

characterised through physical and thermal properties testing including thermal conductivity, density and compression strength, which are explained in detail. Also, the finalised PCM enhanced gypsum plasterboard for this study is also covered in this chapter.

Chapter 5 demonstrates the detailed experimental design, materials and procedure/approach investigating building envelope performance. The data collection section and experiment uncertainty are included in this chapter. The results of the building envelope's performance and evaluating the advantages of the PCM-gypsum plasterboard are presented. This chapter also presents and discusses the experiment results.

Chapter 6 is dominated by the computational modelling of the building envelope's performance. It includes the CFD procedure, relative model selections, boundary conditions settings, governing equations and the solutions method used for this numerical study. It enables the optimal design to be proposed with the most determining parameters affecting the building envelope, via numerically investigating the impact of various parameters on the building envelope's performance and the charging/discharging process of the PCM-gypsum plasterboard. Also, the meshing independent study and the model verification are included in this chapter.

Chapter 7 explains the model validation and the parametric study. It includes the model validation through matching the numerical results with the experimental outcomes and examining the melting/solidification performance. The parametric study was to investigate the impact of several major parameters on building performance during the charging and discharging period. The case study was also conducted using the optimal design from the parametric study to highlight the advantages of this building envelope.

Chapter 8 concludes the research findings along with related recommendations. It concludes the main research outcomes of this PhD project to provide recommendations for future research on this field. The main points of each chapter are also presented in this conclusion chapter. Lastly, the contributions of this research study in terms of academia and the building industry are also mentioned.

Chapter 2. **Literature Review**

2.1 **Introduction**

Nowadays, one of the biggest concerns faced by the UK is the future energy supply challenge. Meanwhile, an 80% reduction in carbon dioxide emissions in the UK is expected to be accomplished by 2050, reducing space heating and cooling energy demands by approximately 30-50%, irrespective of building types. Therefore, designing an efficient envelope and parametric optimisation for the geometrical factors of the envelope is a decisive and promising method to reduce building energy consumption and the production of $CO_{2,}$ by delivering higher building performance with using a limited amount of energy resources. There have been a number of studies done on parametric design and optimisation for the geometrical factors of building envelopes via mathematical, experimental and numerical methods. In particular, one method of reducing building energy consumption and limiting CO_2 emissions can be completed via solar thermal systems like transpired solar collector (TSC) technologies, where solar energy is transformed into thermal energy (Kalogirou 2004).A lot of scholars have been working on the investigation of TSC performance in order to extend the knowledge of TSC technology and improve its application in the building industry, aiming to produce sustainable building designs.

Scholars have also described that one of the methods for improving building performance is to introduce a phase change material (PCM) into the design of the building envelope. These studies have stated the advantages of introducing PCMs into building envelopes such as (i) increasing the thermal mass of the building envelope (Frigione, Lettieri and Sarcinella 2019), (ii) maintaining the room temperature for a longer period of time by reducing the internal temperature swings (Bajare, Kazjonovs, and Korjakins 2011), and (iii) improving the utilisation of the heat produced via absorbing external solar energy and thermal energy generated by the mechanical systems of a building (Kośny 2015). Besides, building materials fulfilled with PCMs increase the thermal energy storage capacity of building components without changing the building fabric's temperature (Xie et al. 2018). In particular, a PCM incorporated with gypsum is one of the most common and popular methods in use. Consequently, integrating PCMs into the building envelope is a promising method of reducing the building's energy consumption and thereby increasing its efficiency (Biswas et al. 2014).

Hence, this chapter gives the theoretical background and literature review on building envelopes, the application of PCMs in building components, the adaptation of PCMs in building envelopes and the transpired solar collector. It also demonstrates the development of building envelopes and PCM implantation in building envelope elements such as external walls, floors, roofs, windows and shading devices, followed by several case studies. This chapter also states the concept/classification, the working principle and the construction of a transpired solar collector (TSC), followed by several implantations of TSCs in the building industry as a case study. This chapter also highlights the potential research field for further study.

2.2 **Classification of building envelopes**

Modin (2014) classified the functions of a building envelope into three different categories: support, control and finish, to meet the desires of people inside/outside the built environment. Oral et al. (2004) stated that building envelopes are critical elements to determine the quality and control of the indoor environmental conditions. Figure 2-1 shows that building envelopes include different types of walls, windows, roofs, foundations, thermal-insulation, thermal mass, and external/internal shading devices (Oral, Yener and Bayazit 2004). It can be indicated that high-performance building envelopes have been popular for designers with the aim of providing good thermally comfortable indoor environments. Currently, several technologies have been developed, such as using passive solar heating (Olenets, Piotrowski, and Stroy 2015), solar walls (a transpired solar collector applied to a building's south-facing external wall) (Ogden et al. 2011), and new materials for the building envelope, e.g. double skin façades (Ahmed et al. 2015), ventilated façades (M Ciampi, Leccese and Tuoni 2003) and highly insulated building envelope components (Chan, Riffat and Zhu 2010; Jaber and Ajib 2011; Iribar-Solaberrieta et al. 2015; Ghaffarianhoseini et al. 2016).

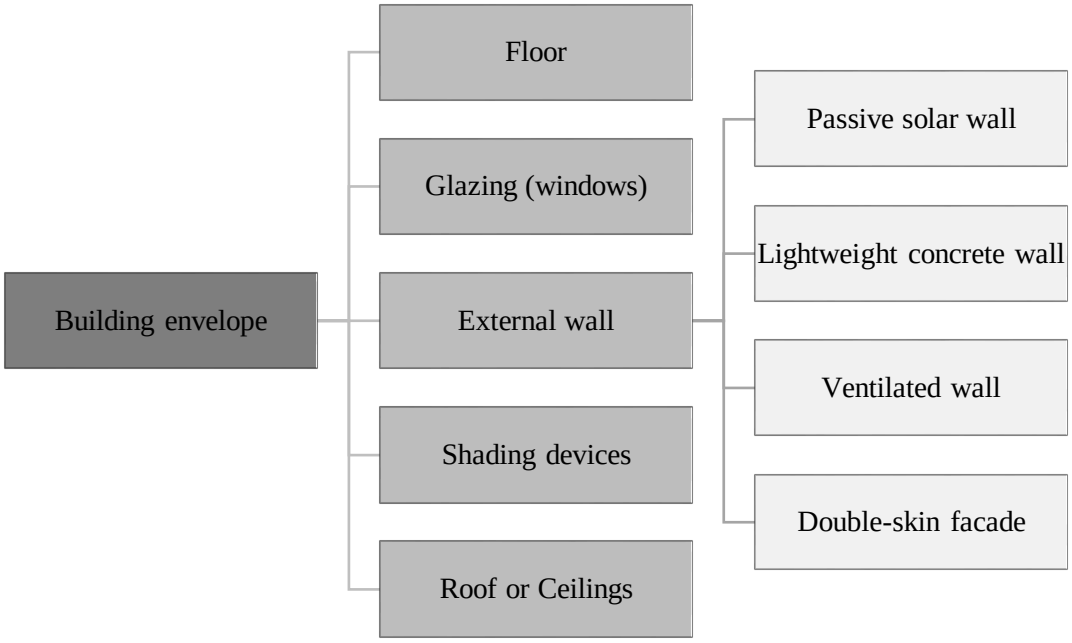

Figure 2-1. Classification of building envelopes

Sherman and Walker (2001) argued that the building envelope is responsible for the majority percentage of heating and cooling energy consumption because of heat loss throughout the building envelope. Goia et al. (2015) demonstrated that the building envelope determines how much energy is consumed for heating and cooling due to heat loss and indoor heat gain. Pearson (2011) believed that the energy loss through the building's fabric is variable and is affected by different components, e.g. the age and type of the buildings, orientation, location, construction techniques, operation, maintenance, and occupant behaviour. Younes et al. (2011) also defined that heat loss through the building envelope to the surrounding environment is a combination of air leakage (air infiltration) and thermal conduction. Thermal insulation and construction materials with a low thermal conductivity less than $0.1\,W/mk$, reduces building energy usage by preventing heat gain/loss through the building envelope (Papadopoulos 2005). In a wall, the position of any thermal insulation will determine its thermal properties. This is very important for measuring heat loss through the building's fabric (for instance, walls), which is crucially important for determining how much energy is needed for the building's operations, for instance heating and cooling (Ji et al. 2016). Scholars have also

described that one of the methods of improving building performance is to introduce energy storage technologies like phase change materials (PCM) into the design of the building envelope. Therefore, it is significantly important to review and acknowledge the implantation of energy storage technologies in building envelope design.

2.3 **Energy storage technologies**

Energy storage (ES) technologies are mainly classified into three different categories: mechanical energy storage, electrochemical energy storage and thermal storage (Renewable Energy Association 2015). Thermal energy storage (TES) is divided into sensible and latent heat storage (Navarro et al. 2016). Latent heat storage (TES) can capture thermal energy as stored energy which can be used at a later time for heating and cooling applications and for the generation of power (Navarro et al. 2016). In the first place, latent heat storage has a higher energy density with a smaller storage volume than sensible heat storage. Latent heat storage materials like phase change materials (PCMs) have become more popular for their applications in building envelopes, since they give a high-energy storage density and have the capacity to store energy at a constant temperature or over a limited range of temperature variations (Mahlia et al. 2014).

2.3.1 ***Phase change materials***

Phase change materials can be classified into four states: solid-solid, solid-liquid, gas-solid, and gas-liquid. There is a wide range of PCMs with different melting point ranges. According to their chemical compositions, PCMs can be categorised as organic compounds, inorganic compounds and eutectic compounds (Figure 2-2). Each group has its typical range of melting temperature and melting enthalpy.

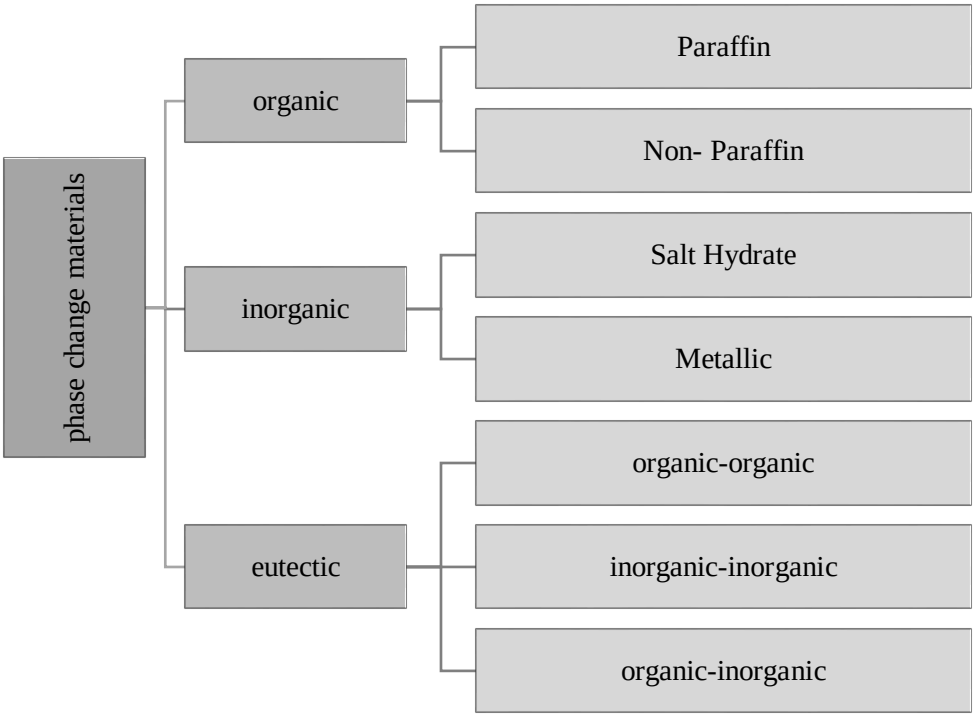

Figure 2-2. Classification of PCMs

Paraffin is one of the most popular organic PCMs used due to its advantages, e.g. (i) non-corrosive, (ii) non-sub-cooling, (iii) safe to use, (iv) low-cost, (v) higher heat of fusion with reliability and (vi) stable energy-storing performance (Zhou et al. 2012; Xu et al. 2014; Sarı et al. 2014). The thermal properties of greatest interest in PCMs are melt temperature, latent heat, specific heat and thermal conductivity (Akeiber et al. 2016a). In particular, improvements in specific heat will be desirable in the next generation of PCMs to increase the amount of energy stored during the sensible heating period of operations. In addition, materials with high latent heats of fusion also tend to have relatively high specific heats that refer to the amount of energy, which would be key benefits for thermal heat storage (Farid et al. 2004). One of the disadvantages of these organic PCM types is their high flammability, which limits them from being exposed to high temperatures (Farid et al. 2004; Xu, Wang and Li 2014). Phase change materials also have their own low thermal conductivities, which has a great impact on the reduction of effectiveness in both energy storage and thermal management application. Low thermal conductivity creates a high thermal resistance and prevents the heat flow from effectively penetrating

into the PCM and initiating the melt process, which leads to the isolation of the melt process (Navarro et al. 2016).

Furthermore, the encapsulation of a PCM is capable of improving thermal conductivity and is divided into (i) macro-encapsulation (with a diameter of 1mm and more); (ii) micro-encapsulation (from1μm to 1mm); and (iii) nano-encapsulation (less than 1μm) (Jacob and Bruno 2015). The encapsulation must be optimised for an effective heat transfer rate with proper corrosion resistance and strong stability and reliability (Memon 2014). Toppi and Mazzarella (2013) indicated that there is no damage/leakages between the microencapsulated PCM and building materials like gypsum during the melting process because of the capsule shell. Konuklu et al. (2015) established that a Microencapsulated PCM can be directly mixed with building materials such as gypsum plaster or concrete, which might cause a lower heat storage capacity. To improve thermal conductivity and heat storage capacity, a PCM is encapsulated using some other materials such as aluminum fins and stainless steel with various thicknesses (Table 2-1). Popular methods have also been found to increase the effective thermal conductivity for phase change materials, as follows (Akeiber *et al.*, 2016a):

a) The use of macro-scale metallic inclusions such as fins, meshes or foams;
b) The use of macro-scale carbon insulations;
c) The use of nanoscale materials to create colloidal phase change material (PCM) suspension with improved thermal properties.

Table 2-1. Summary of the thickness for encapsulating PCMs with various methods

Reference	Material	Thickness (mm)	Height/length (mm)	Width (mm)
Hed and Bellander (2006)	Aluminium pouches	8	160	80
Diarce et al. (2014)	Hollow aluminium profiles	20	148	-

Shi et al. (2014)	Stainless steel	20	560	545

In terms of their implementations, PCMs are popularly used in different areas such as the military, consumer products and especially in buildings, such as domestic hot water, space heating, and air-conditioning systems (Akeiber et al. 2016a; Omrany et al. 2016). PCMs in buildings can especially meet the demands for energy and thermally comfortable environments, such as free cooling methods when applied to the building envelope (Osterman, Butala and Stritih 2015; Thambidurai et al. 2015). However, there are some challenges for applying thermal energy storage systems in buildings as follows:

a) Thermal stability or leakage (Akeiber et al. 2016a);
b) Value of power density that can be delivered to or withdrawn from a storage unit (Renewable Energy Association 2015).

Furthermore, there are some challenges including developing exact analytical solutions for the melting and solidification process and the response time. Challenges still exist in terms of achieving the theoretical performance in terms of charge/discharge rates for many PCM systems and the overall economic evaluation of a thermal energy storage system needs to be developed (Eames et al. 2014).

2.4 **Application of PCMs into building components**

Thermal energy storage with PCMs in buildings are mainly classified into two different groups as active energy storage systems and passive energy storage systems. Each of them also is divided into different categories. Figure 2-3 displays the classification of PCMs in various building envelopes including building materials. PCMs have been applied into different building envelopes such as solar walls, wall boards, floors, ceilings or roofs, concrete and insulation materials, due to their more effective heat transfer (Abbassi, Dimassi and Dehmani 2014; Densley Tingley, Hathway and Davison 2015; Lee, Medina, et al. 2015; Lei, Yang and Yang 2016a).

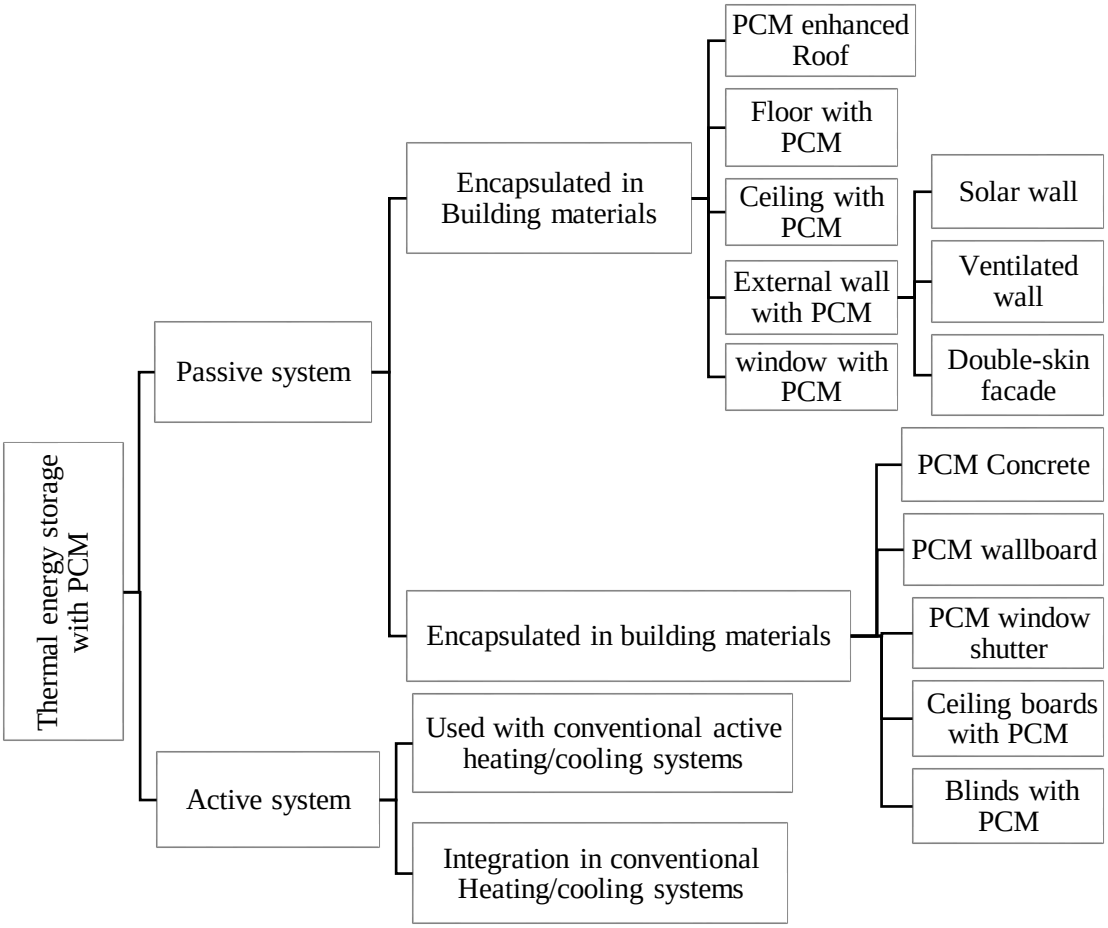

Figure 2-3. Classification of thermal energy storage with PCM and its application in various building envelopes including building materials (Bake et al. 2020)

Therefore, PCM integration with building envelopes provide several benefits (Eames et al. 2014):

a) Capturing the energy for later use, reducing the energy costs for consumers and businesses;
b) Decreasing the usage of fossil fuels by reducing energy demand and enabling a greener energy supply mix where it can enable the interaction of more renewables (especially solar thermal);
c) Improving the thermal efficiency of the envelope.

According to Figure 2-3, it can be illustrated that PCMs have been applied into various building components. Studies have also investigated PCM implementation in building

components. Also, building materials like gypsum or concrete have applied PCMs and their performances have been examined. However, this part has mainly focused on previous researches studying PCM integration into the building envelope (external wall) and PCM integration into gypsum, due to the perspective of this research project.

2.5 **External walls with PCMs**

External walls generally present the majority portion of a building envelope and allow larger solar radiation to pass through due to their large surfaces (Chwieduk 2013). PCMs in external walls reduce temperature fluctuations in terms of solar radiation loads (Chwieduk 2013; Lee, Medina et al. 2015). Ling and Poon (2013) demonstrated that cubicle walls with PCMs have always obtained a smaller temperature value (2–3 °C) than those without PCMs. The cubicles with PCMs reached the same temperature as those without PCMs about 2 hours later. Moreover, the results showed that the tested PCMs enabled a room's air temperature to be maintained within the comfort zone by decreasing its maximum air temperature to a maximum value of 2.9 °C (Kuznik and Virgone 2009a). Also, west-facing rooms integrated with PCMs had a better performance in terms of decreasing the interior surface temperature up to a maximum of 41.4%. A yearly energy saving of 2.9% in an air-conditioning system was achieved for the west-facing case (Mi et al. 2016). Moreover, there are key benefits for PCM composite walls as follows:

a) Wallboards with PCMs decrease air temperature fluctuations in a room and wall surface temperature fluctuations also can be reduced (Kuznik and Virgone 2009a);
b) Overheating effects during hot days can be strongly reduced by PCM materials included in the walls , because the storage energy is released to the room's air when the temperature is at a minimum during the night (Izquierdo-Barrientos et al. 2012);
c) Thermal comfort is enhanced by the radiative heat transfer, as the wall surface temperature is lower when using PCM materials due to increasing natural convection whilst avoiding uncomfortable thermal stratifications (Lee, Medina, et al. 2015).

Furthermore, PCMs are applied into different locations of an external wall, in the inner layer, middle layer, and out layers of the building's wall (Izquierdo-Barrientos et al. 2012). PCM location has a great effect on the performance of walls and the thermal performance of building walls, which can be guaranteed by the PCM's properties (including melting temperature, heat of fusion and thermal conductivity), wall structure and weather conditions (De Gracia and Cabeza 2015; Lee, Medina et al. 2015; Lei, Yang and Yang 2016a). The thermal performance of building walls can be developed by the optimisation of PCM positioning (Jin, Medina and Zhang 2013). For instance, PCMs applied to exterior wall surfaces showed better performance than those applied to interior wall surfaces, as lesser energy penalties in tropical climates (Jin et al. 2014; Lei, Yang and Yang 2016a). An increased amount of PCMs also reduces building envelope heat gain. Efficiency and cost benefits of PCMs are also decreased due to an increased thickness of the PCM layer (Kalnas and Jelle 2015).

2.5.1 *Solar walls enhanced with PCMs*

A Solar wall (Trombe wall) with a PCM is designed for trapping and transmitting solar energy efficiently into a building. It was first described by Edward S. Morse in 1881. Trombe walls have been seen as a wall system capable of significantly reducing the energy consumption of buildings via improving the performance of the walls (Saadatian et al. 2012). A solar wall with latent heat storage is more efficient than conventional concrete walls (Kuznik and Virgone 2009a). Particularly, the PCM enhanced Trombe wall stores the solar thermal gain from incoming solar radiation during the day and releases it into the building space overnight (Jaber and Ajib 2011). The heat is simply stored in the Trombe wall with PCMs in the daytime. At night, the stored heat is discarded by ventilation to the outside of the building, which can prevent daytime overheating problems during the summer period (Xu, Wang and Li 2014; Osterman, Butala and Stritih 2015; Lei, Yang and Yang 2016a). The results also showed that the smaller thickness of the Trombe wall with a PCM was more desirable in comparison to an ordinary masonry wall for providing efficient thermal energy storage (Sharma et al. 2009).

2.5.2 *Ventilated façade or Double skin façades with PCMs*

A ventilated double skin façade (VDSF) offers the possibility of improving the energy efficiency of a building and provides better energy performance than conventional facades (De Gracia et al. 2013; Diarce et al. 2014; Gagliano, Nocera and Aneli 2016; Serrano et al. 2016). A double-skin façade (DSF) can be defined as 'a special type of building envelope, where a second skin, usually a transparent glazing is placed in front of a regular building façade (Poirazis 2004). PCMs in ventilated façades capture solar radiation and use it for heating purposes as well as a cold storage system during the summer season to reduce the energy consumption of HVAC systems (Gagliano, Nocera and Aneli 2016). Moreover, a VDSF presents three potential benefits: free cooling, cold storage and the prevention of solar radiation incidence in different climate conditions (De Gracia and Cabeza 2015).

The use of PCM layers with a double skin façade integrated into PV modules has proved to be effective in reducing the cooling load of an indoor space as well as increasing the solar to electrical conversion efficiency of PV modules (Elarga et al. 2016). Moreover, there are various advantages for the application of DSFs in building envelopes, including permitting radiation to pass through the building due to its transparent characteristics, as well as providing a visual connection with its surroundings (Omrany et al. 2016).

2.6 **PCM-enhanced building materials**

There has been detailed implementation of PCMs in different building materials including concrete, plaster, wallboards and lightweight envelopes. The wallboards or boards are cheap and widely used in a variety of applications, making them very suitable for PCM encapsulation because of their larger heat exchange area (Osterman, Butala and Stritih 2015). PCM enhanced wallboards and concrete have the ability of reducing energy costs, the scale of air-conditioning, peak indoor air temperature and the fluctuations of indoor temperatures (Chan 2011; Jin et al. 2014; De Gracia and Cabeza 2015; Kalnas and Jelle 2015). A PCM for a lightweight building envelope is the most suitable solution for implementing PCMs into buildings. They can be very effective for transferring the heat and cooling loads away from peak demand times. The impacts of PCMs in concrete, lightweight walls and wallboards are different. For instance, PCM enhanced concrete

cubicles present much higher fluctuations of up to 18 °C (Castell and Farid 2014). In addition to the energy saved by the reduced cooling load, the lower surface temperatures of the lightweight wall result in greater comfort (Schossiga, Henninga, Gschwandera and Haussmannb 2005). The heat flow of the wallboard can be reduced by 8.5% to 77.9% with using PCMs (Zeng, Shukla and Liu 2017)

2.6.1 *PCM integration with gypsum*

Building materials integrated with PCMs increase the thermal energy storage capacity of building components without changing the building fabric's temperature (Xie et al. 2018). PCM incorporated with gypsum is one of the most common and popular materials for use in building construction due to the advantages of gypsum, which is low priced, fire resistant, aesthetic, and environmentally friendly. Also, gypsum material can easily be used for internal/external walls and ceilings (Borreguero, Garrido, et al. 2014). Hence, Table 2-2 summarises the articles investigating the performance of PCM integration with gypsum during the last 10 years.

Table 2-2. Summary of studies investigating the effects of PCMs in gypsum

References	Building material	PCM type	Key findings
Kuznik and Virgone (2009)	Copolymer	Microencapsulated paraffin	The PCM wallboard increases the natural convection inside the room and the room air temperature decreases by up to 4.2 °C.
Borreguero et al. (2010)	Styrene monomer	Rubitherm® RT27	The addition of microencapsulated PCM increases the thermal insulation capacity. Also, the maximum/minimum indoor temperature can be maintained at up to 1.3 °C integrating with 7.5% of additional PCM.
Borreguero et al. (2011)	Black gypsum	Rubitherm® RT27	A gypsum block integrated with 5 wt. % of PCM reduces the gypsum plasterboard

			thickness by 8.5% to perform the same insulating behaviour.
Oliver (2012)	Gypsum and reinforcing additives	Micronal® DS 5001X	A PCM enhanced gypsum board with a 15mm thickness would store 5 times the thermal energy of a sealed gypsum board, and the same energy as a 120mm thick brick wall within the relatively comfortable temperature zone (20-30°C).
Shukla, Fallahi, and Kosny (2012)	Gypsum	Microencapsulated PCM	A gypsum plaster board containing roughly 25 wt. % of microencapsulated PCM has a total latent heat capacity of 25kJ/kg.
Toppi and Mazzarella (2013)	Gypsum powder	MICRONAL PCM microcapsules	Density and thermal conductivity changes due to the mass factions of the material compositions. However, it is mostly influenced by the microencapsulated PCM's mass fraction.
Borreguero et al. (2014)	Hemihydrate gypsum	Polymeric-SiO2-PCMs	The addition of a PCM reduces density, thermal conductivity, and compressive strength. Also, this PCM enhanced gypsum block saves 10.20 kW h/m3 and reduce 1.26 kg of CO2 emission per operating cycle.
Borreguero, Garrido et al. (2014)	Hemihydrate gypsum	mSD-(LDPE·EVA-RT27); mSP-(PS-RT27); Micronal®DS 5001X; mSD-CNFs	The addition of 15% microcapsules into gypsum saves 4.5 kWh of energy, reducing 1.395 kg CO2 emissions per operating cycle in a standard room covered with 1 m2 of this gypsum plasterboard.
Serrano et al. (2015)	Gypsum	fatty ester PCM	Gypsum plasterboard integrated with 25% PCM has a higher thermal insulation than

			the common gypsum. It also has 41% higher average heat capacity thanks to the latent heat.
Karaipekli and Sari (2016)	Gypsum powder	form stable composite PCMs (Pumice)	Gypsum blocks with form stable composite PCMs improved the ability of keeping the indoor air temperature at a comfortable zone for a longer time, thereby reducing the building's energy usage.
Serrano et al. (2016)	Hemihydrate gypsum	microencapsulated PCM Micronal®DS 5008	Adding 10% in weight of a PCM, gypsum composite presents the best thermal response, lower thermal conductivity and higher heat capacity.
Lachheb et al. (2017)	Gypsum plaster	Micronal® DS5001X microcapsules	Increasing the amount of additional PCM decreases the heat flux and temperature fluctuations greatly. The heat capacity of gypsum plaster is improved due to increasing additions of PCM.
Jeong et al. (2017)	M-30 gypsum	Hybrid shape stabilized PCM	The hybrid shape stabilised PCM increases the thermal heat capacity and thermal conductivity of the gypsum block, for instance, the addition of 30 wt. % PCM claims the highest value.
Sharifi et al. (2017)	Gypsum	Paraffin blend	The HVAC system energy requirement was reduced by 17% yearly, in particular, 6% of heating requirements and 35% of cooling demand, by using PCM-gypsum plasterboard.
Xie et al. (2018)	Gypsum Powder	Graphite-modified microencapsulated phase	The influence of specific heat and heating conductivity to the heat release time is limited. However, additional PCM layers would increase the wall surface

		change material	temperature and heat flux during the heat storage process.
Singh and Bhat (2018)	Gypsum	Phase change material	The room's inside temperature swings can be reduced by using PCM-gypsum board attached to the roof.
Gnanachelvam et al. (2019)	Gypsum	Microencapsulated PCM	The fire resistance was reduced greatly and the fire intensity for a light gauge steel-framed wall was increased by using PCM enhanced plasterboard.
Li, Yu, and Song (2019)	Gypsum mortar	Microencapsulated PCM (PH-31)	The gypsum composite containing micro-PCM reduces the thermal conductivity while it has a higher specific heat capacity (2.71 times during the temperature interval from 26-32°C).
Srinivasaraonaik et al. (2020)	Gypsum board	Microencapsulated eutectic mixture	Thermal conductivity and compressive/flexural strength decrease with the introduction of microencapsulated PCM in gypsum composites

According to Table 2-2, previous researches have concluded that there are increasing advantages in applying PCM impregnated gypsum plaster board into a building's structure. First, gypsum plasterboard filled with 45% PCM stores at least 3 times more energy than a typical gypsum board and brick wall (Oliver 2012). A gypsum board integrated with a PCM is also more thermally insulating than those without PCMs, since the addition of a PCM reduces the thermal conductivity thereby increasing the heat capacity of the gypsum (Serrano et al. 2015, 2016). For example, a gypsum board integrated with 25% of fatty-ester PCM has a 25% lower thermal conductivity compared to those without PCMs (Serrano et al. 2015). In the meantime, PCM-enhanced gypsum composite shaves the room temperature swing by 46%, as the shape stabilised PCM plate is more efficient in the utility rate of latent heat (Zhou et al. 2007). Thus, gypsum plasterboard with a form stable-composite PCM keeps room temperature in the comfort range for longer hours and diminishes the building's energy usage (Karaipekli and Sari 2016). A study conducted in Canada demonstrated that applying PCM plasterboard to an

existing building envelope could make the internal temperature stay at 6 °C on the daytime and 4°C during the night, respectively (Athienitis et al. 1997).

Due to the increasing benefits of introducing PCM-enhanced gypsum plasterboard into building structures, numerous researches have examined the performance and effectiveness of gypsum plasterboards embodied with PCM (Paraffin, organic/inorganic PCM). It was indicated that integrating PCMs into gypsum could change the complex properties of the proposed gypsums composites. The physical, thermal, and mechanical properties such as density, thermal conductivity and compressive strength are influenced by the mass fractions and thermal properties of the raw materials. Nevertheless, there is still a great demand for research on analysing the impact of introducing microencapsulated PCMs into gypsum blocks in terms of property changes.

2.7 **Recent studies on applying PCMs into building envelopes**

The pivotal comparison of the impact of different types of building envelopes or building materials with or without PCMs in building performance is presented in Table 2-3. Mainly, most of the previous studies have been based on organic PCMs for passively cooling a building, even when applied into the building envelope. The fundamental principle or benefits of a phase change material is good for providing free cooling at the night, mostly. The reason for this focus might be explained by its heat of fusion, its considerable compatibility with most building envelopes and its chemical stability, which may lead to overcooling, fluctuation and thermal leakage problems or challenges.

Table 2-3. Summary of previous researches on the impact of various building envelopes with and without PCMs on building performance

Author	Year	Building envelope (materials)	Method of Study	Building performance	Location
Athienitis et al. (1997)	1997	PCM-based wall lining	experimental and numerical simulation study	Lowered the maximum room temperature by 4°C and reduced heating demand during the night	Canada
Balaras et al. (2000)	2000	Thermal insulation External shadings, light-coloured roof and external walls	EPIQR methodology and software	Reduced energy consumption by 20–40% Reduced the space cooling load by 30% and 2–4%, respectively	Greece
Bojic, Yik and Sat (2002)	2002	External wall thermal insulation	Numerical simulation	Reduced cooling energy and peak cooling load up to 20% and 29%, respectively	Hong Kong
Ciampi, Leccese and Tuoni (2003)	2003	Fully designed ventilated façade	Mathematical modelling	Achieved 40% summer cooling energy savings, typically	Italy

Cheung, Fuller and Luther (2005)	2005	Lighter colour building envelope	Experimental study	30% reduction in solar absorption can achieve 12.6% savings in the annual required cooling energy	Hong Kong
Cabeza et al. (2007)	2007	PCM in concrete walls	experimentally investigated	The indoor temperature of the PCM-enhanced concrete building was 1 °C lower than the reference building without PCM inclusion	Spain
Zhang et al. (2008)	2008	PCM-wallboard	Mathematical and numerical analysis	The most energy-efficient approach of applying a PCM in a solar house is to apply it in its internal wall	China
Zhou et al. (2008)	2008	Shape-stabilised phase change material plates	Enthalpy model and numerical modelling	Create a heavyweight response to lightweight constructions with an increase in the minimum room temperature at night by up to 3°C	China
Kuznik and Virgone (2009a)	2009	PCM-composite wall boards	Experimental assessment	A decrease in maximum room temperature by 4.2°C	France

Muruganantham, Horwath, Ludlam and McDonald (2010)	2010	Organic-based phase change materials	Experimental study	Maximum energy savings of about 30%	USA
Sun et al. (2011)	2011	Photovoltaic-Trombe wall	Experimental and numerical studies	Total efficiency of solar usage is reduced by 5%. Also, the electric conversion efficiency of the PVTW achieves 11.6% while the glazing is fully filled with PV cells	China
Kośny et al. (2012)	2012	Naturally ventilated solar roof with PCM	Experimental study	About 30% heating and 50% cooling load reductions are possible	USA
Peng, Lu and Yang (2013)	2013	Double-skin façade Single-glazed windows	Experimental study	A reduction of up to 26% of annual cooling energy consumption 26% reduction of energy consumption	Hong Kong
Kong et al. (2014)	2014	PCM in concrete wall	Experimental study	Reduce the maximum indoor temperature up to 4°C and relative humidity by 16%	Hong Kong

Soares et al. (2014)	2014	PCM drywalls in lightweight steel-framed buildings	A multi-dimensional optimisation study	Improve the energy efficiency of buildings by 10–60% depending on the climate zone	Portugal
Lee, Medina et al. (2015)	2015	PCM layer in residential building walls	experimental study	30–50% of peak heat flux reductions, 2–6 h delay in peak heat flux and maximum daily heat transfer reductions were estimated as 3–27%	USA
Li et al. (2015)	2015	PCM roof	numerically investigated	PCM roof's effect on the temperature delay in the room beyond 3 hours than that of a common roof	China
Lei, Yang and Yang (2016b)	2016	PCMs in building envelope	Numerical method	Reduced the heat gain effectively in a range of 21–32% throughout the whole year	Singapore
Marin et al. (2016)	2016	PCM in gypsum board	Numerical modelling and validation	The potential of energy consumption reduction both for heating and cooling periods in arid and warm temperate main climate areas	Spain

Nghana and Tariku (2016)	2016	PCMs in building envelope	Experimental study	Reducing indoor air and wall temperature fluctuations by 1.4 °C and 2.7 °C respectively. Also, lowering the heating energy demand by up to 57% during the winter	Canada
Park and Krarti (2016)	2016	Reflectivity coatings on wall	Numerical simulation	Reducing annual energy use in commercial buildings up to 11% for office buildings	Chicago
Yu et al. (2017)	2017	Solar wall	Experimental testing and verification	In winter, heat loss through the solar wall was heavily reduced by about 80–88% than the separate wall	China
Young et al. (2018)	2018	PCM-mortar wall	Experimental study	PCM-composite envelope can decrease or delay the building's energy usage	USA
Venegas et al. (2018)	2018	PCM modified envelope	Numerical study (EnergyPlus)	The addition of a PCM reduced the cooling energy requirement by 8 and 29% in Santiago and Puerto Montt, respectively.	Chile

Zhu and Yang (2019)	2019	Pipe-embedded PCM building envelope	Numerical study	The pipe-PCM integrated envelope could block the negative heat release to the indoor environment, then reduce the building's heating demand and improve the thermal comfort during the heating season	China
Markarian and Fazelpour (2019)	2019	PCM integrated building envelope	Numerical study	PCMs with lower melting temperatures are more effective in heating dominant climates	Iran
Rathore and Shukla (2020)	2020	Macro-encapsulated PCM integrated into building envelope	Experimental study	The thermal amplitude was reduced by 40.67-59.79% and electricity could be saved by roughly $0.4 per day in cooling demand.	India
Yang et al. (2020)	2020	Concrete with PCM	Experimental and numerical study	Concrete with 15% shaped-stabilised PCM satisfies the mechanical performance and has a great advantage in reducing indoor temperature fluctuation.	China

Table 2-3 show the development of building envelopes utilising PCMs. In addition, the table also illustrates the application of phase change materials on different building envelopes or building walls, such as in external walls, in wallboards, in plasters and concrete, in glazing, in various type of roofs and in double skin façades, due to different research studies in different countries as well. More importantly, the benefits of PCMs enhanced within the various types of building envelopes dramatically reduced around 20-40% of the total annual energy consumption. For instance, PCM drywalls in light steel framed buildings can improve energy efficiency by 10-60 % depending on the climate zone. Moreover, solar walls with PCMs as external walls for buildings are good for reducing the heating energy demand by approximately 16 %. However, it is difficult to decide on energy performance in building envelopes due to different aspects, including the limitations and challenges of PCMs in building envelopes as follows:

a) Heat loss is one of the main challenges for PCM enhanced building envelopes because of the temperature difference and the thermal leakage (Younes, Shdid and Bitsuamlak 2011);
b) The fluctuation and instability based on thermal performance with uncertain times for phase change periods, and the low thermal conductivity (Farid et al. 2004; Akeiber et al. 2016a);
c) Thermal stability or leakage (Akeiber et al. 2016a);
d) The value of power density that can be delivered to or withdrawn from a storage unit (Association 2015);

In addition, achieving the theoretical performance in terms of charge/ discharge rates for many PCM systems and the overall economic evaluation of a thermal energy storage system needed to be developed (Eames et al. 2014). As energy storage and building performance are so location-dependent, general savings assumptions are not valid. Therefore, there is further scope for research with the same technologies for various regions and changes in performance.

2.8 **Case studies of PCM applications**

PCM storage is likely to become a viable technology within the next few years. For instance, it can be concluded that PCM-based thermal storage in conjunction with an

electric air-source heat pump and offered as part of a Green Deal, could be technically possible in a retrofit building. Also, the introduction of a thermal store as part of a heating system offers a potential economic impact, through the requirements for initial installation and on-going maintenance. Moreover, the use of latent heat energy storage is finding applications in the built environment with phase change materials used in building cooling systems to displace peak cooling loads and by using microencapsulated PCMs in the building fabric. This paper also displays some case studies on the performance of PCMs in building envelopes, as follows.

2.8.1 *Cool Phase- Notre Dame School Building*

Two COOL-PHASE systems with PCMs were installed in an IT classroom (approx. $70m^2$) where the system was required to overcome high internal heat gains through 30 PCs and glazing in April at the Notre Dame School Building (London) (Anon. 2011) . Also, two control rooms (one room with a similar internal heat gain; another with a much lower internal and external heating load) were chosen to provide the comparison of the performances of the COOL-PHASE systems. During the experiment, temperature and CO_2 levels were monitored every minute and collected by a data logger during the spring term. Therefore, the results show that the average temperatures increased in the control room slightly between the spring and summer terms due to the warmer weather (Figure 2-4).

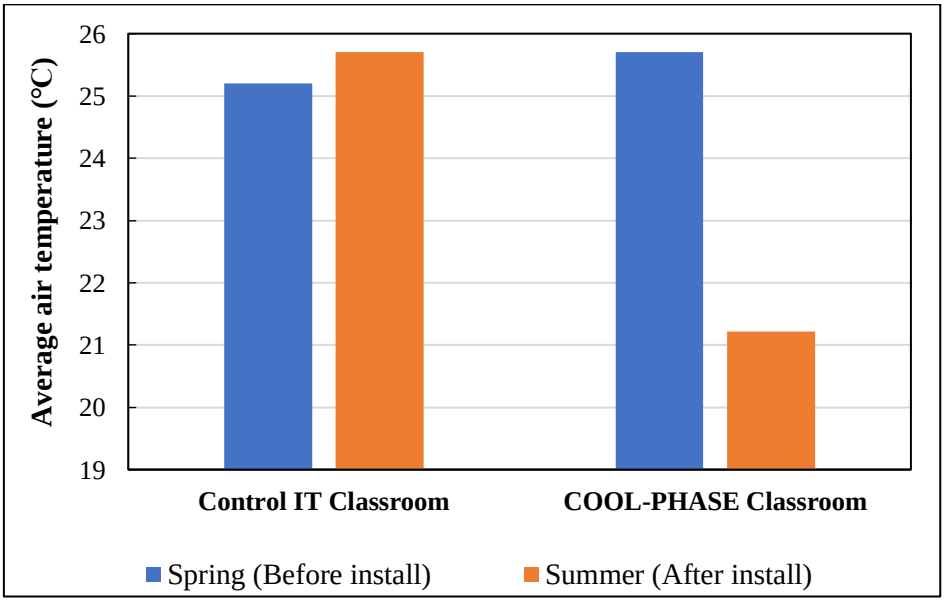

Figure 2-4. Comparison of the temperature before and after the install (*COOL-PHASE system in IT classroom*, 2011)

However, the room with the COOL-PHASE system saw a significant reduction in the average temperatures before and after the install. Therefore, the COOL-PHASE system had a significant impact on average temperatures as a PCM with high-energy storage density stores energy over a limited range of temperature variations. Also, it would deliver financial savings of more than 26% (approximately £10,000) and CO_2 savings of 12.8 tones over the anticipated system lifespan of 20 years.

2.8.2 *Cool Phase- Owen Building at Sheffield Hallam University*

COOL-PHASE® was also installed in a particular "problem" room in the Owen Building at Sheffield Hallam University (Anon. 2012). It is a 90-person teaching room on the tenth floor that had consistently exhibited poor air quality and high temperatures. The room had no mechanical ventilation and was fitted with opening windows to one side; but due to the height of the building these were restricted to a 100mm maximum opening, limiting the effectiveness of the natural ventilation. In November 2009, an initiated environmental check was taken by the University's Estates Department to record the CO_2 levels and temperature changes. COOL-PHASE® was installed in March 2012 and the performance was monitored throughout the late March warm spell. A room temperature peak of 23ºC was recorded when the outside temperatures were hovering around 21ºC. The results also displayed that the temperatures were consistently recorded at 25ºC at a time when November's outside temperatures were reaching only 5ºC. Moreover, the COOL-PHASE system was working harder to bring the CO_2 levels down during these peaks, and COOL-PHASE maintained CO_2 levels at around 600ppm for the rest of the time once the levels had been controlled. Therefore, the system dramatically reduced CO_2 levels because of consuming less energy due to the PCM, whilst controlling temperature fluctuation well within normal comfort zones. At the same time, energy consumption was reduced by up to 90% compared to conventional mechanical cooling systems.

2.8.3 *New Ford retail car showroom*

A new Ford retail car showroom and used car sales office completed in January 2013 has been equipped with Cool-phase, a low energy cooling, ventilation and heat recovery system (Vanegas 2014). The results estimated that the system used intelligently controlled phase change material (PCM) to actively ventilate and cool the buildings, maintaining temperatures within the comfort zone, while radically reducing energy consumption by up to 90% compared to conventional cooling systems. Also, Cool-phase reduces the running costs of buildings while creating a fresh and healthy indoor environment without the use of compressors or hazardous coolants.

2.8.4 *Sustainable building envelope center*

A composite flooring system incorporated under-floor heating and phase change material in the Sustainable Building Envelope Centre (SBEC) (Figure 2-5). A pre-finished steel composite floor was installed on the first-floor level of the building with phase change material added to the concrete mixture just above the steel deck. In this application, the phase change material is used to store, buffer and release heat via the high emissivity pre-finished steel floor deck that acts as a ceiling to the meeting room below. Excess heat load from usage is absorbed by the phase change material and released when the heat load is reduced, providing a constant temperature. Therefore, the room temperature of the building can be controlled without heavy reliance on carbon intensive fuels. The system allows cool or warm water to circulate through a network of water pipes embedded into the concrete to thermally activate the floor, providing a highly effective cooling and heating method for the structure. It can also provide a constant and comfortable room temperature to be maintained during use, thereby reducing CO_2 emissions.

Figure 2-5. PCM in composite floor decking at SBEC, Tata Steel, Shotton works, UK (Allen 2011)

2.8.5 *Sir John Liang Building Coventry University*

PCM technology with 1590 PCM Tube ICEs in total was installed in the Architecture Studio and in two offices within the John Laing Building at Coventry University (Figure 2-6). PCM Tubes are installed and then respond to the surrounding temperature of the room. At the beginning of the day, the TubeICEs are frozen, as the room heats up due to body heat and heat from the sun. The PCM Tubes passively cool the room by absorbing the heat until completely melted. As the temperature cools overnight, so does the PCM. The PCM effectively loses energy to the immediate surroundings, charging for the next day.

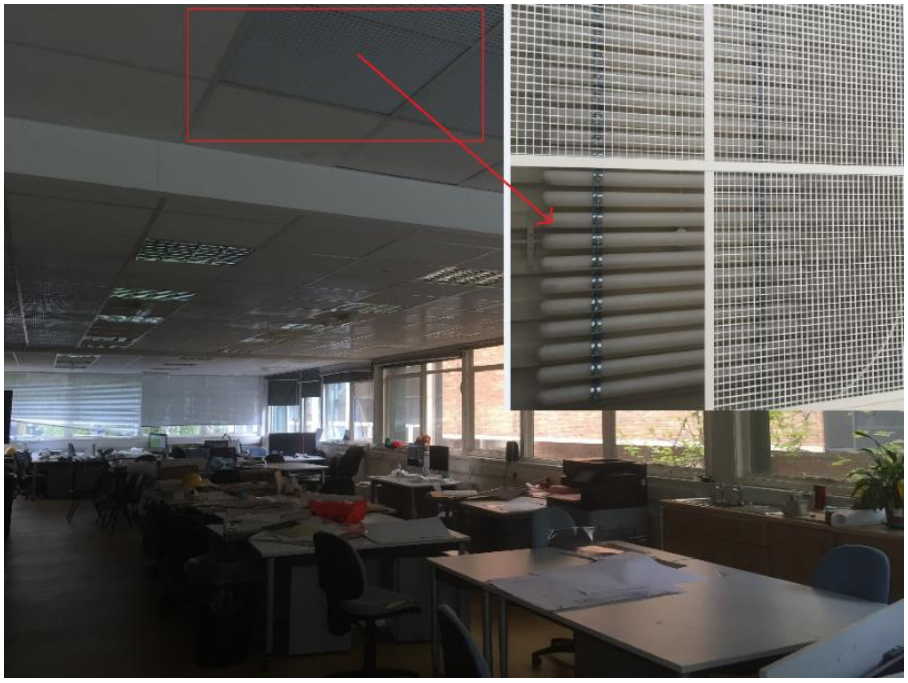

Figure 2-6. Schematic of the PCM TubeICE installation in the Architecture studio in John Laing Building at Coventry University, UK (Ahmed, Abdullahi et al. 2018)

In this project, The PCM technology provided free cooling with 230kWh of energy storage. The spaces and tubes were energy monitored over the next year to gather full performance data and the results showed that the new PCM system could save 10% of total energy compared to the previous system (Table 2-4). The CO_2 emissions would be 48.15 kg/m^2 per year. Associated investment costs of the building renovation were also expected to represent a maximum of 19% on average of the total costs of building an equivalent new building in the same location.

Table 2-4. Comparison of energy consumption of buildings with and without PCM TubeICE (Ahmed, Abdullahi et al. 2018)

	Total system energy (MWh)	Total nat. gas (MWh)	Total carbon emissions $(Kgco_2)$	Total energy (MWh)	Total energy (MWh/m^2)

Previous energy consumption before PCM Tube ICE installation	448.80	418.8	106064.00	448.80	0.12
Present energy consumption after PCM Tube ICE installation	428.90	399.3	101614.00	428.90	0.11
Energy savings (%)	10.58	11.35	9.67	10.58	10.58

It can be concluded from the above case studies that PCM technology with passive cooling is increasingly used in building envelopes, as it has various benefits:

a) Very low running costs;
b) No external units are required;
c) Highly energy efficient system;
d) Long life and a warranty of several years;
e) Creates a healthy and productive environment for occupancy;
f) High performance ventilation and cooling system;
g) Environmentally friendly and sustainable solution that uses no refrigerants.

During the application of PCMs in built environments, the melting temperature of PCMs is the key point to look at during the selection of phase change materials and their applications (Akeiber et al. 2016b). In general, the melting point of a PCM is supposed to be between 10°C and 30°C to provide a thermally comfortable zone for the occupants inside the building. A range of 19 to 24°C is especially regarded as the best melting temperature for PCMs in free cooling systems of buildings (Butala and Stritih 2009). Hence, PCM application in a built environment regarding melting temperature is shown as follows (Cabeza et al. 2011):

i. Up to 21°C for cooling applications
ii. 22-28°C for ease of infrastructure applications
iii. 29-60°C for hot water applications

Among PCMs, paraffin wax is one of the most popular energy storage materials used in buildings used due to its advantages, e.g. (i) non-corrosive, (ii) non-sub-cooling, (iii)

safe to use, (iv) low-cost, (v) higher heat of fusion with reliability and (vi) stable energy-storing performance (Zhou et al. 2012; Xu, et al. 2014; Sarı et al. 2014).

2.9 Key findings of previous studies on applying PCMs in building envelopes

Therefore, it can be concluded that building envelopes play a vital role in the overall energy performance of buildings. Various building envelope components have different impacts on building energy performance. PCMs have been applied into building envelopes as a passive energy technology to reduce the building's energy consumption. Their application varies from free heating/cooling to active roles in novel HVAC designs. Moreover, case studies have provided significant information on PCM enhanced building envelope components, proving their potential to reduce total energy demand in a range of 20-40%. Meanwhile, novel PCM embedded building components, e.g. solar walls with energy storage, can improve the energy efficiency of buildings. It has been reported that improvements in energy efficiency can be made in the range of 10-60% which varies significantly because of several reasons, e.g. size of the building fabric area, location of the building, type of the building, number of occupants, age of the building and so on. Also, the PCM is used as part of the building envelope with a building material like gypsum. However, according to previous research, PCMs had been integrated with the building envelope via a container, which might have possible challenges such as thermal instability/uncertainty and thermal leakage during melting. Hence, it requires a new approach during its application like directly using a microencapsulated PCM with a building material like gypsum. One method of reducing building energy consumption and limiting CO_2 emissions can be completed via a solar thermal system, where the solar energy is transformed into thermal energy (Kalogirou 2004).

2.10 Background to the study of TSCs

However, in order to achieve zero or low carbon buildings, two main strategies have been adopted: (i) use of passive technologies using energy from the natural environment (Ma et al. 2016) and (ii) the integration of renewable energy into the buildings (Ma and Xue 2013; Ma et al. 2016). One method of reducing a building's energy consumption and limiting CO_2 emissions can be completed via a solar thermal system where solar energy is transformed into thermal energy (Kalogirou 2004). Recently, the transpired solar

collector system (also recognised as unglazed transpired solar collectors, UTC) has been identified as one of the most efficient solar thermal conversion technologies (Ogden et al. 2011), where efficiencies of up to 80% can be achieved. Transpired solar collector systems (TSCs) are being popularly used worldwide. A transpired solar collector on the south wall of a single-story industrial building in 2006 was first of its kind to be installed in the UK (Ogden et al. 2011). Several applications of TSC technology have been reported in the literature, e.g. solar heating/cooling, ventilation (Sewalk, Liston and Maher 2009); preheating (Ogden et al. 2011); process air (Badache et al. 2012); solar –industrial drying (Tyagi et al. 2012), etc. For instance, this transpired solar collector in dark, black colours is at Willmott Dixon Community Healthcare Campus, UK (Figure 2-7).

Figure 2-7. Transpired solar collector at Willmott Dixon Community Healthcare Campus, UK (Brown et al. 2014)

A transpired solar collector can considerably strengthen building efficiency by preheating the ventilation air free of cost in commercial, industrial, military and residential buildings (Sewalk, Liston and Maher 2009). A TSC is a collector system with higher efficiency due to ventilating air freely to improve building performance (Sewalk, Liston and Maher 2009; Ogden et al. 2011; Shukla et al. 2012). For instance, several studies demonstrate that TSCs are capable of reaching an immediate efficiency of above 70% when the suction velocity is over 0.02 m/s (Ogden et al. 2011).

2.11 **TSC- Working principles**

Figure 2-8 displays the working principle of building integrated TSCs. The absorber surface uses a perforated metallic sheet (commonly aluminum or steel) and it can be integrated into the building's external wall (Shukla et al. 2012). The metal solar collector is passively heated during the day through diffused and direct solar radiation, then the ambient air is drawn through the perforated collector and into the air cavity or plenum. As the air travels through the plenum (air gap or air cavity), it is heated up and then drawn into the building as ventilation fresh air. Overall, TSCs are highly effective for preheating ventilation air (Ogden et al. 2011; A Shukla et al. 2012). However, in the summer, the warm air in the plenum can be exhausted via using a by-pass damper to prevent overheating inside the built environment, or it can be used for water heating to maximise the usage of TSCs (Shukla et al. 2012).

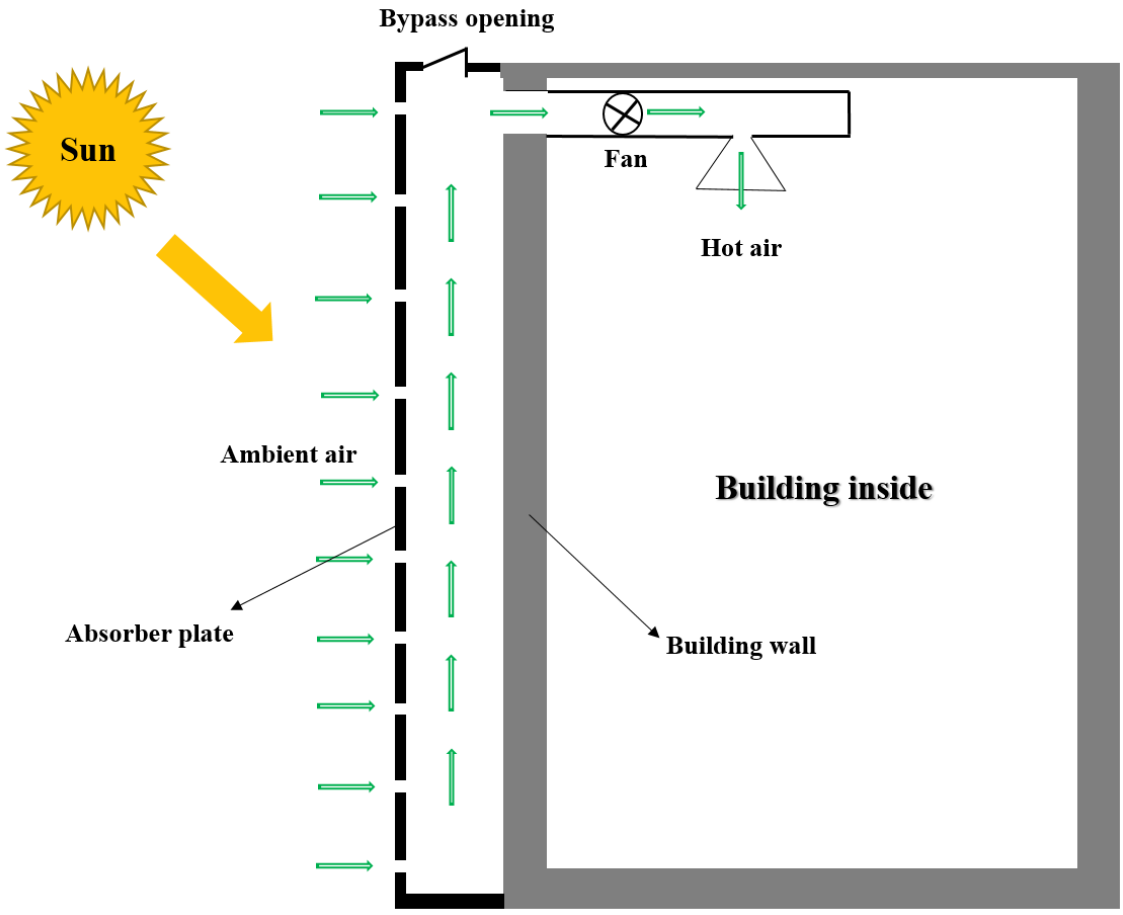

Figure 2-8. Diagram of a building integrated with TSCs

Additionally, the instantaneous thermal efficiency of a solar collector is defined as the ratio of the valuable energy gained to the incident solar energy. TSC (with or without a metal corrugated plate) efficiency (**η**) was assessed from energy ratio transfers, i.e. from the ratio of the heat delivered by the collector shared by the incident radiation absorbed by the surface of the collector (Badache et al. 2012).

2.12 TSC- Collector construction and its parameters

The transpired absorber is normally made of a metal plate with equally distributed perforations for absorbing the solar radiation. The perforated sheet is fixed to protrude around 10-30cm from the south-facing façade (Figure 2-8). The perforating design ranges from 0.5% to 2% of the whole absorber surface area (Dymond and Kutscher 1997). The air cavity or plenum is equal to the space between the plate profile and the structural wall of a building. There is an outlet on the building wall for connecting with the ventilation system by sucking in the air with a fan, which brings the outside air through the perforated holes. The inlet air is heated and drawn up through the air cavity then drives to the ventilation system (Ogden et al. 2011; Ashish Shukla et al. 2012).

The main design criteria while designing a collector for a TSC are (i) profile of metal plate, (ii) pitch of the holes and (iii) size/design of the holes. There are over 300 profiles available in the market with various pitch designs of profiles due to different pitch sizes (PS). These can be classified into (i) profile with longer pitch (PS ≥ 200mm), (ii) profile with medium pitch (100mm≤ PS > 200mm) and (iii) profile with shorter pitch (PS ≤ 100mm) (Younes, Shdid and Bitsuamlak 2011). The absorber profile with a shorter pitch and perforation diameter could cause manufacturing challenges. The profile with a longer pitch is likely to decrease the collector's efficiency and the heat transfer coefficient, and it might decline its thermal efficiency (Rad and Ameri 2016). In particular, the pitch has less impact on collector efficiency than heat exchange effectiveness (Leon and Kumar, 2007a). Therefore, it is important to design the pitch size due to its crucial impact on TSC performance.

Also, there are different types of holes available for TSC design such as round holes, square holes, single slots, elliptical holes and many other special shapes (Papadopoulos 2005). There are various types of pitches including square pitch, staggered pitch and

special pitches with various sizes (Ji et al. 2016). Rad and Ameri (2016) stated that the heat transfer and outlet air temperature increase of the hole diameter weakens the heat transfer to air and outlet temperature. Therefore, the hole diameter and pitch size also affect TSC performance.

In addition, there are various parameters affecting TSC performance such as porosity, geometry of the holes, plenum dimensions, material and absorptance of the collector, air flow rate, plenum velocity, temperature rise, solar radiation, collector surface area, surface layers, wind conditions, collector plate profile and supplementary instrumentation (Tyagi et al. 2012; Perisoglou and Dixon 2015). However, different parameters have various impacts due to the different locations and climates (Shukla et al. 2012; Tyagi et al. 2012). Parametric studies have been undertaken by scholars for finding the influence of various determinants including the porosity, airflow rate, solar radiation and solar absorptivity/thermal emissivity on collector efficiency, heat exchange effectiveness, air temperature rise and valuable heat supplied (Leon and Kumar 2007a). It is concluded that airflow rate and solar radiation have the greatest effects on TSC performance.

2.13 **Numerous forms of the transpired solar collector**

TSCs can be classified into different types based on their implementation (Ogden et al. 2011). Figure 2-9 displays various types of TSCs such as the standalone transpired solar collector, the building integrated transpired solar collector including on a south-facing wall (Sewalk, Liston and Maher 2009) and the rooftop-mounted transpired solar collector (Kozubal et al. 2008). Furthermore, it also describes the different applications or benefits of transpired solar collectors such as summer cooling (Saman et al. no date), pre-ventilation (Croitoru et al. 2016), drying agricultural products (Tyagi et al. 2012) and use in long-term warehouse storage (Sewalk, Liston and Maher 2009).

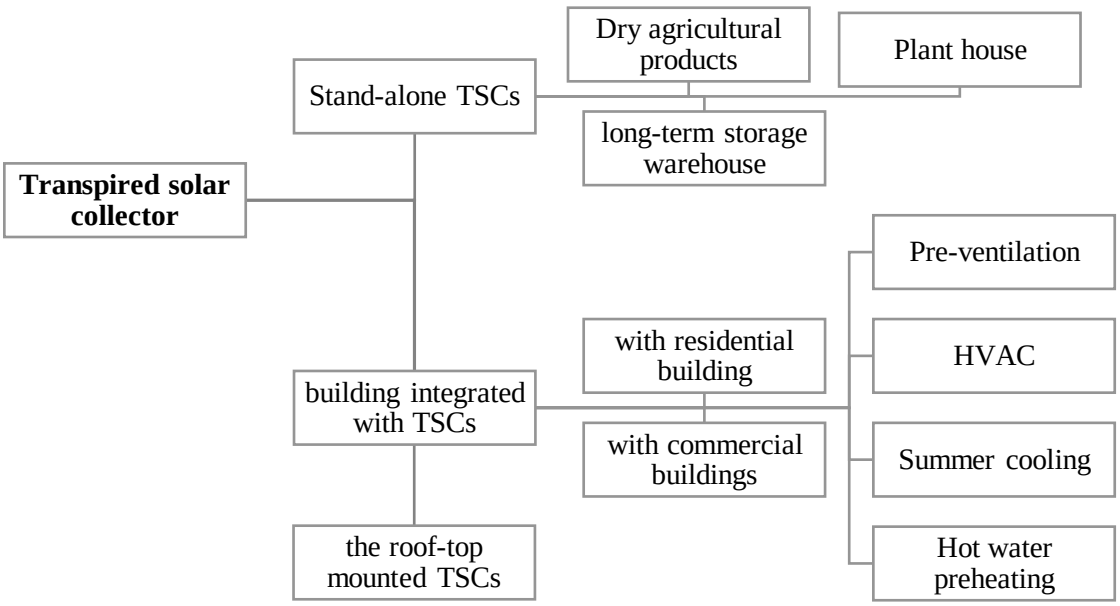

Figure 2-9. Classification and various applications of transpired solar collectors (Bake et al. 2019)

2.13.1 *The stand-alone TSC*

A stand-alone transpired solar collector as a solar thermal system is a basic TSC that contains a porous absorber and is positioned to a bottom plate with sealing around the edges. In terms of applications, stand-alone TSCs have been popular for providing low-temperature process heat for agricultural or industrial purposes, such as crops and drying cardboard, textiles or paint (Leon and Kumar 2007a; Brown et al. 2014).

2.13.2 *The roof-top mounted TSC*

The roof-top mounted TSC lies on the building's roof and it can attain higher energy yields than TSCs integrated within the south-facing barrier because of optimising the tilt and orientation of the absorber freely in order to gain more solar radiation (Kozubal et al. 2008). A roof-integrated with an unglazed transpired solar collector (RIUTC) gains solar energy when it is visible to a high intensity of mainly beam solar radiation, to get the most of the sunlight (Amirante et al. 2017). A RIUTC has the potential to significantly

contribute to domestic heating. For example, it has been applied for summer cooling based on radiative and evaporative cooling techniques (Saman et al. no date). It can also collect solar radiation while preheating the air at the same time, which is also good for providing fresh air for the indoor environment (Saman et al. no date). An experimental study of a RIUTC has created efficiencies in a range of 60% to 80% compared to a glazed solar air collector with 25% efficiency (Eryener, Hollick and Kuscu 2017a). However, a RIUTC in comparison to a TSC applied to the south-facing façade also has high maintenance costs and requires additional facilities to avoid bad weather like rain or snow and more instability of the system's performance due to bad weather conditions (Saman et al. no date). TSCs installed on south-facing façades as new building-integrated TSCs are able to overcome these difficulties and have been used successfully over the years due to their higher efficiency and greater potential benefits for improving building performance, which is given in the next section.

2.13.3 *The building integrated TSC*

A transpired solar air collector system transforms sunlight into heating for a building via the south-facing wall, thereby creating an energy-efficient building with reduced energy usage and carbon dioxide emissions (Genevès et al. no date; Summers, Mitchell, and Klein, 1996; Brown et al. 2014). It can also reduce a building's operational costs via being maintenance-free (Summers, Mitchell and Klein, 1996) and to improve workers' performance via delivering fresh ventilation air for the occupants (Sewalk, Liston and Maher 2009; Ogden et al. 2011). Therefore, TSCs have been popularly used in building the industry and there are some applications of building integrated transpired solar collectors, as follows:

a) Pre-heating ventilation air (Hall and Allen 2015);
b) Preheating water for a district heating network (Frank and Budig 2006);
c) Space heating (Gao, Bai and Mao 2014);
d) Desiccant regeneration for cooling applications (Genevès et al., no date);
e) Drying of agricultural products (Tyagi et al. 2012).

Moreover, there are some potential benefits when a TSCs is applied with other systems as a combined or hybrid system like energy storage or a photovoltaic (PV) system.

2.13.4 *The hybrid system integrated with a TSC*

However, solar energy systems also have restrictions to meet the needs of their own abilities (Kyriaki, Drosou and Papadopoulos 2015). It therefore requires the combination of multiple systems to maximise the usage of resources, which comes to these hybrid systems. There are numerous technologies including Photovoltaic (PV), energy storage (like phase change material) and heat pumps. These can be combined with TSCs in a hybrid system. The combination of PV and TSC systems can replace conservative building components of roofs, skylights or façades (Yang and Athienitis 2016). Buildings integrated with photovoltaic/transpired solar collector systems (BIPV/Ts) complete a better thermal efficiency. For instance, unglazed thermal collectors with additional photovoltaics could provide 10-15% higher collective efficiency (Bigaila et al. 2015). BIPV/Ts also offers an approach for on-site electricity, producing thermal energy for the environmental challenges faced in building (Delisle and Kummert 2014; Li et al., 2014; Gholampour and Ameri 2016). With their contribution to achieving net-zero energy buildings, BIPV/Ts possess the following features (Stamenic, Smiley and Karim 2004; Anderson et al. 2009; Yang and Athienitis 2015, 2016):

a) The system is physically attached to the building;
b) The system generates electricity;
c) The system generates thermal energy ready to be collected and utilised by the building, or the thermal behaviour of the system has an increasing effect on building energy performance.

Although PV as a TSC absorber has the benefits of additional electricity generation, a vertical PV is not as efficient as a roof mounted one due to the sun's angles. Hence, this should be taken into consideration while introducing PVs with TSCs.

2.14 **Case study of TSC implementation in buildings**

Also, the building envelope integrated transpired solar collector is very effective for energy saving via the following components including (i) saving energy from energetic solar gain (Buker and Riffat 2015) and (ii) recaptured and compacted heat loss from the wall (Frank et al. 2005). TSCs improve a building's energy efficiency by seizing this lost

heat in the air cavity during a cold day (Genevès et al. no date). Therefore, TSCs have been used successfully in different types of building around the world over the last decades and various applications of transpired solar collector systems are given in Table 2-5.

Table 2-5. Summary of various case studies on TSCs implementation

Reference	Project	Area of TSCs (m^2)	Location	Year	Impact on building performance
Anon. (no date b)	Erlangen City Hall	150	Germany	2005	It preheats 510m^3/hr cfm of ambient air for the office building and eliminates almost 30000kg of CO_2 emissions yearly.
Anon. (1997)	German Solar Wall Projects	330	Germany	2006	It made approximately 132,000 kWh per year in energy savings and 66000kg of CO_2 can be reduced each year
Reigger, C. (2008)	Pennsylvania Manufacturing Facility	334.45	USA	2006	The International Energy Agency's (IEA) Solar Heating and Cooling Program is reporting efficiencies of more than 70%
Anon. (2007)	Krause factory in Swidnica	2000	Poland	2007	The solar heating system has an overall capacity of 1MW thermal and will save roughly 65000kg of CO_2 annually.
Reigger, C (2008)	Greenwood Elementary School	67.82	USA	2007	It reduces 8618kg of CO_2 and saves $2,553 in heating cost per year with an expected $115,000 in savings over the 30-year project life.
Anon. (no date e)	Sainsbury / Prologis	950	UK	2008	It provides up to 20% of a building's energy requirements

Anon. (2008)	2008 Beijing Olympic Village	83	China	2008	The completed solar wall system expected 10kW of electricity and 20kW of thermal heating energy.
Anon. (no date a)	Elipse BLC building	1800	Latvia	2009	Delivering more than 1MW of thermal energy and displacing over 400 tons of CO_2 each year.
Anon. (no date g)	Flin Flon General Hospital	353	Canada	2009	The system displaced approximately 1,523 GJ of energy a year and reduced CO_2 emissions by 106000kg annually
Anon. (2008)	New hypermarket in Auchan, Miskolc	522	Hungary	2009	It saved Auchan over 245,000 kWh of energy annually and offset 59000kg of CO_2 per year. Natural gas consumption will decrease by 27,900m^3 per year
Butcher et al. (2009)	Northern Arizona University Distance Learning Centre	263	USA	2009	The system will reduce greenhouse gas emissions by 29000kg of CO_2 each year with an estimated financial payback in under 8 years.
Anon. (no date f)	Toyota Car Dealership	400	Spain	2010	It reduced Greenhouse gases by 4600kg of CO_2 each year and delivered 60GJ of renewable energy annually.
Anon. (2004)	Centre Commercial Leclerc de Valréas	224	France	2011	There is an annual saving estimated at €4955 on energy expenditure, reaching 167800kg CO_2 reduction per year.
Anon. (2007)	Toyota Motor Manufacturing France	400	France	2011	There are energy savings of up to 25% of whole traditional heating methods and a reduction of 20000kg CO_2 emissions annually.

Allen (2011)	Sustainable building envelope centre (SBEC)	157	UK	2011	The system installed at the Sustainable Building Envelope Centre (SBEC) has the potential to produce up to 39MWh per year with up to 75% efficiency converting solar radiation to usable heat energy.
Wright (2012)	Deeside leisure centre	216	UK	2011	The system delivered an average of 50MWh of energy per year over a two-year period with 70% conversion efficiency.
Anon. (no date d)	Jaguar Land Rover Training Academy	268	UK	2012	It saved more than 80,000 kWh per year by providing 20% of a building's total energy requirements and reduced over 13000kg of CO_2 on an annual basis.
Anon. (2012)	Cicame Energie Inc.	450	Canada	2012	The Solar Wall system is projected to displace over 35,000m^3 of natural gas a year and offset over 74000kg of CO_2 emissions, annually.
Anon. (2013)	Swalec Smart Energy Centre	140	UK	2013	It was predicted to deliver a heat output per annum of approximately 71MWh. The consequential savings in gas consumption translate into a CO_2 saving of around 15,000kg per annum.
Anon. (2013)	Marks and Spencer	4330	UK	2013	The M&S Solar Wall system is likely to save 1.1GWh energy and eliminate 250000kg of CO_2 yearly.
Anon. (no date j)	Windsor Essex Community Housing	1000	Canada	2014	As one of the tallest Solar Wall systems around the globe, it would replace 4 million cubic meters of natural gas during next 40 years.

Anon. (no date i)	Sherbrooke University Hospital	250	Canada	2014	Supplies 149MWh per year of renewable energy, reducing 40 tons of GHG emissions each year. Also, the energy costs represent a 48% decrease.
LCRI (2015)	The Solcer house	NA	UK	2016	It is estimated that the energy performance is around 70% with a 1.75 grid export-to-input energy ratio and proposes to reduce its solar costs by 50%.
Anon. (no date h)	Peel Regional Paramedic Service Station	490	Canada	2016	It preheats incoming make-up for the facility by collectively 33980m^3/hr of air freely.

According to Table 2-5, one common feature has been found among all the case studies. The TSCs have great benefits in building energy savings and reducing CO_2 emissions and building operation costs. However, the potential benefits in terms of energy saving/generating or reducing CO_2 emissions would be different due to the total area of the TSCs and the different climatic conditions of various countries. Therefore, the climatic conditions of countries is also one of the crucial factors to consider during the implementation of transpired solar collector technology. However, it is indicated that TSC performance could be affected by several parameters such as solar radiation, geometry design (hole diameter and pitch size), plenum width, suction velocity and approach velocity. In order to improve its collector efficiency and total performance to expand its implementation, it is essential to investigate the impact of parametric dominants on TSC performance and there have been a number of researches done by numerical and experimental methods on TSC study, as mentioned below.

2.15 **The parametric dependency of TSC performance**

Different parameters affect the thermal performance of TSCs, since analysing the thermal performance of transpired solar collectors is very compounded (Table 2-6).

Table 2-6. Summary of various factors on the thermal performance of TSCs

Factors	Parameters
Climatic conditions	ambient temperature, solar absorptivity, solar radiation, thermal emissivity, wind effect, weather conditions, humidity, sky temperature
Site conditions	orientation, tilt, surroundings of the site
Geometry of collector	size of the collector, cavity dimensions, surface coatings, absorption, material, porosity
Geometry of holes	pitch, dimensions (hole diameter), hole shape, pattern, plenum thickness, the arrangement of holes
Building parameters	wall *U* value and area of wall (excluding standalone)
Load characteristics	high-temperature rise, low-temperature rise, process air, re-circulation, fan velocity, turbulence intensity

The dimensions of a UTC absorber with its operation conditions affect the thermal performance of unglazed transpired solar collectors (Leon and Kumar 2007a). Recently, investigations on the effects of heat transfer, efficiency, airflow rate and pressure change on TSCs performance have been done by researchers because those determinants are the most important for TSC performance. However, parametric study is crucial for analysing the dependency of different parameters on the performance of TSCs. The thermal performance of transpired solar collector systems has been studied and Table 2-7 displays them in chronological order.

Table 2-7. Summary of various previous experimental studies on TSC performance

Author	Type of TSC	Software/ method	Operation parameters	Results	Special findings
Van Decker, Hollands and Brunger (2001)	TSC	Experimental and mathematical study	Hole geometry, wind speed	In normal operating conditions, 62% of air temperature rise happens on the front surface; 28% of that is in the hole; and 10% of that goes on the back of the perforated plate.	(i) The front surface of the plate is a crucial place where most of the heat transfer happens. (ii) Heat transfer is related to the hole and the thicker plates have greater hole heat transfer.
Frank and Budig (2006)	TSC	Experimental, theoretical study, and TRNSYS	Air flow rate, wind speed	The separated boundary layers have larger heat loss than the attached layers.	(i) Transpired solar collector efficiency varies significantly depending on the wind conditions. (ii) Convective losses from the plate cannot be ignored for the corrugated transpired solar collector.
Badache et al. (2013)	TSC	Investigating experimentally and numerically	Incident solar radiation, inlet air temperature	(i) The collector efficiency is developed by higher air mass flux. (ii) The heat transfer is more significant on the front surface of the absorber plate.	(i) Numerical estimation overrated the obtained efficiency as 13% for the smallest plenum widths. (ii) The alternative lab ambient temperature (±1.5 °C) mostly weakens the outcomes for a reduced amount of mass flux.

Chan, Zhu and Riffat (2013)	TSC	Experimental study	Two different wind directions (normal flow and vertical flow)	(i) The loss of heat is a smaller amount than 0.5% of total energy delivered. (ii) Efficiency and heat exchange effectiveness at different mass flow rate are different.	(i) Heat transfer rate of normal direction is about 10% more than vertical direction at low solar radiation intensity. (ii) Lower absorptivity colour can be used to receive more solar radiation.
Gao et al. (2013)	UTC	Experimental study	Colour effect of the collector, surface temperature, air flow rate	(i) Thermal efficiency of the system was 68.92% and 77.64% usually in low and high air flux, respectively. (ii) The heating demand of the building declined by 6.4% by the integration of UTC.	(i) UTC has better performance compared to other glazed flat-plate solar air collectors. (ii) Increasing air flow rate causes the reduction of air temperature rise but higher thermal efficiency can be reached by growing the air flux.
Badache et al. (2014)	TTC	Experimental investigation	Plenum width, pitch size, holes size, irradiation, and air flow flux	(i) Solar irradiation, slots and pitch dimensions and plenum size has limited impact. (ii) The plenum thickness has a moderate impact on the efficiency of the TTCs.	(i) The relations between factors are not very obvious, but plenum and slot width have obvious connections. (ii) The loss of heat by convection affecting the thermal efficiency of the TTC is determined by solar radiation mainly.

Vasan and Stathopoulos (2014)	UTC	Experimental study and analytical parametric study	Wind velocity distribution, wind angle	(i) Winds at an angle of 45° have the greatest effect on CHTC and heat exchange effectiveness. (ii) Typical wind speeds with a range of 1m/s to 3m/s reduce the UTC thermal efficiency by up to 20 %.	Convective heat transfer coefficient (CHTC) was found to have a dominant impact on heat transfer effectiveness in the prediction of thermal efficiency.
Bunea et al. (2015)	UTC	Mathematical modelling and experimental study	Wind speed, solar irradiation, operation temperature	There are up to 40% and 50% of extra heat gains due to limited solar radiation and condensation, respectively.	There is are improved mathematical model for evaluating the performance of UTC in such weather conditions like condensation, frost, and rain.
Perisoglou and Dixon (2015)	TSC	Experimental monitoring	Wind direction, suction velocity, solar irradiation	(i) The flow exceeds 120m^3/h, the efficiency has the highest point. (ii) The horizontal collector has improved the outcome by completing an efficiency of up to 70% for the highest flow.	(i) The temperature rise declines with the increasing flow. (ii) Particularly for the horizontal collector, at high flows, the suction performs better through high flows.
Vaziri, Ilkan and Egelioglu (2015)	PGSAHs and UTSAH	Experimental study	Air mass flow rate, collector colour	The highest efficiencies can be obtained at an air flux of 0.036 kg/s. (ii) The highest values of efficiency were 55%, 61%, 65%, 74%, 84%, and 85% for	(i) PGSAHs with coloured collectors have better performance than UTSAHs. (ii) Dark coloured PGSAHs perform better than UTSAHs. (iii) Better thermal performance of solar collectors comes from the higher value of the mass flow.

				white, light yellow, violet, red, blue, green, and black PGSAHs, respectively.	
Zhang et al. (2016)	GTC	Experimental and numerical studies with Fluent software	Solar radiation	(i) The indoor temperatures are developed from 12.12 ℃ to 16.17–18.19 ℃ under various operating conditions. (ii) It can lessen the emissions of pollutants by 11.6–69.6% in diverse operating ways.	(i) A glazed transpired solar collector (GTC)-based solar wall system is set as a better method for rough thermal conditions and low air quality. (ii) The recommended solar wall system was operative for boosting the indoor thermal comfort with a higher quality of indoor air.
Chialastri and Isaacson (2017)	BIPV/Ts	Experimental and numerical investigation	solar irradiance, suction velocity (fan velocity)	The BIPV/T collected the highest air temperature rise of 31°C and it generated 31% and 7% averagely for its thermal and electrical efficiencies.	The system with low emissivity coatings produces 64.7°C as an air temperature output and brings a 40% growth in air temperature rise as its greatest cost- effective resolution.
Bokor et al. (2017)	Roof-type TSC	Experimental study and mathematical modelling	Adjustable collector tilts, view factor, solar radiation	Increasing intensity of solar radiation can strengthen the passive cooling ability of the TSC.	A TSC can decrease roof temperature by 30-40°C and a TSC installed with a tilt of 30 degrees generates the highest back plate temperature.
Eryener, Hollick and Kuscu (2017b)	TSCUT	Experimental work	Solar radiation, ambient temperature, plenum air	During a good sunny day, the maximum air temperature rise is around 16-18°C and the TSCUT has a 3 times	The solar collector area of solar towers can be limited to less than a half.

			temperature, and chimney velocities	higher collector efficiency than the traditional solar tower glazed collectors.	
Wang et al. (2017)	TSC	Experimental and numerical study	Pitch and hole size, solar radiation, approach velocity, absorber plate temperature	Dimensional analysis and data fitting can be applied to accurately estimate the thermal performance of a UTC.	Quantitative correlation of the absorber plate temperature and the heat exchange effectiveness is helpful for researchers or designers to select or design a reasonable UTC efficiently.
Eryener and Kuscu (2018)	Hybrid SUT	Experimental study	Solar radiation and solar collector area	A hybrid solar updraft tower generates a hundred times the solar power efficiency compared to conventional solar power.	A hybrid solar updraft tower has a 12-14°C temperature rise on a good sunny day.
Bandara, Amarasekara and Rupasinghe (2018)	UTSC	Experimental work	Solar radiation, wind speed, ambient temperature	When the airflow rate and average solar radiation was $0.0077m^3/s$ and $304.24W/m^2$, the efficiency of the solar collector with a transpired type was collected as 38.41%.	UTSC used as a substitute for the glazed solar collector in the agricultural drying process.

Erenturk and Erenturk (2018a)	UTC	Experimental study	Output temperature	The ANFIS method is the best way to predict the output temperature of a UTC.	Grey modelling method is seen as the simplest way to present the output temperature with the precise accuracy
Poole et al. (2018)	TSC-TES	Experimental investigation	Suction velocity and airflow rate	A one-staged TSC generates a higher air temperature rise, power, and efficiency than a two-stage TSC.	34% of total valuable energy generated to use during the night is stored by TSC-TES, which can substitute 1.35kg of natural gas.
Wang et al. (2019)	TSC	Experimental investigation	Airflow rate, solar radiation, and hole diameter	The collector efficiency and heat exchange efficiency can be increased by 25% and 10% separately by an increase in the uniformity of the infiltration holes.	The preheating effect of fresh air and overall efficiency of the system can be affected greatly by the non-uniform distribution of infiltration holes at the top and bottom of TSC.
Moon and Kim (2019)	UTC-TES	Experimental study	Solar radiation	The UTC generates an average of 13548.21kcal/day and the average stored and released energy achieved was 7739.78 and 1793.47kcal/day, respectively.	The TSC plenum temperature increased up to 65°C with 35°C higher than the outdoor air temperature throughout the day.
Badescu et al. (2019b)	UTC incorporating PCM	Experimental investigation	Solar radiation, PCM plate thickness, hole diameter	A UTC incorporating PCM provided 4°C warmer air than ambient air during the night-time.	UTC integrating with PCM release heat for a longer time period than the usual UTC and thicker PCM plates decrease the air temperature rise.

Gao et al. (2020)	GTC	Experimental study	Hole diameter, hight ratios, fan speed, solar radiation and inlet temperature	The application efficiency increased by roughly 34% when the fan speed increased from 0.25 to 1.25m/s. The thermal efficiency can be increased by 20% and the heat collection efficiency increased by 0.8%/°C with inlet air temperature decreasing when using a glazed transpired solar collector.	.the air temperature rise in GTS was lower than that in a UTC by approximately 3.4°C under the same operational conditions. Also, GTC could achieve higher solar conversion efficiency through using a black corrugated metal plate and newly designed ventilation system
Peci et al. (2020)	UTC	Experimental investigation	Solar radiation, inlet temperature	28 to 48% of ventilation energy demand can be covered by a UTC during sunny days; while a UTC could provide 3 to 28% of ventilation load during cloudy days.	UTC could be a promising approach to reduce ventilation and heating energy consumption.

Table 2-7 shows the typical research done during the last 2 decades via experimental and theoretical study to analyse the impact of each parameter on TSC performance. For example, the larger air flow through the collector results in higher collector efficiency though a reduction in outlet air temperature. Hence, air flow rate impacts strongly on TSC performance in terms of collector efficiency. Wind speed has a significant effect on TSCs performance; however, the hole geometry and solar radiation have rather less impact on TSCs performance. It has been reported that the round hole shape brings a lower heat transfer, around 15% less than the lobed geometry used in the solar collector. More importantly, other parameters, e.g. hole diameter, pitch, solar radiation, suction velocity, plenum size and inlet ventilation air have to be taken into consideration to improve the TSCs performance. The parameters mainly included airflow rate, wind velocity, wind direction, solar radiation, the geometry of the TSCs, and many other factors. However, there is a lack of research on evaluating the effects of multi-parameters on TSC performance, which needs to be tackled. However, lists of numerical and mathematical investigations have been done to analyse the performance of the transpired solar collector and some of these are shown in Table 2-8.

Table 2-8. Summary of various previous numerical and mathematical studies on TSC performance

Author	Models	Type of TSC	Software/ method	Operation parameters	Results	Special findings
Dymond and Kutscher (1997)	Laminar flow	UTCs	Mathematical and pipe network modelling	Air flow distribution	The larger air flow across the collector results in higher collector efficiency.	This common method is used for modelling the airflow phenomenon and various temperatures of UTCs.
Arulanandam , Hollands and Brundrett (1999)	TASC flow	TSCs	CFD and mathematical modelling	Heat exchange effectiveness, wind velocity, suction speed, and plate dimensions	For the same plate geometry, a 10–20% decline in terms of effectiveness with a growth of plate conductivity of 50.196 to 515.121W/m K	Suitable efficiencies can be completed even when lower conductivity materials like plastics are used for the transpired-plate absorber.
Abulkhair and Collins (2005)	RNG k-ε	UTC	Numerical modelling	Wind speed, plate geometry	(i) In a UTC system, suction velocity is much higher than minimum velocity. (ii) A separated flow usually occurs at high wind velocities, but heat loss	A corrugated transpired solar collector loses heat three times greater than a perforated flat solar collector. Wind speed and suction velocity have a huge impact on heat loss.

					is higher when compared to the attached flow.	
Stojanović, Hallberg and Akander (2010)	-	USC	Fin-theory approach	Surface temperature, coating degradation	Comprehensive surface temperatures are essential features for durability studies of the surface coating and its impact on USC and system performance.	(i) The fin-theory model has been capable of analysing energy performances with completed material temperature fields and circulated transfer of heat. (ii) Accuracy of the fin-theory model is better compared to the 3D FDM model.
Badache et al. (2012)	RNG k-ε	UTC	Experimental analysis and Fluent CFD	Air mass flux, solar irradiation, plenum thickness	(i) Heat loss by radiation to the surroundings from the absorber plate is major when the operating conditions have low mass and high irradiation levels. (ii) 2.85% would be the highest efficiency alteration between two plenums sizes (5 and 15 cm).	(i) Plenum thickness has a lower impact compared to the mass flux and solar irradiation on collector efficiency. (ii) Operating the collector at medium or high mass fluxes is good to diminish the loss of heat from UTC to optimise its efficiency. (iii) The collector efficiency could be affected slightly by higher solar irradiation.

Li (2012)	Standard k-ε, RNG k-ε, SST k-ω	Flat UTSC	CFD ANSYS	Wind velocity, suction velocity, perforation row and turbulence intensity	(i) Suction velocity effects the convective heat transfer coefficient (CHTC) more in the perforation row. (ii) Turbulence influences greater CHTC over the plate as the solid row is responsible for a larger area.	(i) The standard k-ε and RNG k-ε models have better performance in terms of accuracy and stability. (ii) The SST k-ω model has a varied performance from all the k-ε models, as its surface temperature is overestimated.
Collins and Abulkhair (2014)	RNG k-ε	UTC	CFD numerical modelling	Wind speed, suction velocity	(i) The temperature behind the absorber drops as the suction velocity increases. (ii) The flow structures are seen to strengthen and grow with increased wind velocity.	(i) Effectiveness and heat transfer were not a function of wind velocity. (ii) In theory, wind speed should have no impact on the calculated heat exchanger effectiveness.
Gao, Bai and Mao (2014)	-	GTC	Mathematical model and discussion	Glazing, pitch design, hole geometry, solar radiation, air flow rate, suction	When 400 W/m2 is for solar radiation: (i) The thermal efficiency and air temperature rise of the GTC are greater compared to that of the flat-	(i) Glazing could decrease convective heat loss due to optical limitations. (ii) The outlet air temperature of the GTC is greater compared to that of the UTC for crosswind velocities beyond 3.0 m/s.

				velocity, wind speed	plate collector by 70% and 9 °C, respectively.	(iii) Hole and pitch diameter have a slight impact on the thermal performance of the GTC.
Li et al. (2014)	Uniform flow	GTC	Mathematical and numerical study	Perforation design, the pitch of perforations, collector size, emissivity of the absorber	The experimental and numerical outcomes have attained good settlement with the same movement and usual deviation of 2.25%.	(i) The model is precise to measure the thermal performance of the collector. (ii) The model is beneficial to operate and develop the vacuum glazed transpired solar collector.
Li and Karava (2014)	-	UTC and UTC/PV	Numerical modelling	Collector geometry, orientation, and incident turbulence intensity, solar radiation, wind speed, suction velocity	The ‘vertical’ installation of the plate enhances convective heat transfer due to the collective impact of the corrugation, wind speed, suction velocity and buoyancy.	It is less effective to improve the energy performance through maximising the geometrical parameters for UTCs with PV panels. However, among all the geometrical parameters studied, the wavelength of the corrugation and the PV panel height were found to be the most important factors.

Misevičiūtė and Rudzinskas (2014)	-	UTC	TRNSYS	Solar radiation, air mass flow rate	(i) The average value of the temperature increase is around 4°C during the cold period. (ii) 5.08 °C as the largest temperature rise is collected in April during the experiment while the highest increase of temperature is 7.42 °C during January.	(i) Heat transfer of the system happens at the forward-facing of the plate the holes and the hind face of the plate. (ii) Collector efficiency is slightly affected by the radiation. (iii) The ventilation air is developed from 2°C to 9°C.
Croitoru et al. (2016)	Uniform flow	UTC	Numerical study	Air flow rate, perforation geometry	(i) The interleaved "×" and "+" perforations and their type (not aligned "+" perforations) introduce better heat transfer performance compared to other lobed geometries. (ii) Type 2 has a higher efficiency under an airflow of 90 $m^3/h/m^2$.	(i) The round hole has a lower transfer with 15% less than the lobed geometry. The black covering of the metal cladding enhances the efficiency by up to 25%. (ii) There is an emphasis on the importance of metal cladding absorbance.
Croitoru et al. (2016)	RNG k-ε	UTC	Experimental study and CFD modelling	Hole geometry and the opening shape of the	Perforation geometry is an important determinant for the performance of TSCs.	(i) The thermal efficiency of the system has a reasonable performance under the materials with low thermal conductivity.

				perforated panel		(ii) Heat transfer of such devices can be evaluated mainly by the temperature difference.
Gholampour and Ameri (2016)	RNG k-ε	Flat UTC/PV	Experimental, theoretical study and numerical modelling	Ambient temperature, suction velocity, solar radiation, suction velocity	The maximum PV coverage was roughly 55% at 400W/m^2 and about 45% at 800W/m2 and the value of the ideal suction rate was 0.045 m/s at 400 W/m^2 and was 0.06 m/s at 800 W/m^2.	(i) PV location had a slight impression on system performance. (ii) Solar radiation is important for designing an exclusive optimal value for PV coverage percentage or suction velocity.
Janusevicius et al. (2016)	-	UTC	TRNSYS simulation	Inlet air temperature	The accuracy of the simulation model predictions has a deviation of 11% due to uncertainty and possible errors from the model fitting.	(i) The effect of frost formation influences operational performance as well as the combination with UTC. (ii) The result from this study could be used to improve the operation process of the ASHP system.

Tajdaran et al. (2016)	RNG k-ε	TSC	CFD modelling	Airflow, wind angle, wind speed, time of day	(i) Surface temperature and air temperature rise grow by higher solar radiation. (ii) Higher values of wind angle have a shrinking impact on temperature rise.	(i) The reduction in heat exchange effectiveness can be led by the growth of the suction ratio and wind velocity. (ii) Wind angle and solar radiation slightly affect the effectiveness of the heat change.
Tian et al. (2018)	NA	PV/T/D panel	CFD simulation	Approach velocity, pitch/hole diameter, plenum size, solar radiation	The thermal efficiency of this system can be in the range of 40% to 85%, due to various approach velocities and different sizes of system geometry.	The heat gained inside the building can be reduced greatly by using a transpired solar collector.
Erenturk and Erenturk (2018b)	NA	UTC	Grey modelling approach and ANFIS	Solar radiation and airflow rate	The grey modelling approach is the simplest method to provide highly accurate results on outlet temperature.	ANFIS could provide optimal prediction results for the thermal performance of this system.
Safijahanshahi and	NA	UTC-HP	MATLAB	Solar radiation, suction velocity	The UTC would reduce the energy consumption and CO^2 emissions by up to 10%.	It was concluded that it is unnecessary to pass the air through the collector if the air is preheated less than 0.3 °C by the collector.

Salmanzadeh (2019b)						
Tajdaran et al. (2020)	NA	TSC	MATLAB	Hole diameter, pitch size, suction velocity, wind speed	Effectiveness reduces on average by 10% per 1m/s wind speed and 6.5% per 0.002 suction ratio.	28% of materials can be saved by the optimised geometry of this proposed system.
Li et al. (2020)	Standard k-ε	TSC	ANSYS Fluent CFD simulating	Solar radiation, wind speed, inlet air temperature	The CO_2 concentrations of indoor environments reduce to less than 1000ppm in winter months because of using TSCs. Also, the solar fraction can be as high as 34.3% during the summertime (hot season).	Such a system is not cost effective but has great potential for energy saving and environmental protection.

Table 2-8 shows the typical research done on investigating the impact of each parameter on TSC performance during the last 2 decades via numerical and mathematical modelling. Scholars have been using various software/methods like CFD, ANSYS Fluent Software and TRNSYS to operate their parametric studies on TSC performance. Generally, the RNG k-ε model has been popularly used by researchers, since the RNG k-ε model has a better performance in terms of accuracy and stability. Most of the numerical modelling focused on the impact of wind speed, airflow rate and solar radiation. Moreover, some of the papers also studied the effects of the geometry of TSCs, especially pitch size and hole diameter. It was found that the hole size and pitch distance have a great impact on the heat exchange effectiveness but less influence on air temperature rise (Table 2-9).

Table 2-9. Comparison of the impact of the main parameters on TSC performance

Parameters	Impacts
Airflow rate	Air temperature rise decreases with an increasing airflow flux or rate (Badache et al. 2012); A larger airflow through the collector has a higher collector efficiency (Dymond and Kutscher 1997); Efficiency increases with an increasing air mass flux (Badache et al. 2013);
Wind effect	Air velocity is one of the most vital determents influencing efficiency (Badache, Hallé and Rousse 2012); Wind velocity has a positive impact on heat exchange effectiveness (HEE) (Tajdaran et al. 2016);

Wind direction or angle	Winds at an incidence angle of 45° to the UTC have the greatest effect on HEE (Vasan and Stathopoulos 2014); Wind direction is the dominant factor in determining the near building flow pattern (Fleck, Meier and Matovic 2002); Wind angle slightly impacts on HEE (Tajdaran et al. 2016);
Solar radiation	Increasing solar radiation has the least impact on collector efficiency (Badache et al. 2012; Misevičiūtė and Rudzinskas 2014); Increasing solar radiation would bring a higher air temperature rise (Tajdaran et al. 2016); The effects of solar irradiation seem to be limited to HEE (Badache et al. 2014); Solar radiation influences the collector efficiency slightly (Leon and Kumar 2007a);
Perforation geometry	The geometry of the perforations is important for the performance of TSCs (Croitoru et al. 2016); The diameter of the perforation and pitch shape have a slight impact on the heat delivered (Li, Li and Li 2016); For specific pitches, any modifications in perforation size influence the heat exchange effectiveness moderately (Leon and Kumar 2007a);
Plenum thickness	Plenum thickness has a lower impact on efficiency compared to air mass flux and solar irradiation (Badache et al. 2012);

	The effects of plenum thickness seem to be limited to HEE (Badache et al. 2014);

The performance of TSCs relies significantly on different parameters (Table 2-9). Wind speed and airflow rate are the most dominant factors in TSC performance in terms of air temperature rise, heat exchange effectiveness and collector efficiency (Badache et al. 2012), while increasing air mass flux leads to the growth of heat exchange effectiveness (Badache et al. 2013). In particular, the peak collector efficiency did not occur at the lowest wind speed, as it occurs at non-zero wind speeds (Fleck, Meier and Matovic 2002). Also, the geometry of the perforations is important in the performance of TSCs (Croitoru et al. 2016). However, the hole diameter and plenum size have a limited effect on TSC performance. Also, Plenum thickness has a lower impact on efficiency compared to air mass flux and solar irradiation. Meanwhile, hole pitch and hole diameter have a slight impact on the thermal performance of glazed transpired solar collectors (Gao, Bai and Mao 2014). The majority of air temperature rise comes from solar radiation and a substantial amount of heat comes from the captured wall heat loss at night. Additionally, painting the collector is also a very significant element affecting the TSC performance, as obviously a dark-coloured unglazed transpired solar collector performs better due to a higher solar absorptivity via its dark colour (Chan, Zhu and Riffat 2013; Gao et al. 2013; Vaziri, Ilkan and Egelioglu 2015). One typical example is that the black coloured perforated plate collector gained the highest values for collector efficiency at 85% among various colours (Vaziri, Ilkan and Egelioglu 2015).

2.15.1 *Impact of airflow on TSC performance*

The airflow rate or approach velocity has the greatest impact on collector efficiency, air temperature rise and heat exchange effectiveness. For instance, a study by Leon and Kumar (2007) demonstrated that heat transfer effectiveness increased by about 23%

when the rate of airflow was from 0.01 to 0.03 m/s. This efficiency increases with increasing the air mass flux and a larger airflow through the collector has a higher collector efficiency (Dymond 1997; Badache et al. 2012, 2013; Badache, Hallé and Rousse 2012). Moreover, the black unglazed transpired solar collector achieved an efficiency of 77.64% and 68.92% with high and low air flow rates, respectively (Gao et al. 2013). Higher mass flux causes a reduction in air temperature rise, as it has a bigger impact on it (Badache et al. 2012).

2.15.2 *Effect of wind on TSC performance*

Wind conditions including speed and direction affect TSC performance, since wind flowing through the collector's surface declines in useful thermal energy to heat the air by effectuating convection heat loss (Vasan and Stathopoulos 2014). Also, wind speed has a significant impact on HEE (Tajdaran et al. 2016). HEE is changed by approximately 50% when the suction ratio is 0.01 and the wind velocity is between 1 and 4 m/s changes (Tajdaran et al. 2016). Additionally, increasing wind velocity by 2m/s enable UTC efficiency to be reduced by about 20% (Vasan and Stathopoulos 2014). In addition, the wind angle or direction plays an important role in TSC performance, especially heat exchange effectiveness, owing to the airflow near the perforated plate which consequently develops the air temperature rise (Tajdaran et al. 2016). In particular, winds at an incidence angle of 45° away from the UTC have the greatest effect on HEE (Vasan and Stathopoulos 2014).

2.15.3 *Impact of solar radiation on TSC performance*

Solar radiation engineers the absorber plate heating process and the impact of solar radiation on TSC performance has been analysed by various scholars. Air temperature rise, surface temperature rise and exergy efficiency can also be improved by increasing solar radiation (Badache et al. 2012; Tajdaran et al. 2016). For instance, increasing

solar radiation from 150 to 600 W/m^2 improves the surface temperature by roughly 33%, achieving a 70% growth in temperature rise (Tajdaran et al. 2016). However, the heat loss from the TSCs might increase via increasing the solar radiation (Gholampour and Ameri 2016). It is generally believed that solar radiation has a great impact on air temperature rise and the surface temperature of the absorber and the least influence on collector efficiency and HEE (Leon and Kumar 2007a).

2.15.4 *Impact of perforation diameter and pitch on TSC performance*

In terms of the impact of pitch design on TSC performance, the air temperature rise first shows a rising trend, then declines while the pitch size increases from 0.03 to 0.18 m (Li et al. 2014). Increasing the pitch size from 0.05 to 0.18 m with the same slit-like perforation (80mm long, 1mm wide) only brings a 0.3% decline in thermal efficiency, since a larger pitch size would improve the jet impingement in a single perforation while it reduces the number of perforations (Li et al. 2014). Additionally, the larger size of hole pitch or hole diameter results in a reduction in exergy efficiency (Gholampour and Ameri 2016). For example, changing the hole diameter from 1.25 to 1.55 mm could only cause a 1.4% decrease in its effectiveness for a pitch of 18 mm (Leon and Kumar 2007a). Leon and Kumar (2007) also examined that decreased HEE comes from an increased perforation pitch, as increasing the size of the pitch from 12 to 24 mm results in an 11.5% drop in HEE. It was concluded that the pitch size and hole dimension have a slighter impact on the heat delivered than the pressure drop of the collector (Li, Li and Li 2016);

2.15.5 *Effect of suction velocity on TSC performance*

The reduction of suction velocity declines the thermal efficiency of a transpired solar collector (Collins and Abulkhair 2014). The temperature behind the absorber is seen to drop as the suction velocity increase. TSC efficiency decreases if the suction velocity

increases (Rad and Ameri 2016). Additionally, in increasing the suction mass flow rate by $0.02kg/s \cdot m^2$, the air temperature rise decreases by nearly 3K (Frank et al. 2005). Therefore, suction velocity affects the cavity flow velocity and has a profound impact on TSC performance and the heat transfer process.

2.15.6 *Effect of plenum thickness on TSC performance*

Plenum thickness has shown a limited impact on collector efficiency. The efficiency between the two plenum sizes (5 and 15cm) is 1.92 and 2.85%, respectively (Badache et al. 2012). Increasing the plenum depth minimises the volume of the convective heat transfer coefficient and fan power as the plenum air velocity falls (Rad and Ameri 2016). Additionally, the collector efficiency decreases by 1.79% via increasing the air cavity thickness between 0.05 to 0.15m (Badache et al. 2014).

2.15.7 *Impact of solar absorptivity/thermal emissivity on TSC performance*

It is generally believed that the efficiency of a solar collector is affected by solar absorptivity and thermal emissivity. For instance, the collector's efficiency can be reduced by approximately 35% due to a drop in solar absorptivity from 0.95 to 0.50. Meanwhile, there is a 12.5% reduction in collector efficiency when the thermal emissivity is increased from 0.25 to 0.85 (Leon and Kumar 2007a). The energy-received and efficiency of the collector is directly affected by solar absorptivity, hence, absorptivity has a greater impact on efficiency than thermal emissivity. However, emissivity impacts only on radiant heat loss from the collector, therefore its influence on efficiency is relatively limited.

2.15.8 *Impact of type of building on TSC performance*

Transpired solar collector systems have been implemented in all types of buildings including institutional, industrial, commercial and residential buildings for pre-heating

the ventilation fresh air for HVAC systems in buildings (Table 2-10). Also, this TSC technology has been used in the Military due to its efficient energy savings and free maintenance and is popular in warehouses and plants for process drying.

Table 2-10. Summary of various application of TSCs in different types of buildings (*Case Studies of Transpired Solar Collector*, no date)

Application	Building Type
Institutional buildings	Hospital, college, school, gymnasium, university, community centre
Industrial Buildings	Distribution centre, warehouse, Manufacturing Plant, Treatment plant
Residential Buildings	Multi-dwelling residence and single-dwelling residence
Commercial Buildings	Airport, office, storage facility, bank, training facility, retail store
Agriculture	Process drying, process heating, chicken coops, utility plants
Military	Military base, Air Force base, Navy

Based on the case studies, it can be assumed that using TSCs has been popular in institutional and industrial buildings including hospitals, schools, warehouses and plants, rather than other types of buildings. TSCs have mostly been used in institutional buildings, as more case studies has been run in them rather than other types of buildings, because such buildings have more funding to apply this new TSC technology (Anon. *Case Studies of Transpired Solar Collector*, no date). During the application of TSCs in real buildings, managing the uncertainty and sudden changes of weather conditions and solar radiation was seen as one of the main challenges, as it is hard to control weather conditions and solar radiation either manually or by human force.

2.15.9 *Impact of various modelling criteria on the evaluation of TSC performance*

There are several papers that concentrate on different turbulence models such as standard k-ε, Re-Normalization Group (RNG) k-ε mode and SST k-ω used in numerical modelling for analysing and evaluating the performance of TSCs (Table 2-11).

Table 2-11. Summary of numerous models and studies reported in the literature

Author	Models	Type of TSC	Software/ method	Meshing	Special findings
Abulkhair and Collins (2005)	RNG k-ε	UTC	Numerical modelling	Unstructured mesh	(i) The loss of heat from corrugated UTCs is more compared to that of a perforated flat absorber plate. It also depends on wind speed and suction velocity.
Badache et al. (2012)	RNG k-ε	UTC	Fluent CFD	Structured mesh grid	(i) 2.85% difference in collector efficiency for two different widths of the plenum (5 and 15cm).
Li (2012)	Standard k-ε, RNG k-ε, SST k-ω	Flat UTCs	CFD ANSYS	Structured mesh	(i) Both models (standard k-ε and RNG k-ε) have enhanced performance regarding accuracy and stability. (ii) The SST k-ω model has a different performance compared to all k-ε models as its surface temperature is overestimated.

Collins and Abulkhair (2014)	RNG k-ε	UTCs	CFD numerical modelling	Body Fitted Co-ordinates	(i) Effectiveness and heat transfer were not a function of wind velocity.
Croitoru et al. (2016)	RNG k-ε	UTCs	CFD numerical modelling	Multi-block meshing approach	(i) Acceptable thermal efficiency of the system could come from materials with low conductivity. (ii) The temperature difference is considered as a key parameter to evaluate the heat transfer of such devices.
Gholampour and Ameri (2016)	RNG k-ε	PV/flat UTCs	ANSYS FLUENT	Fine non-uniform mesh	(i) System performance can be slightly influenced by the location of the PV. (ii) Solar radiation is one of the key determents for a particular value of PV coverage or suction velocity.
Tajdaran et al. (2016)	RNG k-ε	TSCs	CFD software STAR-CCM+	Multi-block meshing	(i) Heat exchange effectiveness can be reduced by a higher suction ratio and wind speed. (ii) TSCs deliver changed operating temperatures due to the time of day. The CO_2 concentration of the indoor environment reduces to less than 1000ppm in winter months because of using TSCs. Such a system is not cost effective but has great potential

Li et al. (2020)	Standard k-ε	TSC	ANSYS Fluent CFD simulating	NA	for energy saving and environmental protection.

It is obvious that different turbulence models have been applied with different impacts on the thermal modelling of TSC performance (Table 2-11). Both the standard and the RNG k-ε models have been widely used for indoor environment simulations. Scholars have been using the Renormalization Normal Group k–ε (RNG k-ε) turbulence model more than the other models, since the RNG k-ε turbulence model performs better considering accuracy and stability for numerical modelling.

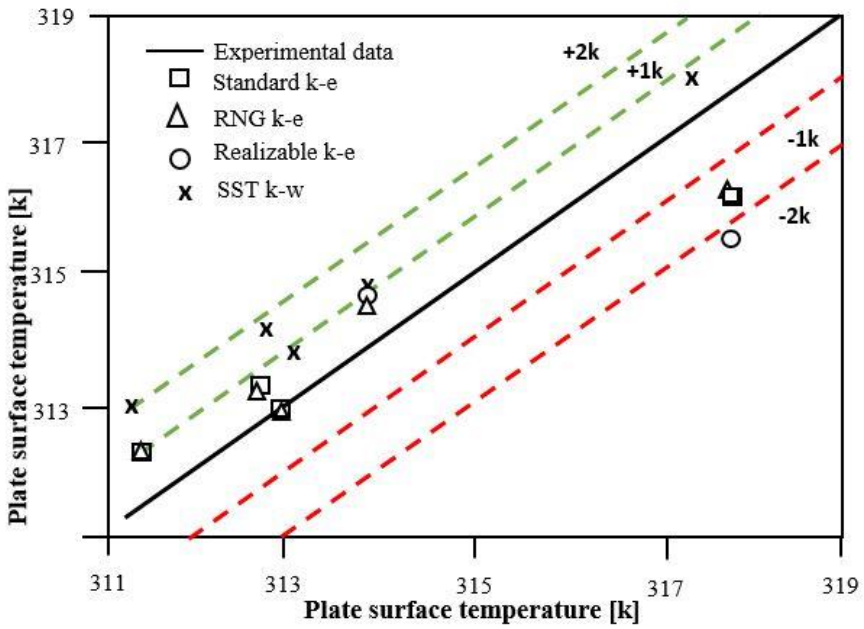

Figure 2-10. Comparison of CFD outcomes and experiment results (Li 2012)

Figure 2-10 displays the various impacts of different turbulence models. The Standard k-ε and the RNG k-ε model bring similar outcomes to the Realizable k-ε model. However, the results are steadier for convergence and are more reliable. The Shear Stress Transport k–ω (SST k-ω) model has different results than all the k-ε models in

that surface temperature is overrated. Both the Standard k-ε and the RNG k-ε model can perform with precise outcomes for thermal modelling. The Standard k-ε model was mostly used for parametric studies since it spends less computing time but has an improved convergence process (Li 2012). However, in terms of accuracy, numerical stabilit, and computing time, the RNG k-ε model is the best option to use (Chen 1995). Most studies have shown that the RNG k–ε model has a better performance than the standard k–ε model in terms of the whole simulation performance (Zhang, 2007). Therefore, scholars have been using RNG k-ε model to make thermal modelling on the performance of transpired solar collector in numerical simulation software. The RNG k-ε model was developed using Re-Normalisation Group (RNG) methods to renormalise the Navier-Stokes equations, to account for the effects of smaller scales of motion (Yakhot *et al.*, 1992).

2.16 **TSC integration with other technologies**

There have been a large number of studies on the performance of transpired solar collectors, including the effects of various parameters and external environmental factors (Wang, Shukla and Liu, 2017). Researches have also studied the advantages of combining TSC with other technologies for instance, thermal energy storage (PCM) (Poole *et al.*, 2018; Badescu *et al.*, 2019a), PV panel (Athienitis *et al.*, 2011; Tian *et al.*, 2018), and heat pump (Safijahanshahi and Salmanzadeh, 2019a). Due to the application of TSC, the power consumption of the heat pump may drop by up to 10% (Safijahanshahi and Salmanzadeh, 2019a). A study shows that the combined techniques of TSC and PCM can store 34% of all useful energy required for night-time operation (Poole *et al.*, 2018). The air temperature rise changes alongside TSC is reduced due to the implementation of PCM (Badescu *et al.*, 2019a). It brings some possible problems such as (i) thermal instability; (ii) higher cost of implementing PCM by using aluminum containers; (iii) leakage during melting process. These problems may affect the thermal

performance of the TSC integrated with the PCM and those issues should be addressed, however, there has been only limited research into the application of PCM to building integrated with solar collectors (BITSC) and its potential benefits.

2.17 **Potential points for further research on TSC study**

It is difficult to compare the significance of each parameter on TSCs performance due to uncertainty like different climate condition and lack of correlation. Therefore, there are some potential points for further research on TSCs performance as following Table 2-12.

Table 2-12. Summary of potential research or limits from specific previous papers

Author	Year	Potential points for investigation
(Fleck, Meier and Matovic, 2002)	2002	There is a need for evaluations about the impact of multiple parameters on system performance.
(Frank *et al.*, 2005)	2005	There is a limited study on evaluating the relationship between the plate and the air through the air cavity.
(Chan, Saffa B Riffat and Zhu, 2010)	2010	There is more need for analysing building performance in terms of energy consumed and thermal comfort with using transpired solar collector
(Ogden *et al.*, 2011)	2011	Analysing the possibility of the system being used for summer cooling based on radiative and evaporative cooling techniques, also the ability of the system to withstand weathering will also need to be considered
(Genevès *et al.*, no date)	2012	UTC needs more optimization to reflect implementation in many aspects of heat recovery;

		Corrugated plates, hole shapes, flow paths, actual pressure drop, slope need further study
(Badache *et al.*, 2012)	2012	There are no or limited studies on the thermal performance of the whole collector involving the plenum and perforation design
(Li *et al.*, 2013)	2013	(i) developing high-resolution Computational Fluid Dynamics (CFD) models for innovative TSC design and simplified thermal analysis models in building energy simulation is expected; (ii) influence of perforation shape design and corrugation aspect radio demand research in the future work;
(S. Li *et al.*, 2014)	2014	Lack of research on developing the physical energy model or comprehensive heat transfer links for the unglazed transpired solar collector

According to Table 2-12, there are some limits of previous research with its potential points for improving the TSCs performance and its application into building section in terms of heating and ventilation. Previous studies have been analysing the impact of different parameters under some assumption, however, the impact of different parameters on TSC performance in a single or couple parameters in same time still need to be analysed. The energy performance on building integrated TSCs system on air temperature rise, increasing thermal comfort, and energy savings in an extreme condition hourly, daily or, yearly also can be studied.

2.18 **Key findings from previous study of TSC**

Second half of this chapter focused on parametric dependencies and evaluation of numerical models on TSC performance alongside with relevant case studies of TSC

integration in building sector. Further parameters and model types used in numerical modelling that affect TSC performance has also been discussed and compared in detail. Based on previous papers on TSC performance, it can be concluded as follows:

a) There are various constraints which affect the performance of TSC, while, wind speed and airflow rate are the most dominant factor in TSCs performance in terms of air temperature rise, heat exchange effectiveness, and collector efficiency and winds at an incidence angle of 45° to the TSCs has the greatest positive effect on heat exchange effectiveness, however, hole diameter and plenum size has limited effect on TSCs performance;
b) Profile with longer pitch mostly have lower collector efficiency and heat transfer coefficient, and this brings a reduction in thermal efficiency. However, Profile with shorter pitch tends to reduce the wind effect. Particularly, the pitch has a slight effect on collector efficiency than heat exchange effectiveness;
c) Plenum depth have slight impact on (improvement of 2.85%) efficiency if the width is increased from 5cm to 15cm. However, the improvement in efficiency in different climatic condition and various types of TSCs will cause further change in efficiency;
d) Regarding the accuracy, numerical stability, and computing time, the RNG k-ε model would be the best option for the numerical modelling. Also, most studies showed that the RNG k–ε model has better performance than the standard k–ε model in terms of whole simulation performance;
e) The impact of multi-parameters optimization on TSCs need more research. Also, the energy performance on building integrated TSCs system on air temperature rise, increasing thermal comfort, and energy savings in an extreme condition also need investigation.

f) There has been only limited research into the application of PCM to building integrated with solar collectors (BITSC) and its potential benefits. This study proposes a new approach to applying PCM into BITSC to address the above-mentioned problems that may arise during the application of PCM to BITSC.

2.19 **Conclusions**

This chapter proposed the literatures related to the performance of energy storage in building envelopes and discuss case studies in the context. It has been found that building envelope provide greater opportunity to integrate and exploit several methods for energy storage which can play vital role in the energy demand reduction of a building. However, there is limited study which particularly focus on the use of energy storage in the building envelope design and its impact on building energy performance in combination with TSC. While, one method of reducing building energy consumption and limiting the CO_2 emissions can be completed via applying the solar thermal system like transpired solar collector (TSC) technologies into the design of building fabric. Thus, with full cognizance of existing knowledge on TSC's performance, the literature related to TSCs performance, Background/concept of TSCs, and relevant case studies are included in this chapter. It mainly focuses on parametric sensitivity analysis including the impact of various parameters on the performance of TSCs. In addition, it not only discusses the key findings from previous literatures on TSC technology and the implementation of PCM on building envelop but also presented potential points for future research on these field. Therefore, it can be indicated that using TSC technology in building envelope design by an introduction of phase change materials would be a novel approach to offer optimal building envelope design proposing higher building performance, which is potentially beneficial to reduce the building energy consumption and carbon dioxide emission to contribute to solving the future energy supply challenge.

Chapter 3. **Research methodology and mathematical modelling**

3.1 **Introduction**

This chapter demonstrate the research method used to investigate the performance of an innovative building envelope that is made of a transpired solar collector and PCM-gypsum plasterboard as part of the envelope. Also, the basic mathematical equations for this building envelope are established in this section. This research study is conducted through literature review, experimental study and numerical modelling (Figure 3-1).

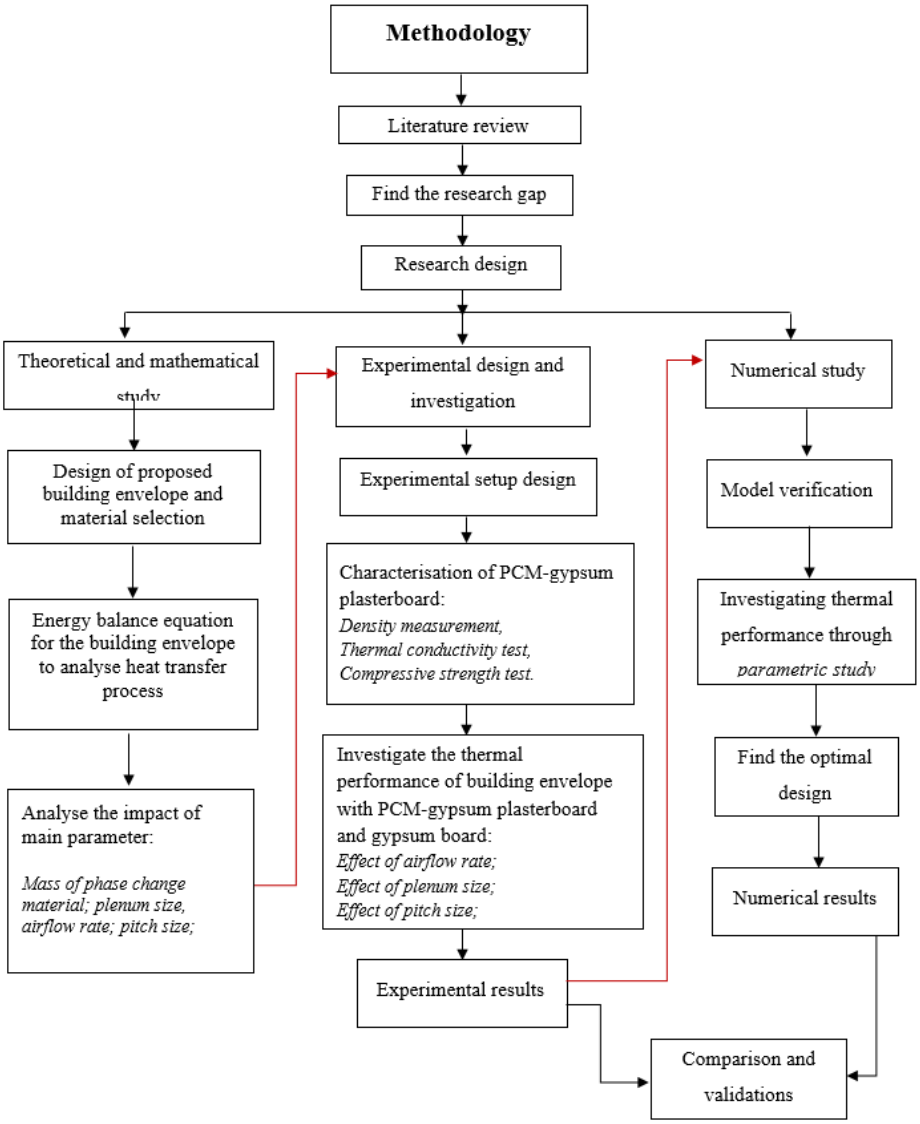

Figure 3-1. Schematics of the research methodology

According to Figure 3-1, the experimental study includes (i) characterisation of PCM enhanced gypsum plasterboard and (ii) investigating the influence of several parameters: the airflow rate, plenum size and pitch dimension on the thermal performance of this innovated building envelope. This chapter presents a detailed analysis of the approaches used to study the performance of the proposed building envelope through in-lab testing and numerical modelling. The chosen research techniques have been presented in more details and justified in the context of the research.

3.2 **Research Approaches**

A research design represents a series of approaches and procedures used to collect data for further analysis in order to address research questions effectively. There are 4 different type of research designs including descriptive, correlational, experimental, review and meta-analytic (Creswell 2014). In this study, the review, experimental and numerical methods are proposed to carry out the research. In the first place, a literature review is a very common method and a crucial tool during the whole research project to review previous research to find conflicting theories or models, to manufacture a research question and catch up on the latest related research done by others (Vogt 2012). Secondly, the experimental research design has been used for many years in research and it is a guided approach for collecting data effectively to match the expectations of an experiment (Tanner 2018). In addition, the experimental approach plays a significant role in science to test theories to establish fundamental concept for scientific knowledge (Franklin, Allan and Perovic 2019). For example, many researchers have used experimental methods to investigate transpired solar collector performance (Cui et al. 2017; Wang et al. 2019; Gao et al. 2020) and the charging/discharging of PCM-gypsum plasterboard (Oliver 2012; Borreguero and Garrido et al. 2014; Serrano et al. 2016). Furthermore, numerical modelling enables a better understanding with less time-

consumption and minimised costs for tackling complicated research problems with greater flexibility (Hussain et al. 2018). Computational fluid dynamics (CFD) has become one of the most common and popular numerical research techniques with the help of the increasing power of computers in physics (Tillman, Duong and Harding 2012). CFD modelling uses numerical methods with the fundamental knowledge of fluid mechanics and algorithms to solve fluid involved problems. Such a research approach has been used widely to study transpired solar collector performance (Li and Karava 2012; Badache et al. 2013; Tajdaran et al. 2016) and the charging/discharging of PCM-gypsum plasterboard (Asimakopoulou, Kolaitis and Founti 2015; Boudali Errebai, Chikh and Derradji 2018). Therefore, this study used experimental and numerical research approaches with the literature review method to complete this research project. Each of the research approaches is discussed below.

3.2.1 *Literature review*

The literature review was carried out at various stages of the research as required by the aim and objectives. The review process ranged from investigations into the basics of the heat transfer mechanism of building envelopes, TSCs and energy storage materials published by other scholars. The main research outcomes were on PCM applications in building envelopes for the past 20 years, especially PCM integration with gypsum over the last decade. The case studies on PCM integration in a building envelope were reviewed. Furthermore, the study on TSC technology was reviewed alongside case studies where TSCs have been implemented in real buildings over the past two decades. Most importantly, the experimental and numerical studies on TSC performance were separately reviewed for the time period between 2000 and 2020 that included the impacts of various parameters on TSC performance. Also, the method used in the experimental and numerical studies of TSCs by previous scholars were reviewed. This provided supportive recommendations for the way this research was done. The

published research outcomes were accessed through journals at the Science Direct website. In all cases, the purpose of the literature review was to focus on the research to ensure the relevance, novelty and validity of the ongoing work to establish and expand the existing knowledge.

3.2.2 *Experimental investigation*

The experimental work was to investigate the in-lab performance of a building envelope that introduced a transpired solar collector and two types of plasterboard: PCM enhanced gypsum plasterboard and gypsum plasterboard. In the first place, the characterisation was conducted on PCM-gypsum plasterboard to analyse the impact of additional PCMs into gypsum plasterboard and to evaluate the advantages of PCM enhanced gypsum plasterboard. Afterwards, once the final PCM-gypsum plasterboard was completed, the impact of several parameters on building envelope performance were studied experimentally. Also, the experimental investigation provided the initial boundary conditions for the numerical study. Hence, the experimental campaign was divided into two main steps which were the characterisation of the PCM-gypsum plasterboard and the investigation of the building envelope's in-lab performance

(i) Fabrication of PCM-gypsum plasterboard

The characterisation of PCM enhanced gypsum plasterboard was a significant step to experimentally investigate the in-lab performance of the newly designed building envelope. PCM-gypsum plasterboard is made by mixing a microencapsulated PCM with multi-finished gypsum. According to previous studies, it can be estimated that the integration of a PCM might change the complex properties of gypsum plasterboard such as density, thermal conductivity and compressive strength. Hence, it was extremely important to test/modify those properties of the developed gypsum plasterboard as the results can vary due to the mass fraction of the mixture compositions and the related

properties of PCMs and gypsum. Therefore, the method adopted during the design characterisation of the building envelope is shown in Figure 3-2.

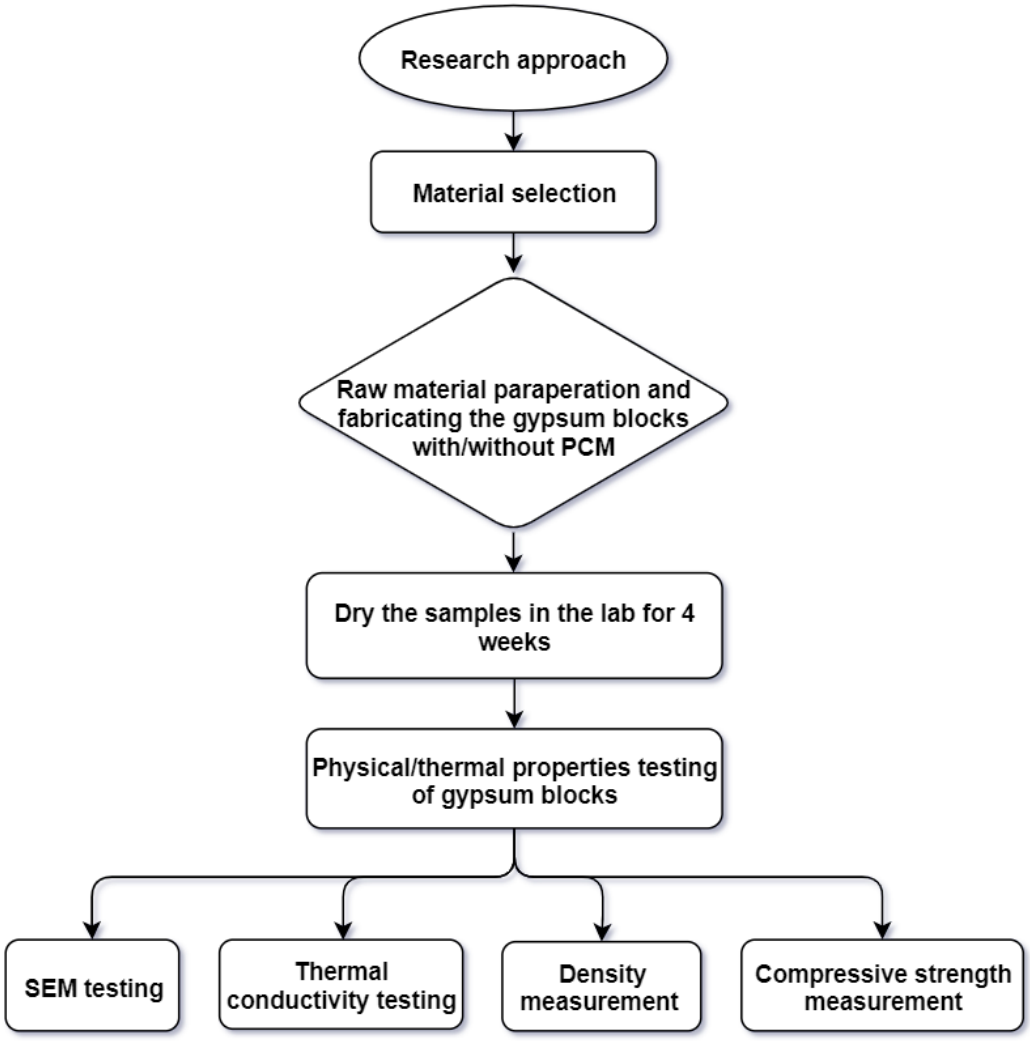

Figure 3-2. Schematic of the research method for characterisation

In order to measure such property changes, this work used 4 different types of samples and each type of sample had at least 4 blocks. These 4 different types were due to the different proportions of additional PCMs. The gypsum blocks were cast and dried for more than 20 days in July 2018 in the indoor environment in the Structural Laboratory at Coventry University. Then, the dried samples were cut into certain sizes which were required for different types of property testing: density, thermal conductivity,

compressive strength and scanning electron microscope (SEM) testing due to the standard EN 13279-2. Hence, the final product of the PCM enhanced gypsum plasterboard was made according to the property testing findings and was applied as part of the proposed building envelope.

(ii) Investigating the in-lab performance of the proposed building envelope

The in-lab performance of the newly designed building envelope was investigated with two different types of plasterboard: PCM-gypsum plasterboard and gypsum plasterboard, respectively. The experimental campaign was to assess the impact of several parameters: the airflow rate, plenum size and pitch size on the thermal performance of the proposed envelope, to analyse the advantages of using PCM-gypsum plasterboard. It was also able to provide the impact of various parameters mentioned above on the system, in terms of air temperature rise, heat exchange effectiveness, collector efficiency and the charging/discharging process of the PCM-gypsum plasterboard. It was therefore beneficial to generate the initial data as the boundary conditions for the numerical study. Hence, each experimental study was divided into different sections based on the different values of each parameter. For instance, the impact of various airflow rates (10, 30, and 50m^3/hr), plenum sizes (140, 200, and 250mm) and pitch sizes (20 and 25 mm) was undertaken on the performance of the innovated building envelope. Hence, this stage of the experimental work was to find out the impact of various parameters on the innovated building envelope performance, including the advantages of using PCM enhanced plasterboard in terms of energy stored. This set of experimental data was used as the boundary conditions for the numerical modelling to validate and evaluate the innovated building envelope's performance.

3.2.3 *Numerical approach*

Numerical modelling, a cost-saving method for any research investigation, does not require any physical apparatus. Numerical modelling is crucial to speed up the investigation process even further. In this research project, numerical modelling was one of the significant approaches to investigating the proposed building envelope performance and it focused on the impact of approach velocity, airflow rate, hole shape/dimension, pitch size, absorber profile material and solar radiation. A numerical approach was used to evaluate and validate the experimental results to find out the optimal design of the innovated building envelope. The melting and solidification of the PCM-gypsum plasterboard were also investigated numerically. Expanding the implementation of the innovated building envelope under the UK's climate was undertaken by simulating various case studies with the numerical approach.

(i) Investigation of the building envelope's performance

In order to examine the performance of the building envelope in order to provide the optimal operational conditions for the innovated building envelope, the numerical investigation was undertaken through ANSYS Fluent Software, using the initial experimental data as boundary conditions. Firstly, the concept of using a numerical approach in terms of equation/method selection, model verification and mesh independence study was studied. Furthermore, the building envelope performance was numerically investigated through studying the impact of the main parameters on the building envelope's performance with/without the PCM gypsum plasterboard. It stated the importance of key parameters for building envelope performance and highlighted the additional benefits of using PCM-gypsum plasterboard compared to the use of gypsum plasterboard.

(ii) Parametric study

In this section, the model was validated through comparing the experimental outcome and the numerical results. Furthermore, the effects of different parameters such as airflow rate/approach velocity, plate temperature, plenum width, hole diameter, pitch size and the thermal conductivity of PCMs on the building envelope and the PCM charging/discharging processes were studied in order to establish an optimal design option to run a case study. Hence, the case study was also included in this section.

3.3 **Mathematical modelling**

3.3.1 ***Introduction***

For this building envelope model, the absorber metal plate was warmed up due to solar energy absorption as total energy input ($Q_{abs,p}$). The air in the plenum was heated up due to convection heat transfer and delivered into the building environment as Q_{out} and the extra/limited amount of thermal energy was stored in the PCM-gypsum plasterboard as Q_{stored} because of the convective heat transfer from the plenum air to the PCM-gypsum plasterboard and the radiation from the back side of corrugated plate. Meanwhile, the net heat losses (Q_{loss}) in the system were caused by convection and radiation from the absorber plate towards the external environment. Hence, the energy flow diagram is explained as shown in Figure 3-3.

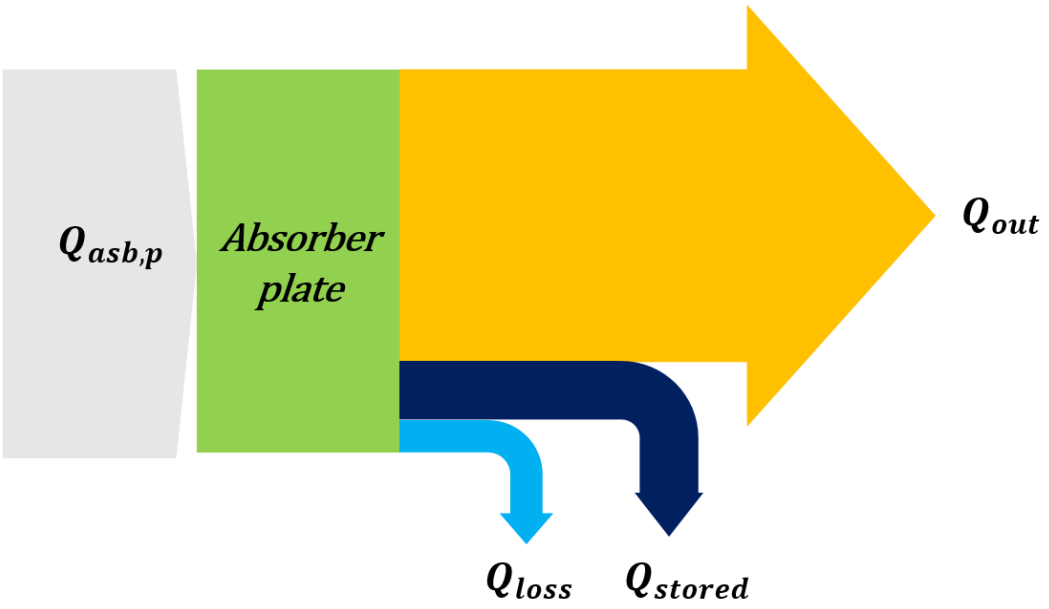

Figure 3-3. Sankey diagrams of Energy flow

The energy balance equations were demonstrated via the calculation of the solar input, mass flux and heat transfer for the corrugated absorber plate, air plenum and PCM enhanced gypsum plasterboard. Figure 3-4 displays the heat transfer mode in this building envelope so that the front surface of the corrugated metal sheet plate received the most percentage of solar radiation as energy input for this building envelope. A little amount of solar irradiation was reflected back to the sky and the surrounding environment because of the greater value of absorptivity (0.95) as the radiative heat loss from the perforated absorber plate could be ignored (Leon and Kumar 2007b; Bokor et al. 2017). In order to reduce the complexity of the mathematical model to deliver easy and simplified calculations, the following assumptions have been made for the present study:

a) The temperature distribution over the perforated plate surface and back wall surface was seen as uniform (isothermal surface) and the metal absorbers were mostly isothermal from hole to hole;

b) The absorber metal plate front and back surface temperatures were assumed to be same. The initial front surface temperature of the plate and the sky temperature of the radiation were considered as the in-lab air temperatures;
c) The suction velocity from the fan was estimated to be equal to the plenum air velocity;
d) There was no radiation and convection heat transfer from the outer surface of the PCM-gypsum plasterboard;
e) The airflow across the perforated holes was assumed homogeneous, while in reality it could be non-homogeneous due to the buoyancy effect or forced flow from the plenum, which depends on whether the buoyancy effect or the forced flow is the dominant factor;
f) The reversal of the flow through the corrugated plate was considered to be insignificant. The flow reversal could happen because of buoyancy and wind effect, when the airflow at the top of the absorber plate was out of the collector rather than within it.
g) The absorber was designed to be grey for all the absorbed and emitted radiation;
h) The heat loss from the plenum edges was generally seen as insignificant for the collector with a larger absorber area.
i) The wind effect on the absorber plate was ignored as the experimental work was investigated under no wind condition;
j) The charging/discharging processes and the heat transfer phenomenon through the PCM-gypsum plasterboard were assumed to be one-dimensional.

3.3.2 *Mathematical equations*

Figure 3-4 presents the heat transfer modes and heat exchanges in the building envelope. The equation of energy balance under steady state for the building envelope with PCM enhanced gypsum plasterboard (PCM-gypsum plasterboard) can be described as follows:

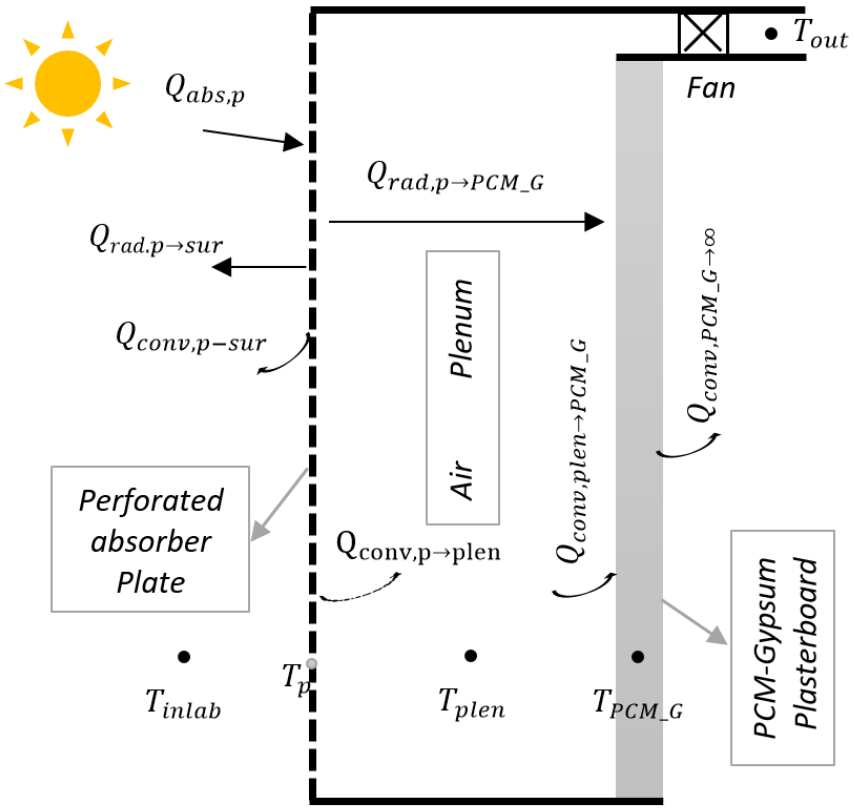

Figure 3-4. Heat transfer scheme of the proposed building envelope for daytime

The thermal heat transfer process and the energy balance equation were analysed in (i) perforated absorber plate, (ii) in the plenum and (iii) in the PCM-gypsum plasterboard (Figure 3-4). Under the suction fan and with no wind (in-lab) conditions, the convective heat loss from the absorber plate ($Q_{conv,p\rightarrow inlab}$) was negligible as the air in the outer surface of the perforated plate could be in the air plenum and it had little impact on heat loss from the absorber plate (Thiele, Sant and Pilon 2015). Hence, the heat loss from

the collector was determined by the consistent radiation to the surroundings ($Q_{rad,p\rightarrow sur}$). The collector's useful energy (Q_u) represents the difference between the absorbed radiation and the radiation losses (Duffie and Beckman 2013).

For the Absorber plate

$$Q_{abs,p} = Q_{rad,p\rightarrow sur} + Q_{conv,p\rightarrow inlab} + Q_{rad,p\rightarrow PCM\_G} + Q_{conv,p\rightarrow plen} \quad (3\text{-}1)$$

$Q_{conv,p\rightarrow plen}$ is the heat gain by the air plenum from the back surface of the corrugated absorber plate and the holes. The term $Q_{rad,p\rightarrow PCM\_G}$ refers to the radiative heat transfer from the absorber plate to the PCM-gypsum plasterboard. $Q_{conv,p\rightarrow inlab}$ gives the convection heat loss from the absorber plate to the ambient air and $Q_{rad.p\rightarrow sur}$ represents the heat loss to the surroundings from the corrugated plate surface by radiation.

$A_s = (1-\sigma)A$ is the surface area of the collector, which is equal to the total absorber surface area (A) minus the area of the holes. The plate porosity (σ) can be measured by (Kutscher, Christensen and Barker 1993)

$$\sigma = 0.907(D/P)^2 \quad (3\text{-}2)$$

The heat gain of the absorber plate is determined by

$$Q_{abs,p} = \propto_p \times I_T \times A_s \quad (3\text{-}3)$$

The heat loss of the collectors can be calculated by

$$Q_{loss} = Q_{rad,p\rightarrow sur} \quad (3\text{-}4)$$

For the Plenum

The plenum air temperature ($T_{air.plen}$) represents the temperature distribution alongside the plenum's height. The plenum air temperature through the air cavity can be negligible, which indicates that the plenum air temperature claims same value as the outlet temperature (Summers, Mitchell, Klein, and Beckman 1996; Safijahanshahi and Salmanzadeh 2019a), hence the energy balance for the plenum:

$$Q_{conv,p\rightarrow plen} = Q_{conv.plen\rightarrow PCM\_G} + \dot{m}_{air}.C_{p.air}(T_{out} - T_{inlab}) \qquad (3\text{-}5)$$

For the PCM-gypsum plasterboard

$$Q_{rad,p\rightarrow PCM\_G} + Q_{conv,plen\rightarrow PCM\_G} = Q_{stored} \qquad (3\text{-}6)$$

Where, Q_{stored} is the amount of energy storage in the PCM-gypsum plasterboard. The heat transfer procedure of the PCM-gypsum plasterboard structure was not easy to calculate as it includes the PCM especially when it is in the phase change period (melting and solidification timeline). In order to make the mathematical calculation straightforward, the PCM-gypsum plasterboard was seen as one single body with different compositions (PCM and multi-finish gypsum) that contained constant and corresponding physical/thermal assets essentially, such as specific heat capacity, latent heat of fusion, thermal expansion, viscosity, melting/freezing temperature and thermal conductivity. Also, the heat transfer process airflow across the CPM-gypsum plasterboard was regarded as one-dimensional and laminar flow. Additionally, for this model, the heat storage during the solidification period of the PCM-gypsum plasterboard was ignored according to the short period of the solar simulator being on. Hence, the energy stored in the PCM-gypsum plasterboard included the sensible energy stored in the gypsum and PCM compositions and the latent heat stored during the PCM's melting period. The Q_{stored} can be decided by calculating the sensible ($Q_{sensible\ heat}$) and latent heat stored ($Q_{latent\ heat}$) in the PCM-gypsum plasterboard via the following equation:

$$Q_{stored} = Q_{sensible\ heat} + Q_{latent\ heat} \quad (3\text{-}7)$$

Where, $Q_{sensible\ heat} = m_{gypsum}.C_{p.gypsum}(T_f - T_{inlab}) + m_{PCM}C_{p.PCM}(T_m - T_{inlab})$ and $Q_{latent\ heat} = m_{PCM}L$, T_f represents the final temperature that the PCM-gypsum plasterboard reaches and T_m gives the melting temperature of the PCM and the latent heat of fusion can be covered by the latent heat of PCM (L) determined by the technical data from the supplier.

3.3.3 *Rate equations*

(i) Convection heat transfer

The convective heat loss can be calculated by using the convection heat transfer coefficient, the surface area for the heat transfer and the temperature variation between the surface and surrounding fluid (Leon and Kumar 2007a). Additionally, it is estimated that a mean value has been introduced for the air velocity in the plenum, since the velocity has various values from zero at the bottom to maximum at the top (Summers, Mitchell and Klein 1996).

a) Absorber plate to inlet environment

The heat loss through the convective heat transfer between the absorber plate and the in-lab ambient air was ignored during this study since the convective boundary layer was continuously sucked off. This study considers 25Pa for the absorber pressure drop that is required to neglect the convective heat loss (Leon and Kumar 2007b) .

b) Absorber plate to plenum air

The convection heat transfer from the back of the absorber plate to the plenum air can be calculated by the following equation:

$$Q_{conv,p\rightarrow plen} = h_{conv,p\rightarrow air.plen} * A_s * (T_p - T_{air.plen}) \quad (3\text{-}8)$$

where the convective heat transfer coefficient between the absorber plate and the plenum can be calculated through the empirical correlation used to estimate the Nusselt number in a study by C.F. Kutscher (1994) and it can be given by

$$h_{conv,p\rightarrow air.plen} = \frac{Nu_1 * K_{air}}{D} \quad (3\text{-}9)$$

where $\mathrm{Nu}_1 = 2.75 * \left(\frac{P}{D}\right)^{-1.21} * Re_1{}^{0.43}$, $\mathrm{Re}_1 = \frac{\rho_{\mathrm{air}} * \upsilon_{\mathrm{hole}} * D}{\mu_{air}}$

c) Plenum air to PCM-gypsum plasterboard

The airflow across the plenum is taken as the laminar flow The Nusselt number for the convection heat transfer between the plenum air and the PCM-gypsum plasterboard is

$$Nu_2 = 0.664 * Re_2{}^{0.5} * Pr_2{}^{0.333} \quad (3\text{-}10)$$

where $\mathrm{Re}_2 = \frac{\rho_{\mathrm{air}} * \upsilon_{\mathrm{hole}} * H}{\mu_{air}}$, $\mathrm{Pr}_2 = \frac{\mathrm{C_{p.air}} * \mu_{air}}{K_{air}}$, and the convective heat transfer coefficient between the plenum air and the PCM-gypsum plasterboard is given by

$$h_{cvonv,air.plen\rightarrow PCM.g} = \frac{Nu_2 * K_{air}}{d_{plen}} \quad (3\text{-}11)$$

The convection heat transfer between the plenum air and the back plate is from

$$Q_{conv.plen\rightarrow PCM\_G} = h_{conv,air.plen\rightarrow PCM.g} * (T_{air.plen} - T_f) \quad (3\text{-}12)$$

(ii) Radiation heat transfer

The heat loss by radiation from the corrugated plate and from the back wall to the outside environment can be calculated using the temperature and emissivity values of the collector modules. It can be estimated using the Stefan-Boltzmann law, including

the total radiating area, the absolute temperature of the radiation body and the Stefan-Boltzmann constant value (σ_{sb}).

a) Absorber plate to the surrounding environment

The radiation heat losses from absorber plate to the surrounding environment happen towards the sky and the ground. The percentage of them is determined by view factors. However, the view factor from the collector to the ground is 0.5 for the transpired solar collector and the surrounding temperature of the in-lab environment is equal to the in-lab ambient temperature. Hence, the radiative heat loss can be defined by the following equation:

$$Q_{rad,p\rightarrow sur} = \varepsilon_p \sigma_{sb} \times A_s \times (T_p^4 - T_{inlab}^4) \qquad (3\text{-}12)$$

b) Absorber plate to the PCM-gypsum plasterboard

The heat transfer by radiation mechanism between the corrugated plate and the back wall can be determined by the next equation (Kutscher 1994; Leon and Kumar 2007b; Bokor et al. 2017):

$$Q_{rad,p\rightarrow PCM\_G} = \sigma_{sb} \times A_s \times (T_p^4 - T_f^4)/(\frac{1}{\varepsilon_p} + \frac{1}{\varepsilon_{PCM.g}} - 1) \qquad (3\text{-}13)$$

The inner surface of the corrugated plate is considered to vary from that of the outer surface, as the front surface of the absorber plate commonly has a coating with a higher absorptivity to receive more solar energy (Leon and Kumar 2007b).

In this study, the thermal performance of the building envelope can be determined in terms of collector efficiency, the air temperature rise and the heat exchange effectiveness (Leon and Kumar 2007b; Wang et al. 2017). Those indicators are able to

fully reflect the gained useful heat, the outlet air temperature and the thermal conversation efficiency of CRBE (Wang et al. 2017).

(i) Useful energy delivered

The collector's useful energy (Q_u) represents the difference between the absorbed radiation and the radiation losses (Duffie and Beckman 2013). With the absorber plate temperature known, the useful energy delivered can be calculated from the following equation:

$$Q_u = \dot{m}_{air} C_{p.air} (T_{out} - T_{inlab}) \quad (3\text{-}14)$$

(ii) Collector efficiency

The collector efficiency is determined as the ratio of valuable thermal energy (heat) delivered as useful energy (Q_u) to the total solar energy received by the corrugated profile. The beneficial thermal energy could increase per unit with the efficiency of the collector. The collector efficiency can be articulated as per Leon and Kumar (2007b) and Wang et al. (2017):

$$\eta = \frac{\dot{m}_{air} C_{p.air} (T_{out} - T_{inlab})}{\propto_p I_T A_s} \quad (3\text{-}15)$$

(iii) Air temperature rise

Higher solar radiation could bring a higher air temperature rise, since the heated air is derived from the outside environment (Tajdaran et al. 2016) and the air temperature can be determined as per Kutscher (1994), Leon and Kumar (2007b) and Bokor et al., (2017):

$$\Delta T = T_{out} - T_{inlab} \quad (3\text{-}16)$$

(iv) Heat exchange effectiveness

Heat exchange effectiveness is based on the overall heat transfer coefficient for the air passing through the absorber plate. It is defined as the ratio of the actual temperature rise of the air as it passes through the absorber to the maximum possible temperature rise (Wang et al. 2017), which is calculated by the following equation (Kutscher 1994; Leon and Kumar 2007b; Bokor et al. 2017):

$$\varepsilon_{HX} = \frac{T_{air.pelnum} - T_{inlab}}{T_p - T_{inlab}} \qquad (3\text{-}17)$$

Heat exchange effectiveness ε_{HX} between the absorber and plenum air can be estimated using the relationship based on the logarithmic mean temperature difference (LMTD) applied for heat exchangers (Kutscher 1994):

$$\varepsilon_{HX} = 1 - exp\left[-\frac{h_{conv,p\rightarrow air} * A_s}{\dot{m}_{air} C_{p.air}}\right] \qquad (3\text{-}18)$$

These two expressions provide a relation between the exit air temperature, the absorber temperature and the ambient temperature.

(v) Pressure drop

Total pressure drop across the collector (ΔP) is the sum of the pressure drop across the absorber plate (ΔP_p), and pressure drops in the plenum, which include the frictional pressure drop (ΔP_{fric}), buoyancy pressure drop (ΔP_{buoy}) and acceleration pressure drop (ΔP_{acc}) (Kutscher 1994; Leon and Kumar 2007b). The buoyancy force tends to push the plenum air up, acting in the direction opposite to that of frictional force.

$$\Delta P = \Delta P_p + \Delta P_{fric} + \Delta P_{buoy} + \Delta P_{acc} \qquad (3\text{-}19)$$

Leon and Kumar (2007) demonstrated that the pressure drop across the absorber plate must be at least 25 Pa to ensure a uniform flow and temperature distribution over the

collector. If the temperature distribution is not uniform, hot spots can develop on the collector's surface, which will increase the radiation loss to the surroundings.

3.3.4 *Data and solution procedure*

The energy balance and rate equations described above were solved to find the outlet air temperature, heat exchange effectiveness, collector efficiency, useful energy delivered and the heat stored in the PCM-gypsum plasterboard, for a given set of input values and for a given time period. The intermediate values included the estimation of the heat transfer coefficients and the heat flux between this transpired solar collector's (TSC) components. For the subsequent times, the initial temperatures were specified equal to the temperature values of the respective previous sections. The iterative process was continued until the end time was reached. As an initial condition, the absorber plate, back plate and plenum air were all assumed to be at an ambient temperature.

According to previous studies (Van Decker, Hollands and Brunger 2001; Frank et al. 2005; Wang, Shukla and Liu 2017), the key parameters affecting TSC performance include perforation diameter, pitch size, plenum width, airflow rate/approach velocity and solar radiation. A parametric analysis through mathematical modelling using Matlab was conducted for a range of perforation diameter–pitch combinations, plenum sizes and airflow rates. A circular hole (1mm diameter) with a square pitch was assumed for the absorber perforations. The input parameters considered for the analysis were (a) approach velocity, (b) plenum size and (c) pitch dimension. Several key parameters with their relative ranges were selected for this study, as below.

a) Approach velocity

According to the approach velocity analysis in previous studies, it was recommended that below an approach velocity of 0.02m/s, the transpired solar collector's performance might be worse than the theoretical outcome due to natural convection effects or non-

homogeneous suction. This, however, does not apply to all cases. For instance, the range of approach velocity has been increased from 0.0125m/s to 0.0375m/s. However, for this study, an approach velocity range of 0.01-0.1m/s was applied.

b) Solar radiation

A solar radiation of 600W/m^2 was used for this mathematical analysis, which is considerably relative to the daily average solar radiation in the UK.

c) Collector plenum depth

The frictional pressure drop across the collector was estimated using the model over a plenum with a certain range of 120-300mm according to previous researches, in order to maintain the minimum friction pressure drop. Hence, in this analysis, a plenum width range of 150-250mm was selected.

d) Pitch size and hole dimension

Considering the past studies on pitch size and hole dimensions (Kutscher 1994; Leon and Kumar 2007b; Wang, Kuckelkorn and Liu 2017), a pitch range of 20-25mm with a perforation hole diameter of 1mm was selected for this present study. A lower size of pitch with relatively very small holes could be challenging to manufacture. It was indicated that a lower collector efficiency and heat exchange effectiveness can by caused by a lower value of pitch.

Table 3-1. Summary of the input parameters and their values selected in this study

Parameters	Range
Inlet (ambient) temperature	18°C
Approach velocity (m/s)	0.01-0.1
Solar irradiation (W/m^2)	600-1000

Pressure drop across the collector (Pa)	Over 25
Perforation diameter (mm)	1
Pitch size (mm)	20-25
Plenum width (mm)	150-250
Absorber plate area (m^2)	1
Absorber material	Stainless steel
Absorber plate colour	Black
Absorptivity	0.95
Emissivity	0.85
Pitch size (mm)	20
Plenum size (mm)	150

The collector's performance was analysed in terms of outlet temperature, air temperature rise, collector efficiency, heat exchange effectiveness, useful energy delivered and heat stored in the PMC-gypsum plasterboard. The impacts of various input parameters were also examined. Hence, the mathematical simulation for TSC performance was investigated for several combinations of pitch and perforation diameter, plenum size and various approach velocities within the selected value of solar radiation. Table 3-1 summarises the input parameters with their relative values and the results are discussed in the following part.

3.3.5 ***Results and analysis***

To study the impact of each parameter (approach velocity, pitch size and plenum size) on TSC performance, each parameter was different while keeping the others constant. This part also illustrates the results of the mathematical modelling analysis.

(i) Effect of approach velocity

The impact of approach velocity on the building envelope's performance was studied through mathematical modelling. For the given collector's operational conditions, any increase of airflow rate leading to a sensible increasing proportion in the approach velocity was due to the linear relationship between airflow rate and approach velocity. The collector efficiency rises as the approach velocity increases. For instance, the collector efficiency achieved 44.5 and 65.5% respectively for an approach velocity of 0.01 and 0.1m/s (Figure 3-5). For such a period of approach velocity, this collector efficiency increased dramatically. These results matched with previous research studies (Kutscher. et al. 1993; Leon and Kumar 2007). Thus, increasing the approach velocity improves the collector efficiency as the higher approach velocity tends to operate the collector at lower temperature levels, which could minimise the overall heat loss from this collector. Furthermore, the impacts of approach velocity on collector heat exchange effectiveness (HEE) are explained in Figure 3-5.

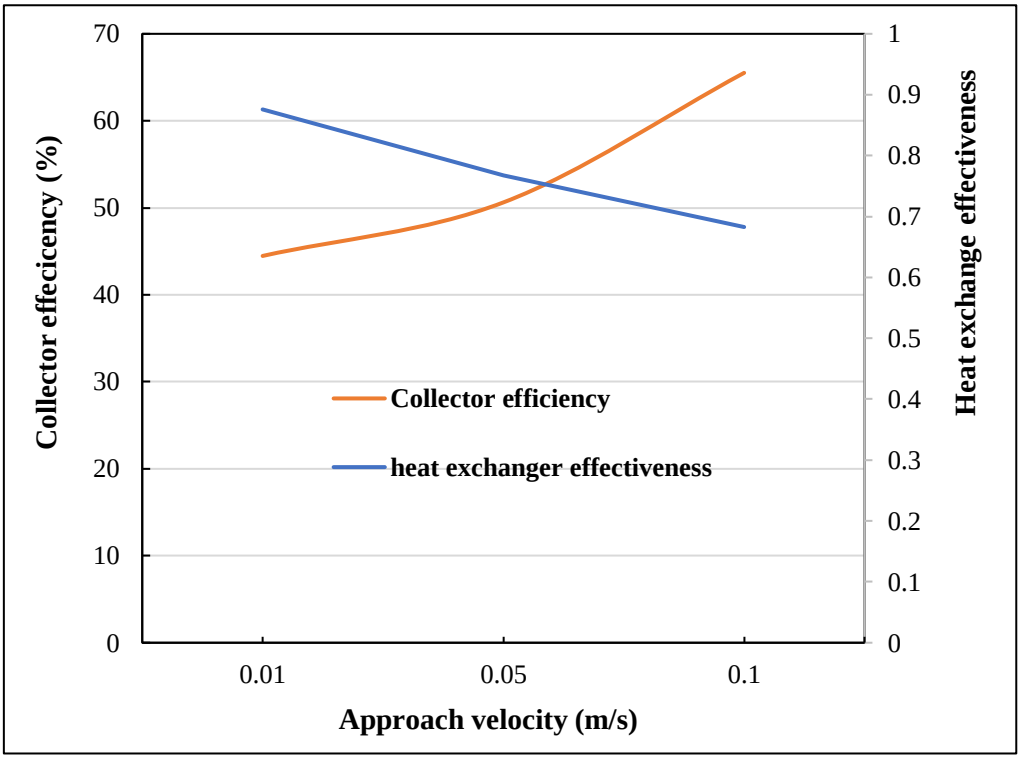

Figure 3-5. Effect of approach velocity on collector efficiency and heat exchange effectiveness

According to Figure 3-5, the heat exchange effectiveness drops with the growing approach velocity for these given collector geometry and operational conditions. Figure 3-5 shows the correlation between the approach velocity and heat exchange effectiveness for an absorber plate with 1.0mm perforations, at 20mm square pitch and 150mm plenum. The increasing range of approach velocity from 0.01 to 0.1m/s resulted in a corresponding decline in effectiveness of 22%. Such changes can indicate that approach velocity impacts significantly on collector heat exchange effectiveness.

(ii) Effect of plenum width

The influence of plenum width on collector efficiency and heat exchange effectiveness was mathematically studied and the results are presented respectively in Figure 3-6. A study demonstrated that collector efficiency decreases with an increasing plenum size

(Rad and Ameri 2016). In this mathematical simulation, **Error! Reference source not found.** shows that by increasing the plenum width from 100 to 300mm, the collector efficiency witnessed a rough 10% drop under a moderately higher approach velocity operation (0.05 and 0.1m/s). Besides, the changes in plenum size are kept relatively unchanged at a lower airflow rate operation like an approach velocity of 0.01m/s. Also, the influence of plenum size on collector heat exchange effectiveness is described in **Error! Reference source not found.**.

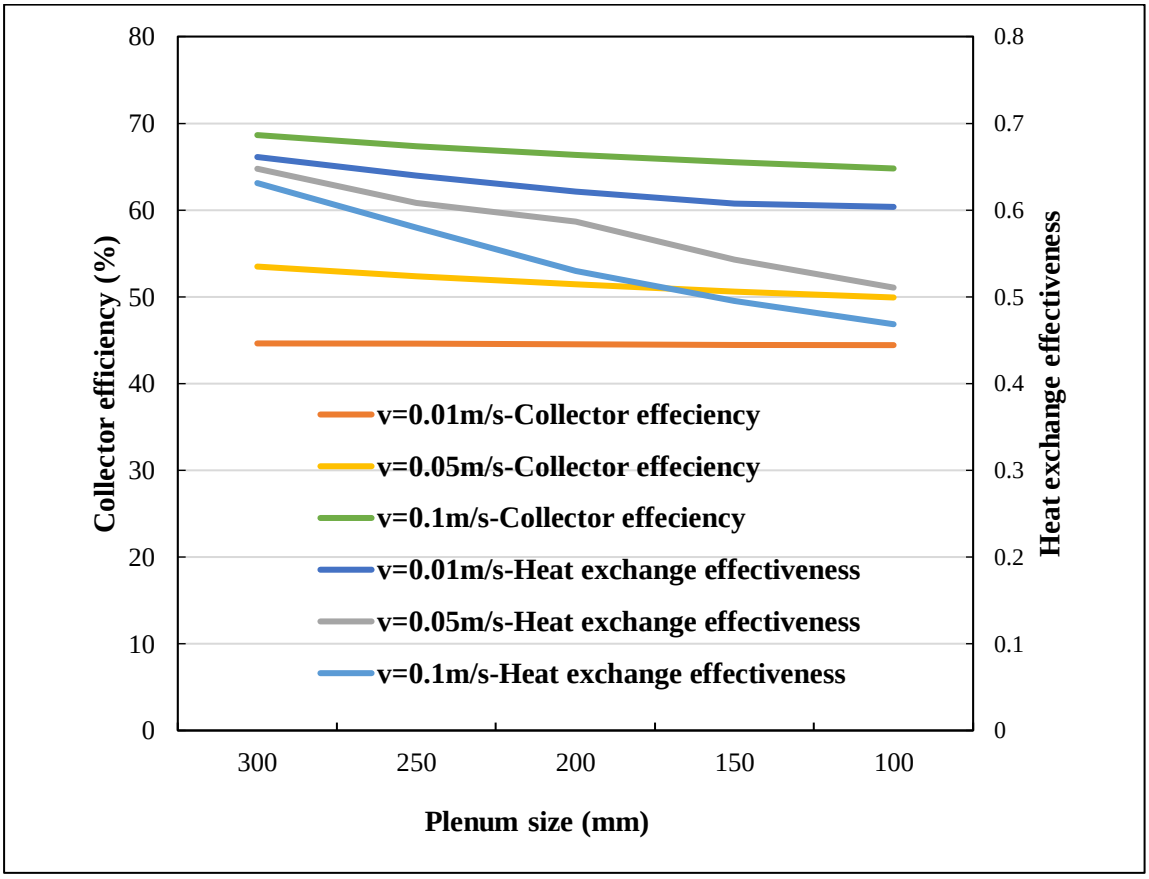

Figure 3-6. Effect of Plenum size on collector efficiency and collector heat exchange effectiveness under various approach velocities (v)

According to Figure 3-6, it can easily be seen that the increasing trend of plenum size enables the collector heat exchange effectiveness to improve. However, the impact of plenum size on collector heat exchange effectiveness varies due to different approach velocities. At a lower airflow rate, the collector heat exchange effectiveness is

insignificantly affected by changes in the plenum size. However, the impact of plenum size on HEE seems moderate under medium and higher approach velocity operations. For example, a plenum width increasing from 100mm to 300mm and an approach velocity from 0.05 and 0.1m/s, separately, will see a change in HEE of over 20%.

(iii) Effect of pitch size

The impact of pitch size on collector efficiency and heat exchange effectiveness are studied through a mathematical approach. It presents the relationship between pitch size and collector efficiency and heat exchange effectiveness for an absorber plate with 1.0mm perforations, with a150mm plenum and under various approach velocities. Figure 3-7 demonstrates the impact of pitch and approach velocity on collector efficiency. Increasing the pitch achieved minimal increase on collector efficiency for a constant airflow rate. For example, an increasing range of pitch size from 10 to 30mm (for an approach velocity of 0.1m/s) results in a roughly 5% decrease in collector efficiency.

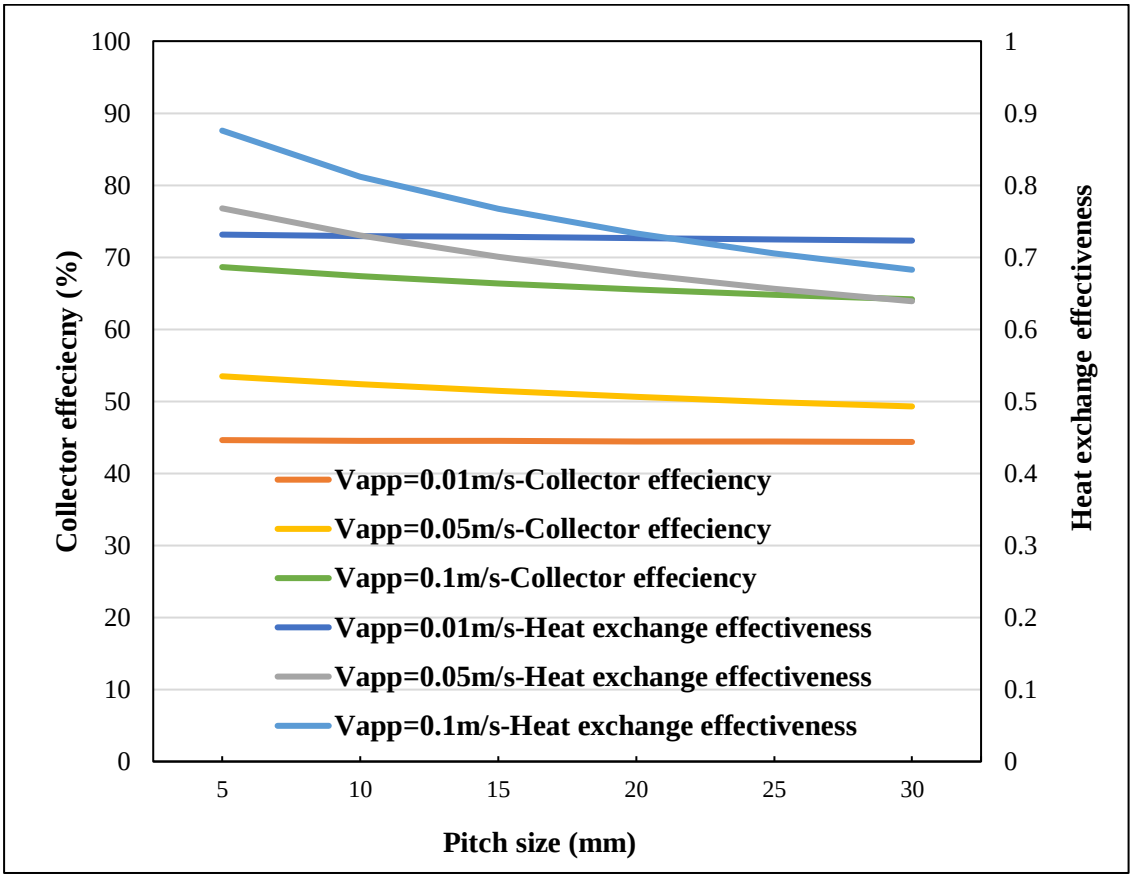

Figure 3-7. Effect of pitch size on collector efficiency and heat exchange effectiveness

In terms of heat exchange effectiveness, Figure 3-7 shows that a higher plenum size can achieve a higher collector heat exchange effectiveness. For instance, for an approach velocity of 0.1m/s, increasing the range of pitch size from 10 to 30mm achieved an approximate 20% drops in HEE. However, for lower approach velocity (0.01m/s) operations, the influence of pitch dimension is marginal and can be ignored.

3.4 **Conclusions**

This section described the mathematical modelling results through analysing the impact of key parameters on collector efficiency and heat exchange effectiveness. A model using heat energy balance and rate equations for a transpired solar collector has been established to estimate its thermal performance in terms of key design and operational

conditions. The observations indicated that the approach velocity significantly impacted on collector efficiency and heat exchange effectiveness. The effect of plenum size on collector efficiency and heat exchange effectiveness seemed moderate. The influence of pitch dimension on collector efficiency was marginal but its impact on collector heat exchange effectiveness was considered moderate.

This section also predicted the benefits of using PCM-gypsum plasterboard to store lesser amounts of energy for later use according to equation (3-7). It also indicated that the impact of approach velocity on how much energy is stored is crucial, as a higher approach velocity enables a higher heat transfer coefficient so that the PCM-gypsum plasterboard can store energy in sensible and latent versions due to the additional function of the PCM. It stored 20% of energy from the plenum, which was achieved by the above parameter ranges due to equation (3-7). Hence, it is believed that up to 15% of PCM is required for use in PCM-gypsum plasterboard and the experimental study was undertaken according to the above observations from the mathematical modelling study.

Chapter 4. **Experimental design of the building envelope components**

4.1 Introduction

This chapter presents a detailed clarification about material selection, the fabrication of the plasterboard, the characterisation of approach/procedure and the testing instruments for the design characterisations of the building envelope, including (i) the structural design of the building envelope and (ii) the characterisation of PCM-gypsum plasterboard. Four type of testing were completed, namely Scanning Electron Microscopy (SEM) analysis, thermal conductivity testing, density measurement and compressive strength. The possible benefits of the proposed building envelope are demonstrated compared to the traditional building wall design. Furthermore, the characterisation procedures with the results are explained and discussed in this part. The finalised PCM-gypsum plasterboard for this research study is also delivered.

4.2 Laboratory fabrication of the proposed PCM gypsum plasterboard integrated TSC envelope

The design of the building envelope has a crucial impact on building energy consumption as the majority of heat loss happens across a building's wall (Hachem-Vermette 2018). Therefore, transpired solar collectors have been popularly used as part of building envelope design (Sadineni, Madala and Boehm 2011). This research study intends to present an innovative building envelope by introducing a transpired solar collector (TSC) and PCM-gypsum plasterboard (Figure 4-1). In this proposed building envelope, the absorber plate is used with perforated corrugate metal plate to create the TSC. The advantages of this newly-designed building envelope compared to the traditional building envelope are (i) the building's fabric thickness decreases so that the building envelope becomes cost-effective; (ii) it would dramatically increase the building envelope's energy performance and reduce energy costs due to the benefits of the TSC that would deliver pre-heated air into the built environment using only free solar radiation; (iii) the PCM enhanced gypsum plasterboard can not only store the extra

heat from the air cavity for later use when the solar radiation is not fully available, but also captures heat loss from inside the building to the outside environment due to the addition of a PCM (Sozer 2010; Shukla et al. 2012; Wang, Shukla and Liu 2017). In this study, the PCM-gypsum plasterboard was made by mixing multi-finished gypsum and microencapsulated PCM homogeneously. Figure 4-1 shows the structural design of a traditional building envelope with this proposed building envelope.

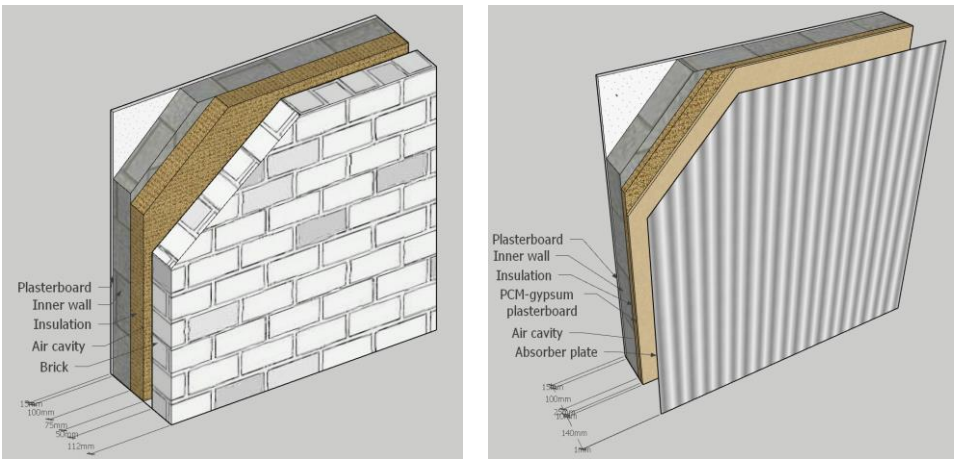

(a) (b)

Figure 4-1. Schematics of (a) traditional wall and (b) proposed building envelope

Furthermore, there are some advantages of this newly proposed building envelope compared to the traditional cavity wall due to the addition of PCM-gypsum plasterboard. In the first place, the thickness of the proposed building envelope is smaller (291mm) than the cavity wall (352mm). It increases the thermal mass and reduces the thermal conductivity due to the lower thermal conductivity of the PCM. Secondly, it enables the capture and storage of the additional heat from the plenum for later use when there is not enough solar radiation. In addition, the proposed envelope can recapture heat loss throughout the building's wall to the air plenum. It can also prevent overheating problems during the hot summertime. Furthermore, this proposed building envelope would have a night cooling feature that would keep the building's

inside temperature constant before occupancy on the next working day. Therefore, the addition of PCM-gypsum plasterboard is the unique and crucially important part of this novel-designed building envelope. It is generally believed that the addition of a PCM would change the properties of gypsum plasterboard. Therefore, it is significantly important to measure the physical/thermal properties of PCM-gypsum plasterboard through characterisation. Therefore, the proposed building envelope includes TSC design (the absorber plate in particular) and the characterisations of PCM-gypsum plasterboard.

4.3 **Fabrication of TSC in the laboratory**

In a building envelope, the transpired solar collector, especially the absorber plate, is as crucial as it absorbs the simulated solar radiation and the preheating of the crossing air due to the absorber plate's higher temperature. A profile is normally made of the metal plate with equally distributed perforations and selective layers for absorbing the solar radiation. The perforated sheet is fixed at around 10-30cm from the south-facing façade and the perforating design ranges from 0.5% to 2% of the whole absorber surface area (Dymond and Kutscher 1997). The air cavity or plenum is equal to the space between the plate profile and the structural wall of the building. Hence, the absorber plate uses a perforate metal profile made with stainless steel, as shown in Figure 4-2.

Figure 4-2. Perforated absorber plate

According to Figure 4-2, a perforated corrugated absorber profile is used as an absorber plate and the 1mm dimension holes with 20 and 25mm pitch sizes were made by an automotive machine in Coventry University's laboratory. According to the technical data from the supplier, the thermal conductivity of such an absorber profile is $16.2W/mK$ and the thermal absorptivity and emissivity are 0.95 and 0.85 respectively. It can indicate that such a higher thermal absorptivity and emissivity ensures the simulated solar radiation is absorbed efficiently. This absorber profile is attached with various distances such as 140mm, 200mm and 250mm to create the air plenum. The back wall uses the PCM-gypsum plasterboard which captures and stores some extra energy from the plenum due to the additional function of the PCM. It is difficult to measure and test how much energy can be stored through this approach. Meanwhile, characterisation of the PCM-gypsum plasterboard is essential.

4.4 **Fabrication of plasterboard in the laboratory**

4.4.1 ***Material selections***

In fabricating the PCM-gypsum plasterboard, multi-finished gypsum was used due to some benefits such as low costs and the common/convenient usage for making gypsum plasters. Microencapsulated PCM was used for this research due to the fact that this PCM had been effectively implemented in building envelopes (Akeiber et al. 2016b; Souayfane, Fardoun and Biwole 2016). However, the heat transfer ability, specific heat capacity, energy storage capacity and stability are important aspects to decide on during the selection of the PCM (Akeiber et al. 2016b). Taking account of the benefits of microencapsulated pure-paraffin PCM (Section 2.3.1), a microencapsulated pure-paraffin powder (MICRONAL® DS 5040X) was selected for making the PCM enhanced gypsum plasterboard.

The MICRONAL® DS 5040X PCM product is microencapsulated with a highly cross-linked polymethacrylate polymer wall, which provides a secure containment system for the high-purity paraffin dry powder. Such a PCM can be directly used with building materials: conventional plasters, plasterboard, floor screeds, wood and concrete, due to the manufacturer's data. The easiest way to combine Micronal PCM is to pre-mix it with the building materials. It is suggested to add PCMs to gypsum-based systems by up to ~30% v/v according to the technical data. The properties are shown in Table 4-1.

Table 4-1. Properties of the mixtures for casting the plasterboard

Mixture	Density (kg/m^3)	Melting temperature (°C)	Thermal conductivity (W/mK)	Heat of fusion (kJ/kg)
Multi-finished gypsum	1250	-	0.19	-

Micronal DS 5040X PCM	300-400	23 ± 1	0.079	⩾ 95
Water	997	0	-	340

Due to the manufacturing information (table 4-2), the particle size of the Micronal PCM ranges from 50 to 300μm. The peaking temperature was 23 ± 1℃ for the fusion process and 22 ± 1℃ for the crystallisation process. Besides, the latent heat storage capacity of this Micronal encapsulated PCM was 95kJ/kg.

4.4.2 *Testing components preparation*

Samples were made due to the different percentages of the additional PCM. Thistle multi-finish plaster and water were mixed homogenously. The concentration of microencapsulated PCM was designed to be lower than 30% in order to secure the mechanical properties and fire resistance features of the final product (Jaworski and Abeid 2011). In this research, the fabrication process of the plasterboard was followed as shown in Figure 4-3. Each type of plaster was made through this process. There were 4 different types, namely (i) gypsum board, (ii) gypsum board with 5% PCM, (iii) gypsum board with 10% PCM, and (iv) gypsum plasterboard with 15% PCM (Table 4-2).

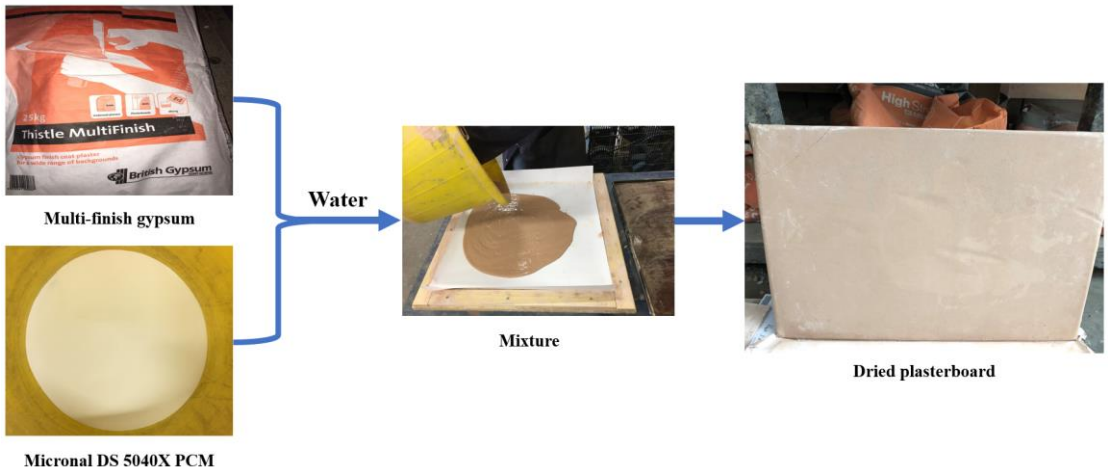

Figure 4-3. Fabrication process of plasterboard in the lab

Table 4-2. Various types of testing component samples

Sample type	Abbreviation	Gypsum (v/v%)	PCM (v/v%)	Water (v/v%)
Gypsum plasterboard	A	50	0	50
PCM-enhanced gypsum plasterboards	B1	45	5	50
	B2	40	10	50
	B3	35	15	50

According to Figure 4-3, the raw materials were mixed uniformly before being poured into a wooden mould having a size of $400 \times 400 \times 10mm$. The moisture of the material can significantly affect the thermal conductivity and the samples were dried for about 28 days after casting according to the provisions of IS EN 1290-2. It was also known that the moisture content of the samples was not more than 4%. The different types of plasterboard samples mentioned in Table 4-2 were made separately following the process shown in Figure 4-3. Afterwards, the dried samples were used for various measurements in order to characterise their physical and thermal properties. These measurement were thermal conductivity testing, density measurement, compressive strength testing and SEM testing.

4.5 **Property measurements of PCM-gypsum plasterboard**

It is important to characterise the PCM-gypsum plasterboard, because the addition of PCMs might change the physical/thermal properties of the plasterboard. Hence, four different measurements were carried out, namely Scanning Electron Microscopy (SEM) analysis, thermal conductivity testing, density measurement and compressive strength. Such measurements also enabled the additional benefits of adding PCMs into

gypsum plasterboard fabrication to be highlighted. During the measuring of each property, each type of plasterboard had at least 3 samples and each testing was performed more than 3 times. Furthermore, the results were displayed with a 98% confidence interval and were compared with the standards for gypsum plasterboard manufacturing.

4.5.1 *SEM analysis*

The scanning electron microscope (SEM) is an electron microscope that scans a surface using a focused electron beam and then produces an image containing information about the surface topography and its chemical composition (Han, Jiao and Fox 2018). In order to examine the distribution of each composition inside the final PCM incorporated gypsum plasterboard, the samples were tested using secondary electron (SE) in a Zeiss Gemini Sigma 500VP scanning electron microscope (SEM) and Energy-dispersive X-ray spectroscopy (EDS) at Coventry University, UK (Figure 4-4). EDS is an analytical technique to determine the elemental compositions or chemical characterisations of a material (Mehrban and Bowen 2017).

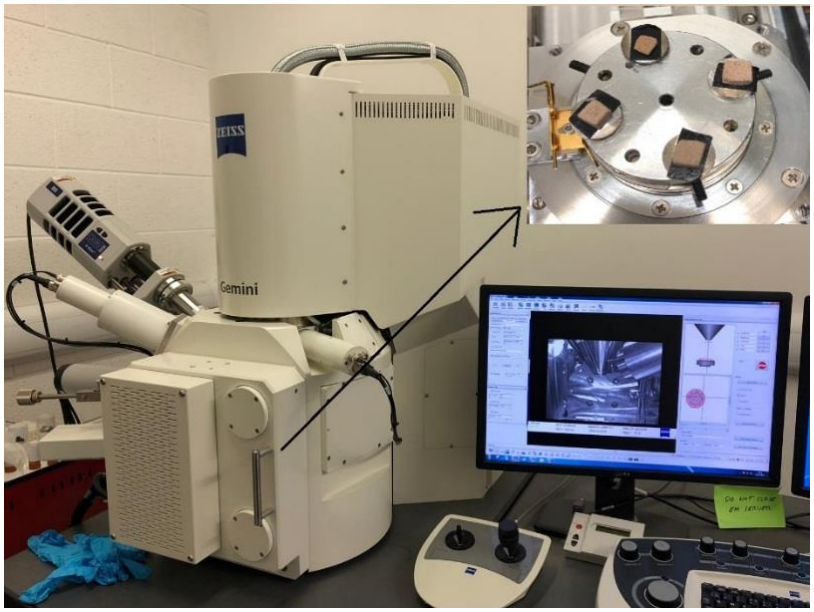

Figure 4-4. Schematic of the SEM instrument at Coventry University

According to Figure 4-4, four samples with dimensions of 2×2×1mm (height, width, thickness) from PCM-gypsum plasterboard and gypsum plasterboard separately were tested through the SEM device and the average results of the four samples were presented. The samples did not require a coating method to be electrically conductive due to their tight thickness.

4.5.2 *Thermal conductivity test*

Thermal conductivity is a pure and basic material property that affects the thermal performance of a material. The addition of a PCM changes the thermal conductivity of the PCM enhanced gypsum plasterboard, so it is significantly important to undertake thermal conductivity testing. The guarded hot plate method through the FOX 314 Heat Flow Meter (HFM) was used to run the steady-state thermal conductivity of the specimens (Figure 4-5). During this testing, a sample with a size of $200 \times 200 \times 10mm$ was placed between two different states of hot and cold plates where the heat flowed in a steady form through the sample square's cross-section and the temperature differences between two surfaces were recorded. One of the upper or lower plates was powered by stepper motors positioned at each corner and another was touched with the sample. Each testing procedure followed the default setting of the HEM (35 °C and 10 °C as hot and cold plate temperatures, respectively) and operated roughly for 1-2 hours. The operating hour varied for the different types of samples. Following equation (4-1), the testing device gave the thermal conductivity result for each sample at the end, when the testing finished automatically. The instrument setting followed the European regulations on thermal conductivity measurements.

$$k = \frac{U \cdot I \cdot L}{a \cdot b \cdot (T_h - T_c)} \qquad (4\text{-}1)$$

where U and I are the voltage and current supply of the electric heater; L refers to the thickness of a sample; a and b are the lengths of sides of a sample; T_h and T_c define the temperatures of the electric heater (hot plate) and the cold plate, respectively.

Figure 4-5. Schematics of the FOX 314 Heat Flow Meter instrument

4.5.3 *Density measurement*

The density was determined by separating the total weight of each ingredient by volume. The specimen's dry weight was tested first before putting it into the water container for measuring the wet weight of the samples under normal laboratory conditions. The samples were placed in a sealed water container and the growth in water height represented the volume of the plasterboard without any voids or moisture (Figure 4-6). Lastly, the density of the gypsum plasterboard was calculated by the equation below (4-2):

$$The\ density\ of\ sample = \frac{Dry\ weight \times Density\ of\ water}{Dry\ weight - Wet\ weight} \qquad (4\text{-}2)$$

Figure 4-6. Schematic of the density testing device

4.5.4 *Compressive strength check*

Compressive strength is the ability of a gypsum board to withstand a load tending to reduce its size. It is usually experimentally determined by a compressive strength test. It determines how the gypsum board reacts when compressed, crushed, crushed or flattened to assess its strength. This also helps us to ensure that the newly designed gypsum board is of a high quality. Hence, the compression strength of the PCM reinforced gypsum plasterboard was tested by the “Cube Crushing” Compression testing Machine in Coventry University’s Structural laboratory (Figure 4-7).

Figure 4-7. Schematic of the "Cube Crushing" Compression Testing Machine

During the test, the test load was applied at a uniform rate of 1N/mm^{2}s and the load rate was added automatically until the plasterboard changed its size. During this process, the applied load was also recorded by a computer. Therefore, the test procedure was repeated for the samples of different phase change materials. The compressive strength (σ) of each sample was automatically calculated and displayed by a computer following equation (4-3), which was then compared with the European Standard EN 13279-2: 2004.

$$\sigma_e = \frac{F}{A_o} \qquad (4\text{-}3)$$

Where F = Load applied$[N]$, A_o = original specimen area $[m^2]$

4.6 **Characterisation results and discussion**

According to the characterisation procedure mentioned above, the thermal/physical properties of the samples were carried out in terms of thermal conductivity, SEM, density and compressive strength measurements. During each property testing, each type of sample had at least 3 pieces with same combination ratio of gypsum and PCM and each sample was tested more than three times. Such a process enabled the reduction of the measurement uncertainty and increased the accuracy and credibility of the measurement data. Such a testing approach assures that the data used for further analysis and discussion in this study are reliable, with higher credibility.

4.6.1 ***SEM analysis***

The SEM/EDS instrument was used for the SEM analysis of two samples: (i) gypsum plasterboard and (ii) gypsum plasterboard with MICRONAL® DS 5040X PCM powder. The results are shown in Figure 4-8.

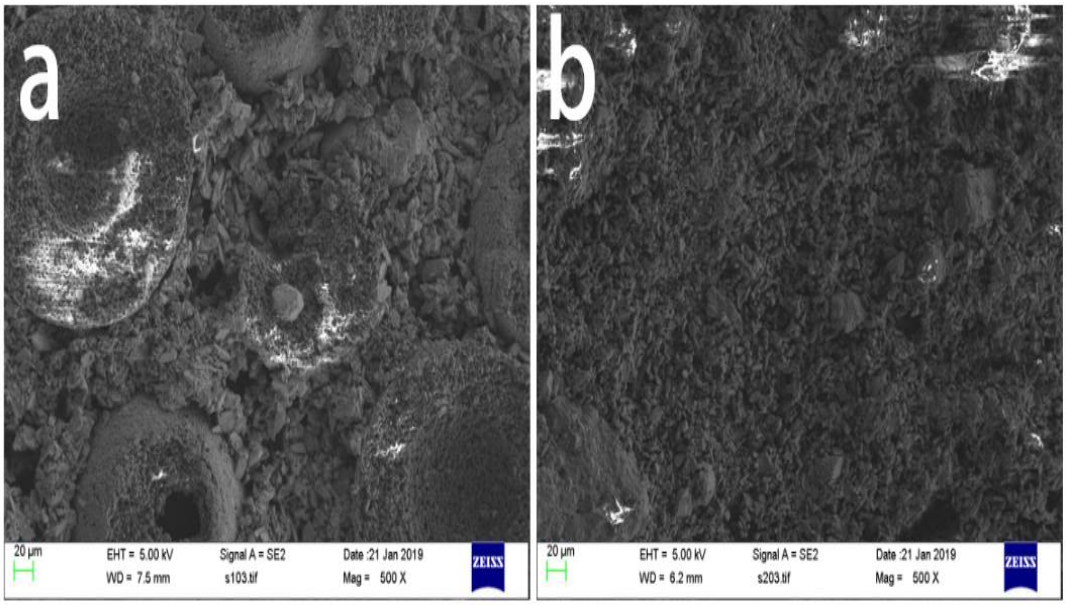

Figure 4-8. SEM image of (a) gypsum plasterboard with 15% PCM and (b) gypsum plasterboard

Figure 4-8 shows the formation of highly interlocking acicular gypsum crystals during the hydration of the hemihydrate. These needles exhibit at a typical µm size, so it is expected that particles of a similar size will have a large effect on the gypsum's properties. However, in Figure 4-8a, there were needle shapes of a component and several spherical shapes of apparatuses. It can be estimated that the diameter of the capsules is in the range of the ideal size of microencapsulated MICRONAL® DS 5040X PCM powder (Anderson Materials Evaluation no date; Salunkhe and Shembekar 2012).

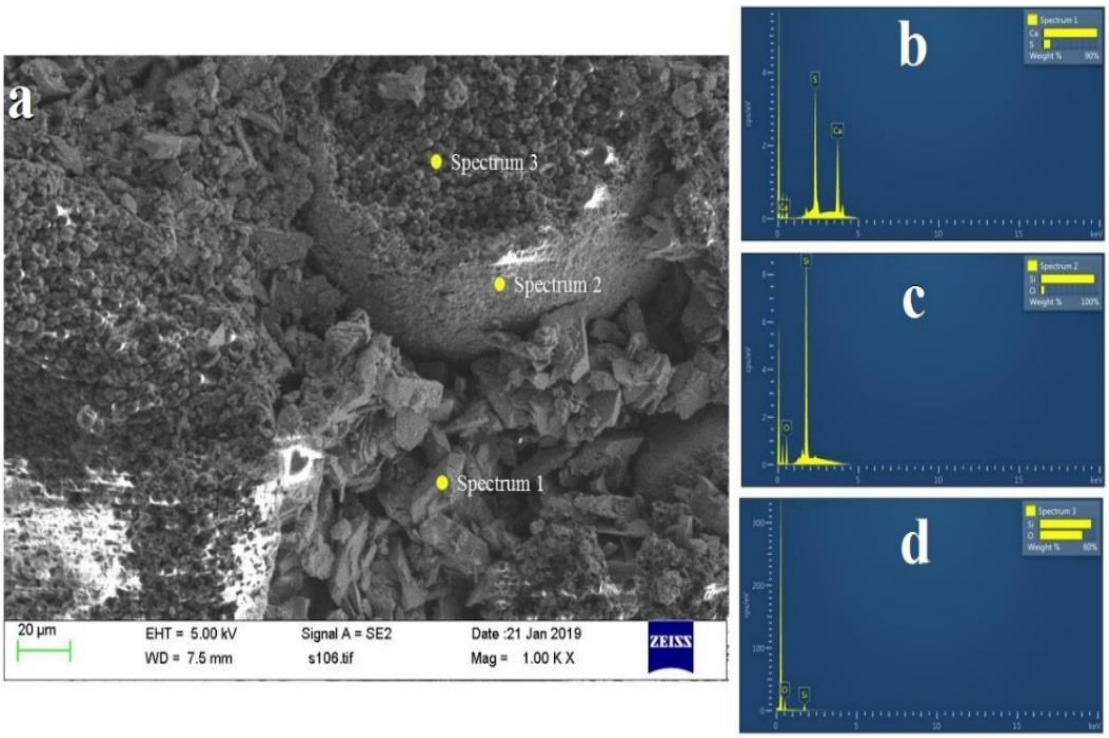

Figure 4-9. SEM micrographs of (a) surface analysis of gypsum plasterboard enhanced PCM and (b, c, d) corresponding EDS analysis of yellow spectrums in (1, 2, 3)

Figure 4-9 shows the surface analysis of the dried PCM enhanced gypsum plasterboard and the EDS analysis of three different spectra. The EDS analysis indicated that there were different major compositions separately at three spectrum points in Figure 4-9a. In return, it could represent various chemical compositions. For instance, the silica shell at spectrum point 1 displayed Calcium (Ca). Sulphur (S) represents the chemical formula of gypsum that can be seen in Figure 4-9b. Meanwhile, silicon (Si) and oxygen (O) demonstrated more at the point of spectrum 3 (Figure 4-9d). Spectrum point 3 showed more of the chemical composition of O and then Si, as the core of MICRONAL® DS 5040X PCM powder has SiO_2 (Borreguero, Serrano et al. 2014). Hence, the results of the SEM imaging and EDS analysis of the PCM-enhanced gypsum plasterboard sample can be valid due to the previous knowledge/formula of the encapsulation process (Lin et al. 2018; Huang et al. 2019).

4.6.2 *Compressive strength test*

This was investigated to check if the compressive strength of the gypsum component integrated with microencapsulated PCM could satisfy the mechanical regulations of the European Standard.

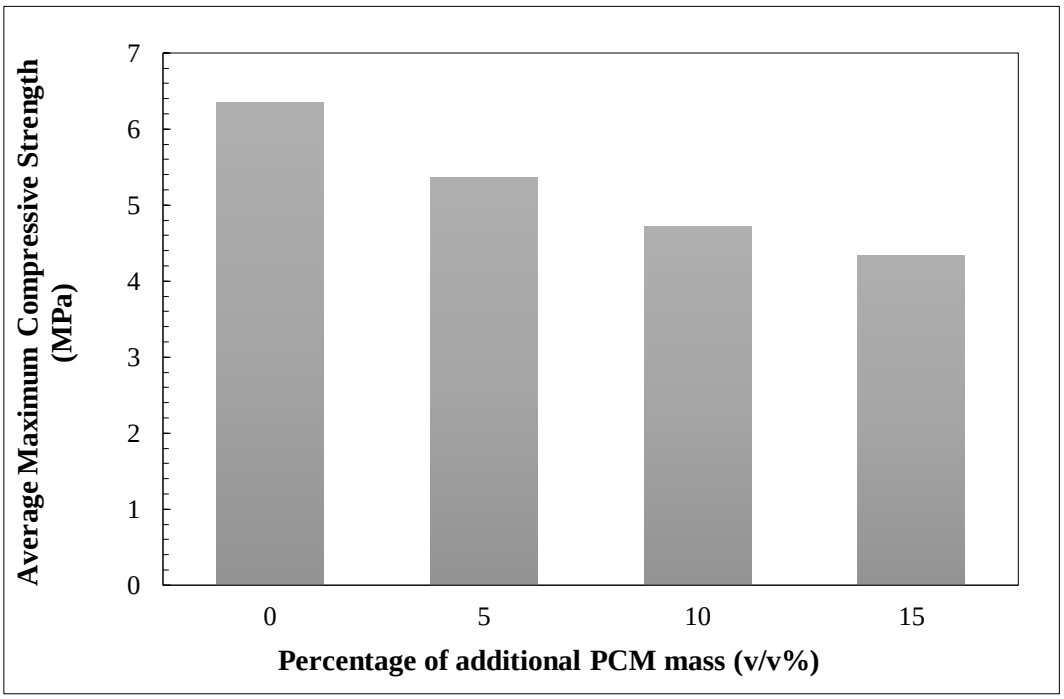

Figure 4-10. The maximum compressive strength of the gypsum plasterboard with various percentages of additional PCMs

Figure 4-10 shows the maximum compressive strength of various gypsum composites filled with different concentrations of phase change materials. The results show that increasing the amount of added phase change material reduces the maximum compressive strength. For example, the addition of 5% and 15% PCM enhances the compressive strength of the gypsum board to 5.36 and 4.34 MPa, respectively. However, the results indicate that the proposed PCM reinforced gypsum board is eligible for use in construction due to the obligation that a building's structure requires gypsum board to be at least 2 MPa or to exceed the maximum compressive strength (EN 13279-2) (Borreguero, Garrido et al. 2014; Borreguero, Serrano et al. 2014).

4.6.3 *Density results*

The density measurements were made using the instrument in Figure 4-6 and calculated using equation (4-2). During this test, each type of sample was tested at least 3 times and the averaged results are shown in Table 4-3.

Table 4-3. The density of various samples

Block	PCM/gypsum (v/v %)	Average Bulk Density (Kg/m^3)
Gypsum	0.0	1897.4
Gypsum plasterboard with PCM	5.0	1752.5
	10.0	1652.4
	15.0	1549.0

According to Table 4-3, increasing the content of the PCM reduces the bulk density because the PCM has a smaller particle size than the gypsum particles and will fill the position between them. Therefore, the gypsum plasterboard filled with 15% PCM has a minimum density of $1549.0 Kg/m^3$ due to the lowest density of the microencapsulated PCM. The bulk density requirement for all the samples was greater than $600 Kg/m^3$, which is in accordance with standard EN 13279-2 (Borreguero, Garrido et al. 2014). However, due to differences in the manufacturing processes of gypsum board, the density results may vary with respect to the density of commercial gypsum board.

4.6.4 *Thermal conductivity of gypsum blocks*

Measuring thermal conductivity is one of the key factors determining a property because it affects the heat flux and specific heat capacity of the gypsum plasterboard. In this study, the thermal conductivity of the sample was tested through HFM. The

thermal conductivity of each type of gypsum board was measured at least three times. All samples were the same size and of different compositions. The average results for each sample are shown in Figure 4-11. In addition, the measurement accuracy was ±1%.

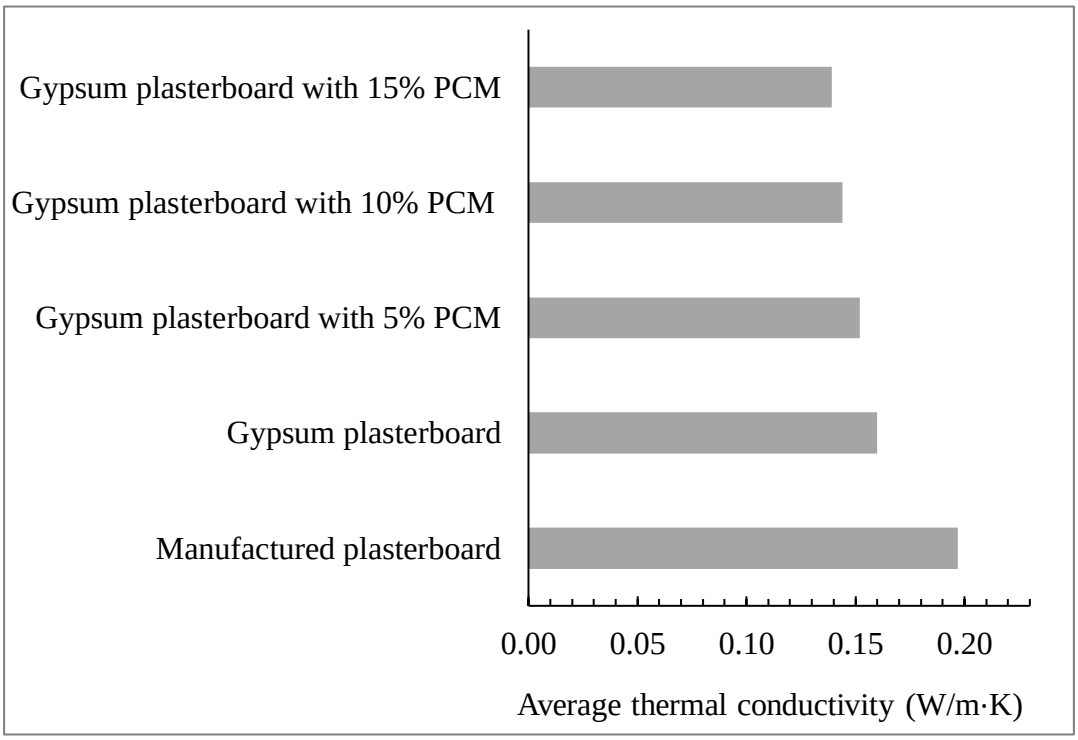

Figure 4-11. Average thermal conductivity for each type of gypsum block

An increase in PCM concentration reduces thermal conductivity because a PCM has a lower thermal conductivity and minimises the total thermal conductivity of the sample. For example, the thermal conductivity of all the gypsum boards was lower than $0.160W/mK$, which is less than $0.19W/mK$ of manufactured gypsum plasterboard (Figure 4-11). In addition, among all the types of gypsum board samples, the gypsum composite with 15% PCM had the lowest thermal conductivity of $0.139W/mK$. It can be indicated that the addition of a PCM can reduce the thermal conductivity of the gypsum board and has a higher heat insulating ability than the manufactured gypsum board. Therefore, PCM-reinforced gypsum plasterboard is a promising material for construction.

4.7 **Finalising the PCM enhanced gypsum plasterboard**

After the property testing/characterisation of the PCM-gypsum plasterboard and especially after analysing the results of the thermal conductivity measurements, the gypsum plasterboard with 15% PCM was finally made to due to its optimal performance. Figure 4-12 shows the PCM-gypsum plasterboard with dimensions of $950 \times 900 \times 10mm$ (height, width, thickness) in Coventry University's Structural Laboratory. There are 3 patch sensors and 3 probe sensors respectively to measure the surface and internal temperatures of the PCM-gypsum plasterboard. These probe sensors are primarily used to measure temperature changes during the charging/discharging of the phase change material.

Figure 4-12. Schematic of framed PCM enhanced gypsum plasterboard

According to Figure 4-12, in order to place this PCM enhanced gypsum plasterboard into an experimental setup for analysing the performance of the envelope, the plasterboard was designed to fit in a wooden frame with a size of 990 x 990 x 10 mm (height, width, thickness) to hold the PCM enhanced gypsum plasterboard tightly and attach it to the inner surface of the building envelope. This can effectively reduce damage during the implementation of the PCM-reinforced gypsum plasterboard.

4.8 **Conclusions**

In this part of the study, the structural design of the proposed building envelope was presented. The potential advantages due to the addition of PCM-gypsum plasterboard and a transpired solar collector compared to the conventional wall design were also mentioned. This chapter mainly focused on the characterisation of the developed gypsum plasterboard integrated with a microencapsulated PCM (MICRONAL® DS 5040X PCM powder). Additionally, the finalised PCM-gypsum plasterboard was also described. The characterisation was undertaken for 4 different types of gypsum samples due to the addition of PCMs. The properties testing included bulk density measurement, thermal conductivity testing, compressive strength measurement and SEM testing. This work conducted the following results:

a) The SEM image shows that multi-finished gypsum powder and microencapsulated PCM were mixed uniformly with the MICRONAL® DS 5040X PCM powder.
b) The density measurement indicated that increasing the PCM content decreases the bulk density. For instance, the gypsum plasterboard filled with 15% PCM had a minimum density as $1549.0 Kg/m^3$ due to the low density of the microencapsulated PCM.

c) An increasing amount of PCM additions would reduce the maximum compression strengths of the gypsum boards. The gypsum plasterboard enhanced with 5% and 15% PCM claim 5.36 and 4.34MPa, respectively.

d) Through the thermal conductivity testing, the gypsum boards with the addition of 15% PCM had the lowest value of thermal conductivity of 0.139W/mK among all the plasterboard samples. Hence, increasing the concentration of the PCM would result in a lower thermal conductivity, since the PCM has a lower thermal conductivity that enables the minimising of the total thermal conductivity of the produced gypsum composite.

Chapter 5. **Experimental investigation of the designed building envelope**

5.1 Introduction

In this chapter, there are detailed explanations of material selection, experiment procedure, measurement devices and sensors for the experimental study. The experimental work was conducted for (i) characterisation of the PCM-gypsum plasterboard and (ii) investigating the building envelope's performance. The experimental setup and the data logger are included in this chapter. Furthermore, the experimental data was statistically analysed through measuring the experimental uncertainty, confidence interval and data cleansing. In addition, the experimental procedure included proposed cases due to various parameters such as airflow rate, plenum size and pitch dimension. The experimental results were analysed and discussed in terms of (i) the advantage of using PCM-gypsum plasterboard and (ii) the impact of the three main parameters: the airflow rate, plenum size and pitch dimension on the charging/discharging of the PCM-gypsum plasterboard and the building envelope's performance. The experimental results also highlighted the benefits of using PCM-gypsum plasterboard.

5.2 Experimental rig design

In order to investigate the performance of the building envelope, the experimental campaign was designed to be undertaken with or without PCM enhanced gypsum plasterboard. During the experimental investigation, the PCM-gypsum plasterboard was framed with a wood mould and attached to the inner surface of the building's façade. The experiment setup is shown as follows (Figure 5-1). Therefore, the light board contained 6 halogen lamps. The specifications and geometry of the experimental setup are given in Table 5-1.

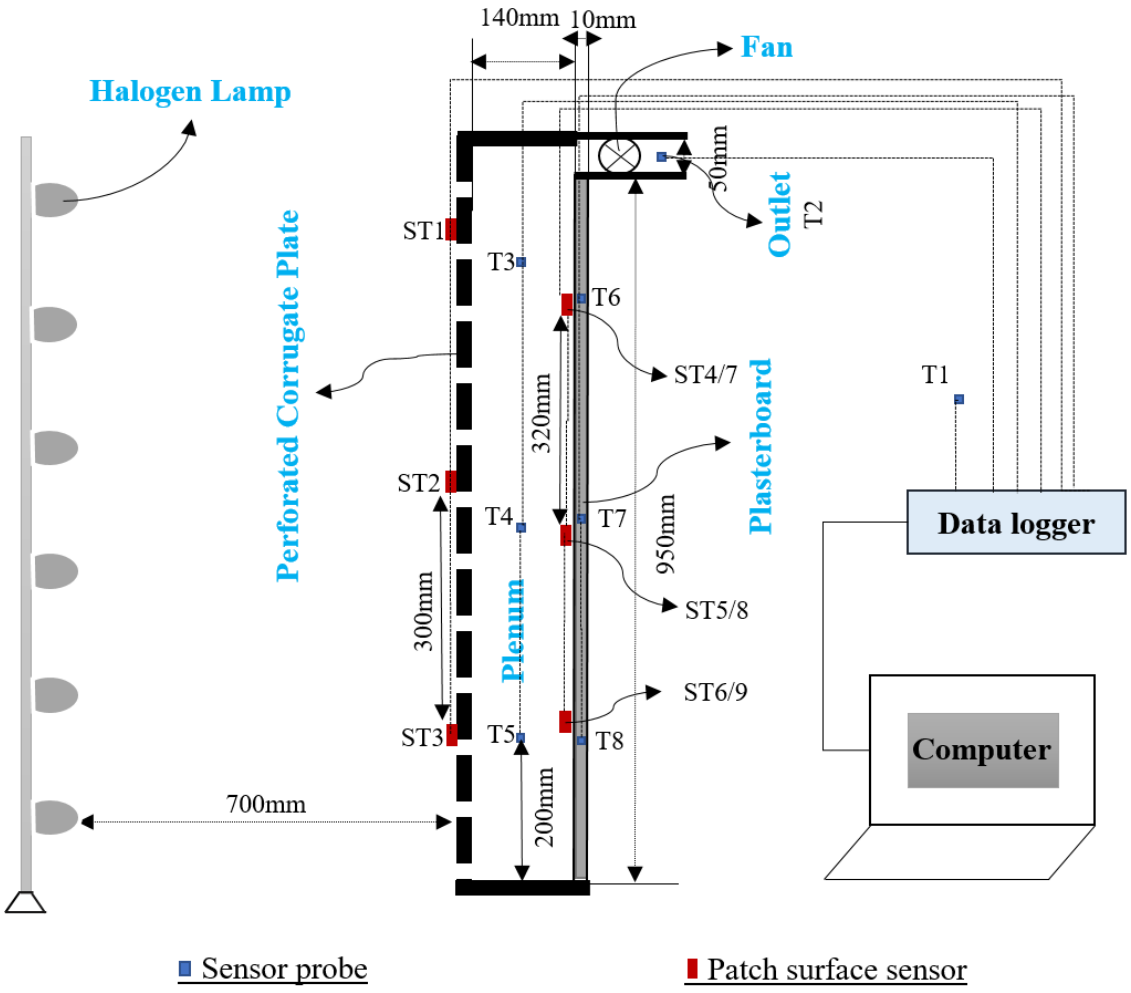

Figure 5-1. Experimental setup in the lab

Table 5-1. Experimental setup specifications

Product	Corrugated metal sheet
Width (m)	1
Length (m)	1
Area (m^2)	1
Top/side wooden wall thickness (mm)	50
Plenum size (m)	0.1
Adjustable collector tilt (°)	90

Perforation diameter (m)	1
Pitch size (mm)	20
Porosity (%)	70
Number of perforations	1293
Colour	Black
Absorptivity	0.95
Emissivity	0.85

Hence, the construction of such a building envelope requires certain types of materials and devices. The requirements for this experimental investigation are listed as follows in detail:

a) A perforated corrugated plate with a size of 1×1m as an absorber profile was attached with various plenum depths such as 140mm, 200mm and 250mm, to create the air plenum;
b) The top/bottom and both sides of the plenum were closed with a wooden wall ($50mm$ thickness) that was made of polyurethane insulation board and Rockwool insulation;
c) The hole diameter of a $\varnothing 100mm$ outlet section was located on the back wall;
d) There was a light board with six halogen lamps (each of $500W$) located within a $700mm$ distance of the absorber plate, simulating the solar radiation intensity of 600 W/m^2;
e) A fan was installed at the outlet to suck the preheated air to be delivered.

Therefore, the TSC structure in this study was thermally insulated with a proper insulation wall on both sides and at the top/bottom of the plenum, as shown in **Error! Reference source not found.**. The experimental setup was established and operated inside the hydronic laboratory, where the airflow and temperature remained

unchanged when conducting the experimental investigation. Therefore, the heat loss from the plenum was negligible and the heat loss from the absorber plate to the surrounding environment was ignored as the wind speed around in the lab was seen as constant at zero.

5.3 **Data collection procedure**

In this experiment, the measurement devices used were: (i) a solar light meter that measured the solar intensity from the light board, (ii) an airflow meter for the fan velocity and air velocity through the plenum and the outlet and (iii), a thermocouple for measuring the temperature at various locations. These locations were inside the plasterboard, in the air plenum, at the outlet and on the absorber plate surface (**Error! Reference source not found.**). **Error! Reference source not found.** presents a data logger recording the temperature through the Platinum Resistance Temperature Detectors probe and patch sensors (with the accuracy of ± 0.30°C), forming a data acquisition system. Sensors were installed in the locations of the experiment platform in the following order:

a) One probe sensor lay at a constant location within the laboratory for measuring the in-lab ambient temperature (T1);
b) 3 probe sensors were also installed inside the mPCM-plasterboard (T6, T7, T8) during the casting to record its temperature change during the charge/discharge process of the mPCM;
c) 1 probe sensor was also installed inside the gypsum plasterboard to measure its inside temperature change (T9);
d) 6 patch sensors (ST4, ST5, ST6, ST7, ST8, ST9) were positioned vertically on the two-line of the back wall surface to test its surface temperature;

e) Three probe sensors (T3, T4, T5) were located vertically on the central line of the plenum at variable distances from the ground at $200mm$, $550mm$, $900mm$ respectively;

f) 3 patch sensors (ST1, ST2, ST3) were on the front surface of the corrugated plate at 100, 400, $850mm$ separately from the bottom of the air cavity;

g) There was one more probe air temperature sensor (T2) on the outlet to record the delivered air temperature.

(a) (b)

Figure 5-2. (a) Platinum Resistance Pt100 Pro Sensor; (b) Platinum Silicone Patch Sensor

The plenum air temperature, outlet temperature, in-lab temperature and the inside plasterboard temperature were measured using a platinum resistance pt100 heavy duty sensor pro, class b (Figure 5-2a) and its specifications are shown in Table 5-2. The platinum silicone patch sensors (Figure 5-2b) were used for measuring the surface temperature of the plate profile and the plasterboard and its specifications are shown in Table 5-3.

Table 5-2. Specifications for the Platinum Resistance Pt100 Heavy Duty Sensor Probe

Sensor Type	PT100 (100 Ohms @ 0°C) to IEC 751, Class B, 4 wire

Probe length	100mm
Probe Diameter	6mm
Minimum Temperature Sensed	-50°C
Maximum Temperature sensed	+200°C
Termination Type	Lead Wire/ 4-wire tails – allows connection to any PT100 instrument 2, 3 or 4 wire
Cable Length	2m
Probe Material	Stainless Steel
Number of Wires	4
Accuracy	Class B

Table 5-3. Specifications for the Platinum Resistance Pt100 Heavy Duty Patch Sensor

Sensor Type	Pt100 (100Ω @ 0oC), thin film Class B to IEC751
Construction	Element encapsulated in a silicone rubber patch with self-adhesive aluminium foil backing
Patch Dimensions	Length 40mm x Width 13mm x Height 5mm 6mm
Minimum Temperature Sensed	-50°C
Maximum Temperature sensed	+150°C
Lead Type	Teflon® insulated, 7/0.2mm twisted 4 core and tails
Termination	4 wire tails
Lead type	3/5m available
Number of Wires	4

During the experiment, ongoing temperature changes were recorded on a minute by minute basis through a data logger (Figure 5-3) and transferred into the computer for further analysis.

Figure 5-3. Data Logger

5.4 Measurement devices

5.4.1 *The solar power meter*

However, for this experimental investigation, measuring the sunlight intensity was crucially important since it could ensure solar irradiation as input energy. This experimental investigation used a light meter as an effective device to measure solar power (Figure 5-4). There are different kinds of solar light meter due to various ranges, resolutions and accuracy. A light meter contains a sensor that converts the light energy into an electrical charge that can give the user a reading (ATP Instrumentation Ltd. no date). In particular, light measurement is performed by drawing a light bulb with a filament that heats up and produces light. Then, the filament is the source of the light and is located at the center of a sphere with light being emitted in every direction. The

total energy of all the light produced is called “luminous flux” (ATP Instrumentation Ltd. no date).

Figure 5-4. Schematic of a DT-1307 solar light meter

For instance, the DT-1307 solar power meter (Figure 5-4) is commonly used to measure sunlight, offering a compact design and robust construction. It is designed for the environmental monitoring of sunlight intensity and is mainly used by solar power installation engineers or scholars for experimental research, when compacting the intensity of the sunlight with the efficiency of the solar panels during installation and maintenance processes. Technical specifications of the DT-1307 solar light meter are shown in Table 5-4, according to the supplier.

Table 5-4. Specifications for the DT-1307 solar power meter

Operating Temp. & RH	5°C – 40°C, below 80% RH
Storage Temp. & RH	-10°C - 60°C, below 70%
Display	3-1/2 digits LCD with maximum reading 1999
Sampling time	Approx. 0.25 second
Resolution	1W/m2 1 BTU/ (ft2 *h)

Accuracy	Typically, within ±10W/m2 [±3BTU/ (ft2 *h)] or ± 5%, whichever is greater in sunlight. Additional temperature induced error ±0.38W/ m2 /°C
Accuracy	< ±3/year
Over - input	Display shows ‘OL’
Range	1999W/m2, 634BTU/ (ft2 *h)
Size	160 (L)*63(W)*28(H)
Weight (including battery)	About 250g

For safety and maintenance:

h) The operating altitude should be below 2000m;
i) The operating environment for indoor use is exposed to pollution level II;
j) Do not put this device in direct sunlight or in a hot and or damp place;
k) This device should be cleaned with a dry soft cloth. Wet clothes, liquid and water are prohibited.

5.4.2 *The Air velocity meter*

It is also crucial to measure the air velocity at the inlet/outlet and the fan speed. A TSI airflow TA440 air velocity meter was used to test the inlet air velocity (Figure 5-5). For each experimental case, the air velocity and fan speed were measured at least 3 times and the average values determined the air velocity.

Figure 5-5. Schematic of the air flow meter

5.5 **Statistical analysis of the experimental data**

5.5.1 ***Experimental uncertainty***

During the experimental work, it was believed that the experiments had inherent errors due to instrumentation, data acquisition and reduction limitations, facility and environmental effects and personal errors, like reading mistakes. With respect to these reasons, the determination and justification of true value demands estimates for experimental errors. The experimental uncertainty/error is crucial for risk assessment in design, both when using the data and in calibrating and/or validating the experiments' outcomes. Therefore, in order to prove the accuracy and precision of the experiments' measurements to justify the credibility of the experimental data, an analysis of error and data was undertaken in terms of total experimental uncertainty (internal and external), confidence interval and significance level.

Most common errors are usually because of the faulty calibration of measuring devices, poorly maintained instruments and reading mistakes by the user. In order to minimise such errors, the air velocity was measured at least 4 times and the average was taken for analysis. In addition, all the measurement devices including the sensor were

calibrated before the experiments took place. Hence, it can be believed that the effects of such errors were reduced to their limits. Besides, it is significant to determine measurement errors while using a calibrated sensor during experimentation. The measurement range and accuracy of the measuring instructions are taken into consideration.

The temperature distribution alongside the absorber plate, in the air cavity, in the PCM enhanced gypsum plasterboard and the fan velocity were measured using the relative testing devices mentioned above. The instruments used to measure these parameters and their technical specifications are summarised in Table 5-5

Table 5-5. Measuring devices and their specifications for the experimental study

Instrument	Manufacturer	Measurement parameter	Measurement range	Accuracy
Platinum Resistance Pt100 Pro Sensor	RS Components Ltd.	In-lab air temperature, plenum air temperature and inside temperature of PCM-gypsum plasterboard	-50~200	± 0.30°C
Platinum Silicone Patch Sensor	RS Components Ltd.	Absorber plate temperature and PCM-gypsum plasterboard surface temperature	-50~150	± 0.30°C
Solar meter	Iso-Tech	Solar flux	0~2000	within ± 10W/m^2
Airflow meter	TSI Incorporated	Air velocity	0~50	±3% of reading

According to a study by Zhou and Zhao (2011), the experimental measurement uncertainty can be calculated by equation (5-1) as follows:

$$U = \pm\sqrt{\left(\frac{\Delta T_{TC}}{T_{TC}}\right)_{PCM\_G}^{2} + \left(\frac{\Delta T_{TC}}{T_{TC}}\right)_{air}^{2} + \left(\frac{\Delta T_{TC}}{T_{TC}}\right)_{surface}^{2} + \left(\frac{\Delta V}{V}\right)^{2}} \times 100\% \qquad (5\text{-}1)$$

In the first place, the uncertainty was estimated due to the sensitivity values specified above, where the sensitivity of the thermocouples and the data logger were roughly± 0.1℃. Also, the reading mistakes for air temperature and surface temperature measurement were estimated as ± 0.2℃ (ΔT_{TC}). Meanwhile, the sensitivity of the velocity measurement of the air was $\pm 0.001 m/s$ and the reading errors were $\pm 0.001 m/s (\Delta V)$ separately.

The relative uncertainties of the PCM-gypsum plasterboard temperature, taking the minimum and maximum temperatures into consideration, can be calculated by

for $T_{min} = 18$℃, the uncertainty is

$$\left(\frac{\Delta T_{TC}}{T_{TC}}\right)_{PCM\_G} = 1.31\%$$

for $T_{max} = 40$℃, the uncertainty is

$$\left(\frac{\Delta T_{TC}}{T_{TC}}\right)_{PCM\_G} = 0.55\%$$

The relative uncertainties of the in-lab, plenum, and the outlet temperature considering the minimum and maximum temperatures approximately becomes

for $T_{min} = 18$℃, the uncertainty is

$$\left(\frac{\Delta T_{TC}}{T_{TC}}\right)_{air} = 1.67\%$$

for $T_{max} = 45$℃, the uncertainty is

$$(\frac{\Delta T_{TC}}{T_{TC}})_{air} = 0.6\%$$

The relative uncertainties of the absorber plate temperature considering the minimum and maximum temperatures become

for $T_{min} = 18℃$, the uncertainty is

$$(\frac{\Delta T_{TC}}{T_{TC}})_{surface} = 1.49\%$$

for $T_{max} = 55℃$, the uncertainty is

$$(\frac{\Delta T_{TC}}{T_{TC}})_{surface} = 0.67\%$$

The relative uncertainties of the air velocity alongside the whole building envelope considering the minimum and maximum temperatures approximately becomes

for $V_{min} = 0.5 m/s$, the uncertainty is

$$(\frac{\Delta V}{V})_{air} = 0.58\%$$

for $V_{max} = 3.65 m/s$, the uncertainty is

$$(\frac{\Delta V}{V})_{air} = 0.12\%$$

Hence, the maximum measurement errors/uncertainties for each parameter are demonstrated in Table 5-6.

Table 5-6. Experimental uncertainty

Parameter	Equipment	Uncertainty

PCM-plasterboard temperature	Platinum Resistance Pt100 Pro Sensor (ΔT_{TC}) Data logger (ΔT_{DT})	1.31%
Air temperature	Platinum Resistance Pt100 Pro Sensor (ΔT_{TC}) Data logger (ΔT_{DT})	1.67%
Plate Surface temperature	Platinum Silicone Patch Sensor (ΔT_{TC}) Data logger (ΔT_{DT})	1.49%
Air velocity	TSI air velocity probe (ΔV) Data logger (ΔT_{DT})	0.58%

Accordingly, the total uncertainty was calculated through equation (5-1) for the uncertainties of each parameter mentioned in Table 5-6 were lower than 5%. Such results ensured the experimental data were reliable with high credibility.

5.5.2 *Confidence interval*

In order to assess the precision of the sample estimates, the confidence levels and confidence intervals were tested for the experimental data in this study. The confidence interval is a range of values calculated by statistical methods which include the desired true parameters with a probability defined in advance. It can be calculated through equation (5-2) (du Prel et al. 2009). In general, a confidence level of 95% is used for statistical analysis which results in the significance level being 0.05. This study also calculated both the confidence intervals and P-values to determine the precision and accuracy of the data through Excel and the results is shown in Table 5-7. The p-values were calculated through regression data analysis in Excel. The confidence intervals and p-values were calculated for the main experimental outcomes such as in-lab ambient

temperature, absorber plate temperature, plenum air temperature, outlet temperature, PCM-gypsum plasterboard and air velocity, respectively.

$$\mu = \bar{X} \pm z \times \frac{\sigma}{\sqrt{n}} \quad (5\text{-}2)$$

Where μ represents the confidence interval, $\bar{X}$ describes the mean of the sample, z is the critical value or confidence level coefficient, σ covers the standard deviation of the samples and n gives the number of samples.

Table 5-7. Results of confidence intervals and p-values for the main parameters

Parameters	Confidence level	Confidence interval	p-value
In-lab ambient temperature	95%	0.0083	<0.001
Outlet temperature	95%	0.0543	<0.001
Absorber plate surface temperature	95%	0.0368	<0.001
Plenum air temperature	95%	0.0571	<0.001
PCM-plasterboard temperature	95%	0.0603	<0.001
Air velocity	95%	0.0988	<0.01

According to Table 5-7, it can be seen that the confidence interval for each experimental parameter data was roughly near 0.05 and the P-value was less than 0.001 for the majority of the data. Such results matched the required significance level of 0.05. The confidence interval and p-value for the air velocity were not as high as the significance level of 0.05. Hence, these statistical data analysis results strongly justify the credibility of the experimental data for further analysis.

5.5.3 *Data cleansing*

Data cleansing is an important process for identifying and removing inaccurate records from experimental data to prepare a higher quality and consistency of the data for further analysis. According to the results of the confidence interval comparing each set of data responding to the mean values, the total proportion of the data was reviewed to identify inconsistencies and inconsistent/inaccurate or duplicated data causing errors or corruptions. Such coarse data was removed/cleared and the rest of data validated accordingly due to the significance level or confidence interval through monitoring and analysing these experimental data. Thus, credible data with a higher quality was used to for the experimental data analysis.

5.6 **Experimental procedure**

In this study, the experimental procedure included measuring the in-lab temperature, plate temperature, plenum air temperature, surface and inside temperature of the PCM-gypsum plasterboard and the outlet temperature for (i) various fan airflow rates (10, 30, 50m^3/hr), (ii) various plenum sizes (140mm, 200mm, 250mm) and (iii), two different pitch sizes (20mm and 25mm) under operational conditions using two different plasterboards: PCM-gypsum plasterboard and gypsum plasterboard, separately. It also investigated the charging/discharging processes of PCM-gypsum plasterboard, for instance, the impact of air flow rate and plenum size on the solidification and melting of PCM-gypsum plasterboard. In this investigation, the in-lab temperature was taken as the inlet temperature. In this project, each set of experiment cases were set to run with the lighting on for 2 hours as the charging period (the lights were on to simulate the solar radiation) and for at least 5 hours with the lighting off as the discharging period (the lamps were off to simulate the night-time/no-sun condition). During the experiment, the lights were to be off at 120 min to prevent the heat flow from being reversed, as the heat might be lost to the environment from the plate if the lights were

kept on for a long period. Furthermore, each experimental case was operated for 7 hours as it was designed to simulate office working, which was beneficial for its implementation in non-residential/commercial buildings. The fan also ran at a constant speed for the whole period of testing. The experimental techniques are shown in Table 5-8.

Table 5-8. Experimental cases to run

Case	Building envelope type	Constant parameters and relative values	Various values	Period
Impact of airflow rate	With gypsum plasterboard With PCM-gypsum plasterboard	Plenum size (150mm), pitch size (20mm), hole geometry (circular hole) and dimension (diameter of 1mm), inlet temperature (18°C), plate temperature (55°C)	Airflow rate (m^3/hr) =10:30:50;	Charging Discharging
Impact of plenum size	With gypsum plasterboard With PCM-gypsum plasterboard	Airflow rate (10m^3/hr), pitch size (20mm), hole geometry (circular hole) and dimension (diameter of 1mm), inlet temperature (18°C), plate temperature (55°C)	Plenum size (mm) =140:200:250;	Charging Discharging
Impact of pitch size	With gypsum plasterboard	Airflow rate (10m^3/hr), plenum size (140mm), hole		Charging

With PCM-gypsum plasterboard	geometry (circular hole) and dimension (diameter of 1mm), plate temperature (55°C)	Pitch size (mm) =20:25;	Dischargin g

5.7 **Building envelope performance- Assessment criteria**

The experiments were undertaken to investigate the thermal performance of this novel-designed building envelope with PCM-gypsum plasterboard and gypsum plasterboard under the same laboratory conditions to determine (i) the advantage of using PCM-gypsum plasterboard, (ii) the impact of several parameters on the building envelope performance and (iii), the charging/discharging of the PCM-gypsum board. For this study, the in-lab environmental temperature was measured and taken as roughly 18°C. Each experimental case was operated for 7 hours including heating the absorber plate for 2 hours (charging period) and cooling down the absorber plate for five hours (discharging time). During the ongoing experiment, the in-lab temperature, absorber plate temperature, outlet temperature, plenum air temperature and surface/inside temperature of the PCM-gypsum plasterboard were recorded on a minute by minute basis through a data logger and transferred to the computer for further analysis. For various scenarios during the experimental operation, the wind effect was ignored and the downlight board with 6 halogen lights was on with an intensity of 600W/m^2 which could be absorbed by the absorber plate profile. Thus, different experimental cases were operated according to various parameters: the airflow rate (fan velocity), plenum size and pitch size. This chapter also analyses and discusses the experimental results. The outlet temperature and PCM-gypsum plasterboard temperature distributions are firstly described to highlight and clarify the advantage of using PCM-gypsum plasterboard compared to gypsum plasterboard. In addition, the impact of airflow rate and plenum size on the PCM charging/discharging is also demonstrated and discussed in this

section. The building envelope performance was analysed through the collector efficiency, the air temperature rise and the heat exchange effectiveness. Those indicators are able to fully reflect the gained useful heat, the outlet air temperature and the thermal conversation efficiency of this innovative building envelope (Wang et al. 2017).

a) Collector efficiency

Collector efficiency is determined as the ratio of valuable thermal energy (heat) delivered by the solar collector to the total solar energy received by the absorber plate profile. Collector efficiency can be articulated as equation (5-2) (Leon and Kumar 2007b; Wang et al. 2017):

$$\eta = \frac{\dot{m}_{air} C_{p.air} (T_{out} - T_{inlab})}{\propto_p I_T A_s} \qquad (5\text{-}2)$$

Where η gives the collector efficiency; $\dot{m}_{air}$ describes the mass flow rate (kg/s); $C_{p.air}$ represents the specific heat capacity of air ($J/kg.K$); T_{out} and T_{inlab} demonstrates the outlet temperature (K) and in-lab air temperature (K) respectively; $\propto_p$ gives the solar absorptance of the absorber perforate plate surface; A_s is the surface area of the collector (m^2); and I_T gives the solar radiation incident on the collector (W/m^2);

b) Air temperature rise

A higher solar radiation could bring a higher air temperature rise (ΔT) since the heated air is derived from the outlet temperature (T_{out}) and the in-lab air temperature (T_{inlab}) can be determined as (Kutscher 1994; Leon and Kumar 2007b; Bokor et al. 2017).

$$\Delta T = T_{out} - T_{inlab} \qquad (5\text{-}3)$$

c) Heat exchange effectiveness

Heat exchange effectiveness (ε_{HX}) is based on the overall heat transfer coefficient for the air passing through the absorber plate and it is defined as the ratio of the actual temperature rise of the air as it passes through the absorber to the maximum possible temperature rise (Wang et al. 2017), which is calculated by following equation (Kutscher 1994; Leon and Kumar 2007b; Bokor et al. 2017).

$$\varepsilon_{HX} = \frac{T_{out} - T_{inlab}}{T_p - T_{inlab}} \qquad (5\text{-}4)$$

Where ε_{HX} is heat exchange effectiveness (HEE); T_{out} and T_{inlab} represent the outlet temperature and in-lab air temperature and T_p gives the absorber plate temperature.

Therefore, the impact of each parameter on building envelope performance was analysed based on the outlet temperature, the PCM-gypsum plasterboard temperature, and thermal performance indicators in the following contents. Furthermore, it also highlighted the benefits of using PCM-gypsum plasterboard on building envelope performance in terms of outlet temperature and generated energy.

5.8 **Experimental results analysis**

5.8.1 ***Influence of PCMs on charging and discharging***

In order to see the correlation between different temperature profiles of building envelopes, the temperature profiles were investigated and discussed for one experimental case. The experiment's operational conditions were a fan speed of 2.26m/s, inlet temperature (18℃), a solar intensity of 600W/m^2, plenum size (140mm), circular hole diameter (1mm) and pitch size 20mm.

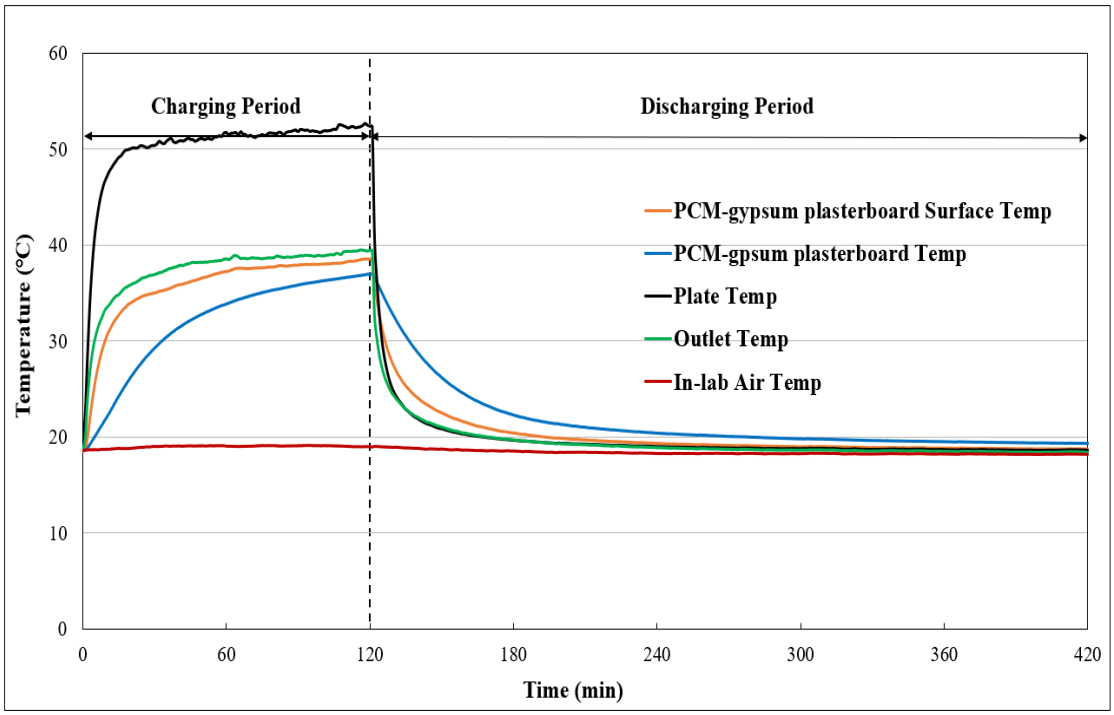

Figure 5-6. Average temperature profiles for different components of a building envelope with PCM-gypsum plasterboard

As shown in Figure 5-6, the plate temperature, the outlet temperature and the surface temperature of the PCM-plasterboard showed a rapid increase within the first 15 minutes, and then stabilised for rest of the 105 minutes. In particular, the plate temperature reached its highest temperature within a very short time due to the higher thermal conductivity and solar absorptance of the metal plate. The PCM-plasterboard temperature displayed an increased trend within the first 60 minutes, then it increased slowly between 60 and 120 minutes where the PCM components inside the PCM-gypsum plasterboard were assumed to be fully melted (v). After switching the lights off, the plate temperature and the outlet temperature went down fast. The PCM-gypsum plasterboard temperature declined slowly to the ambient temperature even compared to the gypsum plasterboard, due to the advantages of the PCM inside. The PCM-gypsum plasterboard stored a certain amount of latent heat and released it slowly during the discharging period.

Under the same experimental conditions, experimental studies were carried out on a building envelope using gypsum plasterboard with/without PCM. These experimental conditions were fan speed (2.26m/s), plenum size (250 mm), pitch size (20mm), circular hole diameter (1mm) and solar intensity (600W/m^2). In both cases, the lamp was turned on for 2 hours, then the plate was cooled by turning off the lamp for 5 hours. The results showed different values at the outlet temperature and the internal temperature of the gypsum board. This provided different useful energy generated and Figure 5-7 shows the temperature changes of the PCM-gypsum board and the gypsum board.

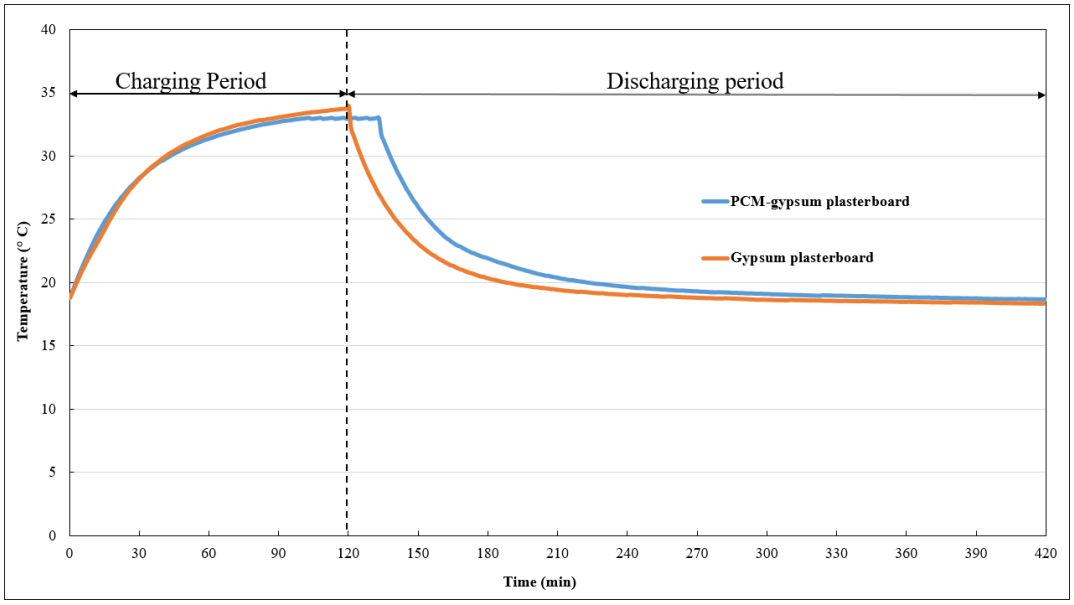

Figure 5-7. Temperature profiles for the PCM-plasterboard and gypsum plasterboard

For both experimental cases, the temperature trends of the PCM-gypsum board and the gypsum board are similar, as shown in Figure 5-7. For illumination during charging, the PCM-gypsum plasterboard and the gypsum plasterboard temperatures rose rapidly during the first 60 minutes and then became relatively stable after 60 minutes of illumination. At the same time, the temperature of the gypsum plasterboard continued to rise until it was extinguished and its final temperature was higher than that of the PCM gypsum plasterboard. It can be assumed that the PCM gypsum board was

completely melted, causing its temperature to remain relatively stable before the lamp was turned off. During discharge, the temperature of the gypsum plasterboard dropped sharply, while the temperature of the PCM gypsum plasterboard decreased more slowly. For example, the temperature of the gypsum plasterboard dropped to about 18 ° C at about 240 minutes, but the temperature of the PCM-reinforced gypsum plasterboard took about 3 hours (300 minutes) to drop to the in-lab ambient temperature (Figure 5-7). One possibility is that the PCM plasterboard can store a certain amount of energy and release it for later use due to the benefits of the additional PCM. The outlet temperature will change in both cases, as described below.

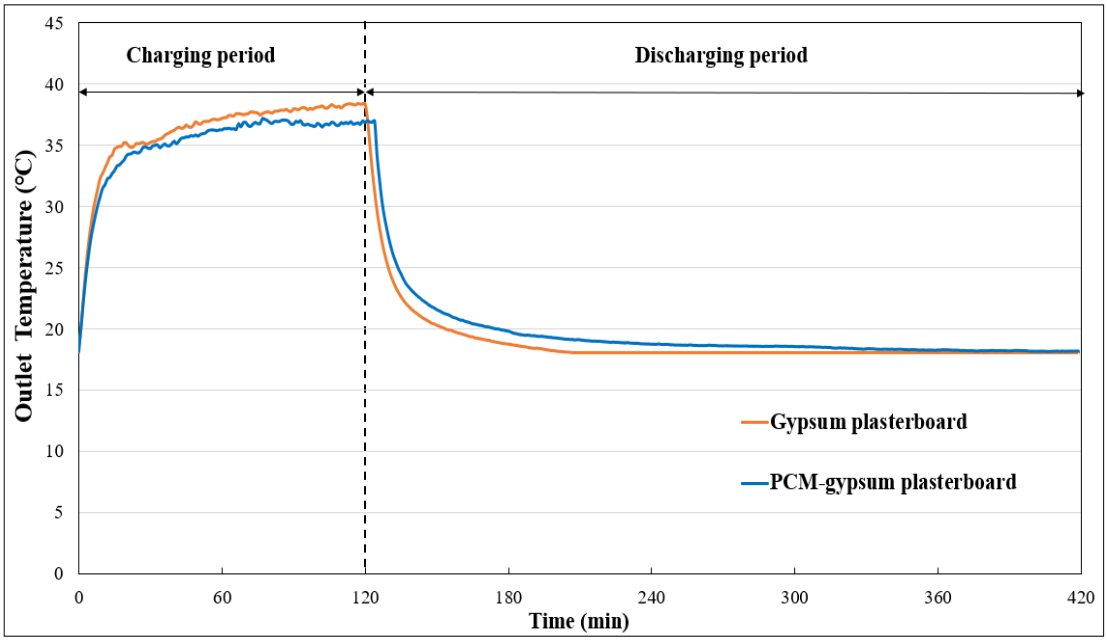

Figure 5-8. Outlet temperature distribution of the PCM-plasterboard and gypsum plasterboard

According to Figure 5-8, the experiment enabled various outlet temperatures to be provided because of using the PCM-gypsum plasterboard and the gypsum plasterboard. During the first 120 mins of the charging period, the outlet temperature for the case with the PCM-plasterboard was lower (roughly 2°C) compared to the gypsum plasterboard (Figure 5-8). Within 15 minutes after switching off the lights, the outlet

temperature for both cases dropped rapidly. The exit temperature for the gypsum plasterboard with the PCM was higher than the gypsum plasterboard without the PCM, since the PCM-plasterboard released the stored latent heat slowly. The outlet temperature for case A was higher than case B for a longer period when the lights were switched off within 2 hours of operation. It can be indicated that the PCM plasterboard stored a certain amount of energy and released it slowly compared to the gypsum plasterboard. It brought attention that the heat generated by these two cases might vary. According to the previous researches, the generated energy (Q_{out}) from both cases could be calculated by following equation (5-5) and the results are shown in Figure 5-9.

$$Q_{out} = \dot{m} c_p \, (T_{out} - T_{in-lab}) \qquad (5\text{-}5)$$

Where Q_{out} is the generated energy; $\dot{m}$ is mass flow rate c_p represents the specific heat capacity of the air; T_{out} gives the outlet temperature, and T_{in-lab} is the in-lab ambient temperature. Hence, the calculation is done for both cases and the results are shown in Figure 5-9.

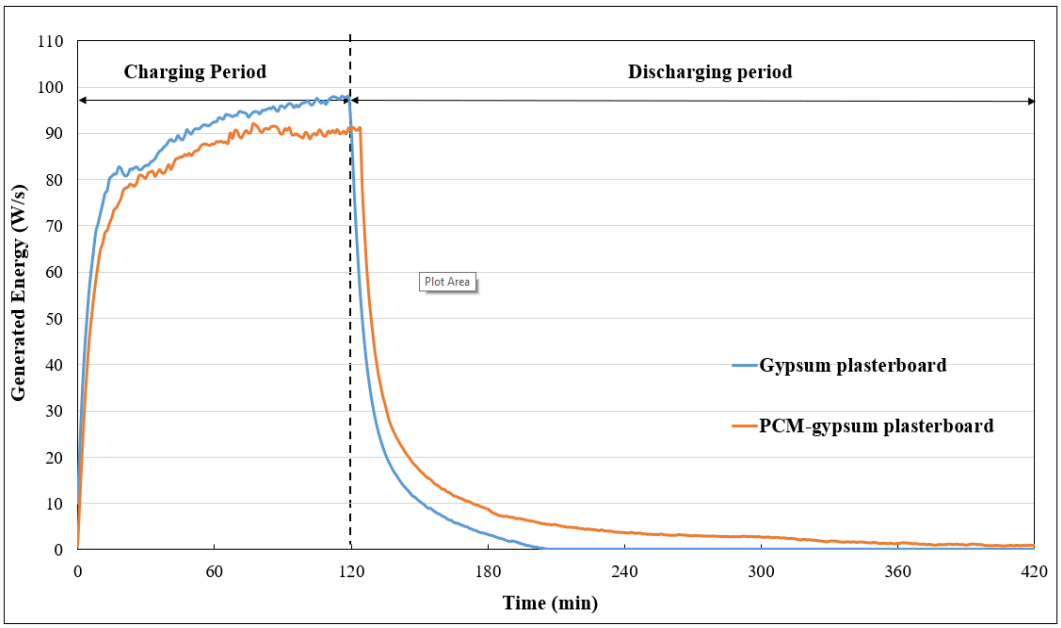

Figure 5-9. Generated energy for the building envelopes with gypsum plasterboard and PCM-gypsum plasterboard

According to Figure 5-9, there was a slight difference in the energy delivered because of the addition of PCM in the plasterboard. In the charging time, the gypsum plasterboard provided higher energy delivered since it stored the heat as sensible energy which was released in a shorter time (Figure 5-9). However, the PCM-gypsum plasterboard stored the extra heat from the plenum as latent heat due to the function of the PCM. It also produced a larger amount of useful energy for a longer time, roughly more than 3 hours, because it released the stored latent heat, which still provided more generated energy than the gypsum plasterboard during the discharging period. In particular, the building envelope with the PCM-plasterboard provided 10W/s higher output energy than the one with gypsum plasterboard due to the additional PCM (Figure 5-9). In this study, the PCM-gypsum plasterboard was not storing a huge amount of energy due to the lesser amount of PCM used in the PCM-gypsum plasterboard. It was designed to capture and store limited amounts of additional extra energy from the plenum rather than storing lots of energy because of the perspective of this research. However, it can be acknowledged that increasing the amount of PCM enables more energy to be stored. It was specifically focused on the charging/discharging process of the PCM-gypsum plasterboard, as shown in Figure 5-10 and Figure 5-11, respectively.

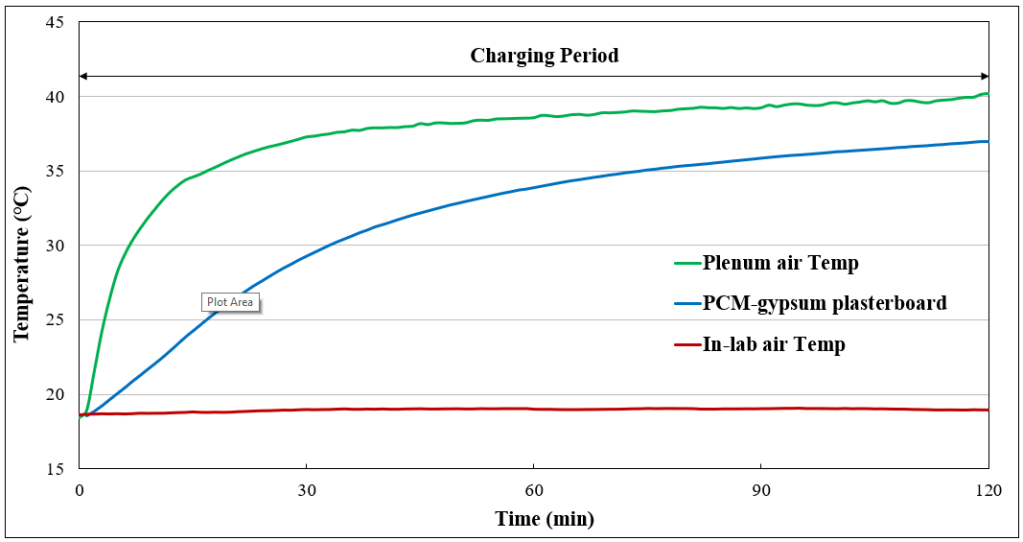

Figure 5-10. Temperature distribution during the charging period for the building envelope with PCM-gypsum plasterboard

The charging period for the PCM-plasterboard and the process included 3 stages: (i) solid-state (storing sensible heat); (ii) mixture (storing latent and sensible heat during the melting); and (iii), liquid state (storing sensible heat). 15 minutes after turning on the lights, the plenum air temperature grew rapidly while the PCM-gypsum plasterboard temperature increased dramatically within 60 mins. In this period, the PCM enhanced gypsum plasterboard stored sensible heat through the gypsum and PCM components. Furthermore, the PCM-gypsum plasterboard temperature became relatively steady and increased slightly after 60 mins. when the melting process was fully completed. Hence, the PCM's phase changed into a liquid state after 60 minutes and reached the maximum temperature of 36.2°C. However, the temperature rise was not dramatically quick compared to the plenum air temperature in the second half of the charging period, which showed the melting phenomenon was happening and was storing latent heat due to the addition of the PCM (Figure 5-10).

However, according to Figure 5-11, the PCM-gypsum temperature decreased slowly rather than the plenum air temperature. For instance, the plenum air temperature went

down quickly within 15 mins of the lighting being off and the PCM-gypsum plasterboard went down slowly and in return kept the plenum air temperature slightly at a constant temperature by releasing its stored heat for a longer period. The PCM-plasterboard with the sensible heat of the gypsum and the PCM components discharged quickly within 30 minutes, then the solidification of the PCM-gypsum plasterboard started. The solidification process continued for roughly 180 minutes when the solidification phenomenon was finished (Figure 5-11).

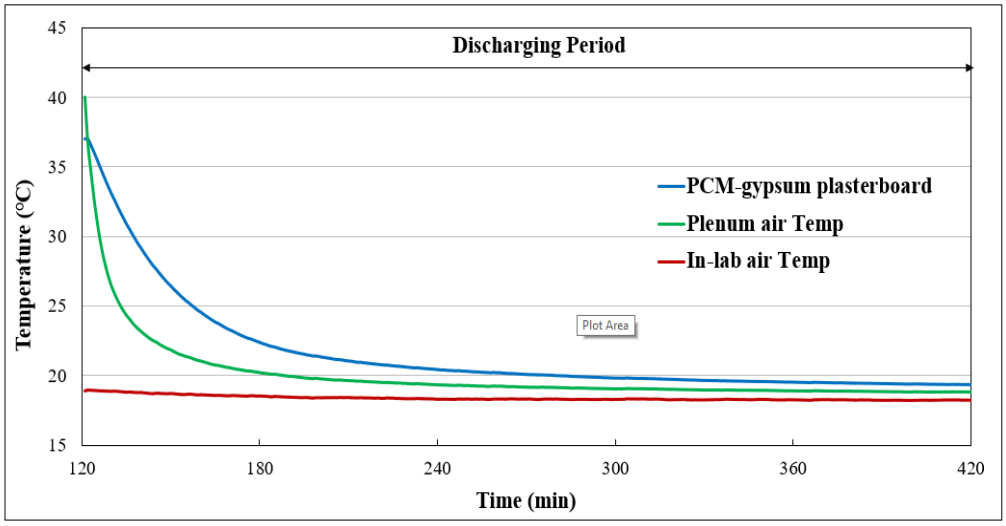

Figure 5-11. Temperature distribution during the discharging period for the building envelope with PCM-gypsum plasterboard

According to the above results analysis and discussion, it can be concluded that the PCM-gypsum plasterboard enables a higher thermal performance of the building envelope to be generated with the additional benefit of using a PCM, although the benefits were not great because of the limited usage of the PCM. During this study, it was intended to store a lesser amount of energy, especially when lots of energy is not required to be delivered into the built environment.

In addition, the heat transfer coefficient was calculated through using the mathematical equation stated in section 3.3.3. The parameters for this case were approach velocity

with 0.1m/s, inlet temperature at 18℃, plate temperature at 52℃ (which was equal to a solar intensity of 600W/m^2), plenum size (250mm), circular hole dimension (1mm), and pitch size 20mm). The various heat transfer coefficient results are shown in Table 5-9.

Table 5-9. The heat transfer coefficient during the charging period

Type of heat transfer coefficient		With PCM-gypsum plasterboard	With gypsum plasterboard
Convection heat transfer coefficient (W/m^2K)	Absorber plate to plenum air	12.9	12.9
	Plenum air to plasterboard	4.1	4.1
Radiation heat transfer coefficient (W/m^2K)	Absorber plate to plasterboard	6.34	6.13
	Absorber plate to the surrounding environment	4.5	4.5

According to Table 5-9, it can be seen that the convective heat transfer coefficient for the building envelopes with gypsum plasterboard and PCM-gypsum plasterboard claimed the same values (12.9 W/m^2K), since the plenum air velocity driving the convective heat transfer process was same for both cases because of the same operational conditions. However, the radiative heat transfer coefficient varied at 6.34 and 6.13W/m^2K separately, due to the different surface roughness of the PCM-gypsum plasterboard and the gypsum plasterboard. Meanwhile, the radiative heat transfer from the absorber plate to the surrounding environment was achieved as 4.5W/m^2K for both cases since the parameter values were unchanged. However, the convection heat

transfer through the corrugated plate to the surrounding environment was ignored, since the experimental work was carried out in an in-lab environment where the wind effect was not considered. Hence, the heat transfer coefficient results could indicate that the effects of different plasterboards vary.

According to the results in this section, it can be concluded that the impact of PCM-gypsum plasterboard could achieve different outlet temperatures, delivered energy and stored energy. These results highlighted the advantages of using PCM-gypsum plasterboard rather than gypsum plasterboard. It is also important to analyse the impact of the airflow rate, plenum size and pitch size on building envelope performance. In order to further analyse the additional benefits of this building envelope with PCM-gypsum plasterboard, the influence of these main parameters on building envelope performance were investigated using the PCM-gypsum plasterboard.

5.8.2 *Impact of airflow rate on thermal performance*

Firstly, the influence of airflow rate on the outlet temperature and the charging/discharging processes were explained for the three different airflow rates (10, 30, 50m^3/hr). Other parameters were inlet temperature (18°C), a solar intensity of 600W/m^2, plenum size (140mm), circular hole diameter (1mm) and pitch size (20mm). Figure 5-12 shows the impact of the three airflow rates on the PCM-gypsum plasterboard temperature. An airflow rate of 10 m^3/hr would allow the PCM-gypsum plasterboard to claim the highest temperature among these three different airflow rates. For instance, the airflow rates of 10 and 50m^3/hr generated higher PCM-gypsum plasterboard temperatures of 42°C and 35°C, respectively (Figure 5-12). The airflow rate of 10 and 50m^3/hr respectively released the stored heat loss within 2 hours and 1 hour separately during the period of discharging. It can be indicated that the airflow rate has a significant impact on the charging/discharging processes.

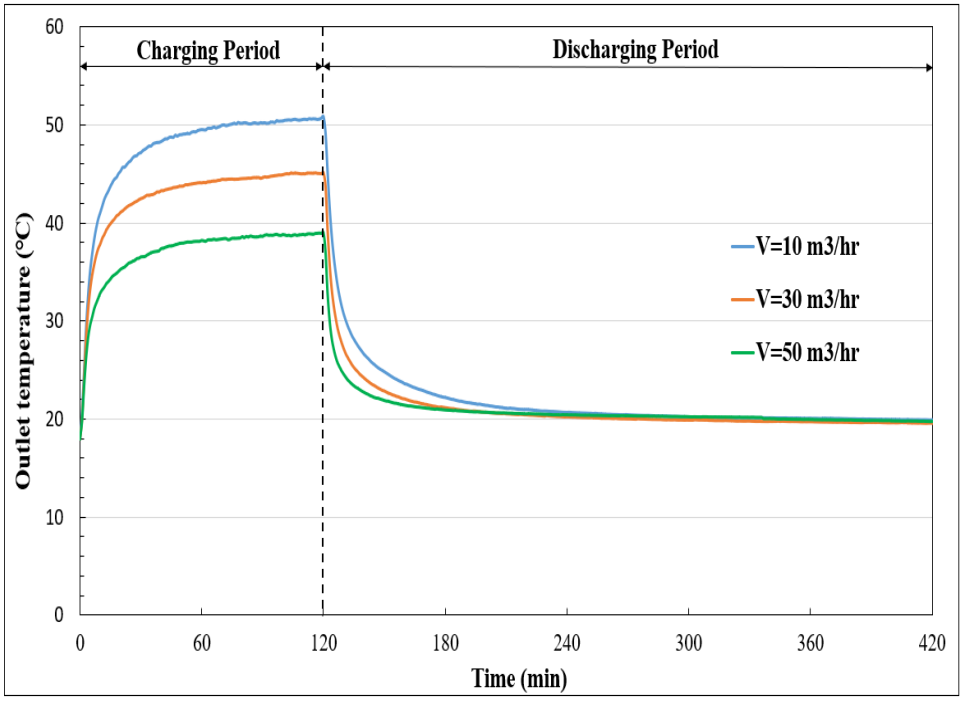

Figure 5-12. The PCM-gypsum plasterboard temperature distribution under various airflow rates for the building envelope with PCM-gypsum plasterboard

It was also important to examine the effect of airflow rate on outlet temperature. A high airflow rate of 50m^3/hr generated an outlet temperature of roughly 39℃ and the low airflow rate of 10m^3/hr claimed the highest outlet temperature of 50.5℃ during the period of lighting-on (Figure 5-13). For the discharging process (switching off the lights), an airflow rate of 10m^3/hr could provide a higher outlet temperature of more than 20℃ for over 2 hours. In the meantime, an airflow rate of 50m^3/hr took only half an hour to make the outlet temperature less than 20℃ (Figure 5-13). Hence, the lower airflow rate provided a higher outlet temperature for a longer period. It can be indicated the airflow rate of 10m^3/hr achieved the highest outlet temperature and the longest energy releasing time during the charging/discharging processes, respectively.

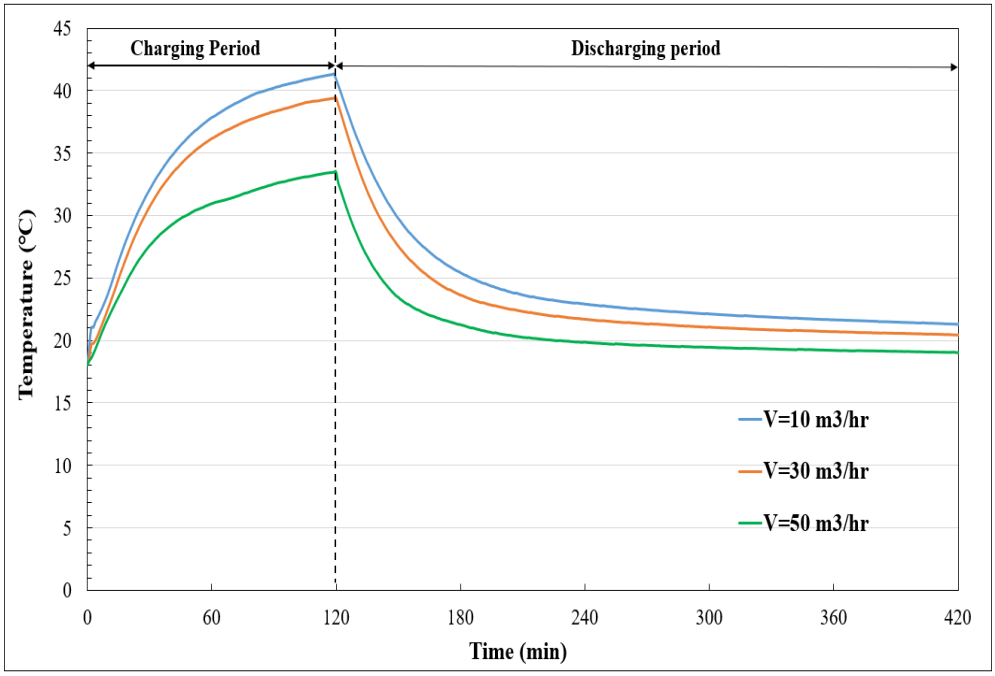

Figure 5-13. The outlet temperature profile under various airflow rates for the building envelope with PCM-gypsum plasterboard

In addition, the effect of the airflow rate on heat exchange effectiveness (HEE) and air temperature rise for the lighting on period was demonstrated under three different airflow rates. The HEE average of 0.7 and 0.5 was achieved respectively by the airflow rate (Figure 5-14), which indicated that airflow has a strong impact on HEE. In terms of air temperature rise, the airflow rates of 10 and 50m^3/hr provided an air temperature rise of roughly 32℃ and 20℃, separately. Hence, the airflow rate greatly influences collector heat exchange effectiveness as well. However, the HEE claimed a constant value after approximately one-hour of lights-on until they were switched off. Figure 5-14 also shows that increasing the airflow rate could deliver a higher collector efficiency. For instance, the collector efficiency was achieved at approximately 40%, 55% and 75% under airflow rates of 10, 30, and 50m^3/hr, respectively (Figure 5-14). It can be concluded that the collector efficiency increases with an increasing airflow rate, as the airflow rate is the key factor rather than the air temperature rise when it comes to calculating the efficiency.

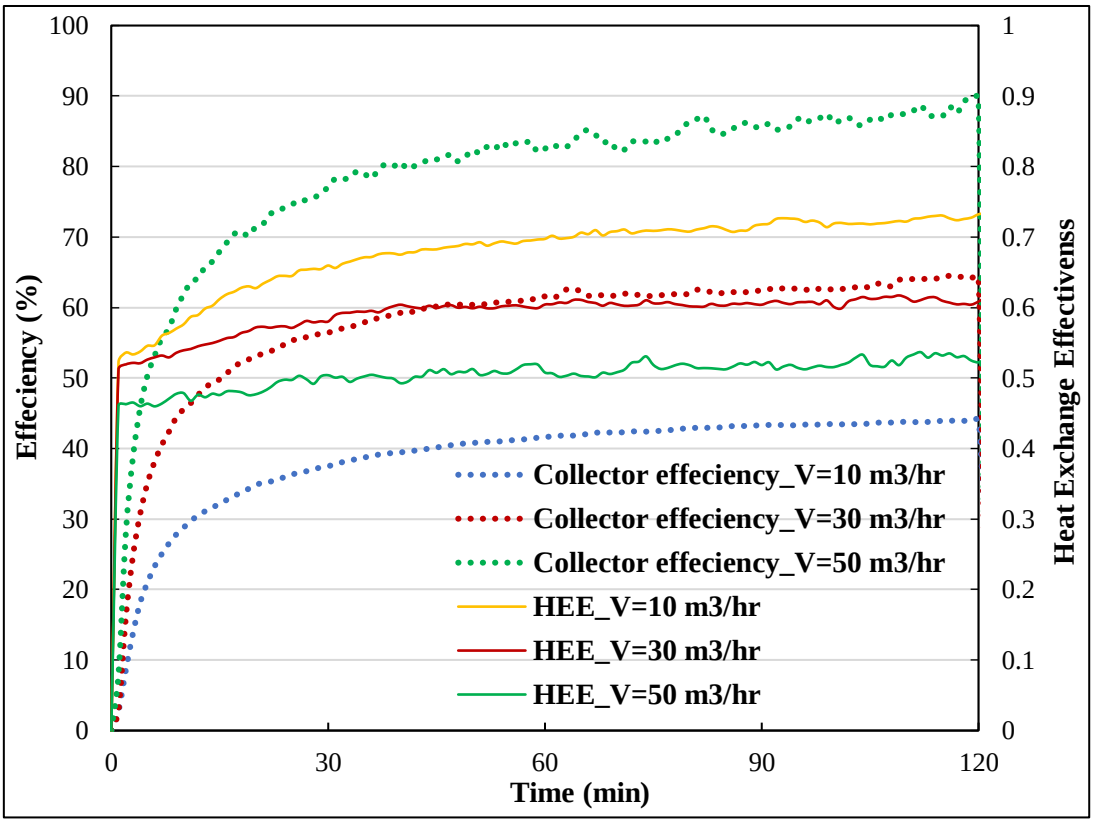

Figure 5-14. Impact of the airflow rate on collector efficiency and heat transfer effectiveness for the building envelope with PCM-gypsum plasterboard

Figure 5-12 and Figure 5-12 demonstrate that reducing the airflow rate could achieve a higher outlet and PCM-gypsum plasterboard temperature, which would store a greater amount of energy in the plasterboard. Thus, the results in Figure 5-14 explain that increasing the airflow rate reduces the heat exchange effectiveness. However, collector efficiency would see an increase with increasing the airflow rate, since the airflow rate is the key factor rather than air temperature rise when it comes to calculating efficiency. In particular, it can be believed that the impact of airflow rate on HEE and collector efficiency are significant.

5.8.3 *Impact of plenum size on thermal performance*

In this study, the investigation was undertaken for three different plenum sizes (140, 200, 250mm) to analyse the influence of plenum size on thermal performance. Other

parameters were inlet temperature (18℃), a solar intensity of 600W/m^2, airflow rate (10m^3/hr), circular hole diameter (1mm), and pitch size 20mm. The experimental outcome displayed that reducing the plenum thickness could achieve a higher PCM-gypsum plasterboard temperature. For example, a plenum size of 140mm gave 35℃ for the charging and 20℃ for the discharging processes within 3 hours after the lighting was off. In the meantime, a plenum size of 250mm generated a PCM-gypsum plasterboard temperature of 32℃ but was down to 20℃ for the solidification process of the PCM-gypsum plasterboard after 60 mins of the lighting being off (**Error! Reference source not found.**). Hence, a smaller plenum size enables higher energy storage to be provided, that could be released for a longer period of later use.

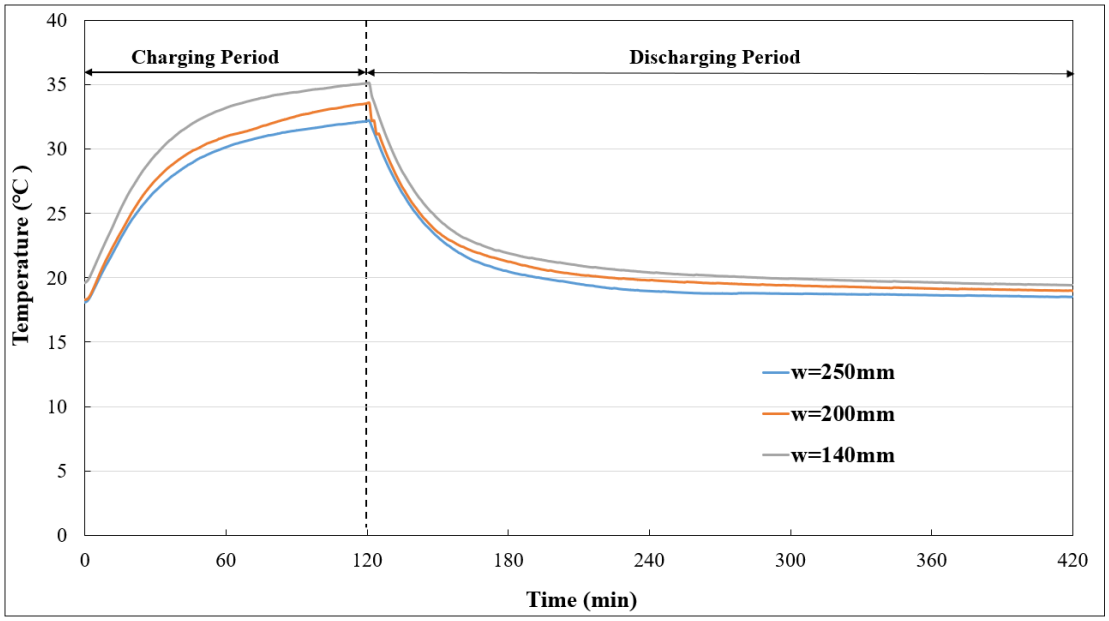

Figure 5-15. PCM-gypsum plasterboard inside temperature under various plenum thicknesses for the building envelope with PCM-gypsum plasterboard

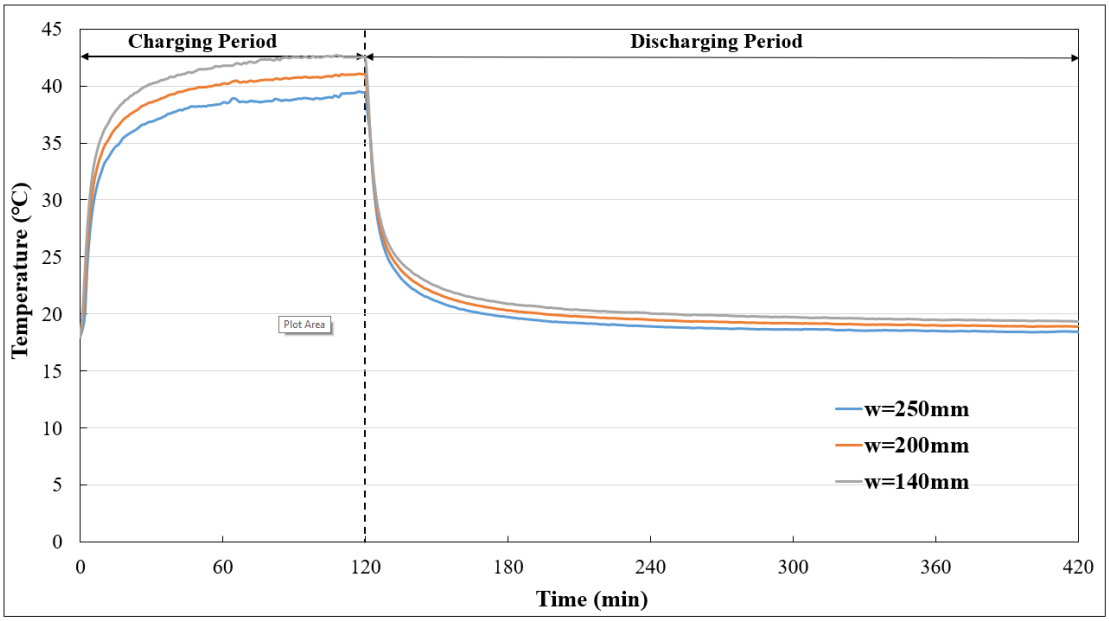

Figure 5-16 . Outlet temperature under various plenum thicknesses for the building envelope with PCM-gypsum plasterboard

Similarly, a smaller plenum size enabled a higher outlet temperature to be provided. A lower outlet temperature could be obtained for higher plenum thicknesses under the same operational conditions. For instance, a plenum size of 140 and 250mm provided outlet temperatures of 38℃ and 33℃ respectively during the charging period (Figure 5-16**Error! Reference source not found.**). In particular, during the lighting-on time, a plenum size of 1400mm could generate a 5℃ higher outlet temperature than a plenum size of 250mm. According to Figure 5-16**Error! Reference source not found.**, it can also be indicated that shrinking the plenum thickness increases the exit temperature for a longer period even during the discharging process. For instance, during the lighting off period, a plenum size of 1400mm could offer more than 20℃ of outlet temperature for 2 hours, while, a plenum thickness of 250mm could provide an outlet temperature higher than 20℃ for roughly 45 mins (Figure 5-16**Error! Reference source not found.**). However, this might vary due to the significant influence of the airflow rate.

Additionally, the plenum size impacts in terms of air temperature rise, heat exchange effectiveness, and collector efficiency. Figure 5-17 shows reducing the plenum thickness increases the air temperature rise, collector efficiency and heat exchange effectiveness (HEE). For instance, the HEE between two plenum thicknesses (140 and 250mm) averages 0.54 and 0.46 (Figure 5-17). According to the calculation, the difference in collector efficiency among various type of plenum size is limited, for instance, the collector efficiency for three various plenum widths achieved similar values with marginal differences. Furthermore, it can be established that increasing the thickness of the plenum size provided the lowest air temperature rise, collector efficiency and HEE. Accordingly, it can be known that the influence of plenum size on the building envelope performance was limited compared to the impact of the airflow rate, which was mentioned above.

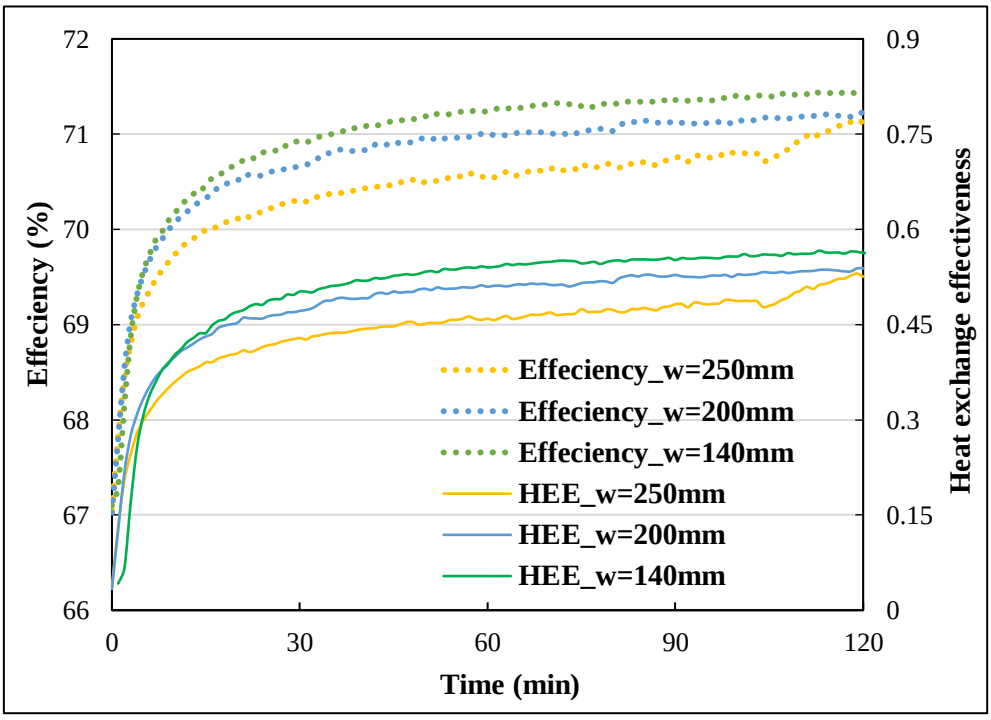

Figure 5-17. Influence of plenum size on collector efficiency and HHE for the building envelope with PCM-gypsum plasterboard

5.8.4 *Impact of pitch size on thermal performance*

The experimental work was undertaken with two different pitch sizes (20 and 25mm) under the same in-lab environment to find out the influence of pitch size on the thermal performance of this proposed building envelope. Meanwhile, other parameters were inlet temperature (18℃), a solar intensity of 600W/m^2, airflow rate (10m^3/hr), circular hole diameter (1mm), and a plenum size of 140mm. Figure 5-18 shows the outlet temperature results for two different pitch sizes for the charging/discharging processes. It can easily be seen that the impact of pitch size is not obvious since the outlet temperature trends are similar and the difference is limited. For instance, the pitch dimensions of 20 and 25mm achieved outlet temperatures of 40 and 38.7 ℃ during the charging period, respectively (Figure 5-18). During the discharging period, the pitch size of 25mm provided a higher outlet temperature by roughly 1 degree Celsius. Therefore, it can indicate the impact of pitch size on collector efficiency and heat exchange effectiveness.

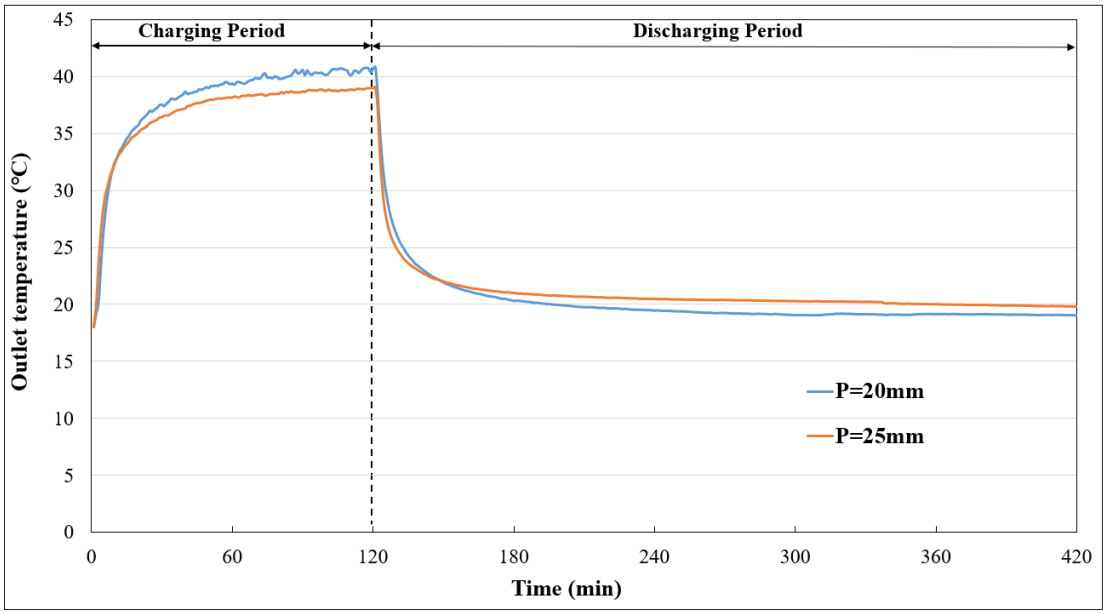

Figure 5-18. Impact of pitch dimension on outlet temperature for the building envelope with PCM-gypsum plasterboard

Also, the experimental results presented in Figure 5-18 could indicate that the pitch sizes of 20mm and 25mm offered higher air temperature rises of 22℃ and 20℃ separately. Thus, a pitch size of 20mm enables a higher air temperature rise to be provided. The impact of pitch size on collector efficiency and heat exchange effectiveness is displayed in Figure 5-19.

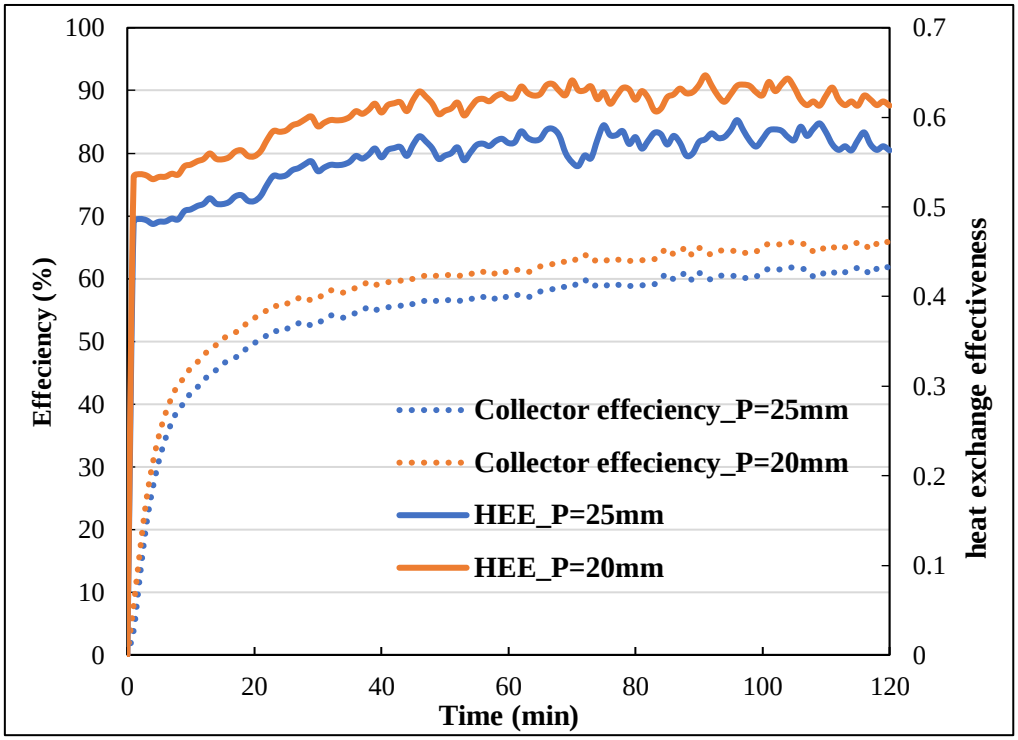

Figure 5-19. Influence of pitch size on collector efficiency and HEE for the building envelope with PCM-gypsum plasterboard

According to Figure 5-19, pitch sizes of 20mm and 25mm had a heat exchange effectiveness of approximately 0.62 and 0.57, respectively. For a constant airflow, increasing the pitch dimension could reduce the HEE as the increasing perforation pitch size from 20mm to 25mm brought a 6.5% decrease in HEE (Figure 5-19). According to the results, it was stated that the larger pitch size reduces the collector efficiency, for instance, an 8% reduction can be obtained from increasing the pitch size from 20mm to 25mm according to the calculation. However, it can be indicated that the influence of pitch design is partial, especially in terms of collector efficiency. Therefore, the results

in Figure 5-18 and Figure 5-19 demonstrated that the impact of pitch dimension is limited in terms of outlet temperature, collector efficiency and HEE. However, the influence of pitch size is likely to be negligible and it might vary when the collector area is greater.

5.9 **Conclusions**

The experimental work was conducted to investigate the performance of the proposed building envelope with PCM-gypsum plasterboard. The results showed that the PCM-gypsum plasterboard stored a certain amount of energy due to the advantages of additional PCM that stored heat during the charging period and released it during the discharging process. However, due to the limited addition of the PCM, the PCM-gypsum plasterboard displayed slight changes in terms of outlet temperature and generated energy. For instance, during the experiment, the PCM-gypsum plasterboard was fully melted after 1 hour of lighting on, where its temperature increased slowly and released the stored heat for 3 hours after turning the lights off.

The effect of airflow rate on building envelope performance were described, including heat exchange effectiveness, air temperature rise, and PCM-gypsum plasterboard charging/discharging behaviours. For instance, a low airflow rate of 10m3/hr could provide a higher outlet temperature of more than 20℃ for over 2 hours. In the meantime, a high airflow rate of 50m3/hr took only half an hour with an outlet temperature of less than 20℃. The lowest air temperature rise and HEE averaged 15℃ and 0.5 respectively, when the experiment ran under the highest airflow rate of 50m^3/hr. On the contrary, the highest HEE of 0.7 can be claimed due to a low airflow rate of 10m^3/hr, which achieved an air temperature rise of 30℃. According to the above results, it can be indicated that airflow has a strong impact on air temperature rise and HEE. In addition, the increased airflow rate decreased the PCM-gypsum plasterboard's temperature as the airflow rates of 10m^3/hr and 50m^3/hr generated higher PCM-gypsum

plasterboard temperatures of 42 and 35℃, respectively. However, during the discharging process of the PCM-gypsum plasterboard, an airflow rate of 10m^3/hr presented the longest time for releasing the stored energy at 2 hours and the airflow rate of 50m^3/hr released the energy stored inside the PCM-gypsum plasterboard for just 1 hour.

Regarding the effect of plenum size, the smaller plenum thickness (plenum size_140mm) generated 35℃ for the charging and 20℃ for the discharging processes within 3 hours. In the meantime, a plenum size of 250mm generated a PCM-gypsum plasterboard temperature of 32℃, but was down to 20℃ for the solidification process of PCM-gypsum plasterboard after 60 mins of lighting-off. Hence, it can be indicated that a wider plenum size stored limited energy that would be released over a longer period for later use. Plenum sizes of 250 and 140mm provided outlet temperatures of 33℃ and 38℃ respectively, during the lighting's on and off periods. During the charging state, a plenum size of 140mm could generate a 5℃ higher outlet temperature than a plenum size of 250mm. Hence, it can also be indicated that increasing the plenum thickness better achieves a lower exit temperature. Meanwhile, it could provide a higher outlet temperature for a longer period even after the lights were switched off. For instance, during the lighting-off period, a plenum size of 140mm could offer more than 20℃ of outlet temperature for 2 hours, while a plenum thickness of 250mm could provide an outlet temperature higher than 20℃ for roughly 45mins. Lastly, the air temperature rise slightly increased with reducing the plenum thickness as the air temperature rise was less among the three various plenum widths. For instance, plenum thicknesses of 140mm and 250mm were able to provide air temperature rises of 18 and 16℃, respectively. HEE also showed an increasing trend with reducing the plenum width. For instance, the HEE was achieved by two plenum thicknesses of 140 and 250mm and 0.54 and 0.46, respectively. It can be indicated that differences in collector efficiency among various types of plenum size is limited. For instance, plenum sizes of

200 and 250mm achieved 70.5% and 71% collector efficiency, respectively. The tightest plenum size of 140mm claimed the lowest collector efficiency averaged at 71.5% during the experiment. Furthermore, the lower thickness of plenum size provided the highest air temperature rise, collector efficiency and HEE. However, the influence of plenum size was limited compared to the impact of the airflow rate, which was mentioned above.

The impact of pitch size was also studied, and the results showed that pitch sizes of 25 and 20mm offered air temperature rises at 20℃ and 22℃ separately. Secondly, a pitch size of 20mm enabled a higher air temperature rise of 2℃ to be provided. Pitch sizes of 20 and 25mm generated a heat exchange effectiveness of approximately 0.62 and 0.57, respectively. For a constant airflow, increasing the pitch dimension could reduce the HEE as increasing the perforation pitch size from 20mm to 25mm had a 6.5% and 8% reduction in HEE and collector efficiency, respectively. The results estimated that that the influence of pitch design on the thermal performance of this building envelope is partial, especially in terms of efficiency.

However, the data for these experiments were used to validate a CFD model developed to further investigate the performance of CRBE in terms of various impacts of different parameters.

Chapter 6. **Modelling of the transpired solar collector with PCM-gypsum plasterboard**

6.1 **Introduction**

This chapter introduces a numerical approach with the procedure of computational fluid dynamics (CFD) modelling to numerically investigate the building envelope's performance. These were setting up the boundary conditions, material selection, turbulence model and determining relative equations for the proposed building envelope performance. A parametric study was done through a numerical investigation to acknowledge the influence of various parameters on building envelope performance in terms of outlet temperature, heat exchange effectiveness and delivered energy. The academic version of ANSYS Fluent 19.1 was used for the simulations. Meanwhile, the selection of various boundary conditions will be justified and their impact on building envelope performance discussed. Besides, the meshing independence study is studied in this chapter in order to find out the optimal meshing method. In addition, the numerical results focus on the effects of approach velocity, plate temperature and inlet temperature on the building envelope's performance. This chapter also highlights building envelope performance with/without PCM-gypsum plasterboard in simulation cases.

6.2 **Background**

Due to the advantages and demands on energy research, the building envelope combining the transpired solar collector (TSC) and the phase change material (PCM) board has attracted scholars' interest and there has been a lot of research done to improve its performance and commercial implementation both experimentally and numerically. Firstly, the thermal behaviour and heat transfer behaviour of this type of building envelope are complex and uncertain, due to the thermal behaviour of the PCM

and temperature variations in time across the building envelope. It is problematic and even difficult to achieve a precise solution through an experimental approach to address the issues that include nonlinear material behaviour and the complex dynamic thermal performance of a system, as experimental investigation demands a long period of working hours, high costs and a certain research environment with expensive instruments and assistance from qualified professionals (Ellobody, Feng and Young 2014). However, the numerical work enables research costs to be cut and reduce the time consumption by reducing computational spending and research hours (Gantenbein and Rindt 2012). In terms of the numerical method, scholars have used various software/methods to study the flow problems including PCM charging/discharging like ANSYS Fluent Software (Koller, Walter and Hameter 2016; Al-Maghalseh 2017; Giovannelli and Bashir 2017a; Youssef, Ge and Tassou 2018), COMSOL (Petrone, Cammarata and Doria 2012), ESP-r (Heim and Clarke 2004), TRNSYS (Ponshanmugakumar et al. no date; Gowreesunker, Tassou and Kolokotroni 2013), and STAR-CCM + (Torlak, Teskeredzic and Delalic 2013; Durakovic and Torlak, 2016). According to recent studies, it can be indicated that Computational Fluid Dynamic (CFD) ANSYS Fluent software has been commonly used to investigate the performance of the PCM charging and discharging phenomena (Gowreesunker, Tassou and Kolokotroni 2013; Youssef, Ge and Tassou 2018). Meanwhile, in terms of approaches to studying PCM charging and discharging behaviours, researchers have stated some approaches to simulate the heat transfer phenomenon across the phase change such as the enthalpy method, the heat capacity method, the temperature transforming model and the heat source method (Al-Saadi and Zhai 2013). A paper has reviewed the advantages and limitations of each mathematical model and concluded that enthalpy is better to numerically investigate phase change behaviour in terms of efficient computing, accurate modelling and flexibility (Al-Saadi and Zhai 2013). The enthalpy method is a modest and effective approach to solve dynamic/moving boundary conditions problems related to PCM charging and discharging (Srinivas Shastri and

Allen 1998). This technique has been popularly applied over the years to the study of PCM melting and solidification phenomena by explaining the latent heat in the energy equations (Lappa 2004). The enthalpy method has been widely used in many research studies (Heim and Clarke 2004; Lamberg, Lehtiniemi and Henell 2004; Zhang, Fung and Siddiqui 2007; Gowreesunker, Tassou and Kolokotroni 2012; Darkwa and Su 2013; Thiele, Sant and Pilon 2015; Giovannelli and Bashir 2017b), as it makes the phase change issue easy to be solved due to the following benefits (Sarbu and Sebarchievici 2017):

a) The governing equation is comparable to the single-phase equation;

b) There is no disorder to be satisfied at the solid-liquid interface as it automatically obeys the interface condition;

c) A mushy (mixture) zone can exist between two phases in the enthalpy formulation;

The heat transfer in the PCM-gypsum plasterboard by convection was negligible compared to the heat transfer due to conduction;

d) The density and enthalpy (latent heat) of the PCM in both phases were constant, independent with temperature, but different for the solid and liquid states;

e) Both the solid as well as the liquid phase are homogeneous and isotropic and the melting process is symmetric within a segment;

f) The chemical composition in the liquid phase of a PCM is an incompressible and Newtonian fluid;

g) The volume change upon phase change is ignored;

h) The laminar flow is set for the melting process of the PCM as Newtonian fluid is assumed;

i) The solid is homogeneously distributed in the mushy region;

j) It is assumed that the PCM has an ideal solidification behaviour. Therefore, the sub-cooling effects are neglected and the solidification temperature is constant.

ANSYS Fluent R19 was used for this numerical study. The experimental specimen's geometries followed a principle of heat transfer alongside the plenum considering the assumptions in the model. 2D modelling was also adopted to reduce the computational time and allow for more refinement and better precision. Lastly, the melting and solidification model through the enthalpy method was used to analyse the phase change behaviour of the PCM-gypsum plasterboard.

6.3 **CFD simulation procedure**

CFD modelling has been one the most recognised methods to simulate heat transfer and flow problems in recent years and it has been widely used in academic research and at a commercial level, due to the following advantages:

a) It provides a quick but precise solution for experimental validation and numerical research;
b) It presents a clear image and inclusive information compared to the analytical and experimental approach;
c) It can calculate and visualise different physical behaviours (fluid dynamics, heat/mass transfer, phase change) on a certain scale with low cost spending and minimum time consumption.

Meanwhile, the accuracy of CFD results depends on the boundary conditions and model selection, solver equations and computer power. Experimental data was used to accomplish the boundary conditions, which provided more accurate numerical findings in this numerical study. Hence, the CFD package ANSYS Fluent was used in this numerical investigation. The procedure can be divided into three steps: pre-processor,

solver, and post processer. The stages related to the CFD technique are shown in Figure 6-1.

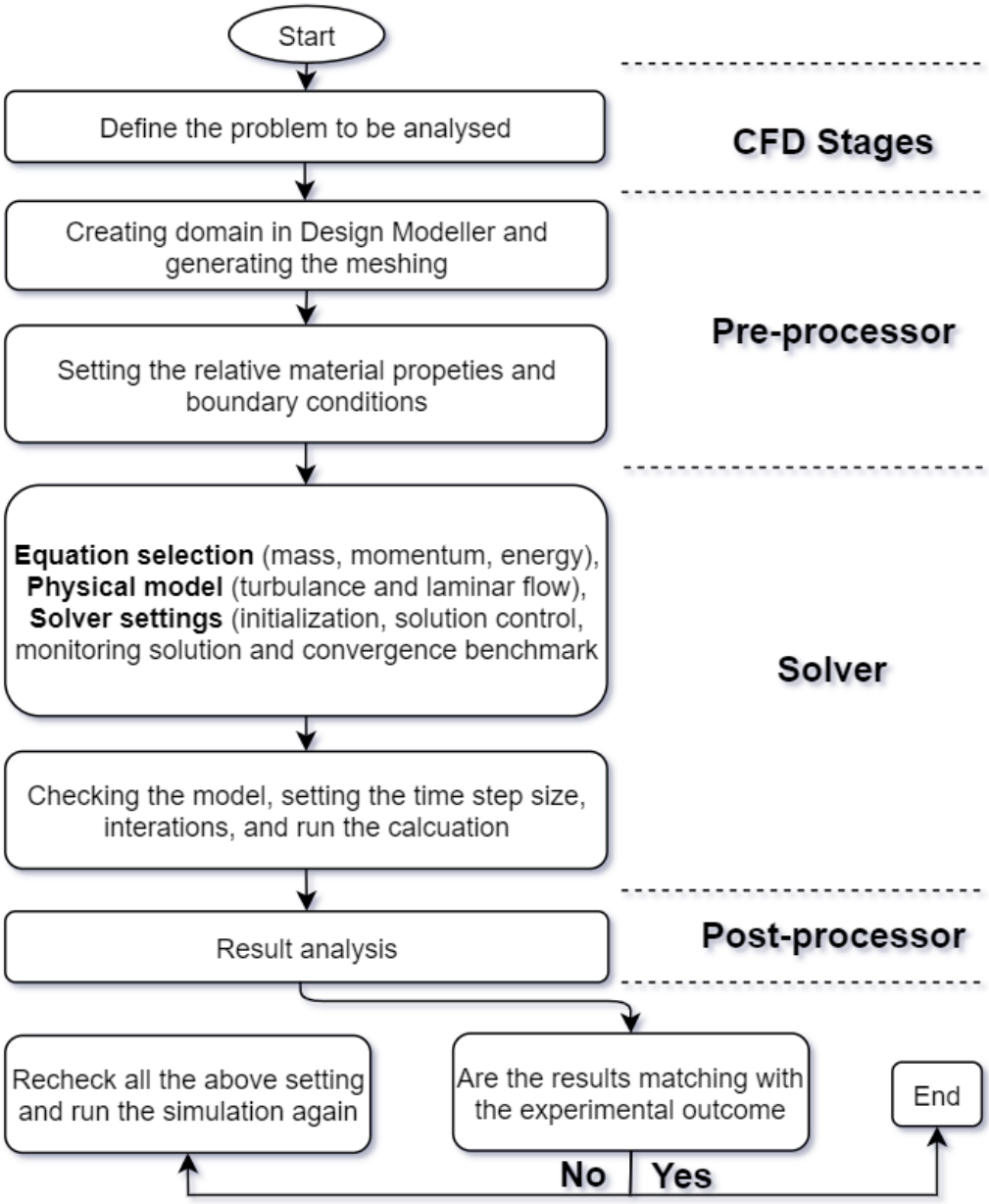

Figure 6-1. CFD procedure

At the end of the result-evaluation section, the simulation is finished if the numerical results match with the experimental outcome, otherwise the numerical modelling can be improved by developing the mesh quality and double-checking the solver process including equation selection, material properties, initialisation, solution control,

monitoring the selection and convergence in order to achieve good quality numerical results. Once the proper meshing method has been selected, further numerical modelling is verified and validated accordingly and the finalised mode is used to investigate the building envelope's performance and the charging/discharging phenomena of the PCM-gypsum plasterboard. The heat transfer, flow problem and charging/discharging across the experimental platform follow a principle of invariance along the horizontal and vertical directions of the plenum, considering the assumptions in the model.

6.4 **The geometry of the CFD domain**

The physical domain of the model was recreated in ANSYS Fluent software to capture multi-scale fluid flow behaviours over the absorber plate, within the perforated holes, through the air cavity (plenum) and the charging/discharging of the PCM-gypsum plasterboard. For the geometrical design of the model, a very small size of perforation holes with a diameter of $1mm$ over the large absorber plate by a dimension of $1m \times 1m$ could bring up a multi-scale geometry, with a 10mm thickness of PCM-gypsum plasterboard at the back (Figure 6-2).

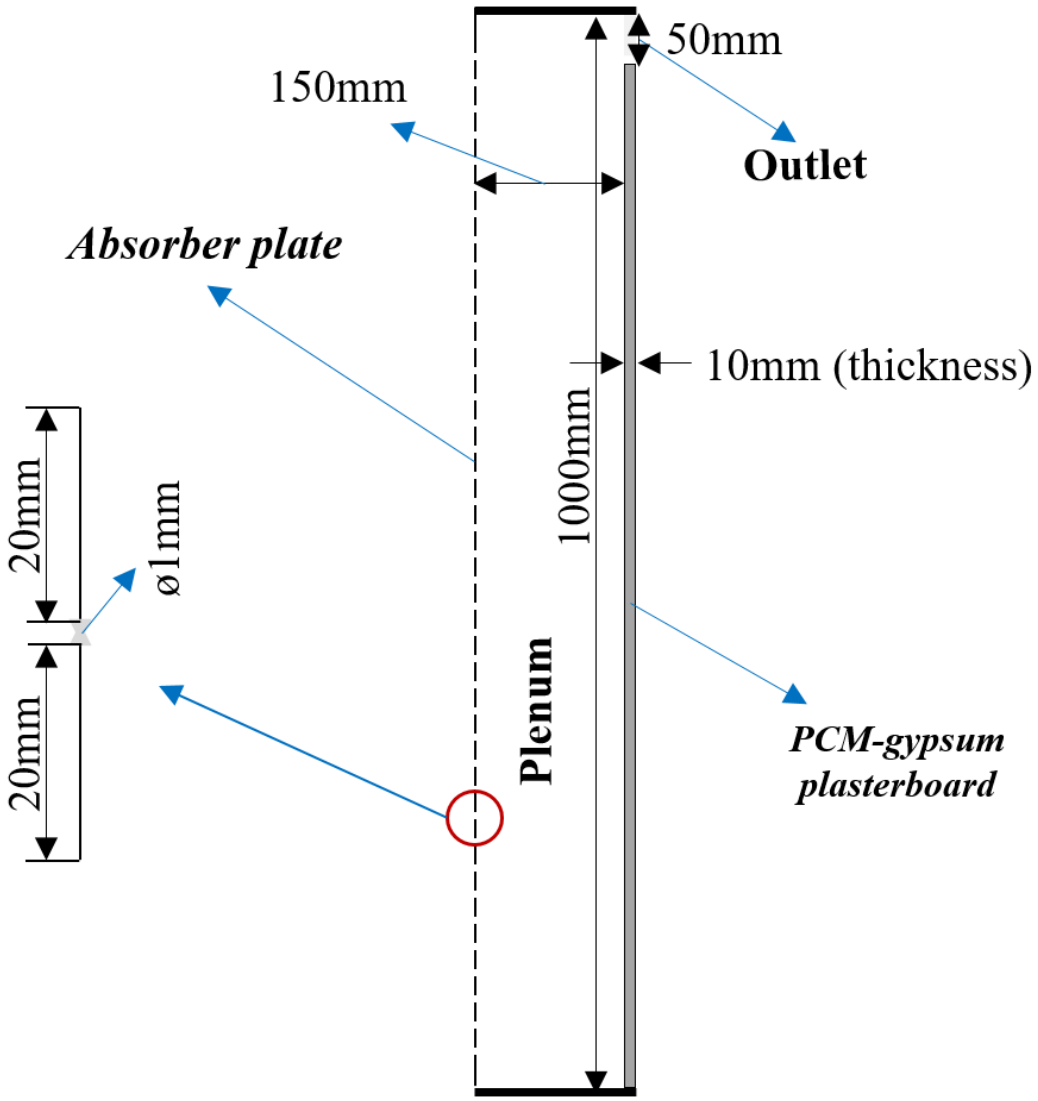

Figure 6-2. The physical domain of the model

6.5 **Method of meshing**

The Finite Element Method (FEM) creates a predictive computational model of the real-world case and reduces the degree of freedom from infinite to finite with the help of meshing (Reddy and Gartling 2010). Meshing enables making the heat transfer and fluid problem solvable via the finite elements that can break up the CFD models into subdomains (representing an element), where the equations are solved with higher accuracy. These equations roughly describe the governing equation of interest via a group of polynomial functions defined over each element. It is agreed that the CFD

solution will present the true solution which is close to the real-world scenarios through meshing refinement with smaller elements. Hence, in this numerical modelling, the geometry was built in the ANSYS 19R.1 and the meshing, including refined meshing, was created. The meshing included a refined mesh in the hole section where more complicated and fluid-structure and heat transfer phenomena occurred, and the mesh refinement was defined via varying all the mesh sizes by the same ratio. The three meshes resolutions denominated as coarse, medium, and fine were created as shown in Figure 6-3. Table 6-1 lists the three meshes used to investigate the experimental validation to determine the final meshing method for further numerical investigations.

Table 6-1. Cases of CFD simulations

Meshing	Nodes	Elements
Coarse	269427	263794
Medium	424757	416162
Fine	581971	500078

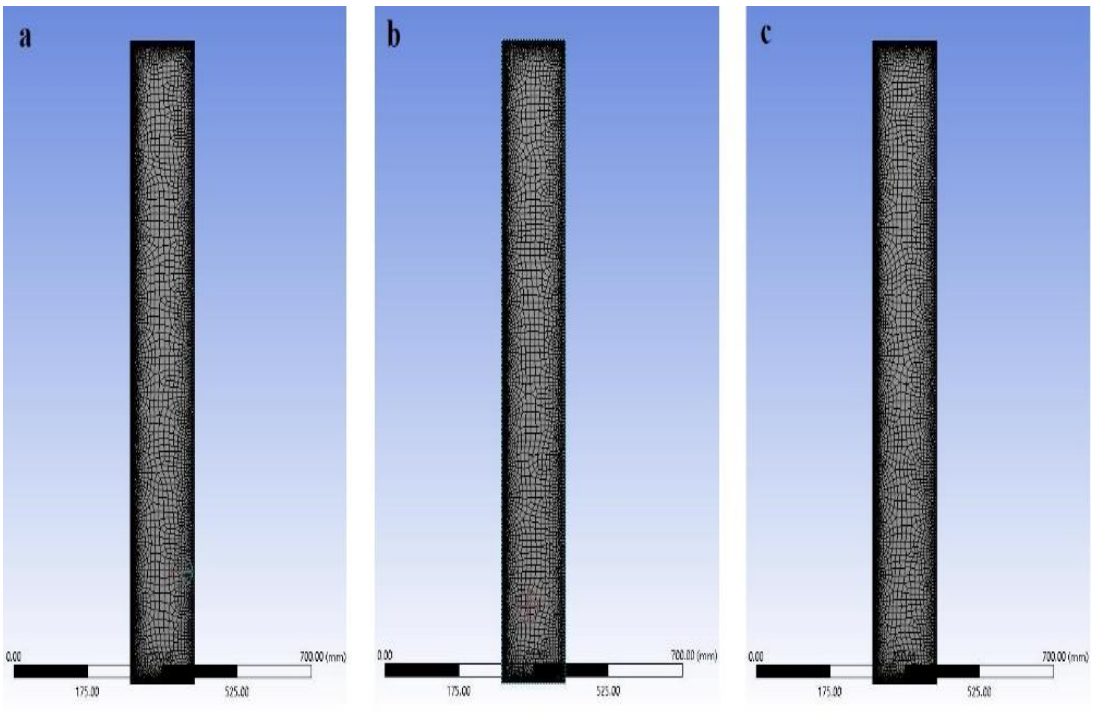

Figure 6-3. Computational meshes: a) coarse mesh (3701 elements), b) medium mesh (12160 elements) and c) fine mesh (48460 elements)

In order to select the optimal meshing method for the numerical study, the effects of various meshing approaches were analysed and evaluated. This procedure was conducted by comparing the experimental and numerical outlet temperatures. Various numerical modellings were operated with three different meshing approaches (coarse, medium, fine) for the chosen experimental conditions with an in-lab temperature of 18°C, a plate temperature of 55° and an approach velocity of 0.01m/s. In the first place, the transient solution model was chosen with relative turbulence and energy equations. The solution was calculated for a 2 hour charging period. Also, the RNG k-ε model was selected to be applied to this numerical study. The RNG k-ε model was developed using Re-Normalisation Group (RNG) methods to renormalise the Navier-Stokes equations, to account for the effects of smaller scales of motion (Yakhot et al. 1992).

Figure 6-4 and Figure 6-5 present the numerical plenum and outlet temperature profile for the three meshing methods (coarse, medium and fine), respectively. It could be

found that the numerical plenum temperature achieved a similar trend as the experimental plenum temperature. However, the average error between numerical plenum temperature and experimental plenum temperature varied among the three meshing methods. For instance, the fine mesh had the lowest error of 3.3%, meanwhile, the coarse and medium meshing claimed roughly 7% and 5.3% average errors.

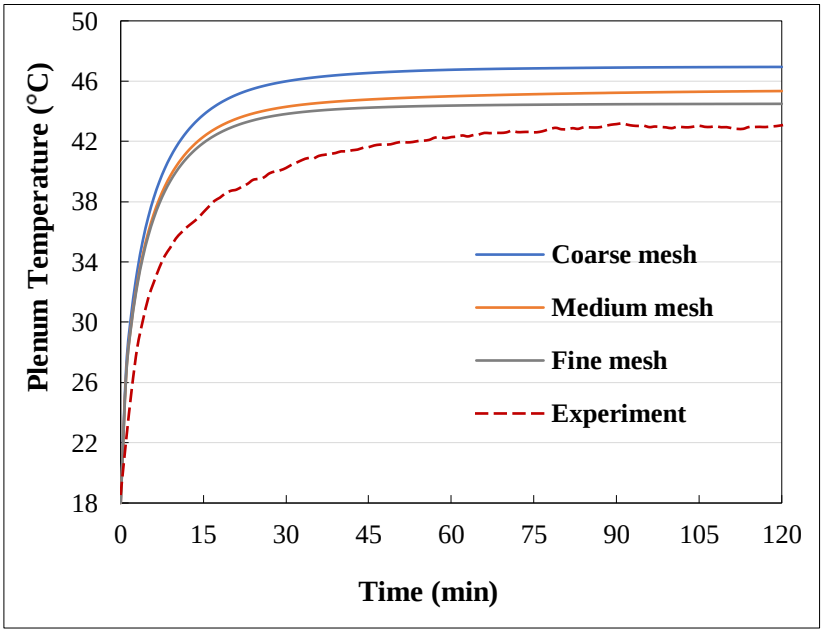

Figure 6-4. Plenum temperature for the three meshing methods

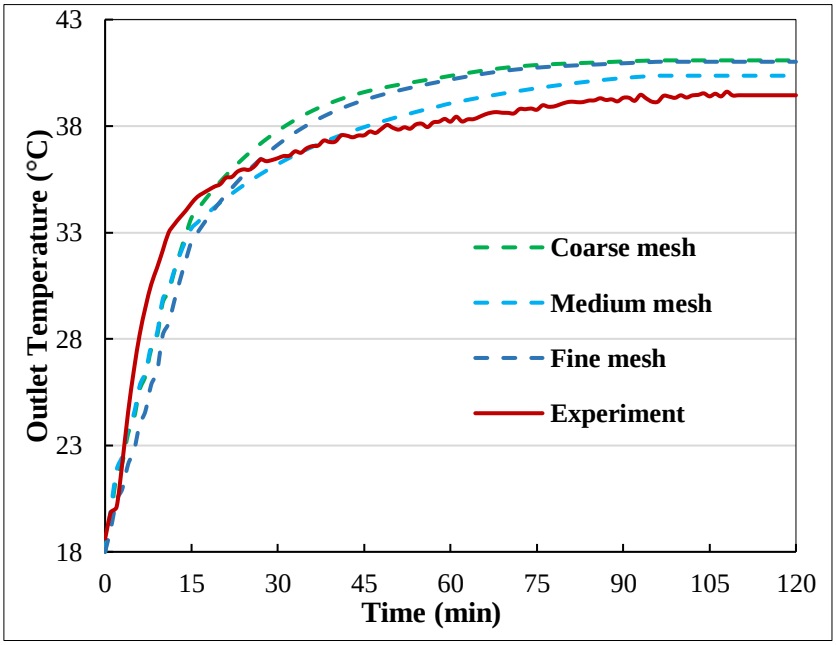

Figure 6-5. Outlet temperature for the three meshing methods

Figure 6-5 presents the experimental and numerical outlet temperatures for the three meshes. The meshing method achieved a relatively similar outlet temperature trend to the experimental outlet temperature. However, the medium mesh had the lowest average error between the experimental and numerical outlet temperatures at 2.3%, meanwhile, the coarse and fine meshes had approximately a 4% error. Also, the medium mesh required less computational time than the fine mesh. Hence, from the results, the medium mesh was used for further numerical analysis since it displayed good agreement with both experimental results (plenum and outlet temperature).

According to Figure 6-4 and Figure 6-5, it can be found that in this model, the plenum and outlet temperatures increased from 18°C (initial temperature) to roughly 45°C and 41°C due to the convection heat transfer from the absorber plate to the plenum air. However, the outlet temperature was unable to achieve the same higher temperature as the plenum temperature because the partial energy was expected to be stored at the PCM wall due to further convection and conduction. Overall, both temperatures showed a good increasing trend during the modelling that satisfied the heat transfer behaviour of the conceptual model. To some extent, it can indicate that this model was verified and good to use. Also, the mesh convergent refinement was unable to change the outlet temperature significantly, which therefore satisfied the mesh convergent benchmark. In addition, the model also met the interactive convergence criterion as it claimed the acceptable range of 0.1% relative error over throughout the iterative process.

6.6 **Materials properties**

The materials used in this numerical study were based on the following experimental materials: steel, gypsum, microencapsulated PCM (Micronal 5040X) and air as the working fluid. The material properties were available in the ANSYS Fluent data to the

expected Micronal 5040X. The density, thermal conductivity and enthalpy were claimed from the technical data sheet from the supplier. The thermal conductivity and specific heat capacity of Micronal PCM were referenced in a study (Fořt et al 2017). Thus, the material properties are shown in Table 6-2.

Table 6-2. Material properties

Material	Density (kg/m^3)	Thermal conductivity (W/m)	Specific heat capacity (J/kg°C)	Dynamic viscosity (kg m/s)	Melting temperature (°C)	Latent heat (J/kg)
Micronal PCM	365	0.079	1480	-	23 ±1	95000
Air	1.25	0.0242	1006.43	0.00001789	-	-
Gypsum	2320	0.5	1090	-	-	-
Stainless steel	8030	16.27	502.48	-	-	-

6.7 **Boundary and initial conditions**

Numerical modelling requires the specific boundary conditions to simulate the conditions detected in the experimental work. The boundary conditions included the inlet velocity (approach velocity) and temperature, the heat flux through the absorber plate, the air cavity and the PCM-gypsum plasterboard. Also, there were various sets of conditions related to the flow field and the thermal conditions of the whole system. There are eight considerable boundary conditions such as inlet, outlet, absorber plate, PCM-gypsum plasterboard (left/right side), adiabatic walls including the plenum (top/bottom), the PCM wall (bottom side), air and the PCM domains (left and right side) (Figure 6-6). Meanwhile, the airflow passing through the perforated hole was

considered as a velocity inlet which was identified due to the fan's airflow rate. The air velocity measured during the experimental campaign was 0.01m/s and the inlet temperature was taken from the experimental in-lab temperature at 18°C. In order to monitor the solar radiation, the plate temperature was set to be 55°C according to the experimental measurement of the plate temperature. During the numerical modelling, the heat loss through the surrounding adiabatic walls was ignored.

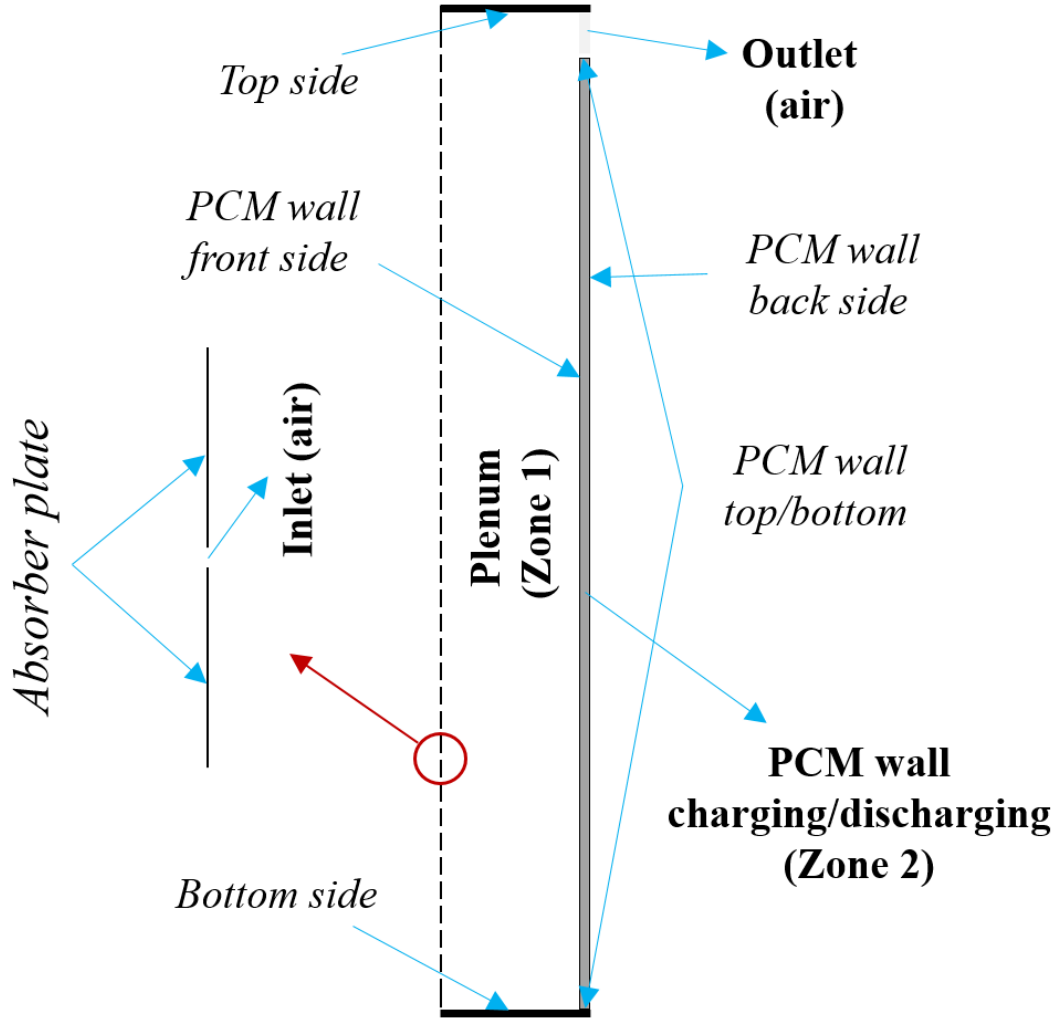

Figure 6-6. Boundary conditions of the geometry

While the air crosses though the perforated hole and is extracted at the outlet, the air is in contact with the back side of the absorber plate and with the front surface of the PCM-gypsum plasterboard. The heat transfer occurs due to convection. The convection

heat transfer demands the convective heat transfer coefficient (h_{conv}) and free steam temperature. The convective heat transfer coefficient of the ambient air in contact with the absorber plate and the PCM wall was decided as follows:

$$h_{conv} = 5.7 + 3.8v_{air.plen} \qquad (6\text{-}1)$$

Where $v_{air.plen}$ is the relative air velocity through the plenum (m/s), which was measured and assumed according to the fan velocity of the experimental work. The air flow across the perforated hole was treated as a velocity inlet and the velocity was assumed at a constant value considering the fan velocity measured in the experiment. The inlet air temperature was set at 18°C, corresponding to the average laboratory ambient temperature during the experiment's operational period. The outlet air flow was regarded as outflow. PCM charging/discharging happens due to conduction heat transfer, which can be simulated through the default melting/solidification model using the enthalpy method available in ANSYS Fluent Software. However, in the absorber plate temperature simulation, the solar irradiation was assumed to be various values to examine the impact of solar intensity on outlet temperature and the PCM wall's charging/discharging processes. The boundary conditions imposed are listed in Table 6-3.

Table 6-3. Boundary conditions for the flow and thermal fields

	Boundary conditions	
	Thermal	Flow
Air inlet	18°C (for validation) 0°C, 4°C, 10°C, 15°C (for charging and discharging)	Uniform velocity inlet: 0.01m/s, 0.05m/s, 0.1m/s, Direction: Normal to boundary

Plate temperature	40°C, 55°C, 70°C, 85°C, 100°C (charging process) 18°C, 14°C, 10°C (discharging)	-
PCM wall front surface	-	-
PCM wall back surface	23°C	-
Air outlet	-	$Pressure_{outlet} = 0$

For any numerical modelling, it is required that the values for each parameter should be initialised. For the present study, the initial temperature at $t = 0$ was the same for all sections: absorber plate temperature, inlet air temperature, plenum air temperature, PCM temperature.

6.8 **Governing equations**

The numerical study was undertaken to calculate the experimental outcome and the CFD modelling, applying the finite volume method to solve the common continuity (conservation), momentum and energy equations in the domain. These equations are known as the Navier-Stokes set of equations and are described in Equation 6-2, Equation 6-3 and Equation 6-4.

Continuity equation

$$\frac{\partial \rho}{\partial t} + \nabla(\rho\, \vec{v}) = 0 \qquad (6\text{-}2)$$

Momentum equation

$$\frac{\partial}{\partial t}(\rho\vec{v}) + \nabla(\rho\vec{v}) = \nabla\left[\mu\left(\nabla\vec{v} + \nabla \underrightarrow{v^T}\right)\right] - \nabla p + \rho g + F \qquad (6\text{-}3)$$

Where ρ describes the density, $\vec{v}$ gives the vector of velocity, μ represents the dynamic viscosity, g is referred to as the acceleration of gravity, and ρ corresponds to the static pressure. Equation 6-2 describes that the net accumulation of the mass must be zero, i.e. mass is conserved. Equations 6-3 and 6-4 define the fluid flow but not the heat transfer, therefore the extra equation is demanded. Equation 6-4 defines the conservation of energy describing the heat transferred and the temperature distributions.

Overall, conventional mathematical approaches are unlikely to be appropriate ways to solve these equations. However, A CFD solver through iterative methods firstly discretised, then linearised and finally addressed these equations. The CFD solution can determine the solution at only discrete volumes (meshes). Furthermore, discretisation is a process where the governing equation is broken down into simpler algebraic forms. In terms of the finite volume method, the solution domains were subdivided into a certain number of small control volumes (known as elements) by a mesh. Therefore, the mesh defined the boundaries of the control volumes while the computational nodes lay at the center of each control volume. However, when it involved a phase change phenomenon, an additional boundary condition appeared related to the interface between the solid and liquid phases of the material. Meanwhile, the phase change problems could be solved effectively through the enthalpy method (Gowreesunker, Tassou and Kolokotroni 2012). Hence, for PCM charging and discharging problems, the energy equation in terms of enthalpy can be written as (Giovannelli and Bashir 2017b)

$$\frac{\partial}{\partial t}(\rho H) = \nabla \cdot (k \nabla T) \qquad (6\text{-}4)$$

The solid-liquid interface can hardly be distinguished and the liquid fraction (β) enables indicating the fraction of the liquid during the period of phase change from a solid to a liquid state in CFD modelling (Giovannelli and Bashir 2017b). The enthalpy (H) of the

microencapsulated PCM is computed as the sum of the sensible enthalpy (h) and the latent heat (ΔH):

$$H = h + \Delta H \qquad (6\text{-}5)$$

Where

$$h = \int_{T_m}^{T} C_p dT \qquad (6\text{-}6)$$

The latent heat of fusion can be defined in terms of the latent heat of the material (L) and the latent heat content value can be between zero at solid-state and L at liquid state, hence

$$\Delta H = \beta L \qquad (6\text{-}7)$$

The liquid fraction (β) can be expressed as

$$\begin{cases} \beta = 0 & if\ T < T_s \quad (Solid) \\ \beta = \frac{T - T_s}{T_l - T_s} & if\ T_s < T < T_l \quad (Mixture) \\ \beta = 1 & if\ T > T_l \quad (Liquid) \end{cases} \qquad (6\text{-}8)$$

There are the states, the solid-state, mushy state and liquid state. According to the combination of the above equations, the enthalpy of the PCM can be expressed as

$$\begin{cases} H = \int_{T_m}^{T} C_{p,s} dT \quad if\ T < T_s \quad (Solid) & (6\text{-}9a) \\ H = \rho \frac{T - T_s}{T_l - T_s} L \quad if\ T_s < T < T_l \quad (mixture) & (6\text{-}9b) \\ H = \int_{T_m}^{T} \rho C_{p,l} dT + \rho \frac{T - T_s}{T_l - T_s} L\ if\ T > T_l \quad (Liquid) & (6\text{-}10c) \end{cases}$$

Hence, equation 6-9a gives the sensible enthalpy that presents the first step when a substance is heated. The liquid fraction formation at the beginning of the phase change

process can be calculated by Equation 6-9b. Equation 6-9c explains the complete phase change process when the sensible heat and latent heat of fusion happen at the same time.

6.8.1 *Model assumptions*

In terms of this model, the following assumptions were made:

a) The perforated absorber plate was placed by an asymptotic boundary layer;
b) The air was incompressible;
c) The air velocity profile was turbulent and fully developed;
d) The air inlet temperature corresponded to the average inlet temperature at the holes across the perforated absorber plate;
e) The heat transfer in the PCM by convection was negligible compared to the heat transfer by conduction;
f) Gravity effect was not considered;
g) The density of the PCM in both phases was constant, independent with temperature but different for solid and liquid states;
h) The latent heat value of the PCM was taken as a constant value for the enthalpy method;
i) The charging and discharging processes were assumed to be one-dimensional problems.

The air was seen as incompressible due to the ignorance of density changes during the flow so that the specific heat and thermal conductivity were claimed as constant (Antony Aroul Raj and Velraj 2011). Tajdaran et al. (2020) stated that an asymptotic boundary layer across the perforations enables computational complexity to reduce dramatically through simplifying the numerical analysis. Besides, it is estimated that

the air velocity is fully developed during the numerical modelling based on the assumption established in a paper by Mosaffa et al., (2014). In this numerical study, during the melting and solidification of PCM-gypsum plasterboard, the PCM density remained constant while the temperature varied for the solid and liquid states of the phase change processes Shukla et al. 2012; Cui et al. 2017; Wang, Shukla and Liu 2017). In addition, the heat transfer during the charging and discharging processes could be considered as a one dimensional problem and incompressible, meanwhile, the conduction was the main factor introducing the melting and solidification due to previous studies (Ling et al. 2019; Bhamare, Rathod and Banerjee 2020; Kim et al. 2020). Furthermore, the thermal resistance across the absorber plate and the PCM-gypsum plasterboard was negligible according to the surface smoothness (Chauhan et al. 2018). Hence, all the above assumptions were done for this numerical study.

6.9 **Turbulence model**

Air movement is one of the main dominant factors in this numerical modelling that demands a correct explanation of the flow type. It is critically important to determine a reliable and accurate turbulence model (Tian 2006). The selection of the turbulence model depends on several factors such as the physics of flow, the availability of the computational model, time consumption and the required calculation accuracy (Migoya and Crespo 2011). There are several papers concentrating on different turbulence models used in numerical modelling such as standard k-ε, Re-Normalization Group (RNG) k-ε mode, and SST k-ω (Li 2012). As a result, the Standard k-ε and the RNG k-ε model bring similar outcomes to the Realizable k-ε model. However, the results are steadier for convergence and more reliable. The Shear Stress Transport k–ω (SST k-ω) model has different results than all the k-ε models as the surface temperature is overrated. Additionally, both the Standard k-ε and the RNG k-ε model can perform with precise outcomes for thermal modelling. Also, most studies have shown that the RNG

k–ε model has better performance than the standard k–ε model in terms of the whole simulation performance (Zhang 2007). Therefore, the RNG k-ε model was applied for the heat transfer process through the plate and plenum and the laminar flow was used for the PCM-gypsum plasterboard melting/solidification process.

6.10 **Solution methods and monitoring**

The ANSYS Fluent software addressed the steady-state, three-dimensional, conservation equations of mass, momentum and energy for this numerical study. The Reynolds-Averaged Navier-Stokes (RANS) equation and the Realizable Renormalization Normal Group k–ε (RNG k-ε) were applied for the turbulence cases, since the RNG k-ε turbulence model performs better considering accuracy and stability for numerical modelling (Li and Karava 2012). A second-order upwind scheme was adopted for all variables except pressure, as the discretisation of pressure was based on a staggered scheme. Also, the SIMPLE algorithm was employed to connect the pressure and momentum equations. The solution was set to reach convergence when the total of the absolute normalised residuals of all the cells in the flow domain became less than 10^{-6} for all variables. The interaction between the boundary layer and the solid surfaces was sorted. For meshing, the proximity and curvature as advanced size function were used and the inflation was also considered. Other sections were automatically program controlled. Also, the residential value for continuity, velocity and turbulence was set at 10^{-6} and 10^{-8} for energy. During the modelling, each interaction and convergence was observed and double-checked. Apart from these values, no critical changes were monitored for velocity, energy and temperature aspects. Due to the ANSYS Fluent recommendations, the fixed default value for the maximum interaction number for each time step was 20. The impact of the time step size was analysed due to conduction problems causing PCM melting/solidification, which would allow a larger time step to be used. However, various step sizes such as 1s, 10s, 30s,

and 60s were investigated for the charging period (2 hours) and were considered the same under other boundary conditions and settings. Table 6-4 shows the effect of time step size on outlet temperature and PCM melting.

Table 6-4. Effect of time step size on liquid fraction and outlet temperature

Time step size (s)	1	10	30	60
Liquid fraction	0.055	0.069	0.061	0.055
Outlet Temperature (°C)	41.87	41.19	41.34	41.15

According to Table 6-4, it can be concluded that the effect of time step size on the PCM melting outcome and the outlet temperature is limited. For instance, time step sizes of 1 second and 60 seconds gave 41.87 and 41.15°C of outlet temperature, meanwhile the liquid fraction claimed the same value. The time step size of 10s claimed the highest liquid fraction, while the liquid fraction difference was higher compared to the others. The outlet temperature difference was significantly limited among all the time step sizes. However, a time step size of 60s spent much less computational time than the 1s time step size during the charging period. On the other hand, for the solidification period, the larger step sizes were applied due to the pure conduction problem of PCM melting/solidification (Tay, Belusko and Bruno 2012). In addition, during the experimental work, the data logger collected the data on a 60s basis. Thus, it was decided that a time step size of 60s would be used during the numerical simulation.

6.11 **Model verification**

This section describes the model verification through analysing the airflow behaviour across the model and the mass flow calculation at the outlet and inlet. The airflow profile across the model was observed for the different approach air velocities (0.01m/s, 0.05m/s, and 0.1.m/s) and the mass flow rates at inlet and outlet positions were

investigated. With the respect to the above-mentioned air velocity settings, the air velocity contours were gained for the condition when the model would reach its convergence (the fluid was fully developed). The results as velocity contours are presented in Figure 6-7.

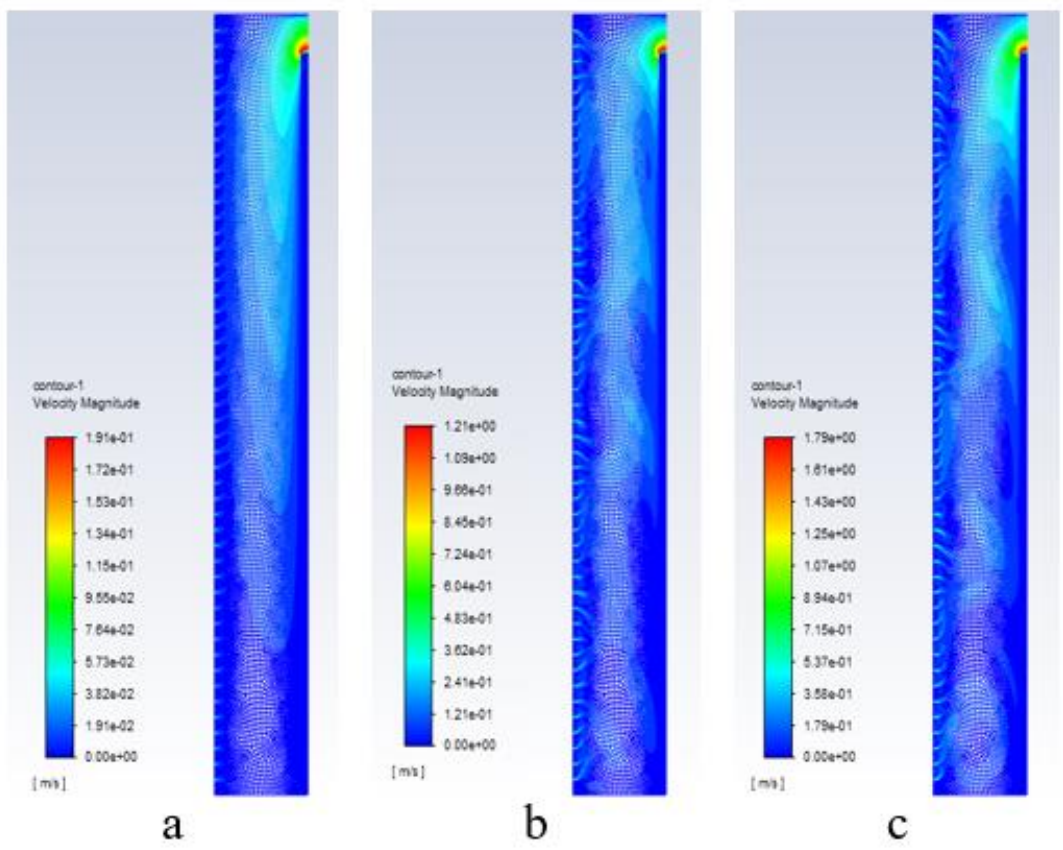

Figure 6-7. Velocity contours at (a) 0.01m/s, (b) 0.05m/s and (c) 0.1m/s

According to Figure 6-7, it was obvious that various approach velocities presented different velocity magnitudes across the model. Each velocity contour had a relative velocity magnitude, for instance, velocities of 0.01m/s and 0.1m/s had various magnitudes at 0.191m/s and 1.73m/s, respectively (Figure 6-7). Such results show different velocity contours across the model. It can be indicated that increasing the air velocity achieved a higher airflow across the model. Meanwhile, the air velocity first flowed through the inlet and the plenum and was then delivered at the outlet. The outlet

had a much higher velocity magnitude than in the plenum, because the cross-section area of the outlet was much smaller than the plenum cross section. In order to verify the model, the mass flow rates at the inlet and outlet were investigated if the model met the energy conversion. Table 6-5 displays the mass flow rates at the inlet and outlet locations for different air velocities when the model reached its convergence.

Table 6-5. Mass flow at inlet and outlet for the various air velocities

Approach air velocity	Mass flow rate (kg/s)	
	Inlet	Outlet
0.01m/s	0.00597	0.005906821
0.05m/s	0.029534	0.0295341
0.1m/s	0.047255	0.04725457

Table 6-5 shows that the mass flow rate at the inlet and outlet positions claimed the same values that could satisfy the mass conversion of the air alongside this model. Meanwhile, there were ignorable mass flow rate differences between the inlet and outlet sections since the roughness of the plate and the PCM-gypsum board were not applied to this model. Figure 6-7 also illustrates that the higher air velocity enabled a higher velocity magnitude to be provided. A lower air velocity (0.01m/s) created a more uniform flow compared to other air velocities. Therefore, this numerical model was verified for further use in the numerical study. Also, this model performed well for the system at the PCM back wall.

6.12 **Numerical investigations**

According to previous studies on TSC performance and the equations used in this numerical model, there are several key parameters such as airflow rate (approach air velocity), inlet temperature and plate temperature (simulating solar radiation) affecting TSC performance. For example, studies have stated that the impact of airflow rate on

overall collector efficiency is recognisable since the higher airflow rate introduces a higher velocity which then boosts the heat transfer between the back side of the absorber plate and the plenum air (Badache et al. 2014; Poole et al. 2018). Furthermore, the solar radiation (known as plate temperature in the present study) has a critical impact on system performance and PCM phase change phenomena (Badache et al. 2014; Charvát et al. 2019). Additionally, a higher air temperature rise can be achieved by increasing the solar radiation which would also affect the collector efficiency and heat exchange effectiveness (Leon and Kumar 2007a). In order to analyse the impact of the inlet temperature to check this model's implementation under different inlet air temperature conditions, the numerical study also discussed the effects of inlet temperature through modelling. Hence, this numerical study was undertaken for the following four different categories: building envelope with/without PCM-gypsum plasterboard, charging/discharging period for analysing the impact of the approach velocity, plate temperature and inlet temperature (Table 6-6).

Table 6-6. Parameters considered and their relative values

Case	TSC type	Constant parameters and relative values	Various parameters and their values	Period
Impact of approach velocity	TSC	Plenum size (150mm), pitch size (20mm), hole geometry (circular hole) and dimension (diameter of 1mm), inlet temperature (18°C), plate temperature (55°C)	Air velocity (m/s) =0.01:0.05:0.1	Charging
	TSC with PCM			Discharging
	TSC	Plenum size (150mm), pitch size (20mm), hole geometry		

Impact of plate temperature	TSC with PCM	(circular hole) and dimension (diameter of 1mm), inlet temperature (18°C), airflow rate (lower airflow rate)	Plate temperature (°C) =40:55:70;	Charging
Impact of inlet temperature	TSC TSC with PCM	Plenum size (150mm), pitch size (20mm), hole geometry (circular hole) and dimension (diameter of 1mm), plate temperature (55°C), airflow rate (lower airflow rate)	Inlet temperature (°C) =10:14:18	Charging

Table 6-6 shows the different cases designed for operating the numerical study. It includes the impact of air velocity, plate temperature and inlet temperature. The impact of each of the parameters were considered for the charging and discharging periods of the building envelope with/without PCM-enhanced gypsum plasterboard at the back. Also, the impact of thermal conductivity on the melting/solidification behaviour of PCM-gypsum plasterboard was studied. For all the numerical cases, the wind effect was neglected and a circular hole with a dimension of 1mm was applied for the hole geometry with 20mm as the pitch size and 140 mm as the plenum size. Also, it was assumed that the air flow across the plenum was considered as uniform airflow. Each charging period was simulated for 2 hours of charging, since the system would see heat reverse if charged for a longer time according to the experimental observation. Meanwhile, the discharging period was also simulated for 5 hours due to the experimental outcome. The system performance results in terms of outlet temperature, heat exchange effectiveness and energy delivered are presented and discussed through the numerical study.

6.13 **Results and discussion**

The influence of approach velocity, plate temperature (simulating solar irradiation) and inlet temperature on the building envelope performance were analysed and discussed in terms of outlet temperature, delivered energy and heat exchange effectiveness. Meanwhile, the effect of using the PCM was also studied due to the building envelope with/without PCM-gypsum plasterboard cases. Such parameters on the performance of a TSC with PCM enhanced gypsum plasterboard are also illustrated in terms of outlet temperature during the charging/discharging period, heat exchange effectiveness and delivered energy during the charging period only. Furthermore, the results would indicate and conclude on the impact of using PCM-gypsum plasterboard on outlet temperature, heat exchange effectiveness and outlet energy for the charging duration period. Therefore, the influence of approach velocity, solar radiation and inlet temperature were analysed and discussed as follows. Meanwhile, it can also highlight the importance of using PCM-gypsum plasterboard under different operational conditions. In all the numerical modelling cases, the charging period and discharging periods were designed as 2 and 7 hours, respectively. In addition, the absorber plate used a perforated metal profile with 1mm diameter circular holes with a pitch size of 20mm and a plenum size of 140mm.

6.13.1 ***Effect of approach velocity***

The impact of various approach velocities on the thermal performance of a building envelope with/without PCM-gypsum plasterboard. were studied, based on various approach velocities including 0.01m/s, 0.05m/s and 0.1m/s. For this modelling, other boundary conditions stayed unchanged such as plate temperature (55°C) and inlet temperature (18°C). Figure 6-8 presents the results of the outlet temperature profile for the charging and discharging periods under various approach velocities.

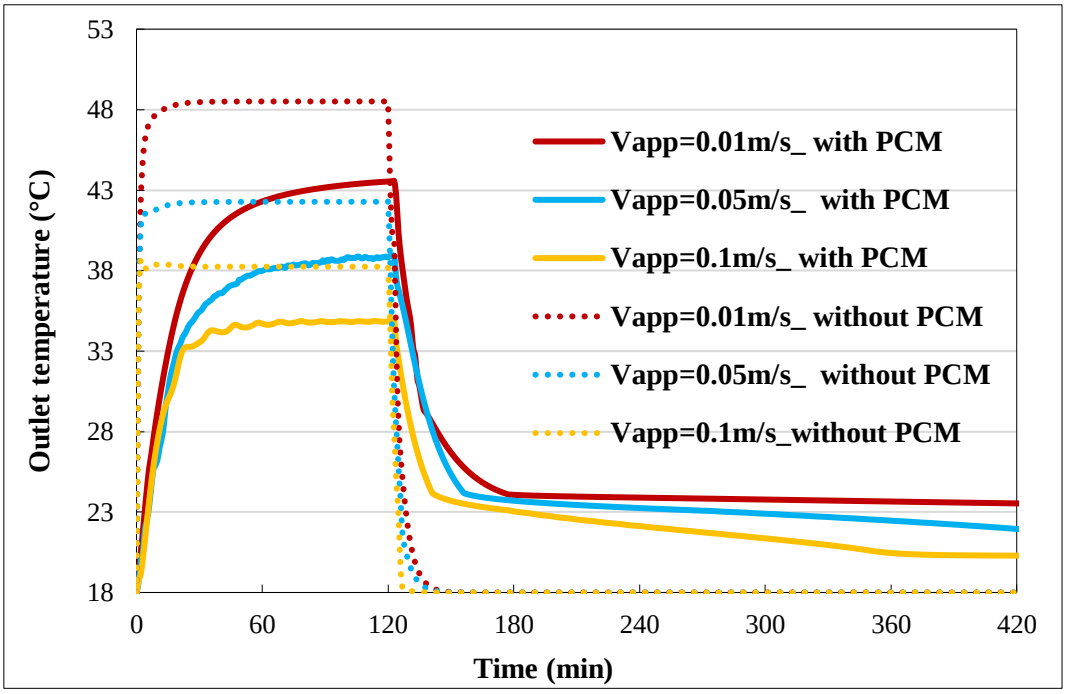

Figure 6-8. Outlet temperature for the charging and discharging periods under various velocities

Figure 6-8 shows that various approach velocities achieved various results for the outlet temperature of the building envelope with/without PCM-enhanced gypsum plasterboard during the charging/discharging periods. It can easily be seen that the building envelope without the PCM back wall enabled a higher outlet temperature to be delivered compared to the other. In addition, a smaller approach velocity (0.01m/s) could achieve the highest outlet temperature compared to all the approach velocities. For example, Figure 6-8 displays that the approach velocities 0.01m/s and 0.1m/s separately delivered outlet temperatures of 48°C and 38°C at 120 mins for the building envelope without PCM-gypsum plasterboard (Figure 6-8). Meanwhile, the approach velocities of 0.01m/s and 0.1m/s delivered outlet temperatures of 43°C and 35°C respectively, during the charging process whilst using the PCM-gypsum plasterboard back wall. In addition, the case with the PCM back wall took 30 minutes to reach the highest outlet temperature and the case without the PCM only took roughly 5 minutes

to reach the peak outlet temperature (Figure 6-8). Such results can indicate that the PCM-gypsum plasterboard stored a certain amount of energy.

However, during the discharging period, the operational case without the PCM back wall could reduce the outlet temperature dramatically to 18°C within a short timeline of 30 minutes. Meanwhile, Figure 6-8 also indicates that the PCM-gypsum plasterboard released the stored heat to the plenum air in order to deliver a relatively higher outlet temperature for a longer time period. For instance, the approach velocities of 0.01 and 0.1m/s provided 23.5 and 20.3°C separately during the discharging period. Furthermore, for the discharging period, the case with the PCM back wall could provide a higher outlet temperature than those without the PCM-gypsum plasterboard. In addition, the usage of a PCM back wall was obvious in that it could reduce the outlet temperature since some certain amounts of energy might be stored in the PCM back wall. Besides, the impact of the approach velocity on heat exchange effectiveness are shown in Figure 6-9.

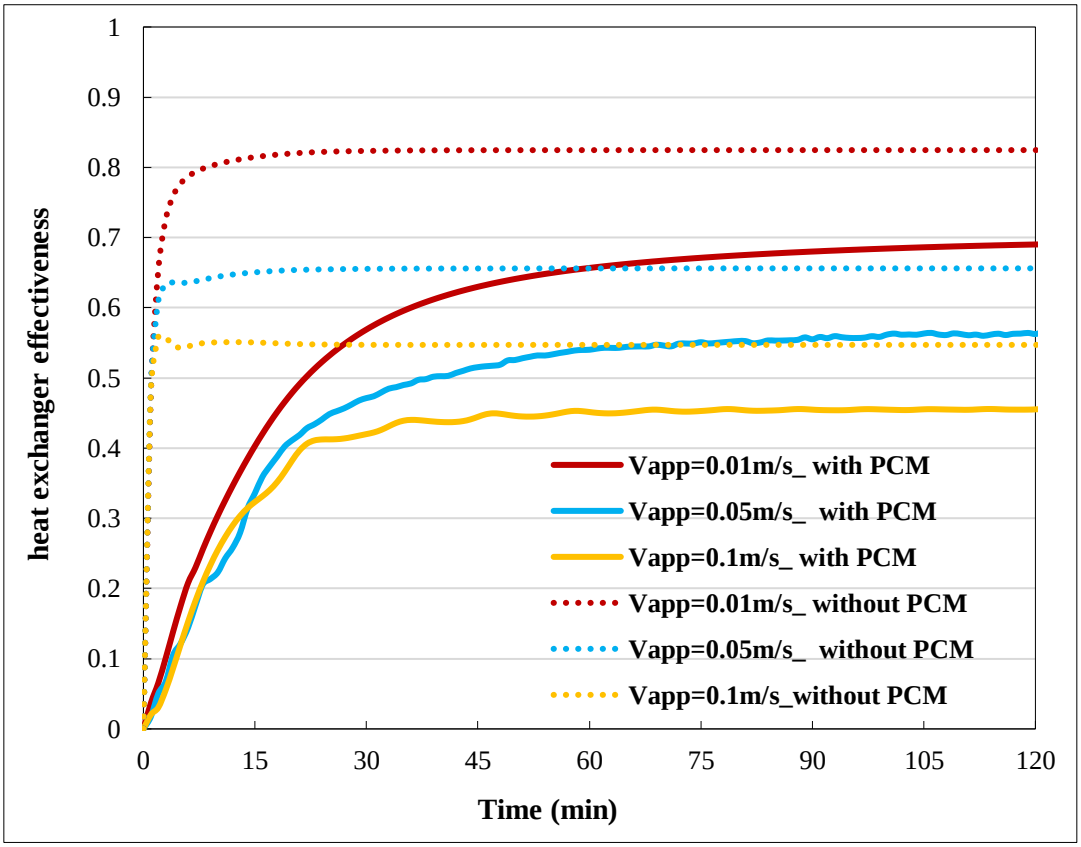

Figure 6-9. Impact of approach velocity on the heat exchange effectiveness of building envelopes with/without PCM-gypsum plasterboard during the charging period

It can easily be seen that the impact of approach velocity on heat exchange effectiveness (HEE) for the charging period was varied. The HEE average of 0.7 and 0.82 was achieved by the lower approach velocity (0.01m/s) for the building envelopes with and without PCM-gypsum plasterboard, respectively (Figure 6-9). Additionally, the results in Figure 6-9 demonstrate that the highest approach velocity (0.1m/s) condition claimed the higher HEE at 0.46 and 0.56 for the cases with and without the PCM back wall, respectively. It can be indicated that using PCM-gypsum plasterboard reduces HEE as a certain amount energy stored in the back wall that results in a lower outlet temperature in order to achieve lower HEE. Besides, increasing the approach velocity greatly affects HEE, since a higher approach velocity could deliver great amount of delivered air with

a lower temperature, causing the reduction of HEE. Also, it is worth mentioning that the HEE claimed a constant value after approximately 45 minutes of the charging period (Figure 6-9). It could also be predicted that the approach velocity would greatly influence the HEE. The impact of approach velocity on the energy delivered is shown in Figure 6-10.

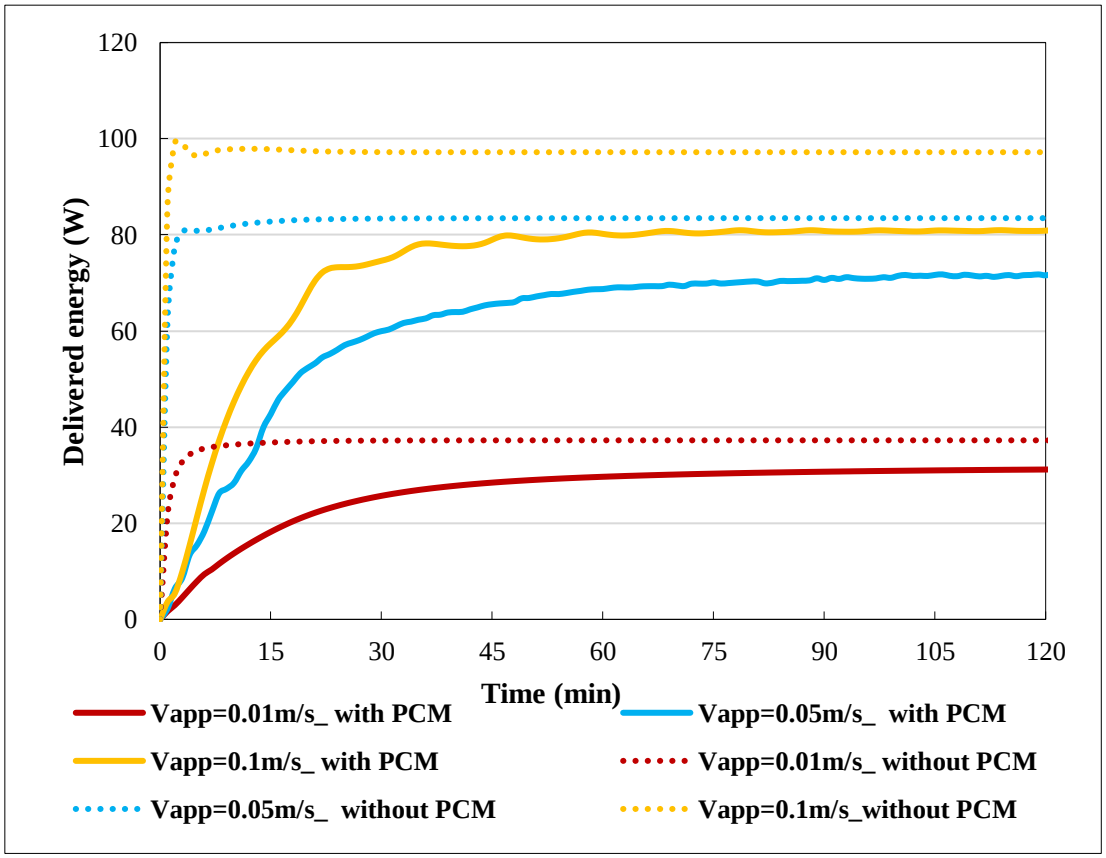

Figure 6-10. Impact of approach velocity on energy delivered for building envelopes with/without PCM-gypsum plasterboard during the charging period

According to Figure 6-10, there is a slight difference in the energy delivered from both, because of the addition of PCM in the plasterboard. In the charging period, the gypsum plasterboard provided higher delivered energy since it stored the heat as sensible energy which was released in a shorter time. However, the PCM-gypsum plasterboard was storing the extra heat from the plenum as latent heat due to the function of the PCM. It can be estimated that the case with PCM-gypsum plasterboard could produce a larger

amount of outlet energy for a longer time because of releasing the stored latent heat, which still provided more generated energy than the gypsum plasterboard during the discharging period. Furthermore, the system with a higher approach velocity enables higher output energy to be achieved due to a higher airflow rate. Besides, the simulation case without the PCM back wall stored a limited amount of energy in the PCM back wall as sensible heat. However, the case with the PCM-gypsum plasterboard could not only store sensible energy, but also latent heat due to the advantage of additional PCM components. Meanwhile, in this study, the PCM-gypsum plasterboard did not store a huge amount of energy due to the lesser amount of PCM used in the PCM-gypsum plasterboard. It was designed to capture and store an additional limited amount of extra energy from the plenum rather than soring lots of energy, because of the perspective of this research.

It can be acknowledged and highlighted that increasing the amount of PCM enables more energy to be stored. Therefore, the impact of approach velocity on thermal performance is significantly important, especially for energy delivered. This numerical study also highlighted the advantages of using PCM-gypsum plasterboard in building envelope performance, particularly during the discharging process where the building envelope with the PCM-gypsum plasterboard could release stored energy for a longer period to provide a higher outlet temperature, even without solar radiation. However, the impact of plate temperature on outlet temperature was marginal during the discharging period. The effect of various outlet temperatures was ignored, as the plate temperature was equal to the inlet temperature during the discharging period where there was no solar radiation, so that the plate temperature kept an ambient air temperature.

6.13.2 *Effect of plate temperature*

The impact of plate temperature was analysed and discussed through running the simulation under various plate temperatures at 40, 55, 70°C for the cases with/without PCM-gypsum plasterboard. For this investigation, other boundary conditions stayed constant, such as an approach velocity of 0.01m/s and an inlet temperature of 18°C. According to Figure 6-11, it can be found that a higher plate temperature can achieve a higher outlet temperature for both cases with and without PCM-gypsum plasterboard. For instance, plate temperatures of 40 and 70°C delivered outlet temperatures of 38 and 67°C respectively, without the PCM back wall. Meanwhile, the case with the PCM back wall enables approximately 29 and 48°C to be provided separately for plate temperatures of 40 and 70°C. A plate temperature of 55°C could achieve outlet temperatures of 38 and 50°C for the cases with and without the PCM back wall, respectively (Figure 6-11). It can be concluded that using the PCM back wall could reduce the outlet temperature since a certain amount of energy is stored in the PCM-gypsum plasterboard due to the advantage of the PCM, so that the outlet temperature reduced during the charging period.

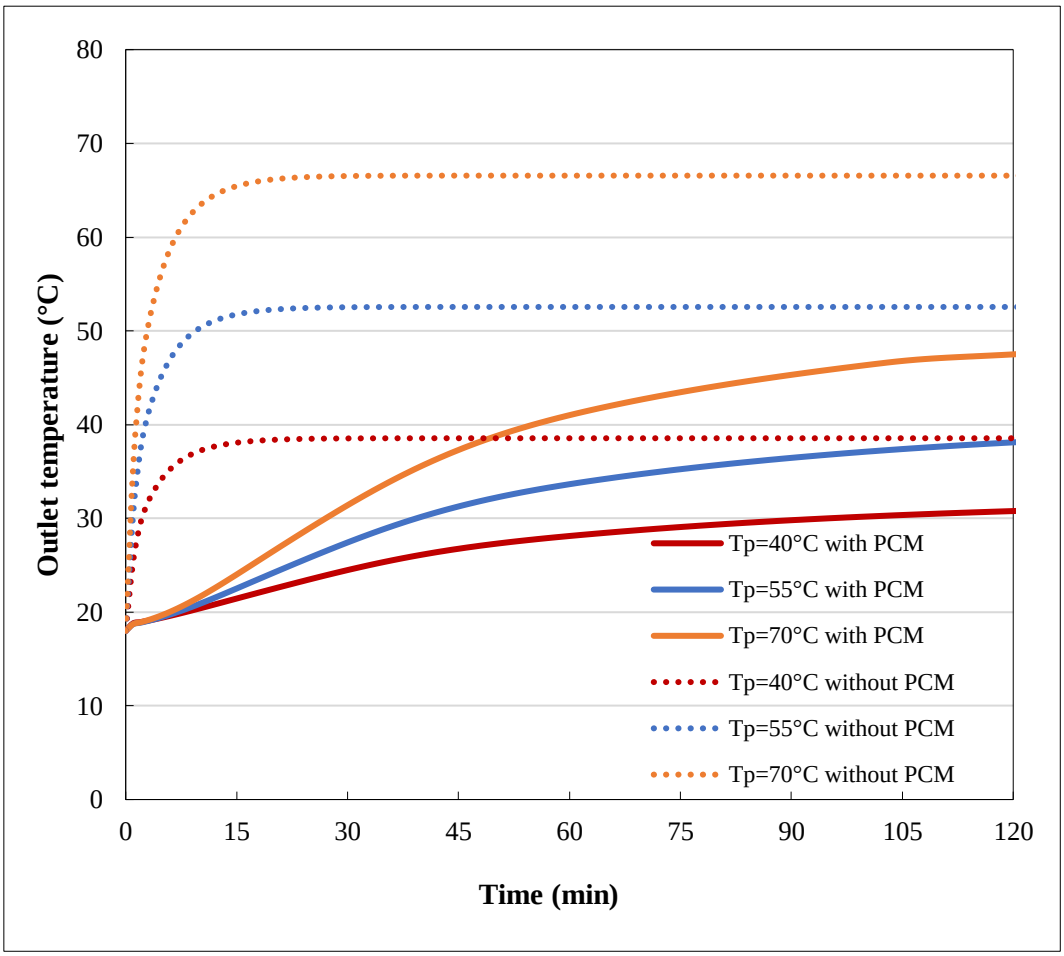

Figure 6-11.Impact of plate temperature on outlet temperature for building envelopes with/without PCM-gypsum plasterboard during the charging period

The impact of plate temperature on HEE is presented in Figure 6-13. Impact of plate temperature on energy delivered during the charging period for the building envelope with PCM-gypsum plasterboard

. The HEE is so various due to the different operational conditions. For instance, the cases without PCM-gypsum plasterboard achieved the same values of 0.92 as the HEE for various plate temperature operations (Figure 6-13. Impact of plate temperature on energy delivered during the charging period for the building envelope with PCM-gypsum plasterboard

). However, the impacts of various plate temperatures on HEE for the cases with the PCM back wall were slightly different, as shown in Figure 6-13. Impact of plate temperature on energy delivered during the charging period for the building envelope with PCM-gypsum plasterboard

. Under conditions using the PCM-gypsum plasterboard, the lower plate temperature could deliver higher HEE during the charging period. For example, plate temperatures of 40 and 70°C achieved HEEs of 0.57 and 0.54, respectively. In addition, for the case without the PCM back wall, the HEE increased sharply within 15 mins of the charging time and stayed steady. However, the simulation cases with the PCM-gypsum plasterboard had a steadily increasing trend of HEE during the charging period and reached a relatively steady state after 75 mins of charging.

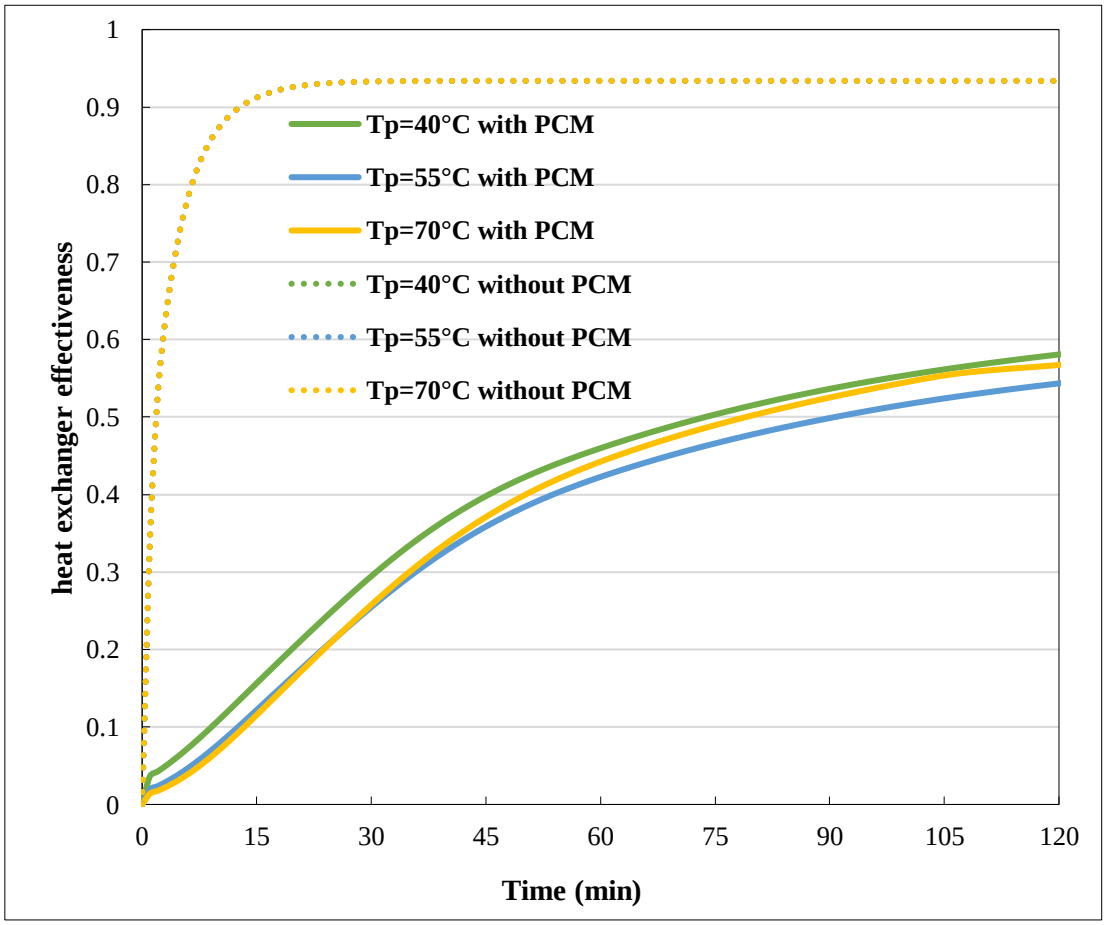

Figure 6-12. Impact of plate temperature on heat exchange effectiveness during the charging period for the building envelope with PCM-gypsum plasterboard

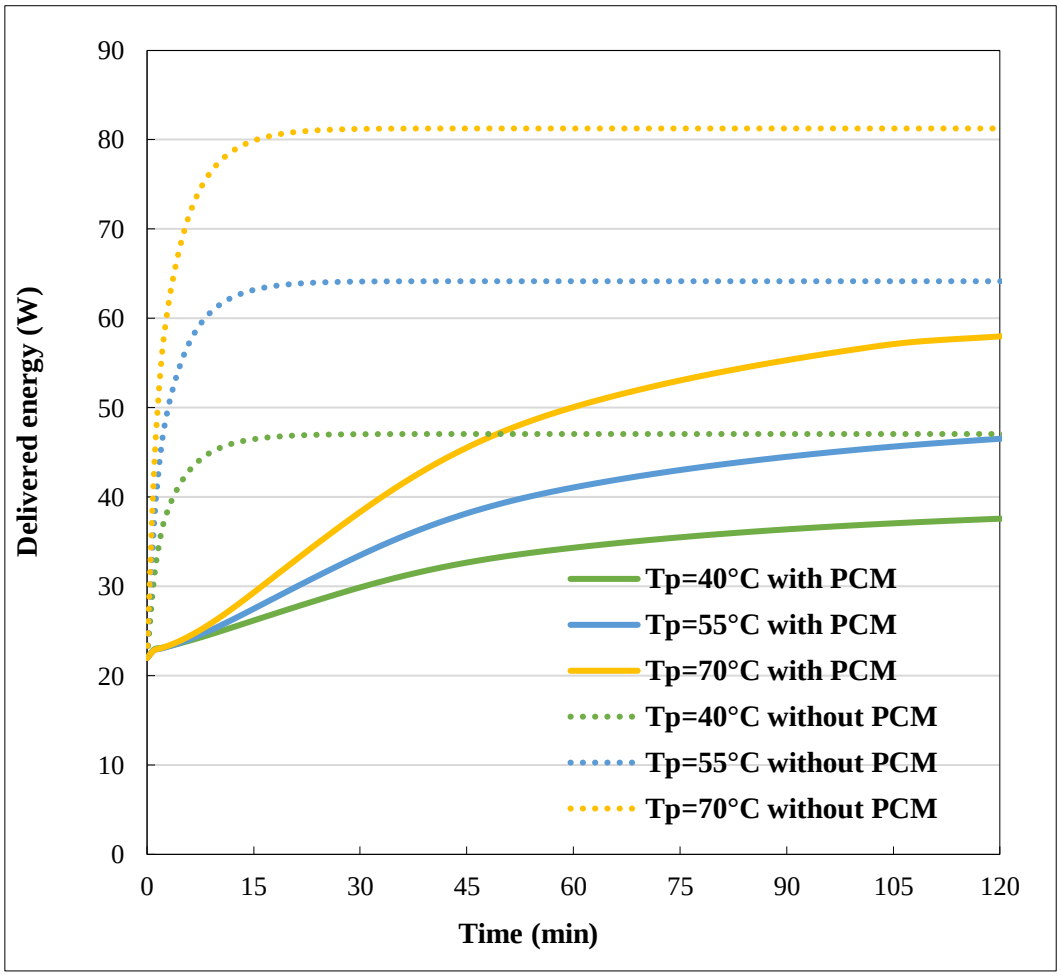

Figure 6-13. Impact of plate temperature on energy delivered during the charging period for the building envelope with PCM-gypsum plasterboard

In addition, Figure 6-13 displays the output energy for different operational cases. It can easily be seen that increasing the plate temperature can deliver higher output energy. For instance, plate temperatures of 70°C and 55°C achieved 80 and 63W of output energy for the simulation cases without the PCM back wall. However, for the numerical cases with the PCM-gypsum plasterboard, plate temperatures of 70 and 40°C achieved the highest output energy of 60 and 40W during the charging period. It can be concluded that the output energy for the simulation cases without the PCM back wall

reached relatively constant values after 15 minutes of charging. Meanwhile, the delivered energy for the numerical cases with the PCM back wall showed increasing curves and achieved relatively steady values after 75 minutes of charging. It can be indicated that the PCM back wall would finish the melting process at around the 75 minutes mark. Then, the energy would not be further stored in the back wall, so that the delivered energy reached a relatively constant value in the last quarter of the charging period. In addition, it could be that the impact of the plate temperature was light, especially for the outlet temperature and HEE under conditions with no PCM back wall.

6.13.3 *Effect of inlet temperature*

Figure 6-14 demonstrated the effects of different inlet air temperatures on building envelope performance in terms of outlet temperature during the charging and discharging processes for the cases with/without PCM-gypsum plasterboard. For this analysis, three inlet temperature values of 10, 14, 18 °C were considered and other conditions stayed the same, such as an approach velocity of 0.01m/s and a plate temperature of 55°C. In addition, Figure 6-14 shows that increasing the inlet temperature can increase the outlet temperature in the early period of the charging duration, especially in the first 60 minutes, for the simulation cases with the PCM back wall. However, the outlet temperature difference due to the various inlet temperatures seems to be reduced as the charging period goes on. For instance, the inlet temperatures of 10 and 18°C achieved outlet temperature differences of approximately 3.0°C and 1.1°C respectively, at 60 mins. and 120 mins.

In addition, for the numerical cases without the PCM back wall, various inlet temperatures would eventually provide same outlet temperature as the charging period went on. Meanwhile, the airflow rate stayed constant due to the same approach velocity and the plate temperature claiming the same values, so that the outlet temperature would be the same for all cases.

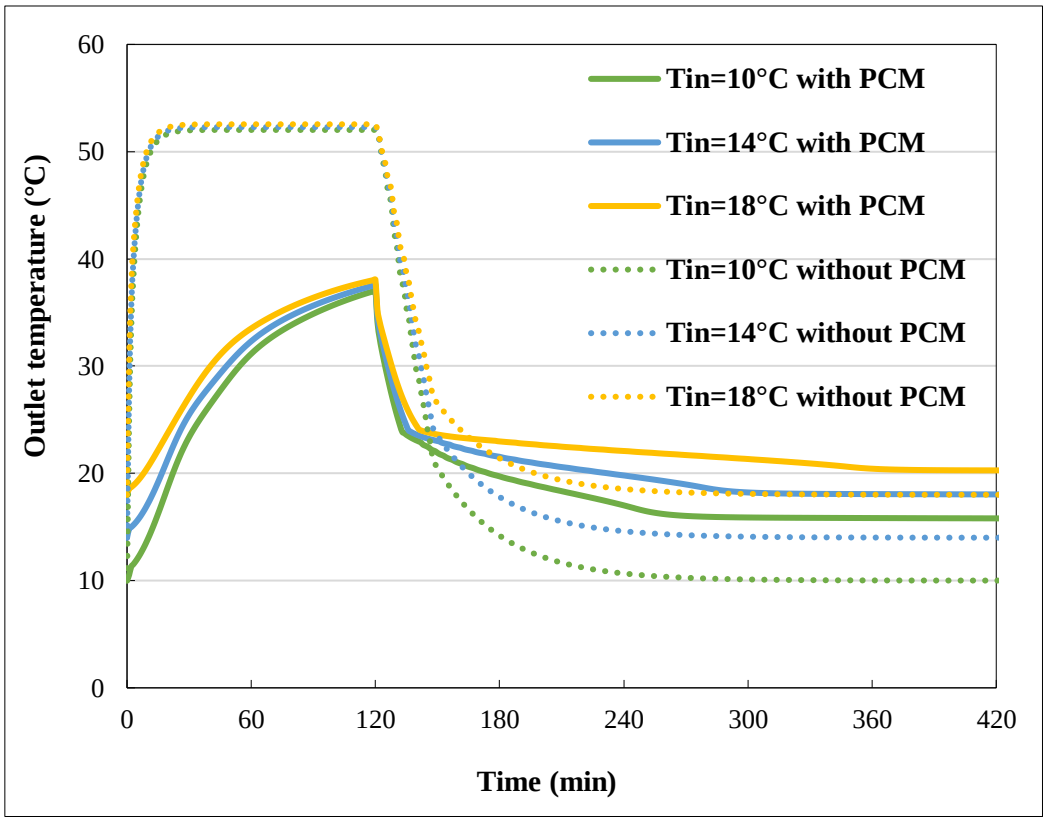

Figure 6-14. Impact of inlet air temperature during the charging/discharging period for building envelopes with and without PCM-gypsum plasterboard

However, during the discharging process, the building envelope with the PCM was able to provide a higher outlet temperature compared to the one without the PCM. For instance, the building envelope with the PCM-gypsum plasterboard could provide 2°C higher than the one without the PCM-gypsum plasterboard when the inlet temperature was 18°C (Figure 6-14). Meanwhile, decreasing the inlet temperature enabled the discharging process to be boosted. For example, inlet temperatures of 10°C and 18°C achieved the outlet temperature of 20°C at 150 and 200 mins, respectively, during the discharging period (Figure 6-14). Such results indicate that using PCM-gypsum plasterboard has the advantage of providing a higher outlet temperature for a longer period due to the benefits of the PCM storing energy. Besides, it can be concluded that increasing the inlet temperature was greatly influential, particularly during the charging period.

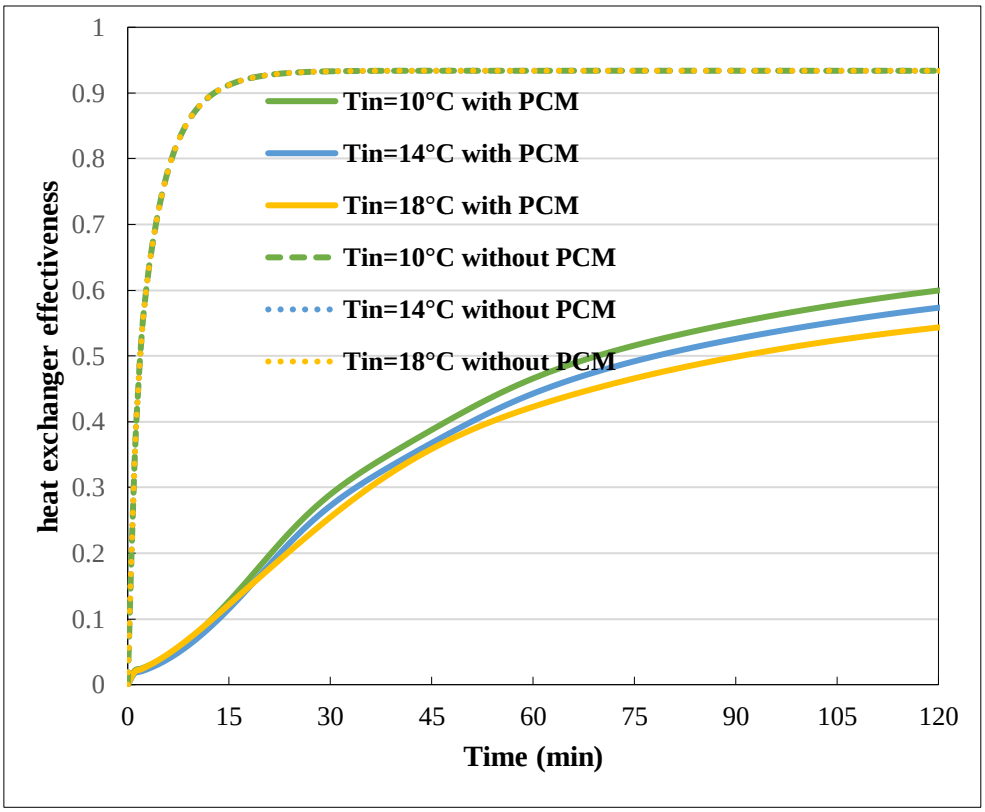

Figure 6-15. Impact of inlet temperature on (a) heat exchange effectiveness during the charging period for building envelopes with/without PCM-gypsum plasterboard

Therefore, the same principle would apply for HEE, as the inlet temperature variation was limited and it would not affect the HEE, especially when the simulation case was running without the PCM-gypsum board. For instance, all the different inlet temperatures achieved same HEE of 0.92, as shown in Figure 6-16, illustrating that a lower inlet temperature provided a slightly higher HEE. For instance, the inlet temperatures of 10 and 18°C produced 0.54 and 0.6 respectively, when using the PCM-gypsum plasterboard.

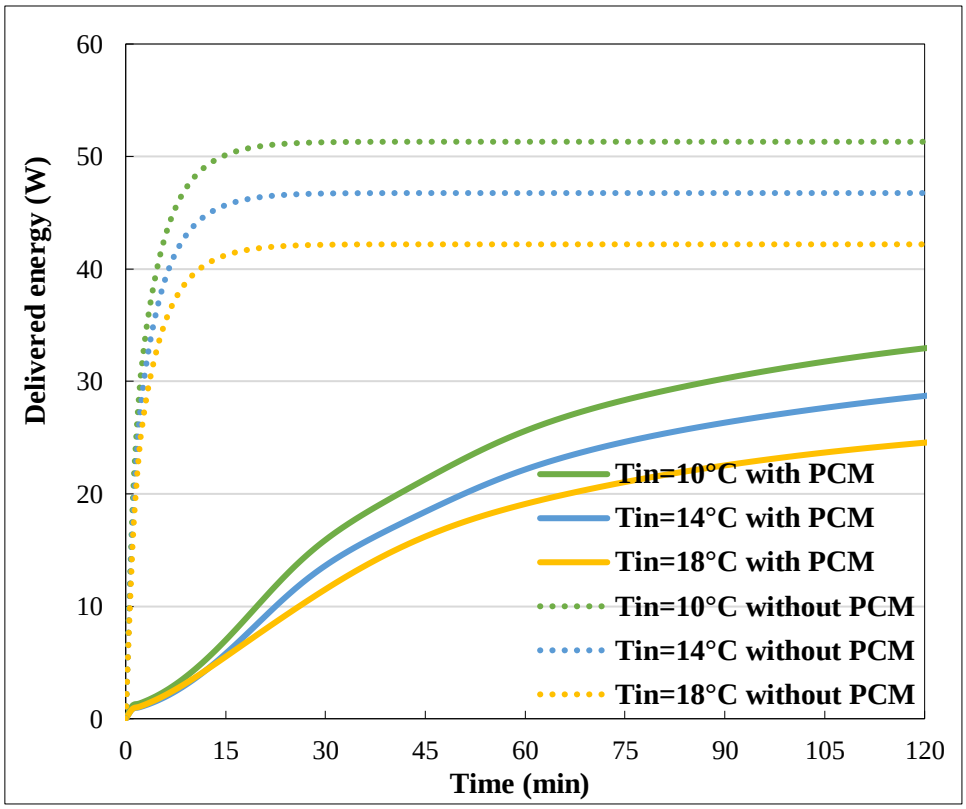

Figure 6-16. Impact of inlet temperature on energy delivered during the charging period for building envelopes with/without PCM-gypsum plasterboard

However, various simulation cases under different inlet temperatures showed limited changes in the system's output energy (Figure 6-16). For instance, for the simulation cases with the PCM gypsum plasterboard, inlet temperatures of 10 and 18°C produced the highest output energy of 25 and 32W at the 120 mins charging point. Meanwhile, for the numerical cases without the PCM back wall, the inlet temperatures of 10 and 18°C separately achieved 42 and 51W at 120 minutes (Figure 6-16). It can be concluded that the system with the PCM back wall provided lower output energy since a certain amount of energy was stored as latent heat in the PCM-gypsum plasterboard during the melting process. Also, the plate temperature and approach velocity were same, so that the inlet temperature was able to deliver a higher output temperature due to the higher temperature rise. However, it can be indicated that the impact of inlet temperature on

building envelope performance might be limited, especially on outlet temperature and HEE.

6.14 **Conclusion**

Therefore, this chapter introduced detailed explanations on the numerical study approach and the results on building performance with/without PCM-gypsum plasterboard. According to the research background of this field, the computational fluid dynamics (CFD) modelling through ANSYS Fluent 19.1 was used for this numerical study. The CFD model was established and the relative boundary conditions were justified based on the relative assumptions for this numerical study. Also, the meshing independence studies were investigated, and the medium mesh was used for further numerical study. Then, the model was verified according to the fact that the flow behaviour and mass flow changes among the models satisfied the energy conversion.

According to the literature review, the key parameters were investigated to study their impact on the building envelope's performance in terms of outlet temperature, heat exchange effectiveness and delivered energy. Such an investigation was beneficial to highlight the advantages of using PCM-gypsum plasterboard.

The effects of approach velocity on building envelope performance with/without PCM-gypsum plasterboard were described, including outlet temperature, heat exchange effectiveness and energy delivered. The outlet temperature was higher at the approach velocity because a smaller amount of delivered air could be heated when the heat transfer fluid moved through the plenum at a higher approach velocity compared to the others. Also, the simulation cases without the PCM back wall were able to provide higher outlet temperatures comparing to those with the PCM-gypsum plasterboard. It was concluded that using PCM-gypsum plasterboard has the advantage of reducing the HEE, as a certain amount energy is stored in the back wall that results in a lower outlet

temperature in order to achieve a lower HEE. Furthermore, the system with a higher approach velocity was able to achieve a higher output energy due to a higher airflow rate. Besides, the simulation case without the PCM backwall as a limited amount of energy was stored in the PCM back wall as sensible heat.

Regarding the effect of plate temperature (simulating solar radiation), the plate temperatures of 40 and 70°C delivered outlet temperatures of 38 and 67°C respectively, under conditions without the PCM back wall. In addition, using the PCM back wall could reduce the outlet temperature, since a certain amount of energy was stored in the PCM-gypsum plasterboard due to the advantages of the PCM, so that the outlet temperature was relatively reduced during the charging period. The cases without PCM-gypsum plasterboard achieved the same values of 0.92 as HEE for various plate temperature operations. However, the impact of various plate temperatures on HEE for the cases with the PCM back wall were slightly different. Furthermore, increasing the plate temperature can deliver higher output energy. For instance, the plate temperatures of 70°C and 55°C achieved 80 and 63W of output energy for the simulation cases without the PCM back wall.

The effects of different inlet air temperatures on this system's performance were studied in terms of outlet temperature, heat exchange effectiveness and the output energy for 2 hours of the charging duration under the simulation cases with/without PCM-gypsum plasterboard. The results showed that various inlet temperatures would eventually provide the same outlet temperature during the charging period. The inlet temperature was able to deliver a higher output temperature due to a higher temperature rise, so that the lower inlet temperature operation was able to achieve a higher output energy when using the PCM-gypsum plasterboard.

However, it can be indicated that the impact of approach velocity on building envelope performance was significant among these parameters according to the results shown

above. Hence, the results on the impact of approach velocity were used to validate this model through comparing the numerical and experimental results in the next chapter.

Chapter 7. **Validation and the parametric study**

7.1 Introduction

This chapter explains details of the validation methods/procedures and the parametric study using the validated model. In this study, the model validation was conducted through (i) analysing the melting/solidification behaviour during the charging/discharging periods, and (ii) comparing the numerical outlet temperature results with the experimental outlet temperature for various airflow rates. This section also includes the parametric study for several key parameters. After analysing the impact of various parameters on building envelope performance with/without the PCM-gypsum plasterboard, the airflow rate was seen as one of the significant factors affecting building envelope performance. Therefore, the validation study was undertaken for this airflow rate factor in terms of outlet temperature, to find out the validation error between the numerical and experimental outcomes. Besides, the validation was also done through the enthalpy method. Due to the results of the numerical study mentioned in the previous chapter, the parametric study was undertaken for the charging and discharging periods for serval key parameters such as airflow rate, solar radiation, inlet temperature and the thermal conductivity of the PCM.

7.2 Validation for the outlet air temperature

It is significantly important to confirm if the model is correctly implemented with respect to the conceptual model through model validation. This can be done by comparing the numerical outcomes with the experimental results in order to determine if the CFD process is acceptable. For the validation study, the simulations were run for 2 hours of charging and 5 hours of discharging periods using the medium mesh method and following the same boundary condition settings as the experimental operations. These were absorber plate profile (stainless steel black painted sheet), plenum size (140mm), pitch size (20mm), hole geometry (circular hole) and dimension (diameter of 1mm), inlet temperature (18°C), and plate temperature (55°C). Secondly, the various

airflow rates of $10m^3$/hr, 30 m^3/hr and $50m^3$/hr were regarded as lower airflow rate, medium airflow rate and higher airflow rate, respectively. The residual value of 10^{-6} was set for continuity, velocity and turbulence. 10^{-8} was set for energy. Each iteration and convergence were checked and monitored. In addition, a pressure-based double precision solver was selected to solve the set of equations with the SIMPLE pressure-velocity coupling scheme. The second-order upwind discretisation scheme was imposed on the pressure, momentum, density, energy and first order upwind for the kinetic and dissipation turbulence. The maximum number of iterations for every time step was sixty. Based on the numerical results, the validation percentage error calculated the error between the numerical outlet temperature and the experimental outlet temperature, which can be determined by the following equation:

$$Average\ percent\ error\ (\%) = \left[\frac{\sum(\frac{T_{exp}-T_{num}}{T_{exp}})_t}{N_t}\right] \times 100 \qquad (7\text{-}1)$$

Where T_{exp} describes experimental Temperature (°C), T_{num} gives the numerical Temperature (°C), t covers the time (s) and N_t corresponds to the number of time-steps.

Therefore, Figure 7-1 demonstrates the temperature variations during the charging period between the experimental data through data recordings and the numerical outlet air temperatures through computational modelling on a time- dependent scale of one data every single minute. In all cases, the inlet temperature was taken as 18°C which was equal to the in-lab ambient temperature.

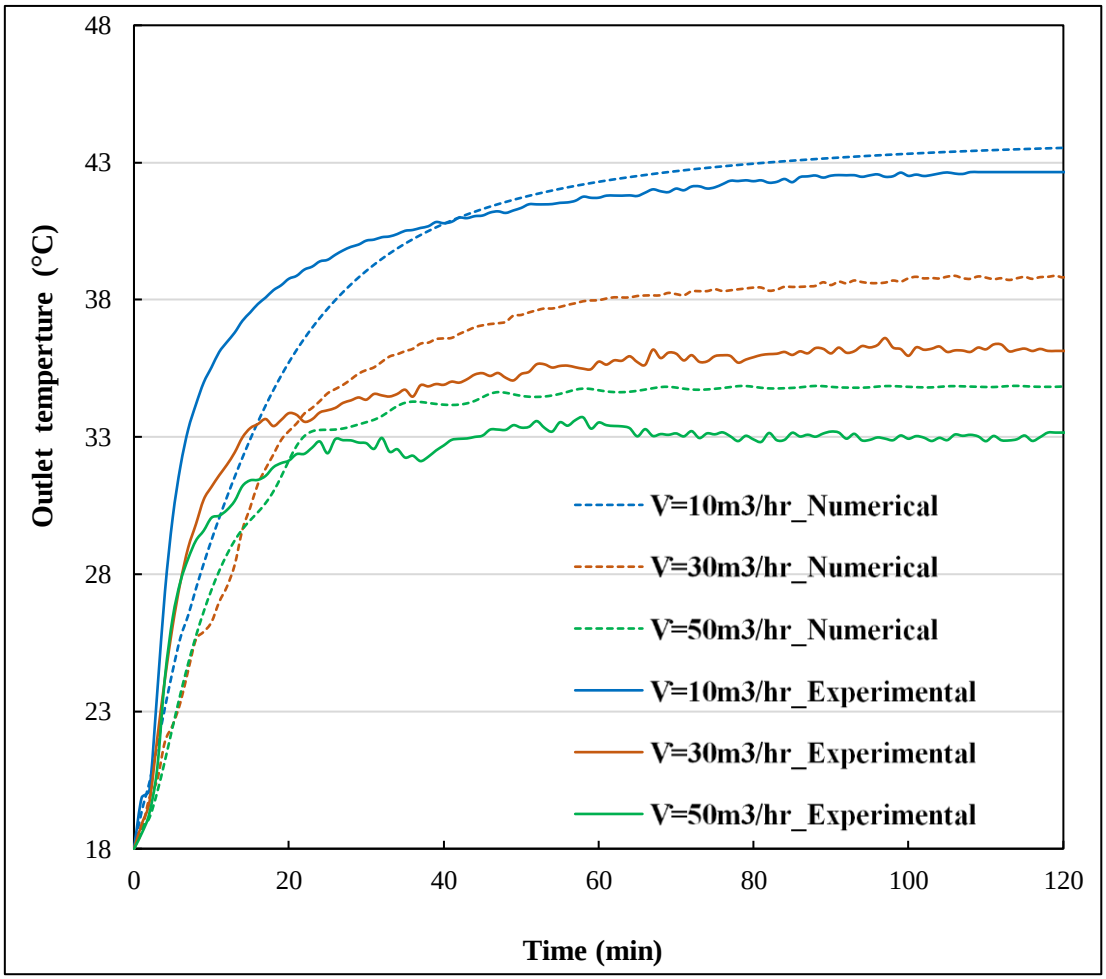

Figure 7-1. Outlet temperature during the charging process for different airflow rates

Figure 7-1 displays the numerical and experimental outlet air temperatures for different airflow rates during the charging process. The outlet air temperature curve differentiates the phase change behaviour of the PCM wall. First and foremost, the outlet temperature showed a rapid rate of increase with the sensible heating of the PCM, then a relatively steady temperature growth during the PCM melting period. There is a similar temperature changing trend for the experimental and numerical outlet air temperatures with a maximum variation of 2°C for various airflow rates. This might be caused by several factors, such as lower air tightness leading to higher heat loss and lower thermal conductivity of the PCM wall. However, these were ignored and no heat loss was considered during the simulation. Hence, for most of the cases, the numerical outlet

temperature claimed higher values than the experimental operations. According to Figure 7-1, it concludes that a lower airflow rate is able to achieve the highest outlet temperature among the various airflow rates in both the numerical and experimental work. When the air crosses in a lower airflow through the plenum, it is capable of capturing a higher amount of heat from the back side of the plate because of a higher heat transfer coefficient, so that a higher outlet temperature can be delivered compared to the system running at a medium and higher airflow rate. However, from the results presented in Figure 7-1, it can be known that there is a good agreement between the experimental and numerical outcomes for such cases, thereby finding assurance in this model for the charging process.

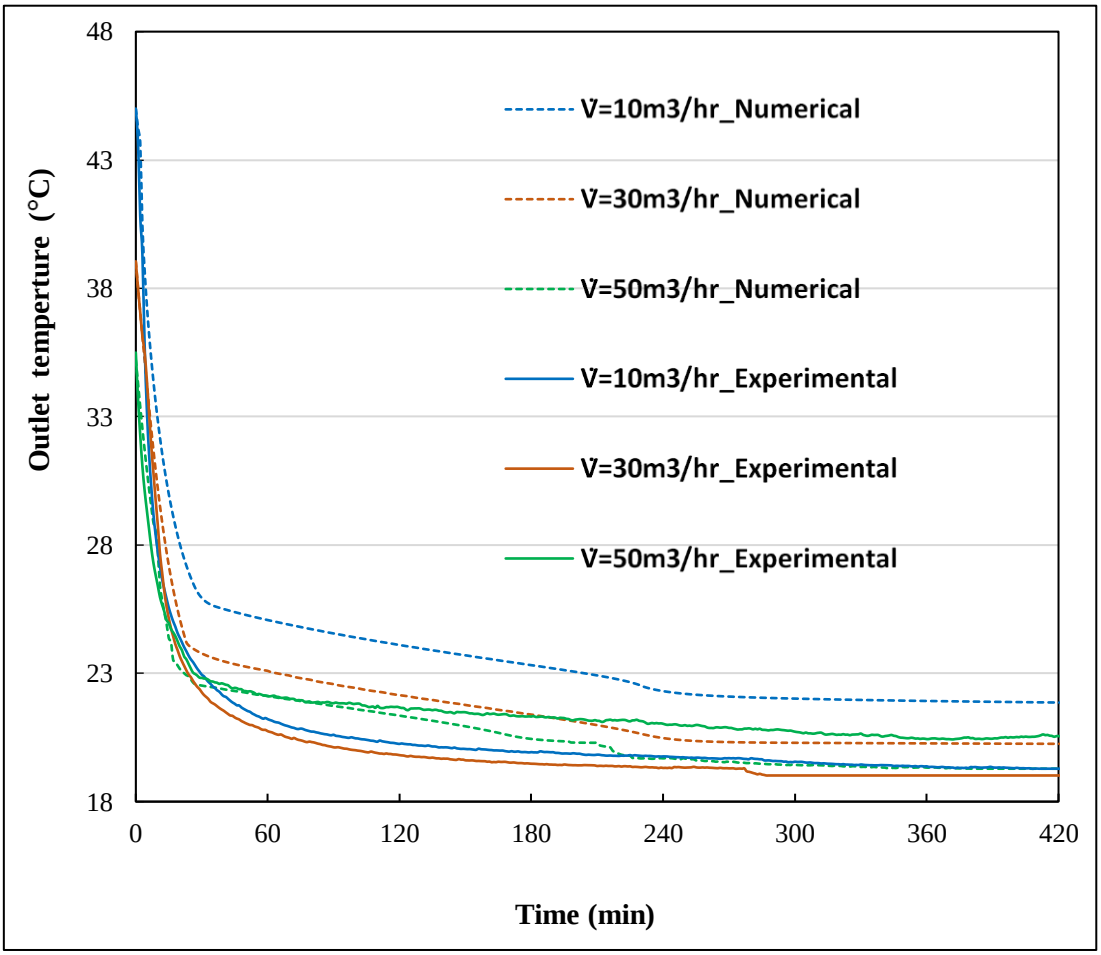

Figure 7-2. Outlet temperature variations during the discharging process for different airflow rates

The temperature variations during the discharging period between the experimental and numerical outlet air temperature results are presented in Figure 7-2. It can be indicated that the outlet air temperature between the experimental and numerical results illustrated a similar temperature changing trend with a maximum temperature difference of 3°C. This was caused by heat loss from the experiments that was ignored in the numerical modelling. However, the numerical results succeeded in a good agreement with the experimental data. From the results displayed in Figure 7-2, the outlet temperature decreased rapidly to the melting temperature of the PCM wall, followed by a slowly stabilised decline of outlet air temperature. Then, the outlet temperature showed a steady outlet temperature rate due to the PCM wall releasing the stored heat. This is able to provide a higher outlet temperature than the initial inlet temperature of 18°C. In addition, the higher airflow rate spent a shorter solidification period among the various airflow rate cases because it caused a higher convective heat transfer between the air crossing through the plenum and the PCM wall. This would increase the speed of releasing the heat from the PCM wall to the plenum. Therefore, according to the results shown in Figure 7-1 and Figure 7-2, the validation percentage error can be calculated using equation (7-1) and is shown in Table 7-1.

Table 7-1. Results of the validation percentage error on outlet temperature for various airflow rates

Type of airflow rate	**Validation percentage error (%)**	
	Charging period	Discharging period
Lower airflow rate (10 m^3/hr**)**	2.04	8.36
Medium airflow rate (30 m^3/hr**)**	6.90	7.30
Higher airflow rate (50m^3/hr**)**	4.87	2.84

According to Table 7-1, it is easily found that the validation percentage error (overall consistency between the experimental and numerical outcomes) is different for various simulation cases due to a changing airflow rate. The results in Figure 7-1 and Figure 7-2 demonstrated that the numerical outlet temperature is relatively higher than the experimental outlet temperature due to several factors. For instance, the experimental data measurements were influenced by the uncertainty of the measurement devices, in-lab conditions and the experimenter. Each experimental measurement instrument displayed their acceptable uncertainty, like air temperature (1.67%). Secondly, the in-lab conditions were under a controlled environment. Additionally, in a numerical simulation, the heat loss and surface roughness were ignored alongside many other assumptions. Therefore, the numerical simulations could achieve a higher outlet temperature than the experimental investigation. However, the maximum validation percentage error (8.36%) was relatively acceptable compared to a study that illustrated the highest percentage error between the numerical and experimental outcomes was 13% (Badache et al. 2013). Hence, it can be concluded that the numerical results showed good agreement with the experimental outcomes due to the graphs in Figure 7-1 and Figure 7-2. Also, the validation study was conducted through analysing the melting/solidification behaviour with the default enthalpy method available in ANSYS Fluent.

7.3 **Validation using the enthalpy method**

The enthalpy method was explained in a section of the numerical study and was used to address the phase change process of the PCM. The solidification and melting model of ANSYS Fluent software applied the enthalpy method. ANSYS Fluent solves the temperature by integrating between the energy and the liquid fraction, as shown in Equations 5.3 and 5.8. Such a governing equation is commonly used to simulate the phase change behaviour of PCMs in previous studies like Iten, Liu and Shukla (2016).

This present model was validated through comparing the outlet temperature during the PCM's melting and solidification periods with the experimental data achieved by various airflow rates that were presented in the experimental study.

Figure 7-3 and Figure 7-4 present the PCM mass fraction contours for the PCM-gypsum plasterboard during the melting and solidification period with an inlet air temperature of 18°C, a plate temperature of 55°C and a lower airflow rate of 10 m^3/hr. The mass fraction contours showed that the PCM wall costs different time periods of 4 hours and 12 hours for melting and solidification, respectively.

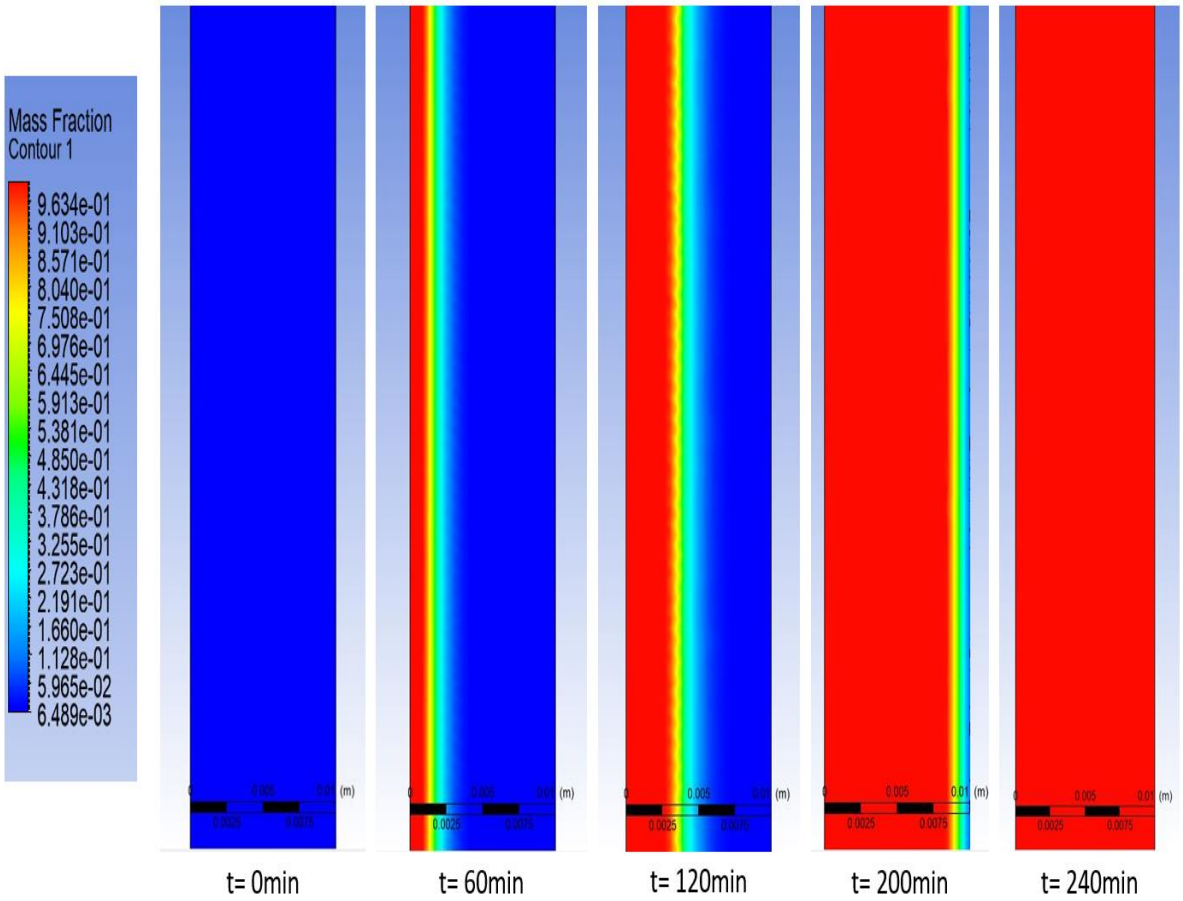

Figure 7-3. Mass fraction contours for PCM-gypsum plasterboard during the charging period

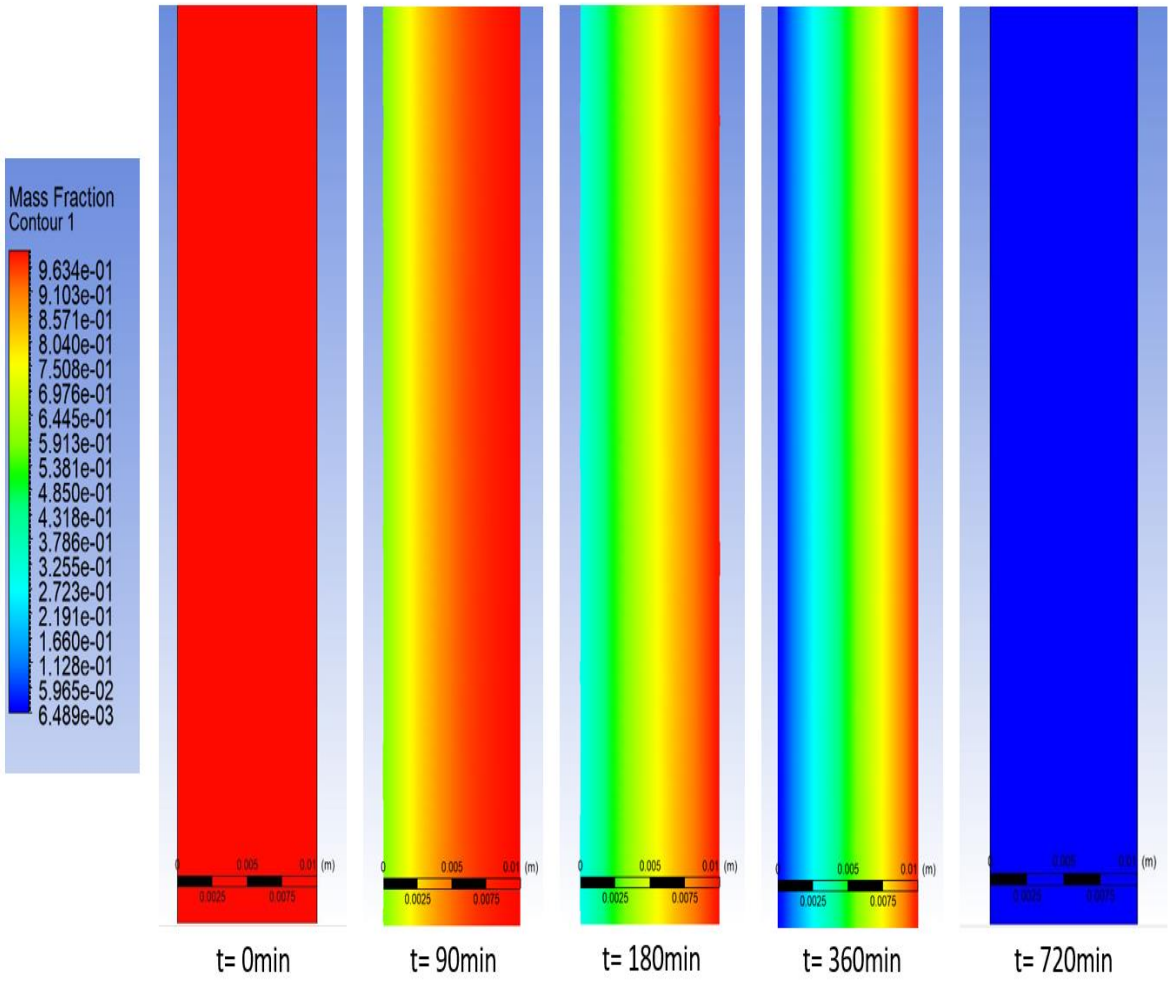

Figure 7-4. Mass fraction contours for PCM-gypsum plasterboard during the discharging period

In addition, this numerical outcome of the mass fractions matched the scenario observed in the experimental work. This is the fact that the solidification period took a longer time than the melting process under the same operational conditions, e.g. inlet temperature and airflow rate considering the phase change behaviour was happening uniformly. For instance, it illustrated that the melting and freezing processes took 240 and 720 minutes, separately. Therefore, this numerical investigation used the default melting and solidification model through the enthalpy method available in ANSYS Fluent 19.1, achieving good agreement between the numerical and experimental results.

One of the main advantages of using such a model is to show the liquid fraction of the PCM wall versus time, which is challenging to observe in any experiment, especially when using a mixture of microencapsulated PCM.

Thus, the experimental validation was undertaken successfully through this ANSYS Fluent CFD model, satisfying the outlet air temperature during the charging and discharging processes of the PCM wall. Also, it can be believed that the good agreements between the experimental and numerical results could be achieved through a suitable numerical model with proper thermo-physical properties during the melting and freezing periods. In this numerical model, the default enthalpy method presented the most promising results with a percentage error varying from 2.04% to 4.87% for the outlet temperature during the charging period. Furthermore, it presented a percentage error of 2.84% to 8.36% for the outlet temperature during the discharging period due to various airflow rates. In addition, the various airflow rates were able to provide different outlet temperature results and affect the phase change behaviour of the PCM wall (Table 7-1). For instance, a lower airflow rate would provide a higher outlet temperature among all the various airflow rates, especially during the charging period. From the outlet results, it can be found that the numerical modelling achieved higher outlet temperature values compared to the experimental cases, because the heat loss from the experimental setup due to lower insulation was neglected during the numerical work. Such factors could moderately influence the experimental temperature outcomes due to slight air movements and temperature changes in the lab conditions. Therefore, this CFD model, through the default enthalpy method in ANSYS Fluent software, was used for the parametric study investigating the effects of various parameters on system performance in terms of outlet temperature and phase change behaviour.

7.4 **Parametric study**

According to the equations used in this numerical model and previous studies, the thermal performance of this building envelope can be determined by several significant parameters such as airflow rate, inlet temperature, plate temperature (simulating solar radiation) and thermal conductivity of the PCM. For the validation period, the fundamental boundary conditions were absorber plate profile (stainless steel black painted sheet), plenum size (140mm), pitch size (20mm), hole geometry (circular hole) and dimension (diameter of 1mm), inlet temperature (18°C), plate temperature (55°C), and airflow rates ($10m^3$/hr). Also, the medium meshing method was used for the parametric study. However, a study has stated that the impact of airflow rate on overall collector efficiency is recognisable, since the higher airflow rate introduces higher velocity, which then boosts the heat transfer between back side of absorber plate and the plenum air (Badache et al. 2014; Poole et al. 2018). Furthermore, the air velocity across the plenum also affects the PCM's phase change behaviour across the melting and solidification durations (Poole et al. 2018; Badescu et al. 2019a). Those studies also indicated the effects of inlet air temperature on the system's performance of PCM phase change behaviour. The inlet temperature has an especially great impact on collector efficiency and the charging/discharging behaviour of the PCM due to the formulation of the numerical model and the previous study (Karthikeyan et al. 2014). Besides, the solar radiation (known as the plate temperature in the present study) has a critical impact on system performance and PCM phase change phenomena (Badache et al. 2014; Charvát et al. 2019). In addition, the thermal conductivity of a PCM greatly influences its melting and solidification (Karthikeyan et al. 2014; Panchabikesan et al. 2019). Thus, Table 7-2 displays the various values of the key parameters used in this parametric study: airflow rate, inlet temperature, plate temperature and thermal conductivity of the PCM. In order to analyse and discuss the thermal performance of such a building envelope through parametric study, the results are focused on outlet

temperature, liquid fraction (β), and energy stored during the charging and discharging periods. The energy stored (Q_{stored}) during the charging and discharging periods can be calculated by the following equation (7-1). Such results could indicate the heat exchange effectiveness and the collector efficiency, relatively. Therefore, this parametric study kept many model-settings and solution selections the same as the one used for the validations, which showed good agreement with the experimental outcomes. Also, heat loss and wind effect were neglected in this study.

$$Q_{stored} = m_{gypsum}.C_{p.gypsum}\left(T_{gypsum} - T_{inlab}\right) + m_{PCM}C_{p.PCM}\left(T_{melting} - T_{inlet}\right) + m_{PCM}\beta L \quad (7\text{-}1)$$

Where T_{gypsum} represents the final temperature of the PCM-gypsum plasterboard and $T_{melting}$ gives the PCM melting temperature of the microencapsulated PCM (MICRONAL® DS 5040X) used in this study. The latent heat of fusion (L) can be determined due to the technical data from the supplier.

Table 7-2. Parameters considered with their relative values

Parameters	Values
Airflow rate (m^3/hr)	10; 30; 50;
Inlet temperature (°C)	10; 14; 18
Plate temperature (°C)	40; 55; 70; 85;
Plenum width (mm)	100; 150; 200;
Pitch size (mm)	20; 22; 25;
Hole diameter (mm)	1; 2; 3;
Thermal conductivity of PCM (W/mK)	0.16; 0.5, 1;

7.4.1 *Results and discussion*

The effect of airflow rate, inlet temperature, plate temperature (simulating solar irradiation), plenum width, pitch size, hole diameter, and thermal conductivity of the PCM on the system's performance are analysed and discussed in terms of outlet temperature, liquid fraction and heat stored during the charging and discharging periods in this section.

7.4.2 *Effect of airflow rate*

The impact of varying the airflow rate of the system's performance in terms of outlet temperature and melting behaviour during the charging period was covered in this analysis by investigating the influence of three different airflow rates ($10m^3$/hr, $30m^3$/hr, and $50m^3$/hr). Meanwhile, the other boundary conditions remained unchanged for these trials, such as a plate temperature of 55°C, an inlet temperature of 18°C, and the amount of PCM. Hence, Figure 7-5a describes that various airflow rates greatly impact on outlet temperature, for example, the airflow rates of $10m^3$/hr, $30m^3$/hr, and $50m^3$/hr achieved outlet temperatures of 44, 39, 35°C respectively, when the charging period reached the 2 hour mark. Hence, higher outlet temperatures can be produced by smaller airflow rates since a smaller amount of delivered air can be heated when the heat transfer fluid moves through the plenum at a higher airflow rate compared to a lower airflow rate. Meanwhile, the impact of airflow rate on charging behaviour is shown in Figure 7-5b.

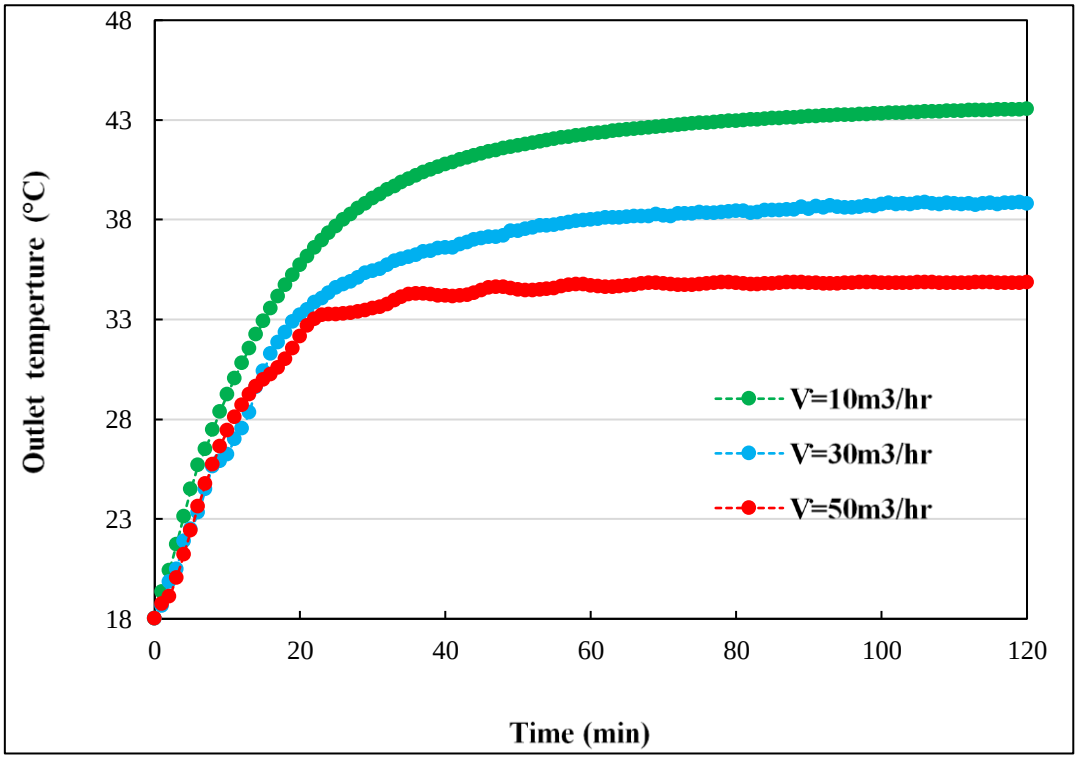
Outlet temperture (°C)
48
43
38
33
28
23
18
0
20
40
60
80
100
120
Time (min)
V=10m3/hr
V=30m3/hr
V=50m3/hr

(a)

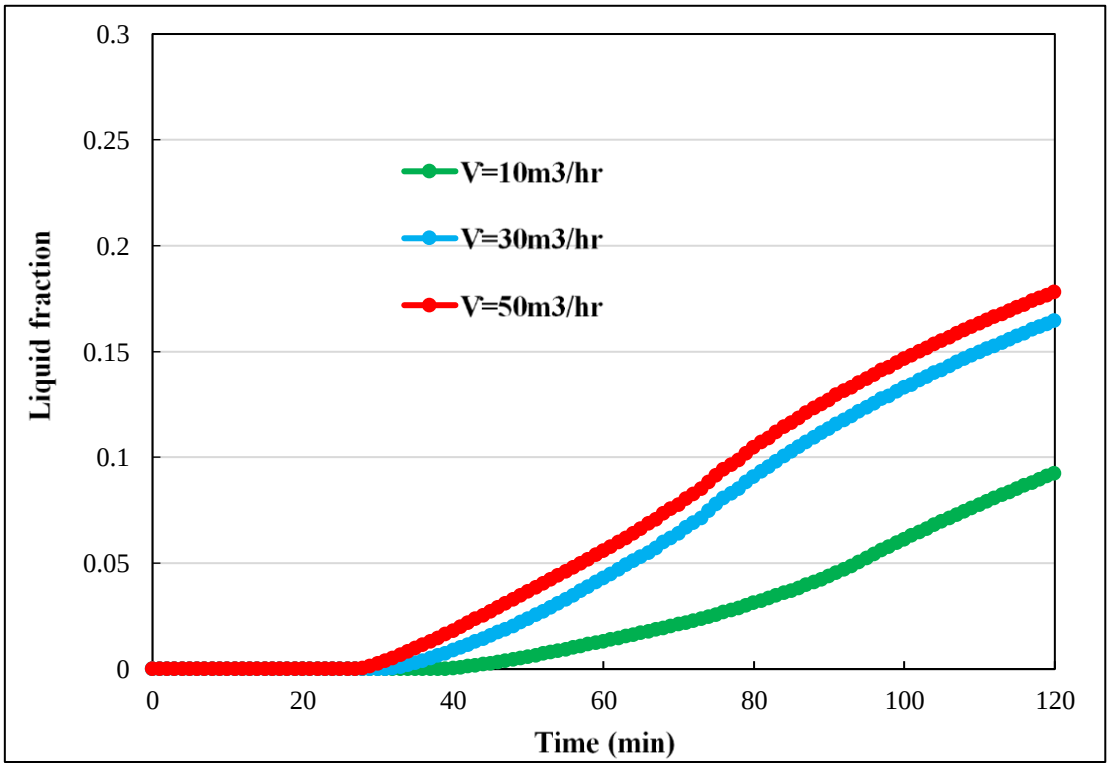
Liquid fraction
0.3
0.25
0.2
0.15
0.1
0.05
0
0
20
40
60
80
100
120
Time (min)
V=10m3/hr
V=30m3/hr
V=50m3/hr

(b)

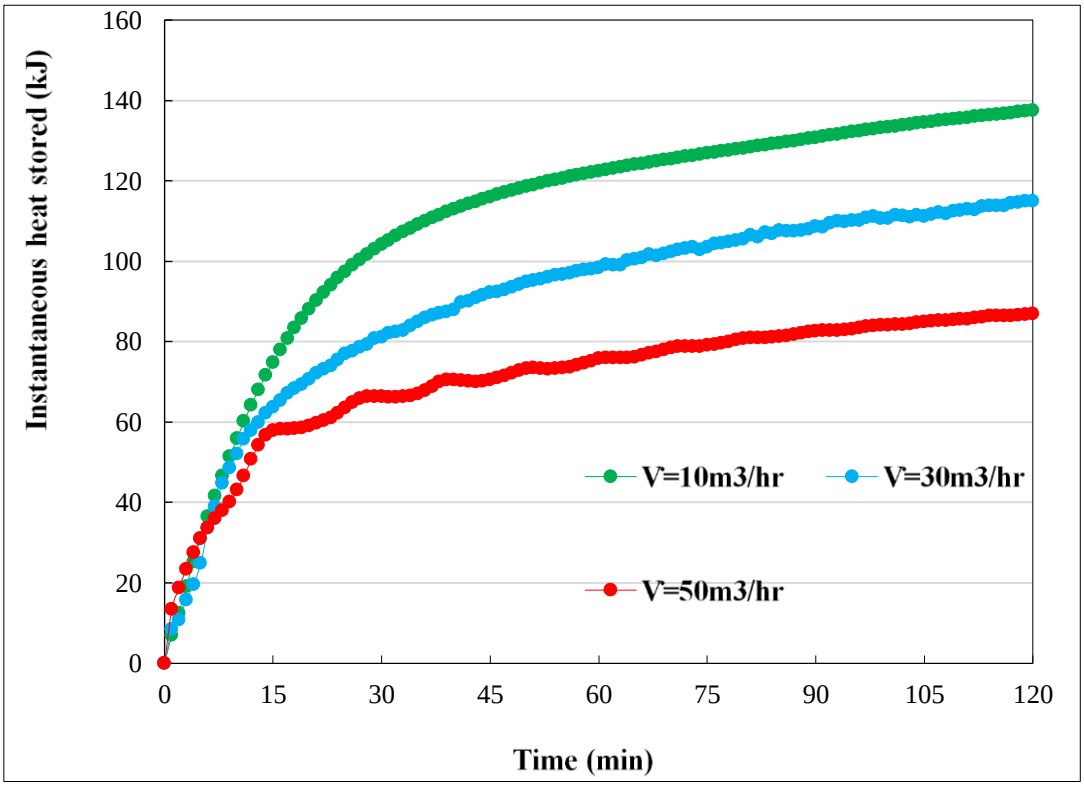

(c)

Figure 7-5. Impact of the airflow rate on (a) outlet temperature and (b) PCM liquid fraction and (c) energy stored during the charging period

According to Figure 7-5b, a lower airflow rate increases the charging of the PCM wall. For instance, after 2 hours of charging, the liquid fraction ratios were 0.17, 0.16, and 0.094 respectively for airflow rates of 10, 30 and 50m 3/hr. In order to achieve a 10% melting of the PCM wall, the lower airflow rate required more than 2 hours. Meanwhile, the higher airflow rate needed only 1.25 hours. This can be explained by the fact that the higher airflow rate could result in a higher surface heat transfer coefficient so that it could improve the rate of heat storing/releasing due during the phase change process. Due to the same quantity of PCM, the cumulative latent heat stored in the PCM wall remained the same for these three airflow rates. However, the rate at which the instantaneous energy stored was different for the various airflow rates was due to the temperature of the PCM-gypsum plasterboard increasing. Figure 7-5c shows that the

building envelope with 10 and 50m^3/hr achieved a higher instantaneous heat storage of 140 and 82kJ, respectively. It can be concluded that increasing the airflow rate could dramatically reduce the heat stored during the charging period. From Figure 7-5, it can be predicted that the system with a lower airflow rate would be beneficial when a higher outlet temperature was highly required. Figure 7-6 presents the results of outlet temperature, liquid fraction and heat storage for all three airflow rates during the discharging period.

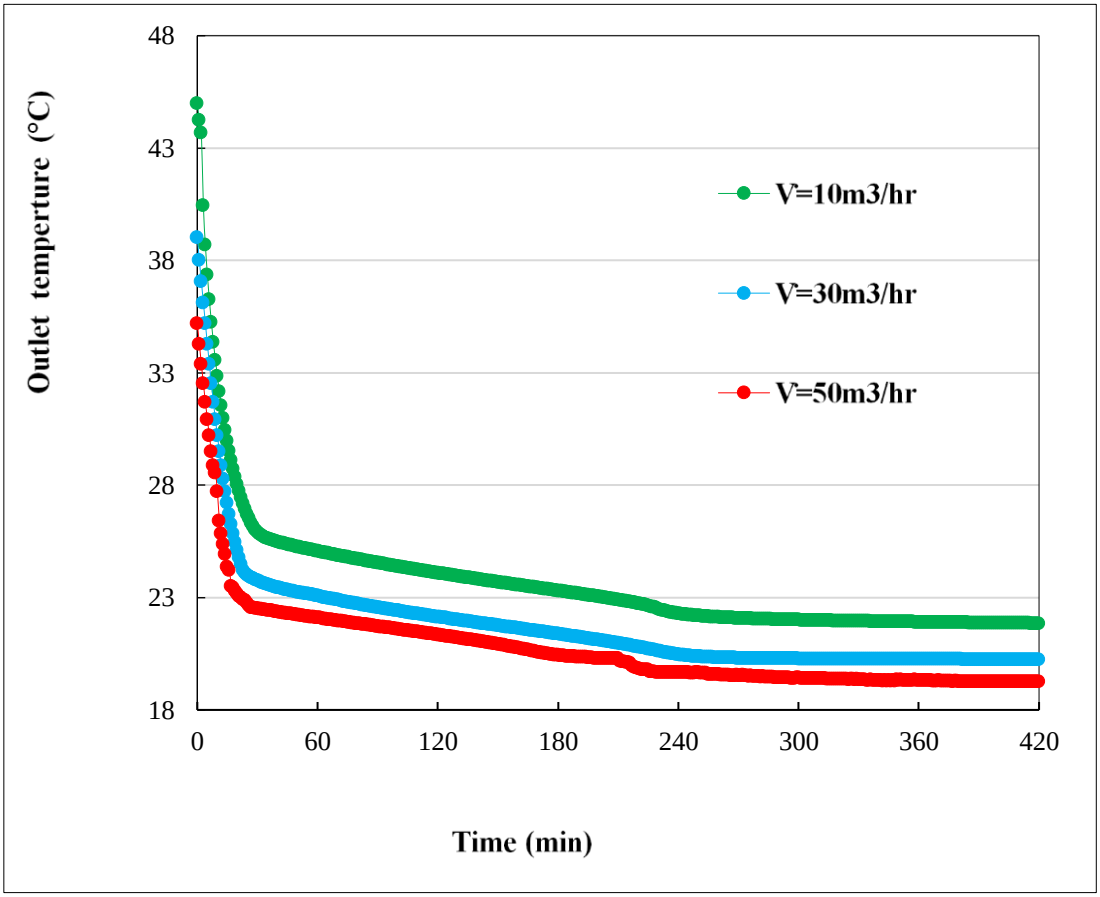

(a)

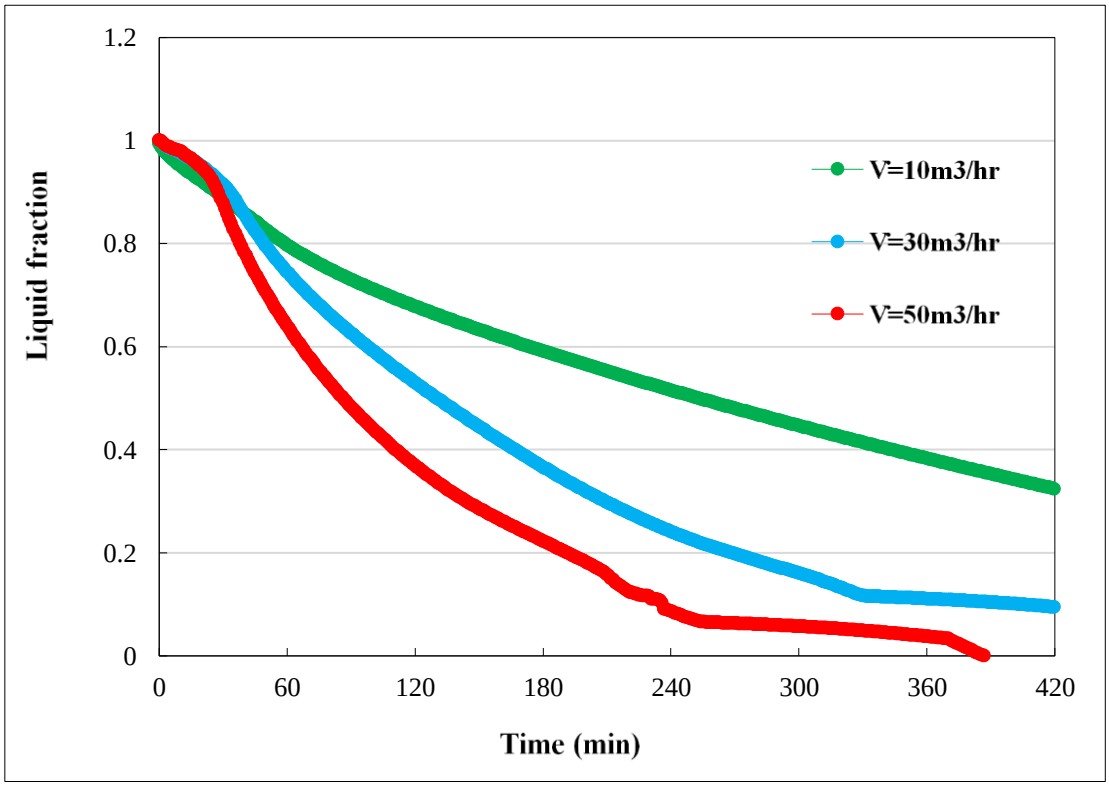
Liquid fraction
1.2
1
0.8
0.6
0.4
0.2
0
0
60
120
180
240
300
360
420
Time (min)
V=10m3/hr
V=30m3/hr
V=50m3/hr

(b)

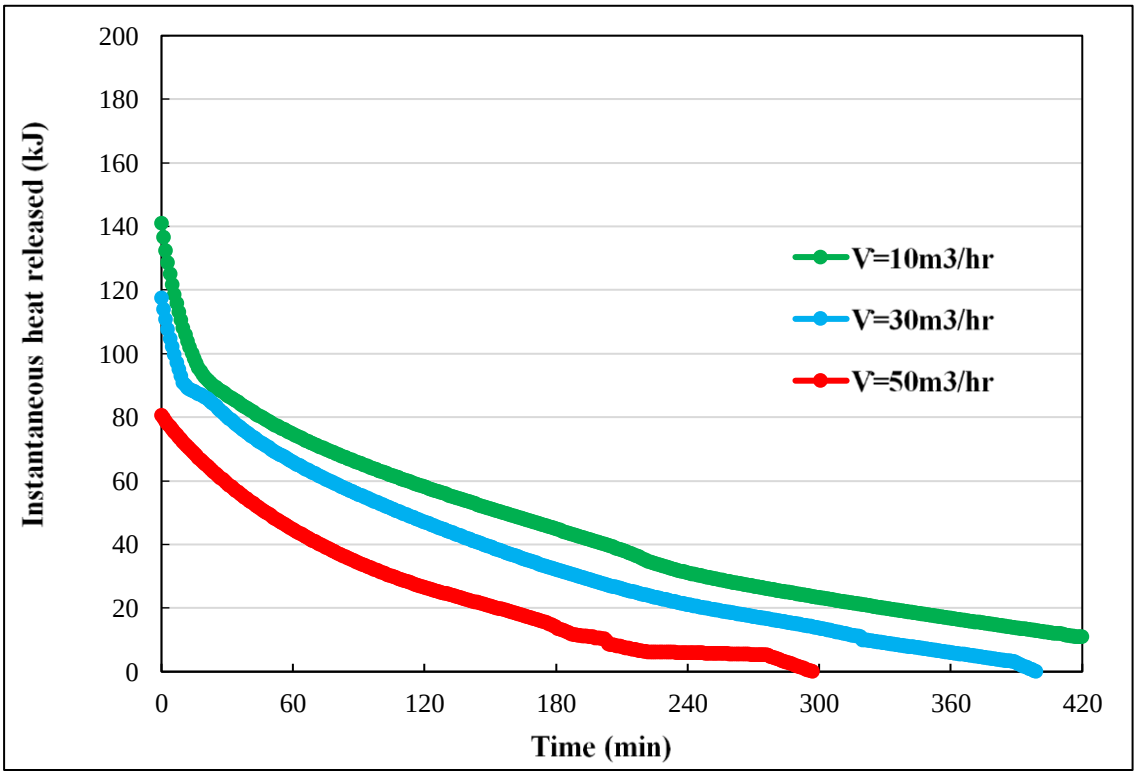
Instantaneous heat released (kJ)
200
180
160
140
120
100
80
60
40
20
0
0
60
120
180
240
300
360
420
Time (min)
V=10m3/hr
V=30m3/hr
V=50m3/hr

(c)

Figure 7-6. Impact of the airflow rate on (a) outlet temperature and (b) liquid fraction and (c) energy stored during the discharging period

According to Figure 7-6, it can easily be seen that variation in airflow rates greatly affected the outlet temperature, liquid fraction and heat releasing rate. Figure 7-6a demonstrates that the outlet temperature decreased sharply within the first 30 minutes of discharging overall. The building envelope's outlet temperature had the highest reduced rate since a higher airflow rate boosted the PCM-gypsum plasterboard to release the stored heat quickly. Even after 4 hours of discharging period, the outlet temperature was relatively higher, above 22°C ,due to the benefits of the PCM releasing the stored heat (Figure 7-6a). It can be believed that the lower airflow rate enabled the heat releasing period to extend for a longer period than the higher airflow rate (Figure 7-6b). The PCM-gypsum plasterboard under the higher airflow rate finished the solidification process in about 6 hours and the lower/medium airflow rates completed the discharging period in more than 7 hours (Figure 7-6b). Also, the higher airflow rate provided higher solidification rates. From Figure 7-6b, it can be found that the airflow rates (10, 30, and 50m^3/hr) had liquid fractions of roughly 0.5, 0.23 and 0.8 respectively, at 240 minutes of discharging time. The variation in airflow rates also affected the heat releasing rate, as shown in Figure 7-6c. The highest airflow rate had the highest rate at which the stored energy was released. The lowest and medium airflow rates used 6.5 and 5 hours respectively, to release the heat entirely. Thus, it can be concluded that the different airflow rates can greatly affect the solidification behaviour of PCM-gypsum plasterboard in terms of outlet temperature, liquid fraction and the heat releasing rate. Figure 7-6 demonstrates that the building envelope operating under a lower airflow rate could achieve a longer period of discharging by which it could provide a higher outlet temperature. In addition, Figure 7-5 also presents that the lower airflow rate can provide the highest outlet temperature and heat stored in the PCM-gypsum plasterboard. Hence, it can be estimated that, the building envelope operation under the airflow rate of

10m^3/hr could have the best performance among the various airflow rates. Hence, the airflow rate of 10m^3/hr was used for rest of the parametric studies and the case study investigations as the optimal design selection of airflow rate.

7.4.3 *Effect of inlet temperature*

Figure 7-7 demonstrates the effect of different inlet air temperatures on this system performance in terms of outlet temperature and liquid fraction ratio for 2 hours of the charging duration. For this analysis, three inlet temperature values of 10, 14 and 18 °C were considered, as these were relatively close to a lower solar heating application. However, the other main parameters such as the plate temperature of 55°C and the airflow rate of 10 m^3/hr stayed unchanged. From Figure 7-7a, it can be observed that increasing the inlet temperature can increase the outlet temperature in the early period of the charging duration, especially in the first 60 mins. However, the outlet temperature difference due to the various inlet temperatures seems to be reduced as the charging period goes on. For instance, the inlet temperature of 10 and 18°C achieved outlet temperature differences of approximately 3.0°C and 1.1°C, respectively, at 60 mins and 120 mins.

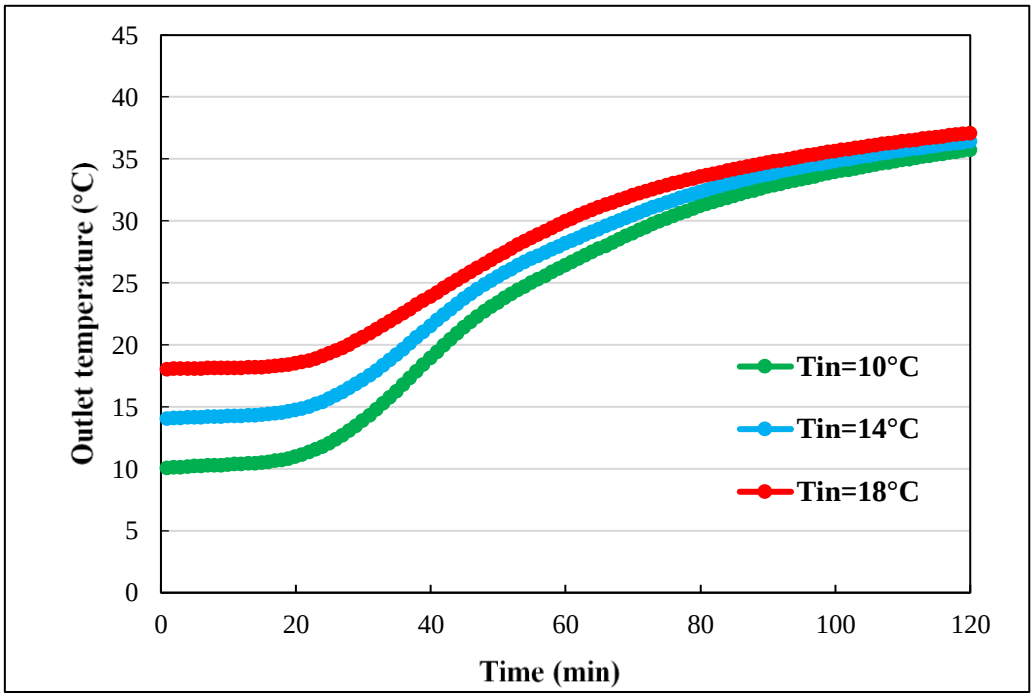
Outlet temperature (°C)
45
40
35
30
25
20
15
10
5
0
0
20
40
60
80
100
120
Time (min)
Tin=10°C
Tin=14°C
Tin=18°C

(a)

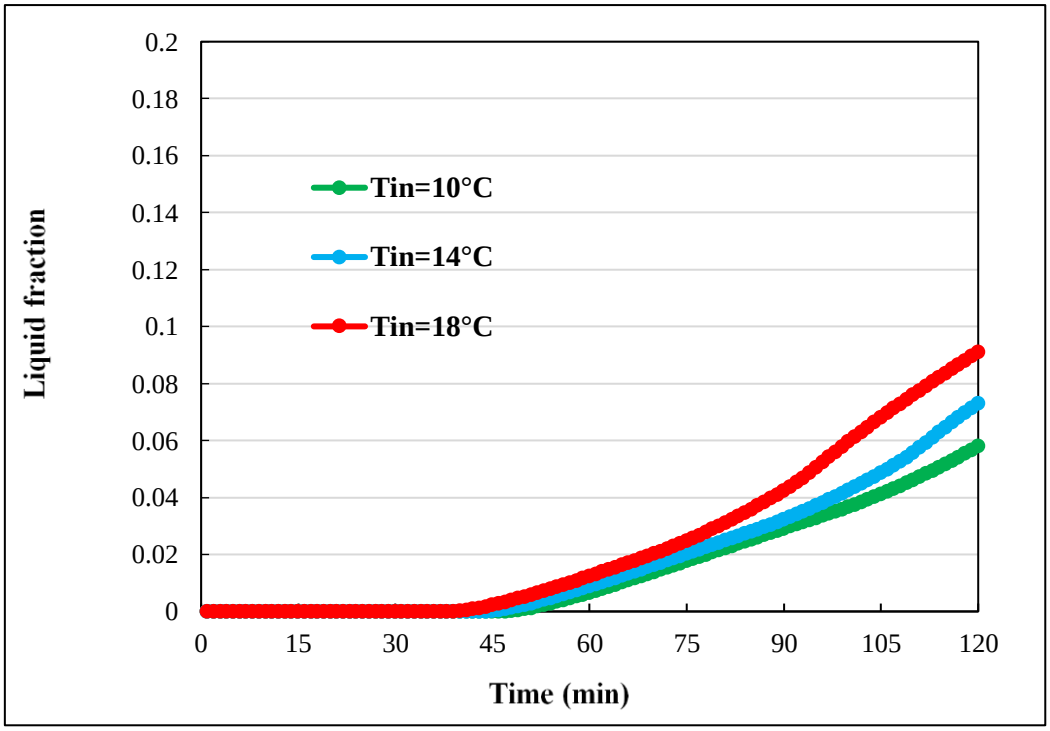
Liquid fraction
0.2
0.18
0.16
0.14
0.12
0.1
0.08
0.06
0.04
0.02
0
0
15
30
45
60
75
90
105
120
Time (min)
Tin=10°C
Tin=14°C
Tin=18°C

(b)

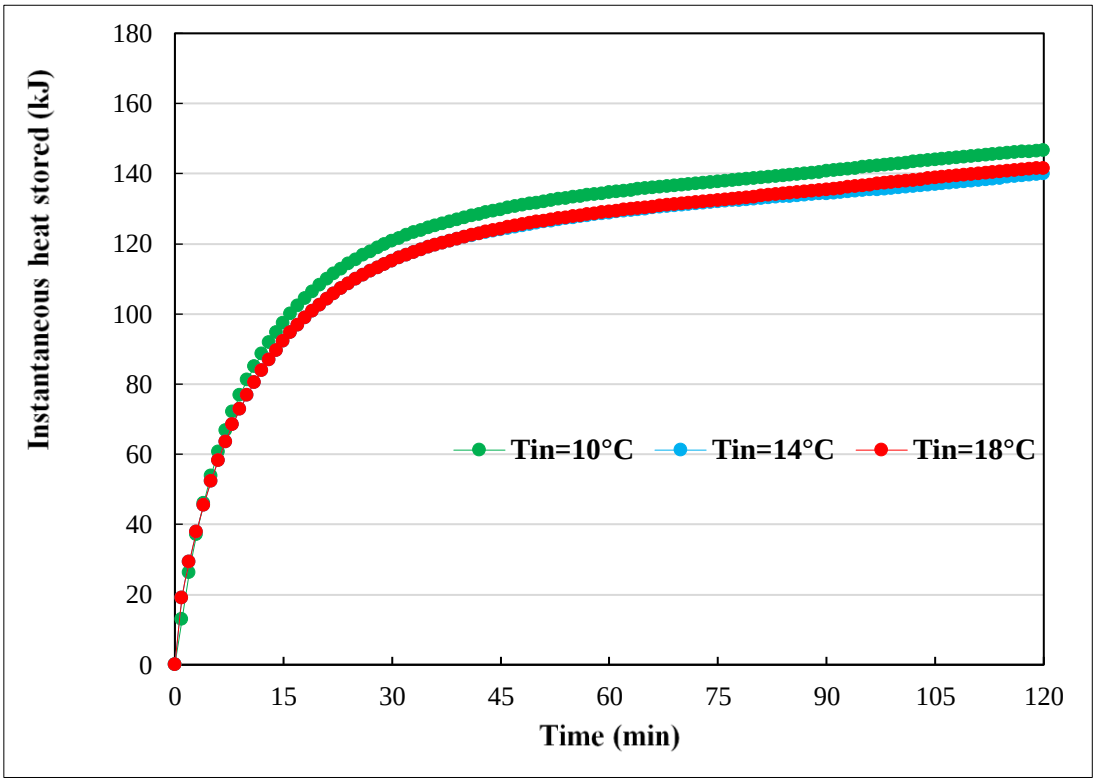

(c)

Figure 7-7. Impact of the inlet temperature on (a) outlet temperature and (b) liquid fraction and (c) heat stored during the charging period

In terms of the charging behaviour of the PCM wall, Figure 7-7b displays that the decrease in inlet temperature from 18°C to 10°C reduces the potential temperature variation between the plenum air and the PCM wall, which is likely to increase the charging time. For instance, the inlet temperature of 18°C took roughly 90 mins to finish the liquid fraction ratio of 0.05. Meanwhile, a charging period of 115 mins was required by the inlet temperature of 10°C to achieve the same liquid fraction ratio. Various inlet temperatures could create temperature difference variations across the plenum between the plenum air and the PCM wall. In return, this would bring a reasonable drop in instantaneous heat transfer alongside the plenum. With respect to the charging period, the total latent energy stored inside the PCM wall would be kept unchanged as the amount of PCM was the same for all the cases. However, Figure 7-7c

demonstrates that the different values of inlet temperature are likely to slightly impact the rate of energy storage and the instantaneous energy stored. For instance, the instantaneous energy stored at 120 minutes was shown as roughly 140kJ for all the inlet temperature trials. Therefore, it has a slight impact on the melting behaviour and outlet temperature only in the early period of the charging process. However, it can be estimated that changing the inlet temperature on a small scale has a marginal influence on system performance and melting behaviour when the charging time increases.

Figure 7-8 presents the results of the outlet temperature, liquid fraction and heat stored for all three airflow rates during the discharging period. It can be found that various ranges of inlet temperatures influence the outlet temperature, liquid fraction and heat releasing rate differently during the solidification period. Figure 7-8a demonstrates that the outlet temperature decreased sharply within the first 30 minutes of the discharging period and gradually reached a relatively steady state. However, increasing the inlet temperature achieved a higher outlet temperature. For instance, inlet temperatures of 10°C and 18°C provided outlet temperatures of around 16 and 20°C separately. Meanwhile, after 150 mins. of the discharging process, the outlet temperatures could be claimed as roughly 16°C, 19°C, and 21.7°C respectively, for the inlet temperatures of 10, 14, and 18°C (Figure 7-8a).

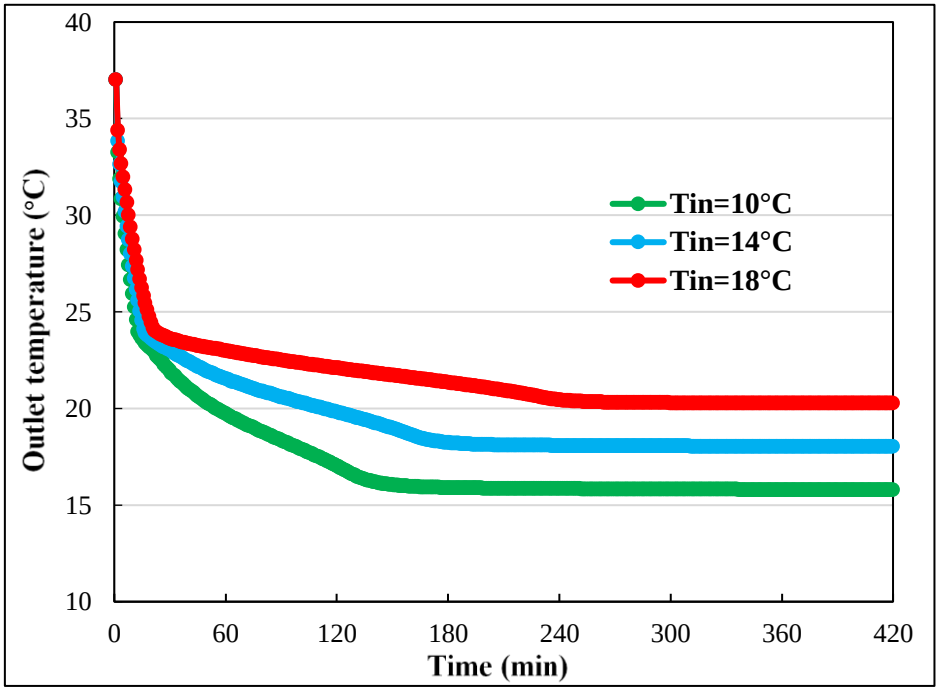
Outlet temperature (°C)
40
35
30
25
20
15
10
0
60
120
180
240
300
360
420
Time (min)
Tin=10°C
Tin=14°C
Tin=18°C

(a)

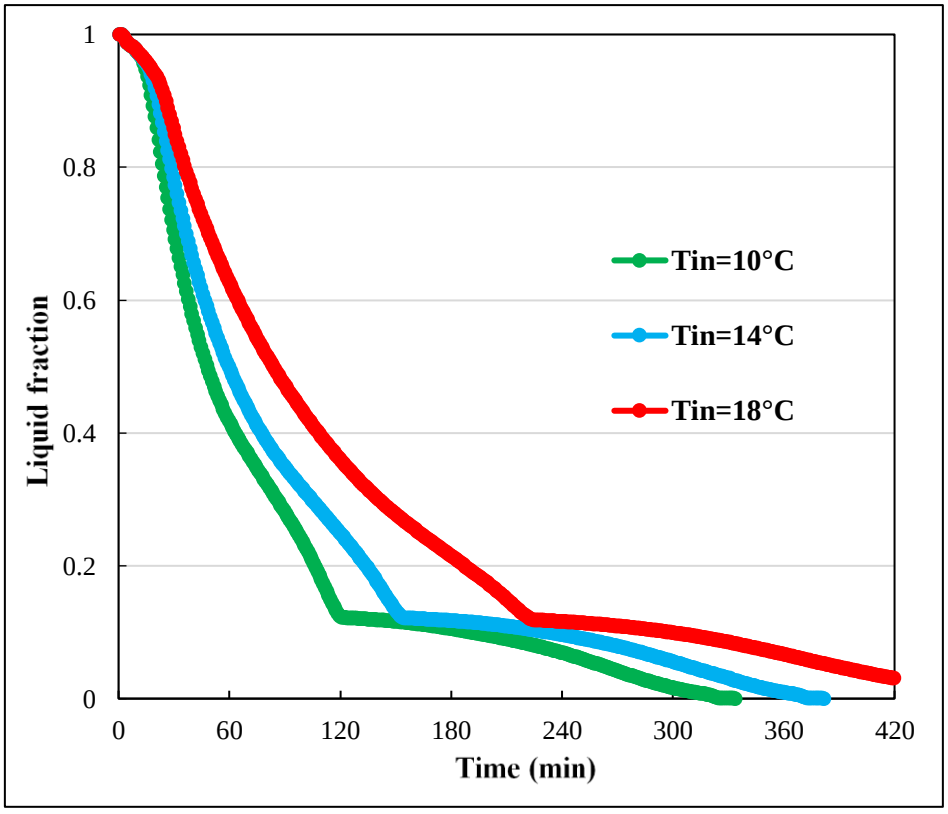
Liquid fraction
1
0.8
0.6
0.4
0.2
0
0
60
120
180
240
300
360
420
Time (min)
Tin=10°C
Tin=14°C
Tin=18°C

(b)

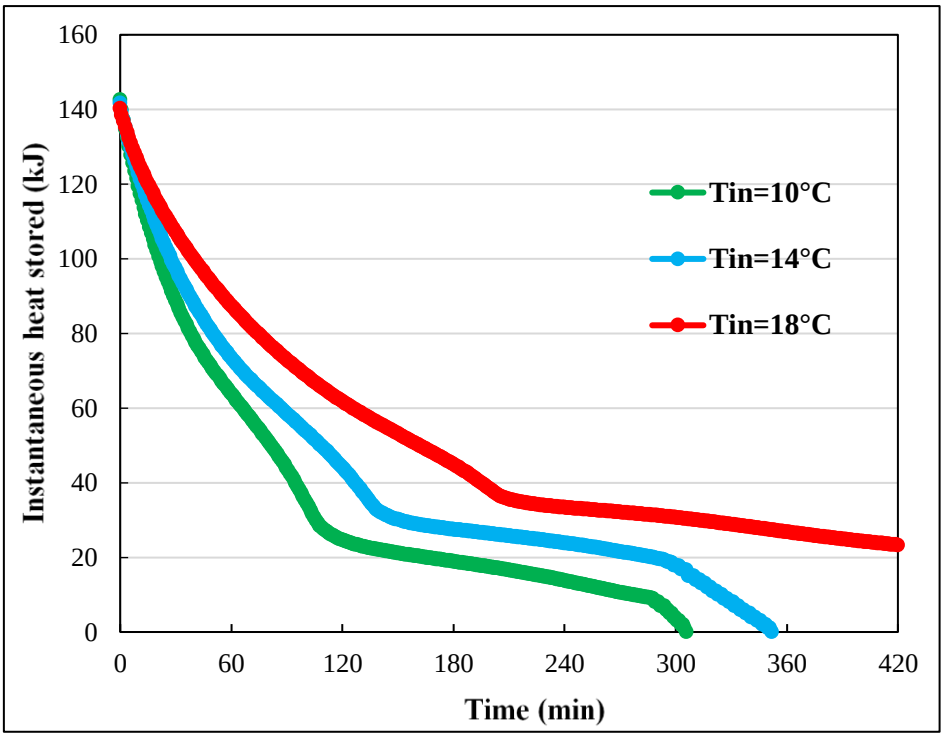

(c)

Figure 7-8. Impact of inlet temperature on (a) outlet temperature and (b) liquid fraction and (c) energy stored during the discharging period

According to Figure 7-8b, it is believed that different inlet temperatures critically affect the liquid fraction and the higher inlet temperatures spent a longer time to finish the solidification period. For instance, at the 120 minutes discharging point, the liquid fractions were 0.12, 0.24, 0.35, respectively, for the inlet temperatures of 10, 14 and 18°C. Meanwhile, the liquid fraction was zero (assuming the completion of solidification) at 5.5 and 6.25 hours for the inlet temperatures of 10 and 14°C (Figure 7-8b). Such results indicated that decreasing the inlet temperature improved the freezing speed as the PCM-gypsum plasterboard released the storage energy quickly thorough convection heat transfer because of the lower inlet temperature. Figure 7-8c demonstrates the impact of various inlet temperatures on the instantaneous heat stored

during the solidification period. It was obvious that the range of various inlet temperatures dramatically influenced the heat realising rate though convective heat transfer behaviour. The stored heat in the PCM-gypsum plasterboard would be completely released at roughly 5 and 6 hours for the inlet temperatures of 10 and 14°C. Meanwhile, the inlet temperature of 18°C took a longer time to release the stored heat (Figure 7-8c). For example, after 3 hours of the solidification period, the instantaneous heat stored were 19, 28 and 45kJ respectively, for the inlet temperatures of 10, 14, and 18°C. Such results can indicate that the building envelope's energy releasing rate is reduced under relatively higher inlet temperatures, which is beneficial for effective later use. Thus, it can be concluded that various inlet temperatures greatly affect the outlet temperature and releasing rate of the stored energy during the discharging process. However, the effect of various inlet temperatures on the charging period is limited. However, the inlet temperature of 18°C has a greater advantage during the discharging process especially for the releasing rate of energy stored. Hence, the optimal design for the case study determined the inlet temperature at 18°C.

7.4.4 *Effect of plate temperature*

The impact of various plate temperatures (simulating solar irradiation) on the building envelope's performance included outlet temperature and liquid fraction for 2 hours of the charging period. For this investigation, four different plate temperatures with a 15°C increment at 40, 55, 70 and 85°C were included. Other boundary conditions stayed unchanged, such as inlet temperature at 18°C and an airflow rate of $10m^3$/hr. Figure 7-9a shows that increasing the plate temperature could achieve a higher outlet air temperature. For instance, plate temperatures of 40 and 85°C produced outlet temperatures of 30.62 and 52.30°C, respectively. According to Figure 7-9a, it can be illustrated that the simulation cases under various plate temperatures showed relatively higher increasing trends in the first hour of charging and then displayed steadily

increasing curves between 60 and 120 minutes of charging duration. It can also be presented that the outlet temperature difference for various simulation cases with different plate temperatures firstly showed an increasing difference as the charging time increased, reaching an unchanged outlet temperature gap as the outlet temperature reached its peak. In addition, the impact of various plate temperatures on melting behaviour is presented in Figure 7-9b as the result of the liquid fraction.

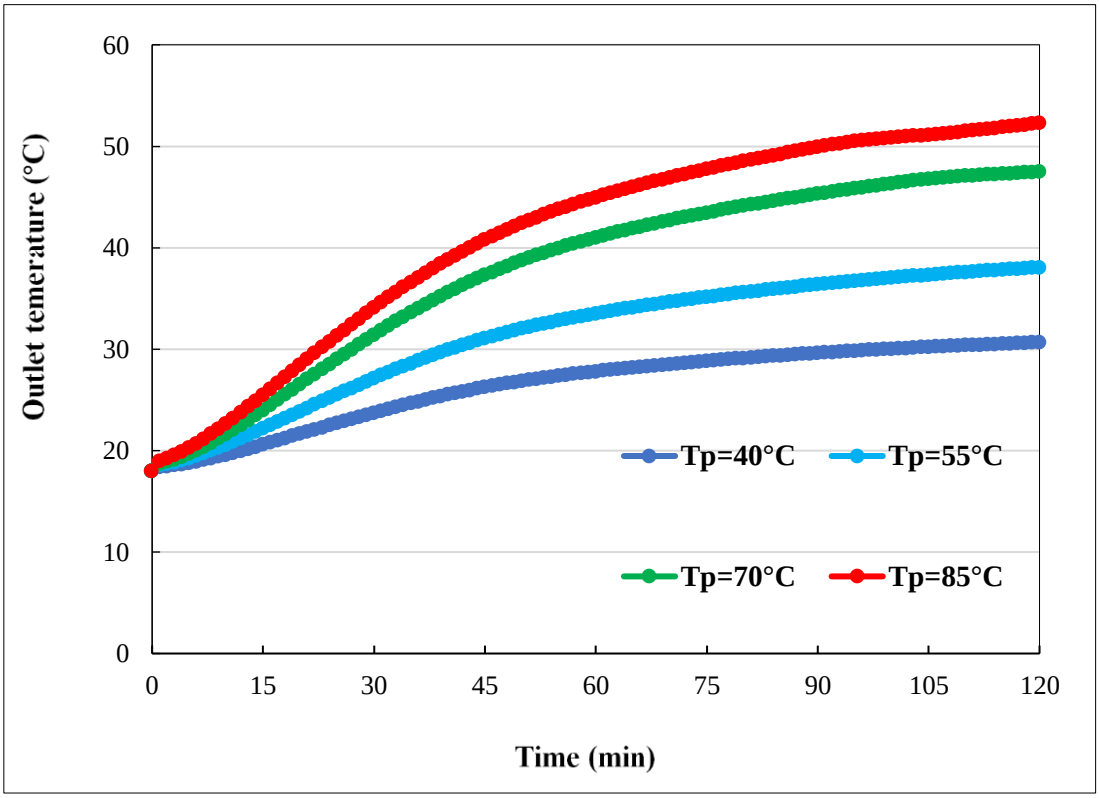

(a)

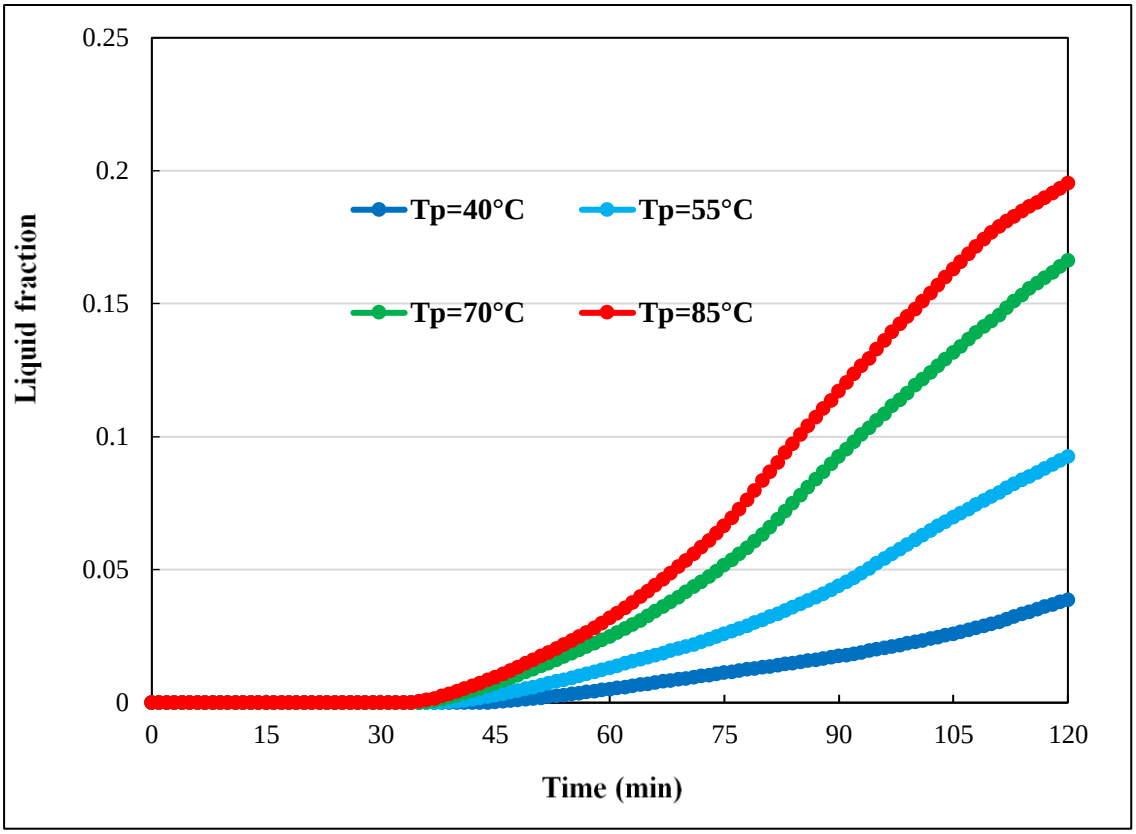
Liquid fraction
0.25
0.2
0.15
0.1
0.05
0
Tp=40°C
Tp=55°C
Tp=70°C
Tp=85°C
0
15
30
45
60
75
90
105
120
Time (min)

(b)

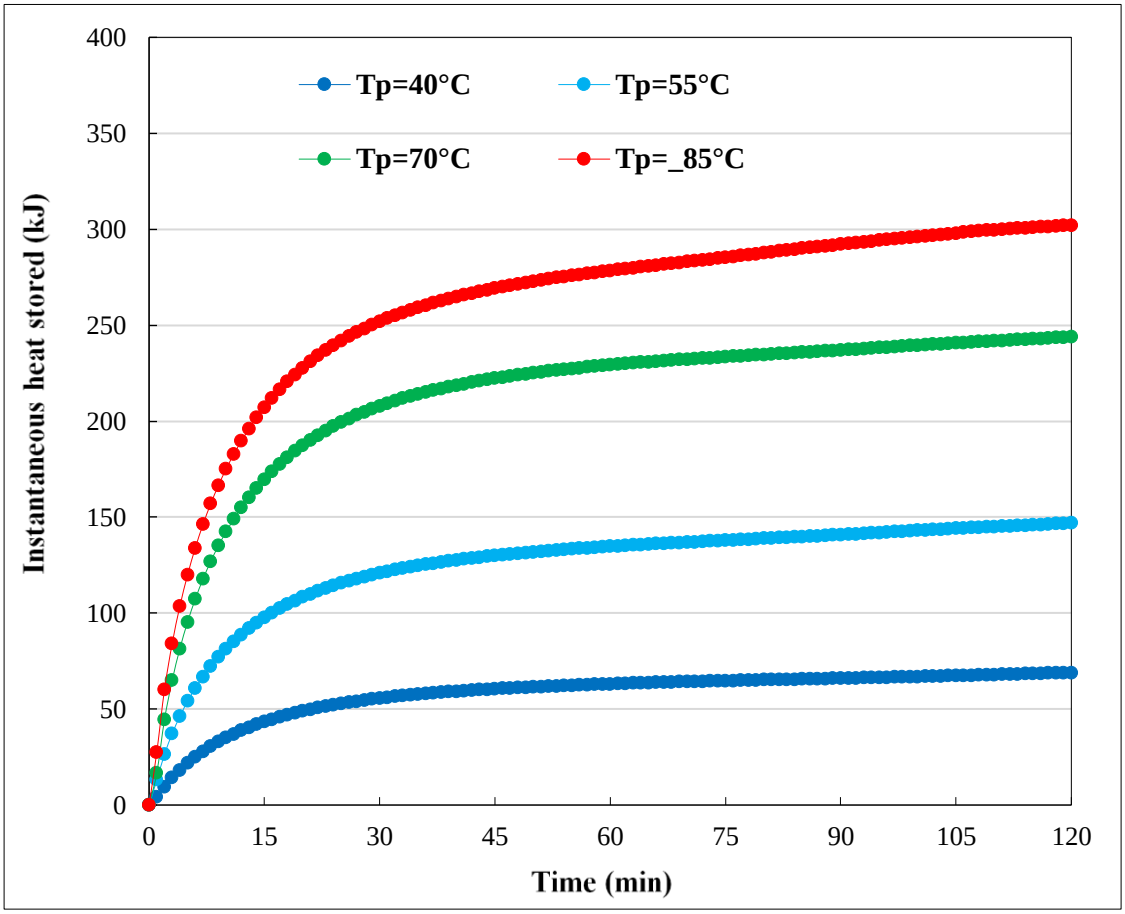

Figure 7-9. Impact of plate temperature on (a) outlet temperature and (b) liquid fraction and (c) heat stored during the charging process

The results in Figure 7-9b introduced that the simulation cases with higher outlet temperatures showed higher liquid fractions. For instance, the numerical model could achieve roughly 0.2 and 0.1 of liquid fraction for the PCM-gypsum plasterboard during 2 hours of the charging period by plate temperatures of 85 and 55°C, separately. Plate temperatures of 70 and 55°C respectively spent roughly 1.25 and 2.10 hours in order to melt 10% of PCM-gypsum plasterboard. (Figure 7-9b). It can be concluded that increasing the plate temperature enhanced the melting process of the PCM back wall. Also, under such plate temperature operations, the PCM-gypsum plasterboard stored a certain amount of sensible heat in the first 35 minutes of the charging period and then stored it as latent heat during the charging period between roughly 35 mins. and 120

mins., when the liquid fraction was gaining values above zero (Figure 7-9b). Even the total latent heat stored was same when the melting was fully finished due to same amount of PCM being used. Figure 7-9c shows that the instantaneous heat stored during the time of the charging period for the PCM-gypsum plasterboard would be varied due to the different plate temperatures (solar radiation). For example, the building envelope operating at plate temperatures of 40 and 85°C achieved approximately 68 and 302kJ, separately, at the 2 hour mark of the charging duration. Hence, according to Figure 7-9, the results demonstrate that the impact of plate temperature (simulating solar radiation) greatly impacts on the outlet temperature and charging behaviour of the PCM-gypsum plasterboard. This is similar to the effect observed for the variation in the airflow rate. However, the effect of various outlet temperatures was ignored as the plate temperature was equal to the inlet temperature during the discharging period where there is no solar radiation, so that the plate temperature kept to the ambient air temperature.

7.4.5 *Effect of plenum size*

The impact of plenum size was studied through analysing the influence of three plenum sizes (100, 150 and 200mm) on building envelope performance in terms of outlet temperature, liquid fraction, collector efficiency, HEE and instantaneous heat stored/released. For this investigation, three different plenum depths at 100, 150 and 200 mm were included. Other boundary conditions stayed unchanged such as an inlet temperature of 18°C and an airflow rate of $10m^3$/hr (approach velocity as 0.01m/s). Figure 7-10a shows that that the outlet temperature had a similar trend under various plenum sizes. Various plenum widths influenced the outlet temperature during the charging period and increasing the plenum could reduce the outlet temperature. For instance, plenum sizes of 100 and 200mm achieved outlet temperatures of approximately 43 and 41°C respectively, at 120mins (Figure 7-10a). Figure 7-10a's results can indicate that the impact of changing the plenum width was not significant.

The effect on heat exchange effectiveness is also seen in Figure 7-10b. It is clear that decreasing the plenum size has the impact of potentially increasing the HEE and collector efficiency. For example, the plenum sizes of 100 and 200mm provided the highest HHE at 0.68 and 0.62, separately (when the plate temperature was fully heated by solar radiation) (Figure 7-10b). This result could conclude that increasing the plenum size enables the outlet temperature and HHE to reduce marginally. Thus, the collector efficiency could be reduced by decreasing the plenum size due to the HEE results. Figure 7-11 illustrates the impact on phase change behaviour and heat stored.

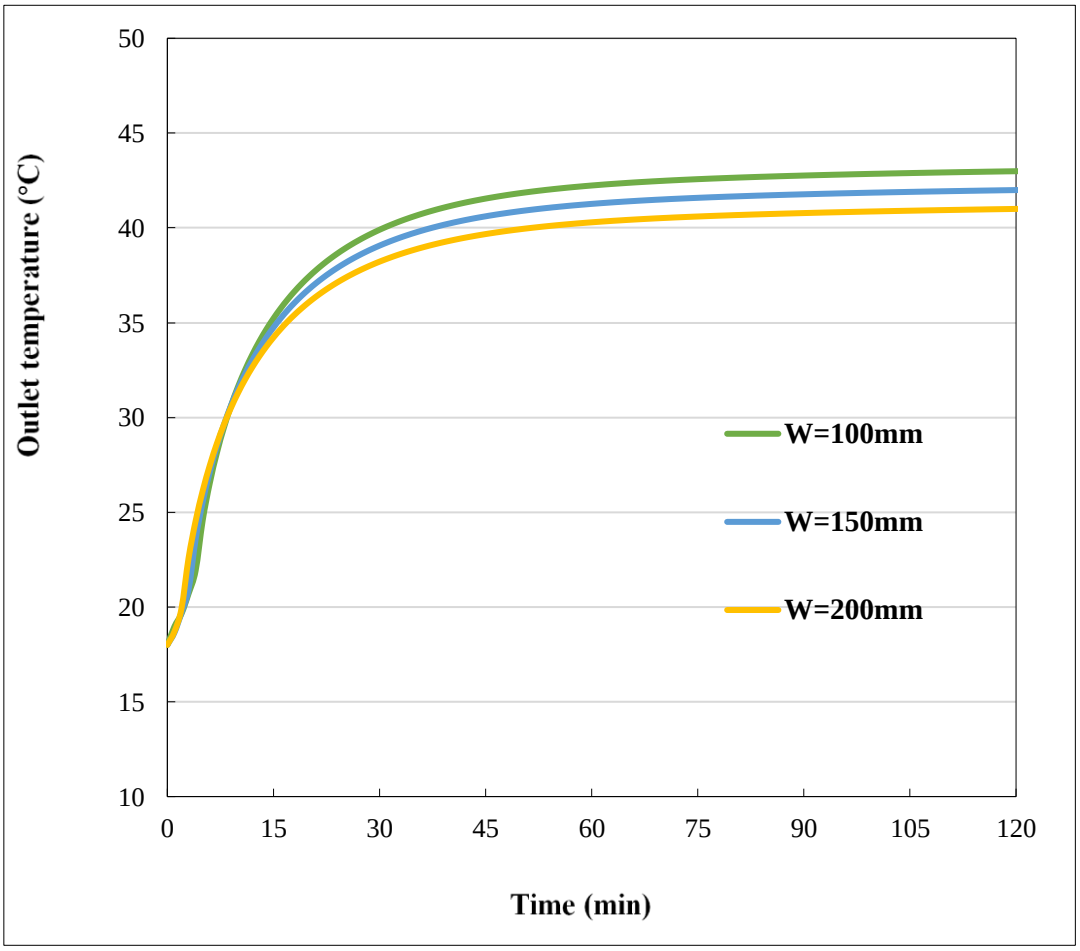

(a)

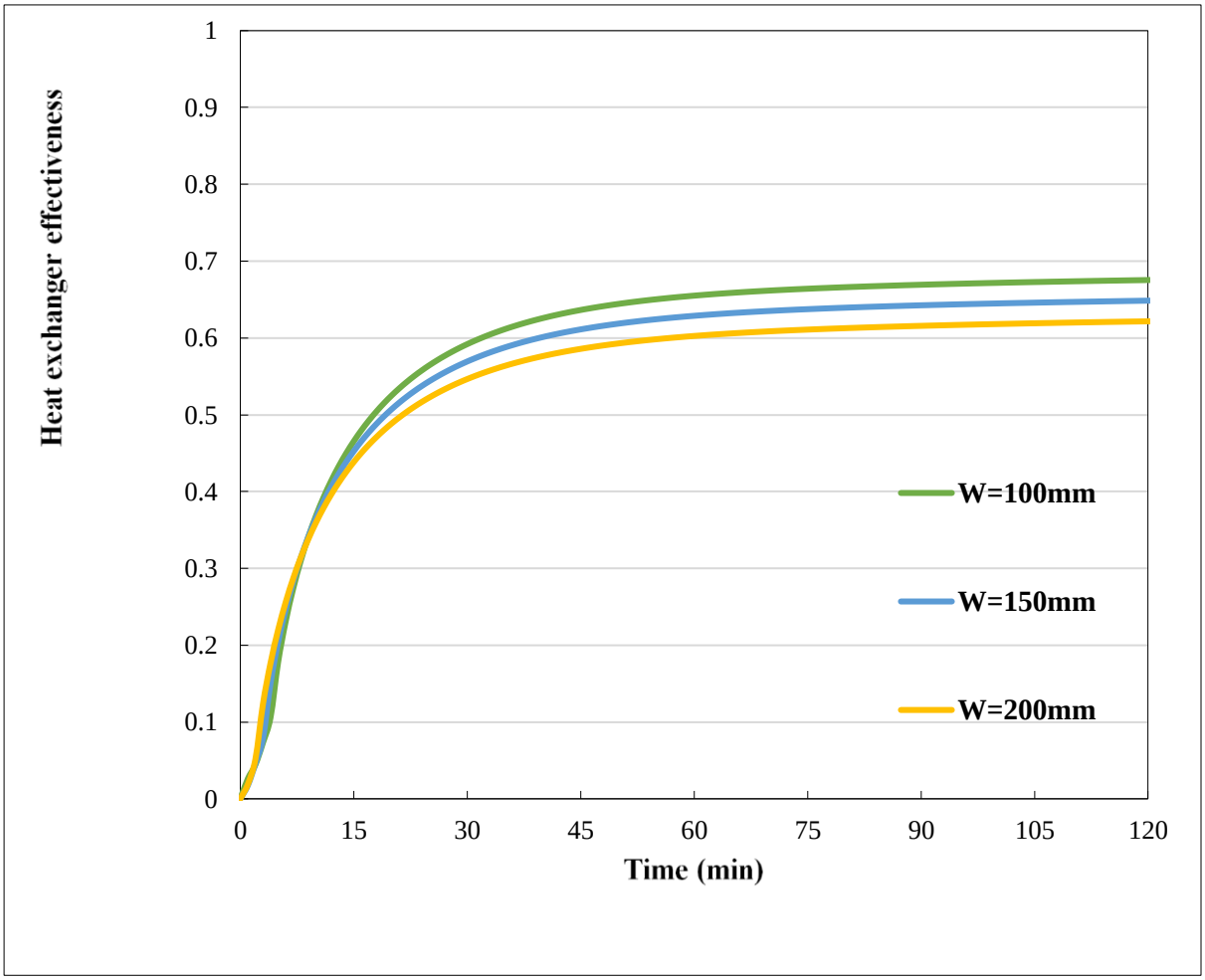

(b)

Figure 7-10. Impact of plenum size on (a) outlet temperature and (b) HEE during the charging process

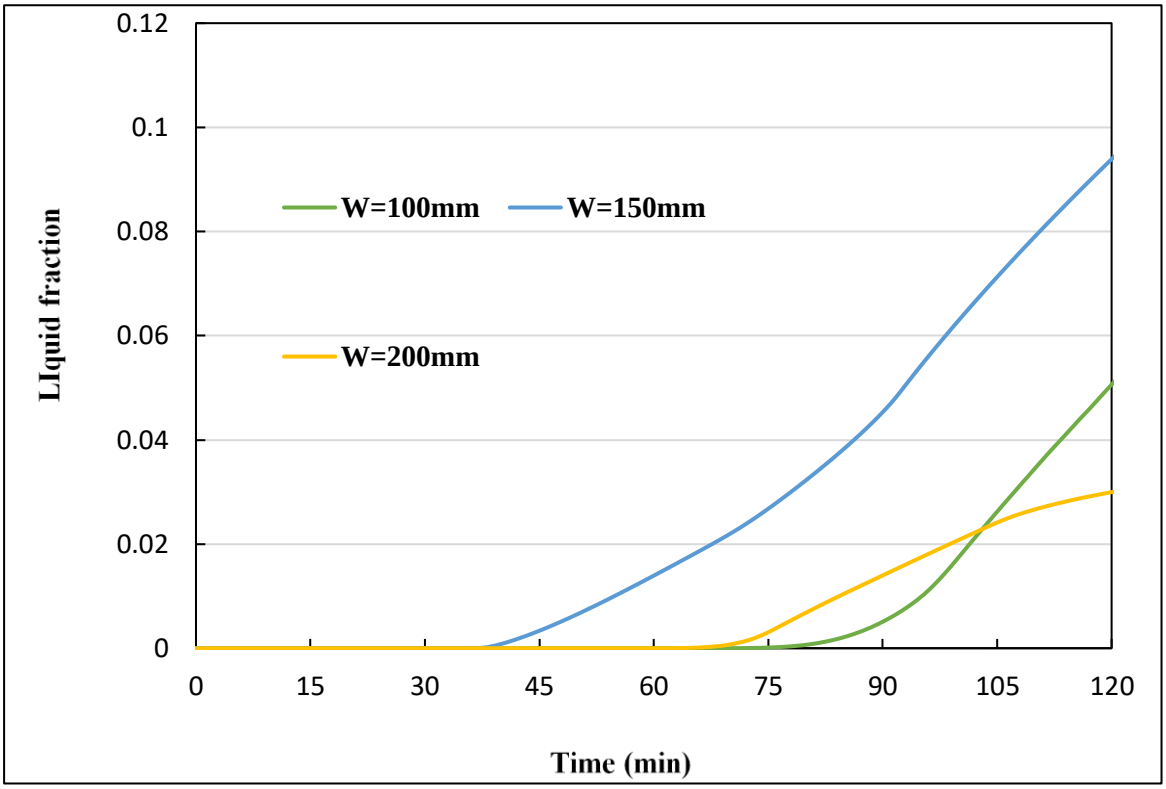
0.12
0.1
0.08
0.06
0.04
0.02
0
LIquid fraction
W=100mm
W=150mm
W=200mm
0
15
30
45
60
75
90
105
120
Time (min)

(a)

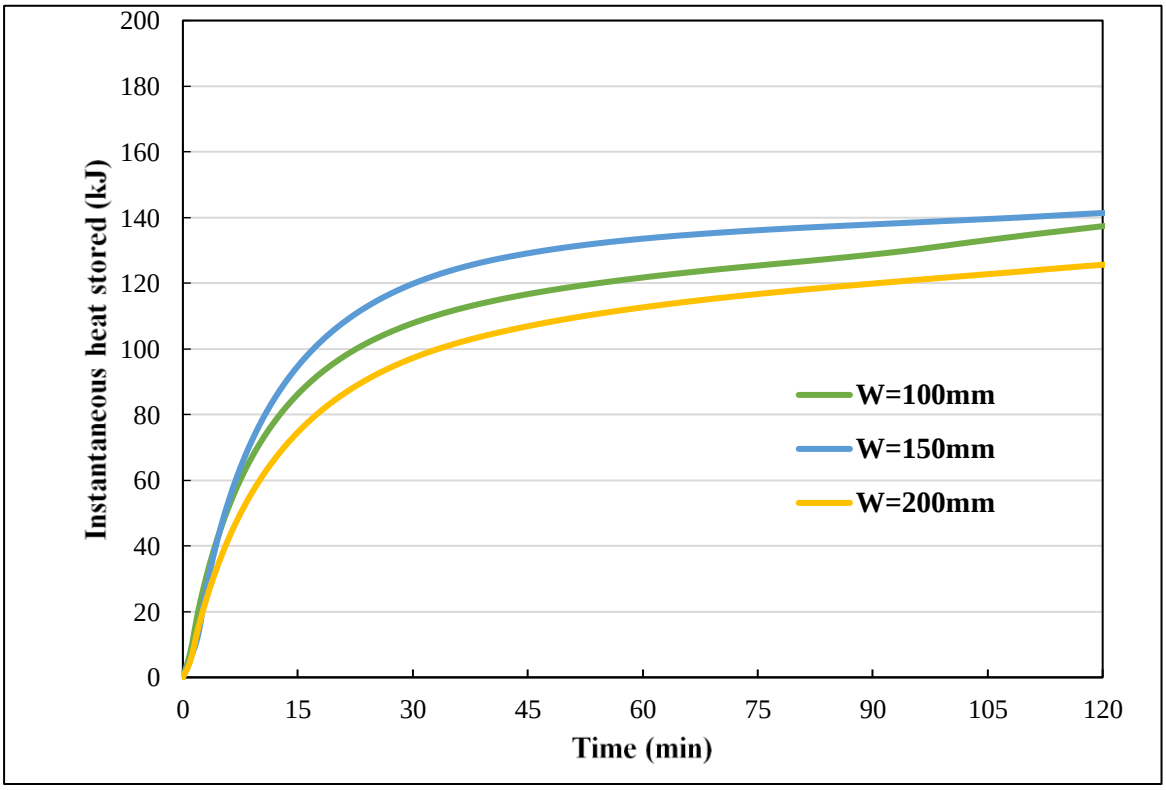
200
180
160
140
120
100
80
60
40
20
0
Instantaneous heat stored (kJ)
W=100mm
W=150mm
W=200mm
0
15
30
45
60
75
90
105
120
Time (min)

(b)

Figure 7-11. Impact of plenum size on (a) liquid fraction and (b) instantaneous heat stored during the charging process

Figure 7-11 presents the impact of various plenum sizes on the phase change behaviour of PCM-gypsum plasterboard and its instantaneous energy stored during 2 hours of the charging period. The plenum size had limited influence on the liquid fraction and energy stored. Meanwhile, among all the plenum sizes, the plenum width of 150mm had the greatest liquid faction and instantaneous energy stored at 0.093 and 142kJ, respectively (Figure 7-11). Also, the plenum sizes of 100 and 200mm separately achieved a liquid fraction of 0.05 and 0.03, respectively. Meanwhile, the instantaneous energy stored were at 138 and 124kJ, separately. The results in Figure 7-11 can indicate that increasing the plenum size could melt a smaller amount of PCM and store a smaller amount of instantaneous energy. Hence, changing the plenum size has a marginal impact on building envelope performance during the charging period. Meanwhile, Figure 7-12 demonstrates the impact of plenum size on outlet temperature, liquid fraction and instantaneous energy stored during the discharging period.

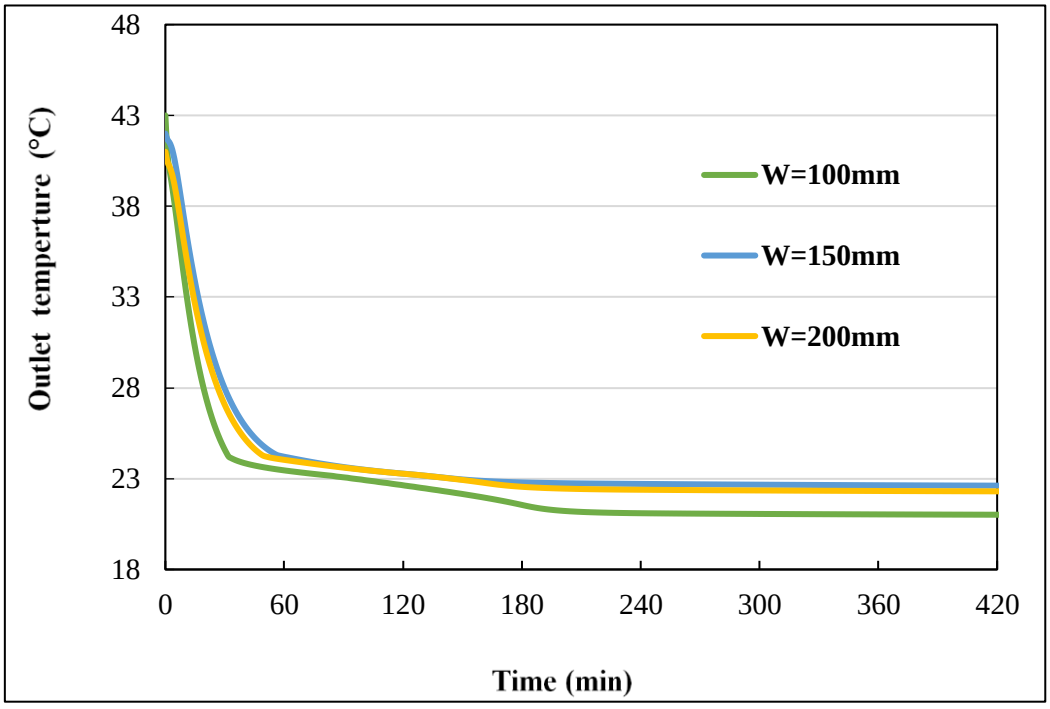

(a)

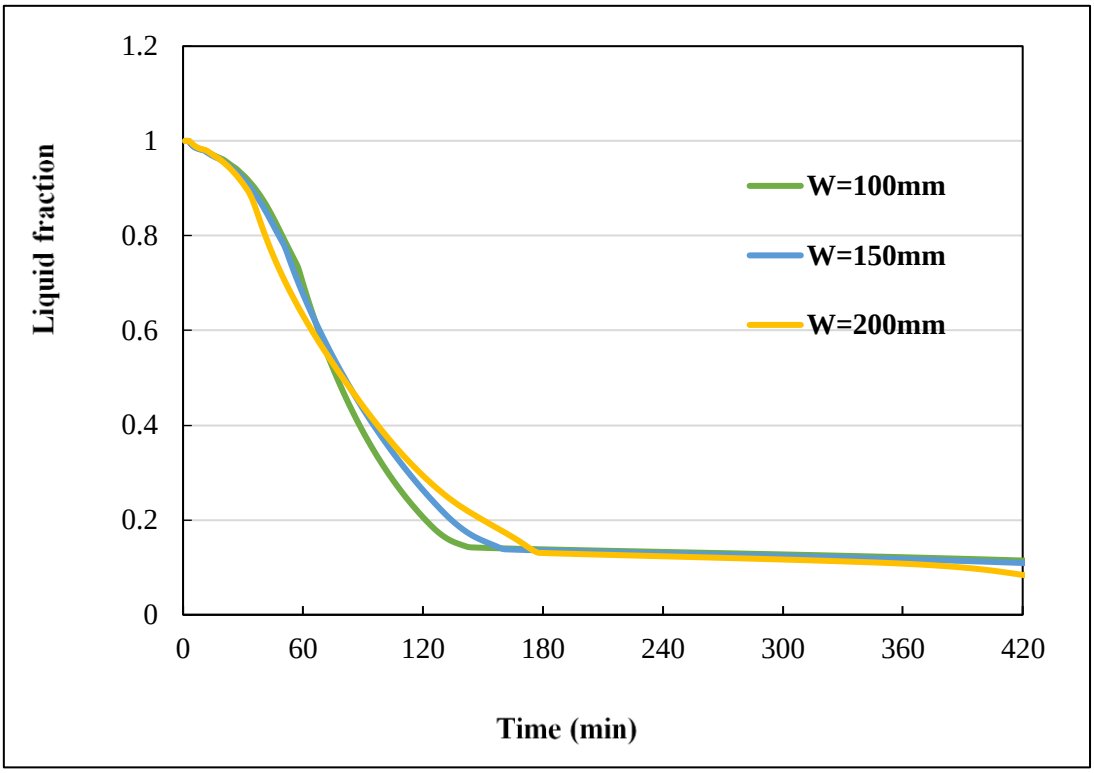
Liquid fraction
1.2
1
0.8
0.6
0.4
0.2
0
0
60
120
180
240
300
360
420
Time (min)
W=100mm
W=150mm
W=200mm

(b)

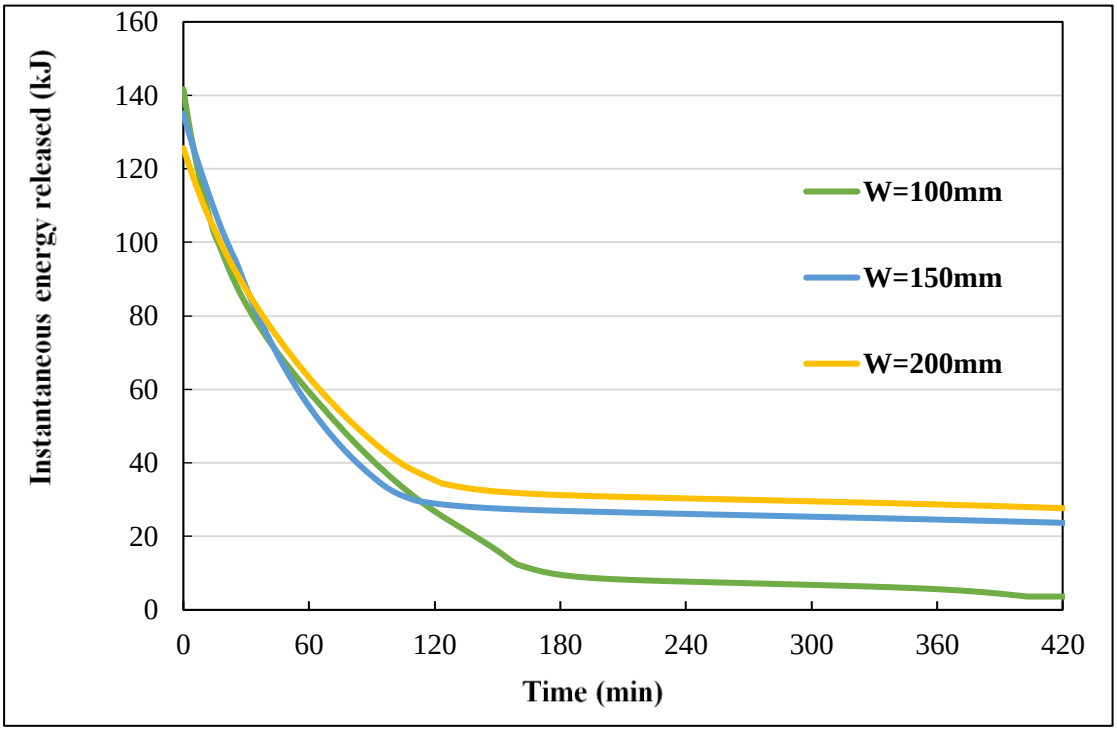
Instantaneous energy released (kJ)
160
140
120
100
80
60
40
20
0
0
60
120
180
240
300
360
420
Time (min)
W=100mm
W=150mm
W=200mm

(c)

Figure 7-12. Impact of plenum size on (a) outlet temperature, (b) liquid fraction and (c) instantaneous energy released during the charging process

Figure 7-12 displays the results of the impact of various plenum widths on outlet temperature, liquid fraction and instantaneous energy stored during the discharging period while keeping the inlet temperature and airflow rates at 18°C and 10m^3/hr respectively. Meanwhile, the hole diameter and pitch dimension were 1mm and 20mm. According to Figure 7-12a, it can be believed that the impact of plenum size on outlet temperature during the discharging period is limited. For instance, plenum sizes of 100 and 200mm reduced the outlet temperature to 23 degrees at 100 and 150 mins. It can be predicted that shrinking the plenum size would greatly and quickly reduce the outlet temperature. Such an observation can be seen for the liquid fraction changes shown in Figure 7-12b. In order to achieve a liquid fraction of approximately 0.2, plenum widths of 100, 150 and 200mm consumed 120 mins, 125 mins, and 150 mins, respectively. It can be stated that increasing the plenum size would decrease the liquid fraction speed. Hence, the instantaneous energy is released differently due to the liquid fraction and outlet temperature changes. For instance, the plenum size of 100 released the stored energy quickly with a larger amount among all the plenum sizes (Figure 7-12c). Such results can be explained, since shrinking the plenum size under the same approach velocity, the plenum air velocity increases and boosts the convective heat transfer coefficient between the PCM-gypsum plasterboard surface and the plenum in order to release the stored heat quickly during the solidification process.

Such results in Figure 7-12 can present that various plenum widths can influence the outlet temperature, liquid fraction and instantaneous energy release, bringing an effective impact on efficiency. However, the impacts are limited. Meanwhile, it is clear that decreasing the plenum width could reduce the solidification time of the PCM-

gypsum plasterboard. However, a plenum size of 150mm would be the optimal choice for designing the plenum dimensions according to the results shown in Figure 7-10, Figure 7-11 and Figure 7-12.

7.4.6 *Effect of pitch dimension*

The impact of the pitch size was investigated through analysing the influence of three pitch dimensions (20, 22 and 25mm) on building envelope performance in terms of outlet temperature, liquid fraction, collector efficiency, HEE and instantaneous heat stored/released. For this investigation, three different pitch depths of 20, 22 and 25mm were included and other boundary conditions stayed unchanged, such as an inlet temperature of 18°C and an airflow rate of $10m^3$/hr (approach velocity at 0.01m/s). Figure 7-13 displays the influence of various pitch dimensions on outlet temperature and HEE. The impact of various pitch sizes had an increasing trend in terms of outlet temperature and HEE. During 2 hours of the charging period, the outlet temperature and HEE reached relative steadiness after 45mins. Hence, after 45 mins. of charging, the pitch dimensions of 20 mm and 25 mm achieved 42 and 40°C. respectively. The HEE were claimed as 0.65, 0.64, and 0.60 separately, for three different pitch dimensions (20, 22 and 25mm) (Figure 7-13). Besides, increasing the pitch size could relatively reduce the efficiency as the outlet temperature decreased. However, it can be believed that increasing the pitch size has a limited impact on outlet temperature and HEE. Also, the impact of various pitch dimensions on the phase change of PCM-gypsum plasterboard is explained in Figure 7-14.

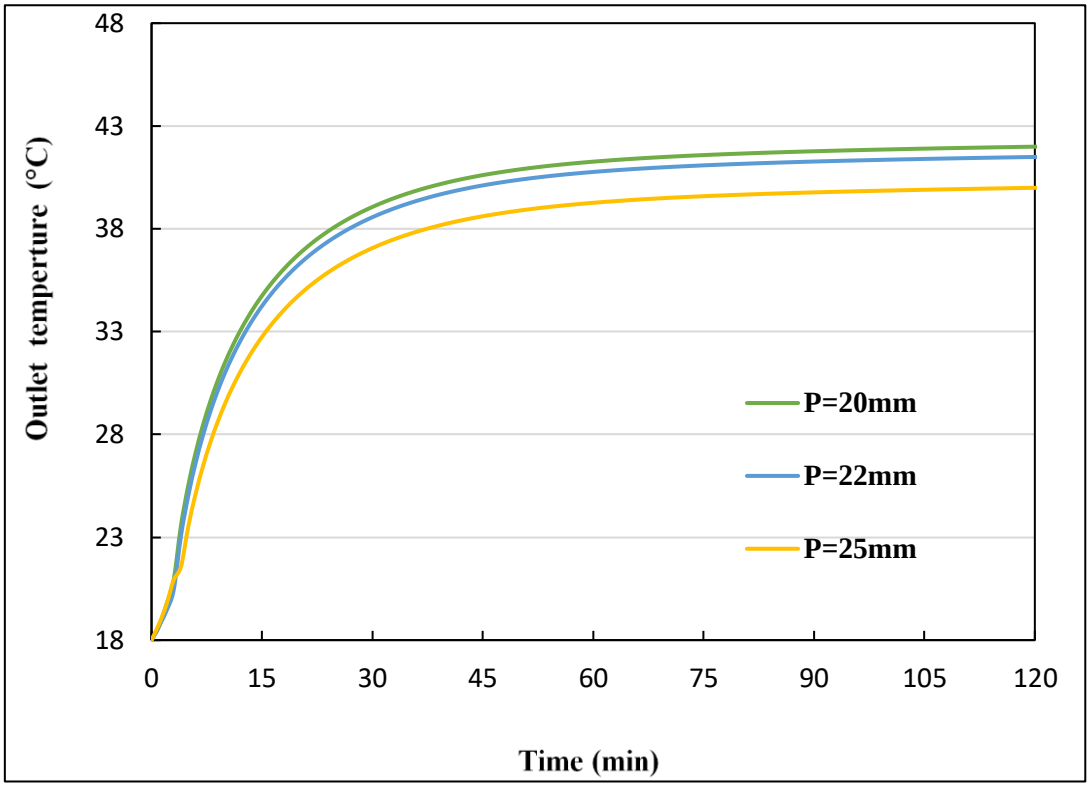
Outlet temperture (°C)
48
43
38
33
28
23
18
0
15
30
45
60
75
90
105
120
Time (min)
P=20mm
P=22mm
P=25mm

(a)

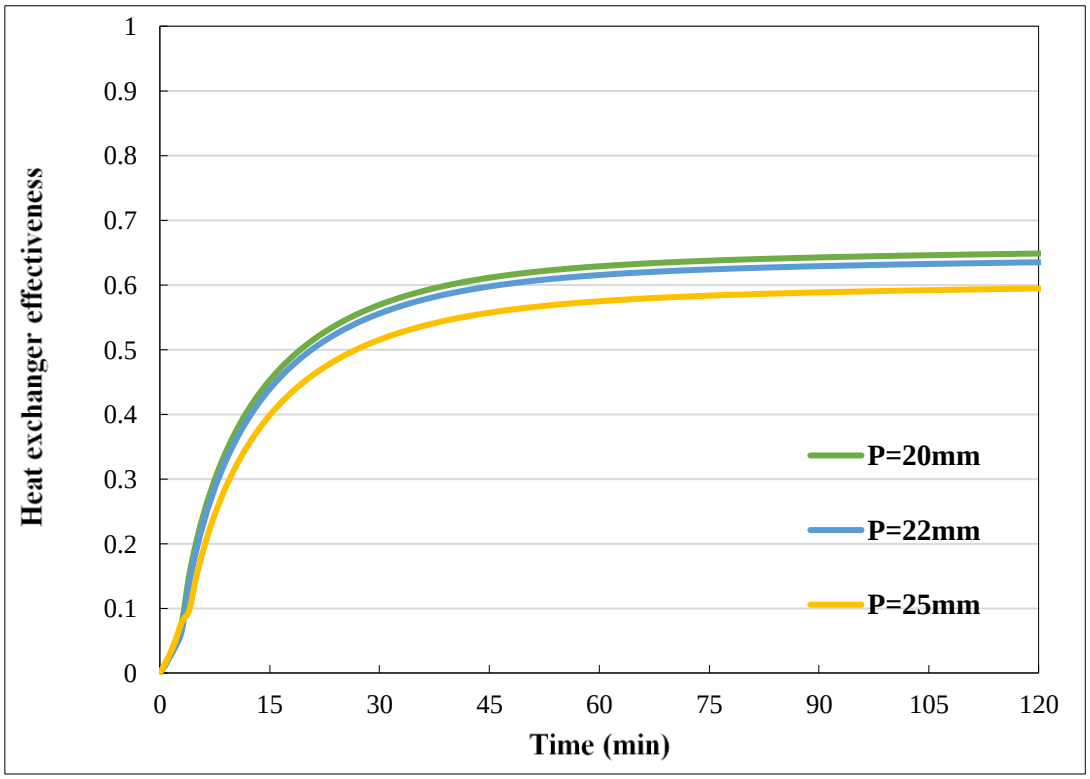
Heat exchanger effectiveness
1
0.9
0.8
0.7
0.6
0.5
0.4
0.3
0.2
0.1
0
0
15
30
45
60
75
90
105
120
Time (min)
P=20mm
P=22mm
P=25mm

(b)

Figure 7-13. Impact of pitch dimension on (a) outlet temperature and (b) HEE during the charging process

Figure 7-14a showed the impact of various pitch sizes on the liquid fractions of PCM-gypsum plasterboard during 2 hours of the charging period and it is believed that reducing pitch size enables a higher liquid fraction to be achieved. For example, pitch dimensions of 20 and 25mm claimed 0.092 and 0.03, respectively. Meanwhile, the PCM-gypsum plasterboard started melting at 40mins and 60min respectively under separate pitch sizes of 20 and 25mm (Figure 7-14a). Different liquid fractions could impact on the instantaneous energy stored and it achieved different results (Figure 7-14b). It showed that increasing the pitch dimensions could increase the instantaneous heat stored in the PCM-gypsum plasterboard as the plenum air temperature increases by increasing the pitch dimensions. For example, pitch sizes 20 and 25mm achieved instantaneous energy storage at 140 and 160kJ, respectively (Figure 7-14b). It can be stated that a smaller pitch size could have a higher liquid fraction. However, higher instantaneous stored energy can be delivered by a higher pitch size.

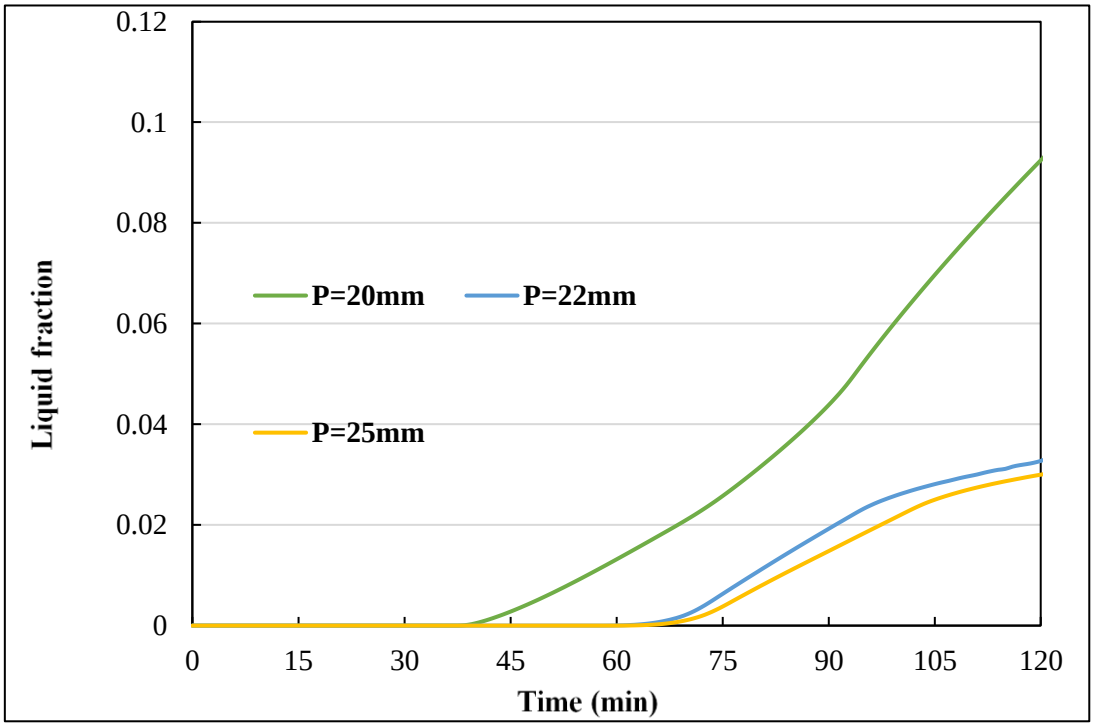

(a)

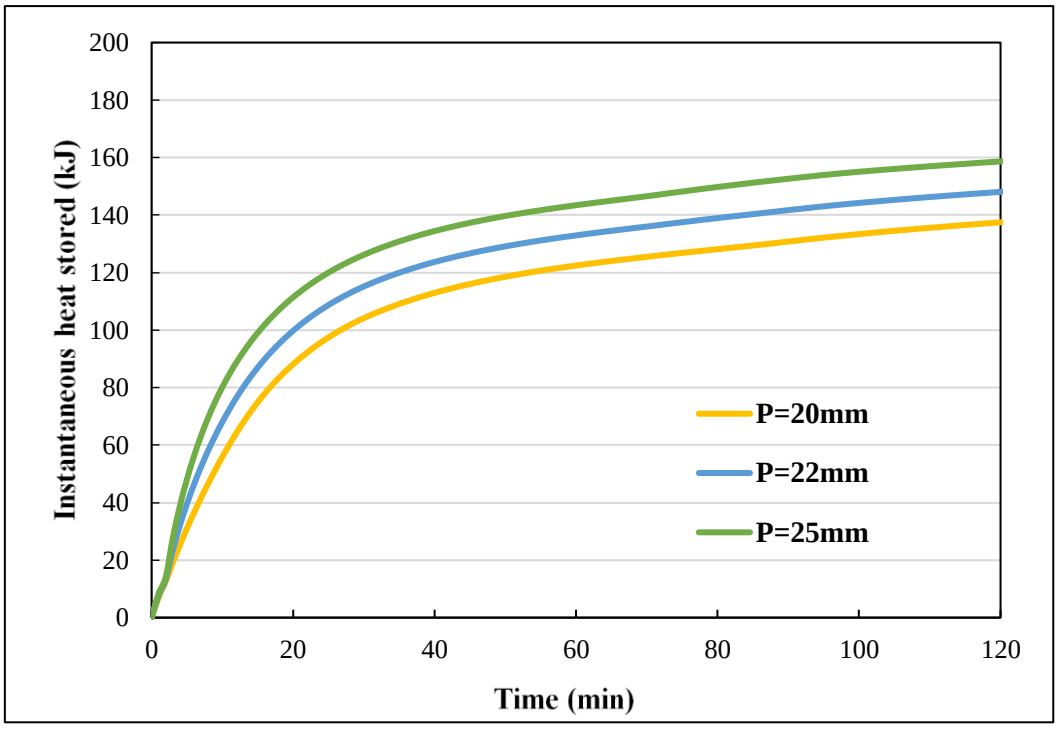

(b)

Figure 7-14. Impact of pitch dimension on (a) liquid fraction and (b) instantaneous heat stored during the charging process

Figure 7-15 demonstrates the impact of pitch dimension on outlet temperature, liquid fraction and instantaneous energy stored during the discharging period while keeping the inlet temperature and airflow rate at 18°C and 10m^3/hr, respectively. Meanwhile, the hole diameter and plenum size were 1mm and 150mm. Figure 7-15a shows the impact of various pitch dimensions on outlet temperature during the discharging period and it is believed that a smaller pitch size would greatly reduce the outlet temperature quickly. For instance, a pitch dimension of 20 and 25mm achieved outlet temperatures of 21°C and 22.6°C at 7 hours of discharging period (Figure 7-15a). Meanwhile, pitch sizes 20 and 25mm used 35 and 50 mins to decrease the outlet temperature to a melting point of 24°C (after releasing the sensible heat stored in the PCM-gypsum

plasterboard). However, changing the pitch dimensions had a minimal impact on outlet temperature, as they had similar trends in graph size. Such a changing trend can be seen in the liquid fraction of PCM-gypsum plasterboard due to various pitch sizes (Figure 7-15b). The impact of pitch dimension on the liquid fraction (solidification process) varies. For example, a pitch size of 20mm used the largest period of time to complete the freezing of the PCM-gypsum plasterboard at 180 mins. The pitch dimensions of 22 and 25mm spent 132 and 144 mins, respectively, to reach the solidification temperature of 23°C (Figure 7-15b). In terms of instantaneous energy released, a pitch size of 20mm would release a higher amount of instantaneous stored energy in a shorter period of time, as it would greatly increase the outlet temperate during the discharging period, which in return would increase efficiency (Figure 7-15c). Hence, it can be concluded that the impact of pitch size on liquid fraction is insignificant. Such results shown in Figure 7-15 can illustrate that the impact of pitch size on the releasing rate of instantaneous energy and liquid fraction is obvious, however, the impact on outlet temperature during the discharging process is insignificant. Meanwhile, it can be summarised that a smaller pitch size is beneficial for building envelope performance during the charging/discharging period according to the results presented in Figure 7-14, Figure 7-14 and Figure 7-15. Hence, a pitch size of 20mm would be the best design option among the three pitch dimensions.

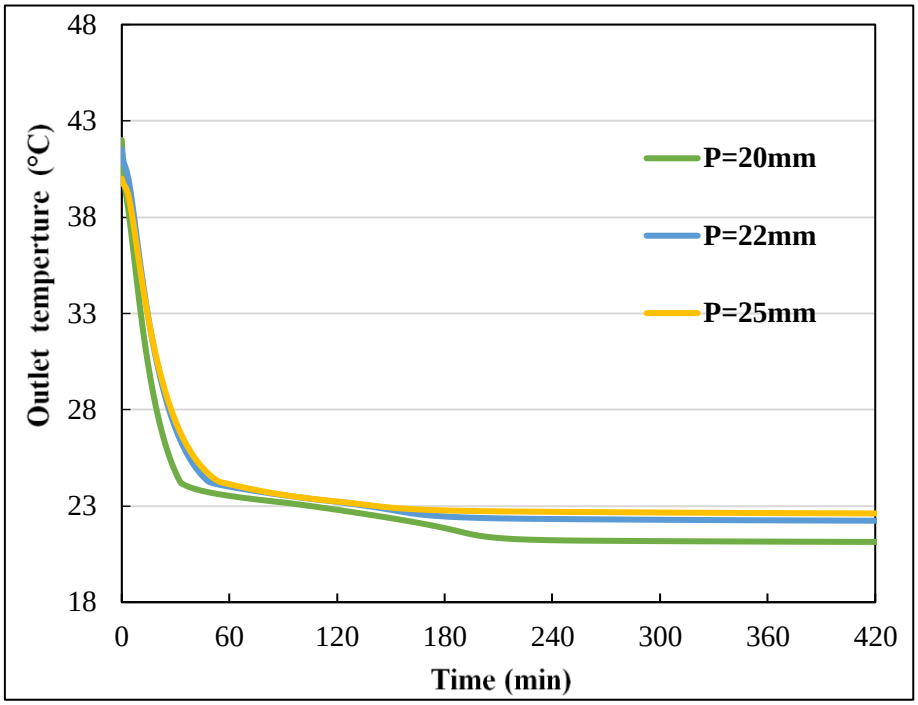
48
43
38
33
28
23
18
Outlet temperture (°C)
0
60
120
180
240
300
360
420
Time (min)
P=20mm
P=22mm
P=25mm

(a)

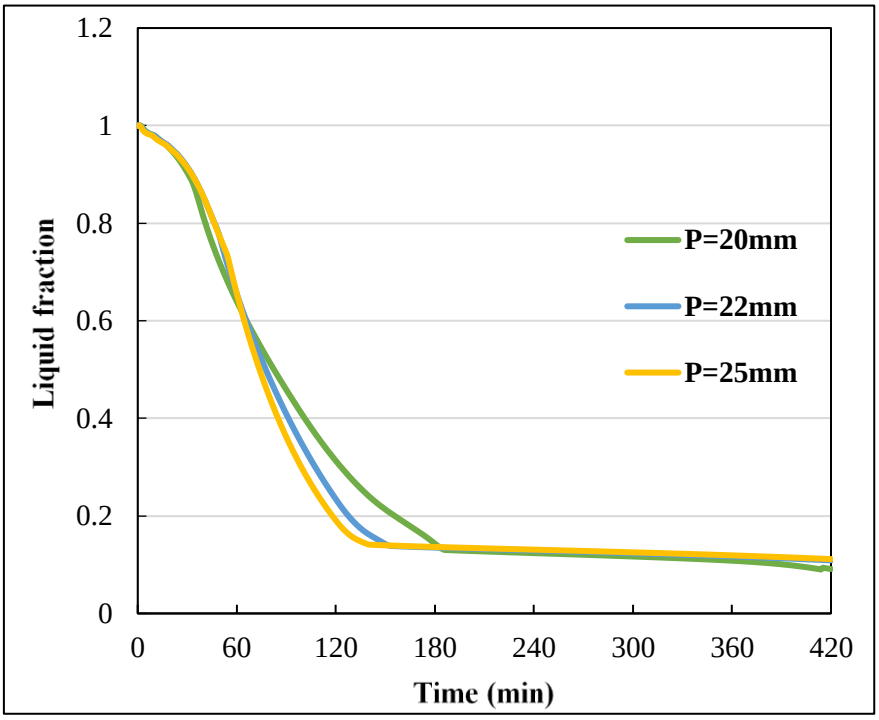
1.2
1
0.8
0.6
0.4
0.2
0
Liquid fraction
0
60
120
180
240
300
360
420
Time (min)
P=20mm
P=22mm
P=25mm

(b)

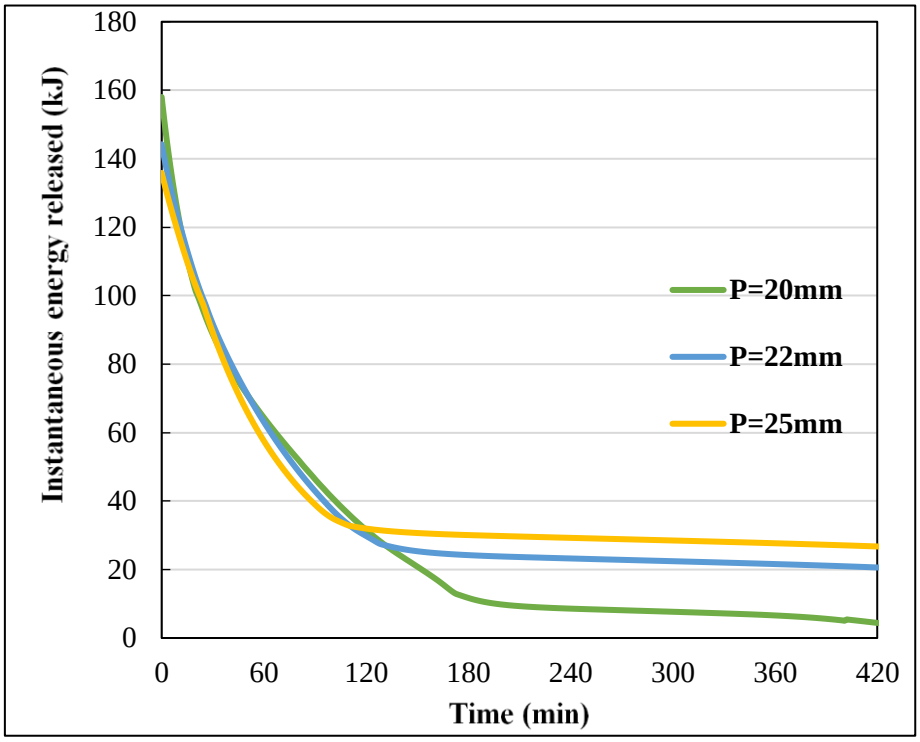

(c)

Figure 7-15. Impact of pitch dimension size on (a) outlet temperature, (b) liquid fraction, and (c) instantaneous energy released during the discharging process

7.4.7 *Effect of hole diameter*

The impact of hole dimension was investigated through analysing the influence of three hole diameters (1, 2, 3mm) on building envelope performance in terms of outlet temperature, liquid fraction, collector efficiency, HEE and instantaneous heat stored/released. For this investigation, three different circular hole diameters at 1, 2 and 3mm were selected. Other boundary conditions stayed unchanged such as an inlet temperature of 18°C, a pitch size of 20mm, a plenum width of 150mm and an airflow rate of 10m^3/hr (approach velocity at 0.01m/s). The impact of various hole diameters on outlet temperature and HEE is shown in Figure 7-16. Figure 7-17 illustrates the effect of hole diameter on liquid fraction and instantaneous energy stored in the PCM-gypsum plasterboard. The outlet temperature and HEE graph claimed similar trends for

the three different hole diameters. Figure 7-16a presents that increasing the hole size could reduce the outlet temperature since the larger hole accesses a larger amount of airflow. Under the same solar radiation or plate temperature, the building envelope delivered a reduced outlet temperature. For instance, hole diameters of 1 and 3mm achieved outlet temperatures of 40.5 and 43°C, respectively (Figure 7-16a). This result could indicate that increasing the hole diameter delivers a lower outlet temperature, thereby reducing HEE and collector efficiency. Figure 7-16b illustrates that the hole diameters of 1 and 3mm achieved aHEE of 0.68 and 0.6 at a relatively steady state. Hence, it can be believed that increasing the hole diameter enables HEE to be reduced. Thereby, the efficiency could decrease due to a lower outlet temperature and a lower airflow rate caused by increasing the hole diameter. Hence, the hole diameter has a crucial impact on building envelope performance in terms of efficiency and HEE. Besides, the melting and instantaneous heat stored varies because of different hole diameters (Figure 7-17).

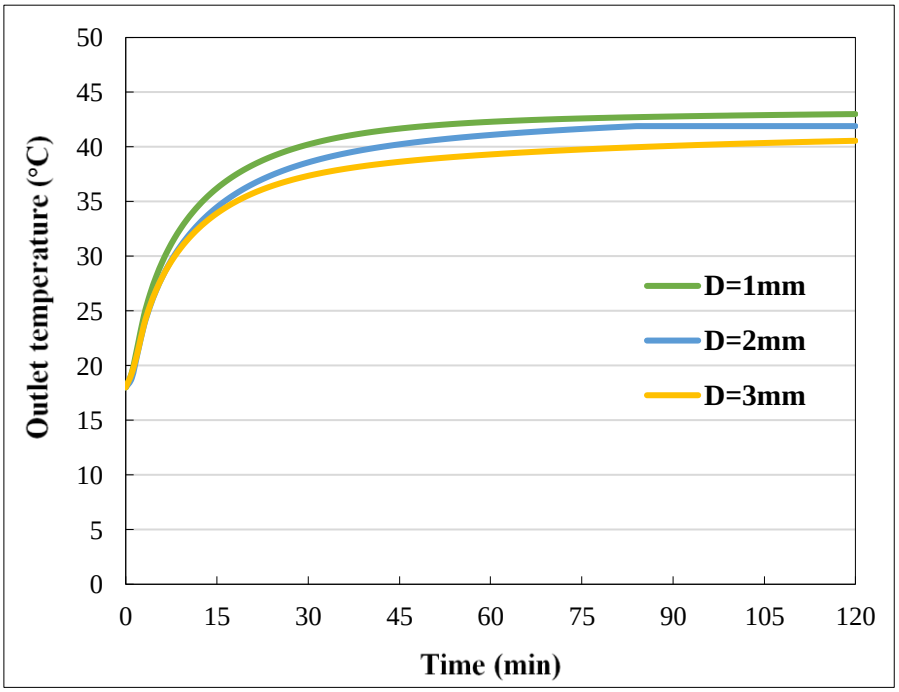

(a)

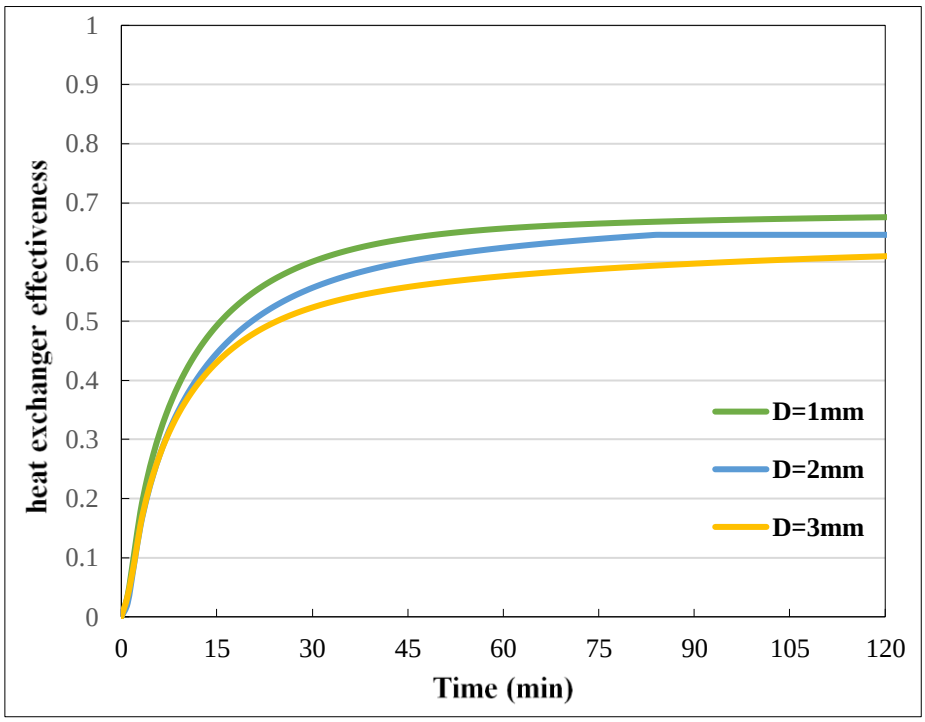

(b)

Figure 7-16. Impact of hole dimension on (a) outlet temperature and (b) HEE during the charging process

According to Figure 7-17, it can be believed that the influence of the hole diameter on the liquid fraction and instantaneous heat stored varies. Figure 7-17a explains that a smaller hole size achieved a greater liquid fraction. For instance, hole diameters of 1 and 3mm provided liquid fractions of 0.09 and 0.032. Meanwhile, the PCM-gypsum plasterboard started melting at the 45 and 60 mins mark under 1 and 2mm diameters, respectively (Figure 7-17a). However, the instantaneous heat stored for three different hole diameters were 140, 125 and 110kJ, respectively, during the charging period since the larger hole had a smaller airflow rate that greatly affected the heat storage behaviour of the PCM-gypsum plasterboard (Figure 7-17). This is because a higher airflow rate could increase the convection heat transfer between the plenum air and the PCM-gypsum plasterboard, which greatly influenced the charging behaviour.

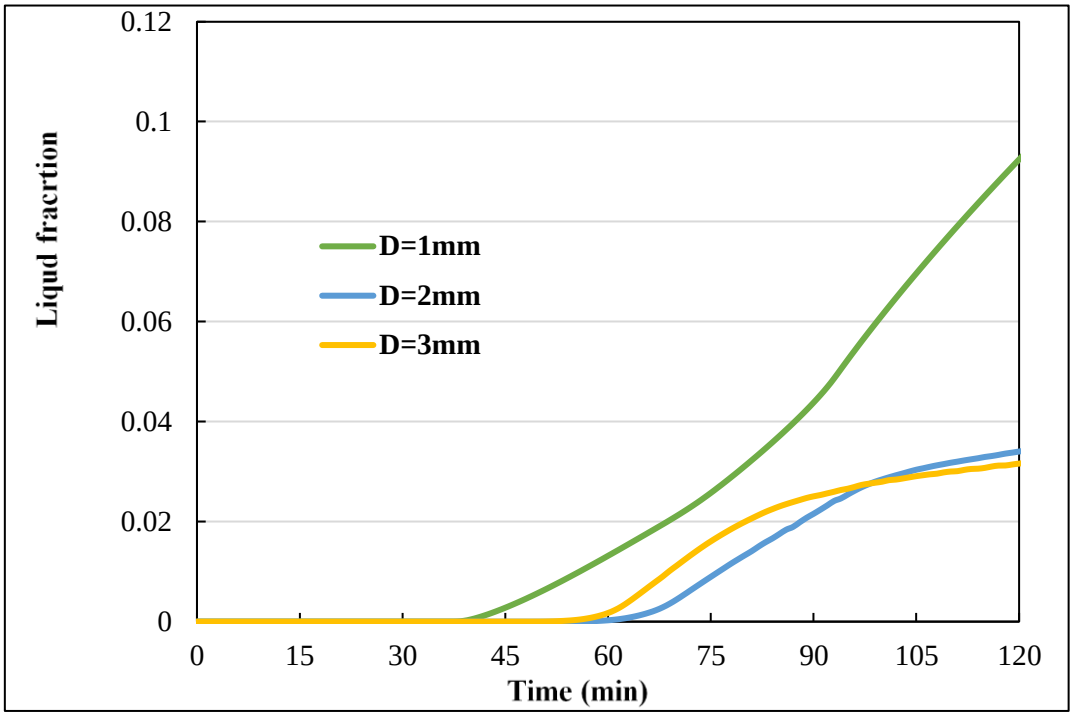
Liqud fracrtion
0.12
0.1
0.08
0.06
0.04
0.02
0
D=1mm
D=2mm
D=3mm
0
15
30
45
60
75
90
105
120
Time (min)

(a)

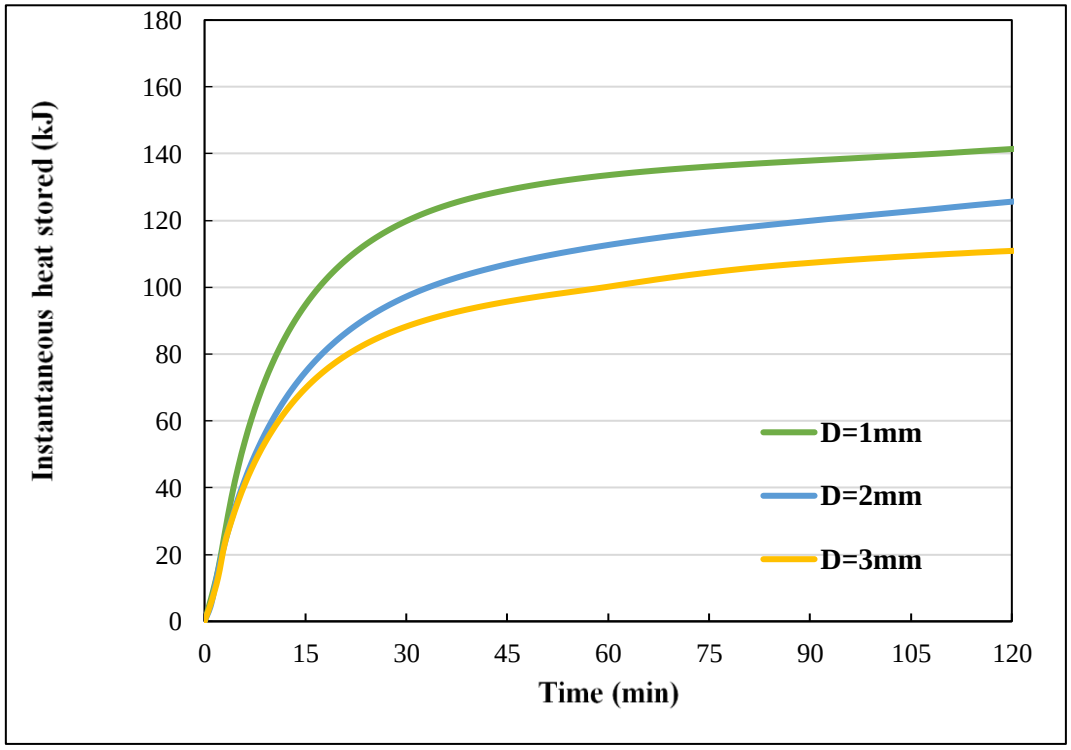
Instantaneous heat stored (kJ)
180
160
140
120
100
80
60
40
20
0
D=1mm
D=2mm
D=3mm
0
15
30
45
60
75
90
105
120
Time (min)

(b)

Figure 7-17. Impact of hole dimension on (a) liquid fraction and (b) instantaneous heat stored during the charging process

Figure 7-18 presented the impact of hole diameter on outlet temperature, liquid fraction and instantaneous energy stored during the discharging period while keeping the inlet temperature and airflow rate at 18°C and 10m^3/hr, respectively. Meanwhile, the pitch dimension and plenum sizes were 20mm and 150mm. Figure 7-18a presents the effect of three different hole diameters on the outlet temperature during the solidification process of the PCM-gypsum plasterboard. For example, the hole diameters of 1 and 3mm reduced the outlet temperature to the solidus temperature of the PCM-gypsum plasterboard (23°C) by consuming 110 and 165 mins of discharging (Figure 7-18a). Also, the building envelope with a 1mm hole diameter would provide a lower outlet temperature at 21°C during the solidification process. Hence, it can be indicated that a smaller hole diameter would greatly and more quickly reduce the outlet temperature among the three different hole sizes. However, a smaller hole diameter might use a longer time to complete the freezing of the PCM-gypsum plasterboard. For instance, a hole diameter of 1mm used the highest rate of 180 mins to reach the lowest point of the solidification process (Figure 7-18b). Besides, the effect of hole diameter change on liquid fraction behaviour is marginal. Meanwhile, the hole diameter of 1mm had the highest releasing rate of instantaneous energy during the discharging period, according to the results shown in Figure 7-18c.

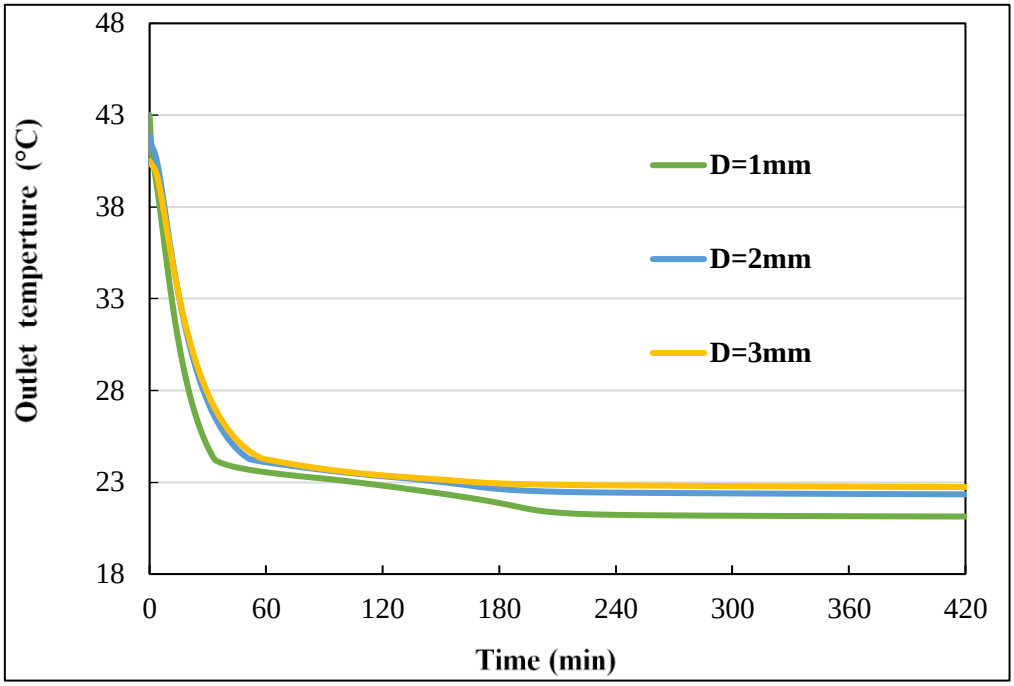
Outlet temperture (°C)
48
43
38
33
28
23
18
0
60
120
180
240
300
360
420
Time (min)
D=1mm
D=2mm
D=3mm

(a)

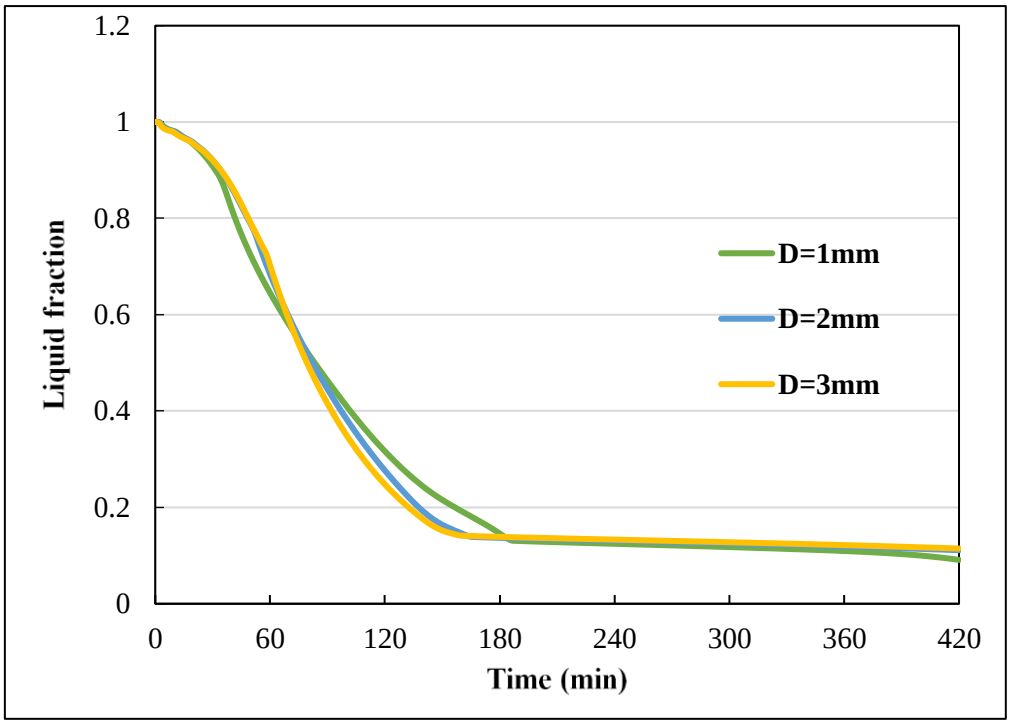
Liquid fraction
1.2
1
0.8
0.6
0.4
0.2
0
0
60
120
180
240
300
360
420
Time (min)
D=1mm
D=2mm
D=3mm

(b)

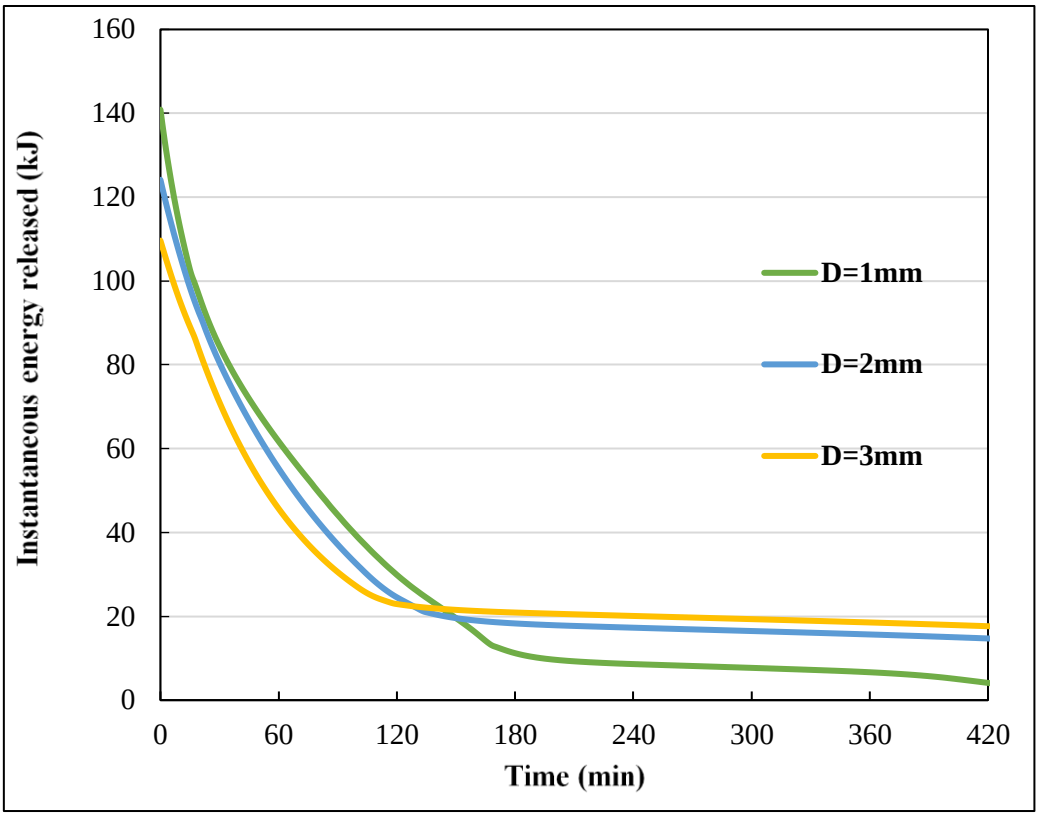

(c)

Figure 7-18. Impact of hole diameter on (a) outlet temperature, (b) liquid fraction, and (c) instantaneous energy released during the charging process

The results in Figure 7-18c can indicate that a smaller hole size greatly enables the solidification process to be completed by releasing the maximum amount of instantaneous heat stored. It can be explained by the fact that a smaller hole diameter could increase the plenum's air velocity, that increases the convective heat transfer coefficient in order to quickly boost the solidification behaviour. However, the influence of hole diameter on building envelope performance is limited. It can be concluded that a hole diameter of 1mm is significantly beneficial for building envelope performance due to the results displayed in Figure 7-16,Figure 7-17 and Figure 7-18. Hence, a hole diameter of 1mm was selected as the optimal design option.

7.4.8 *Effect of thermal conductivity of the PCM*

In the application of a PCM, a low thermal conductivity has been seen as one of the major disadvantages as the rate of storing/releasing the heat depends on its thermal conductivity. In order to improve the thermal conductivity of a PCM during its usage, there are several approaches that can be used such as using an additional container made of aluminum, metal or fins. Scholars have acknowledged that these materials are recognised as among the best methods to improve the thermal conductivity of a PCM during its application. In order to study the impact of various thermal conductivities of the PCM on the system's performance, this analysis included the impact of three different values of 0.16, 0.5, and 1.0W/mK. Figure 7-19 shows the variation in thermal conductivity of the PCM regarding outlet temperature and liquid fraction within the charging duration, while maintaining the inlet temperature, plate temperature and airflow rate at 18°C, 55°C, and 10 m^3/hr, separately.

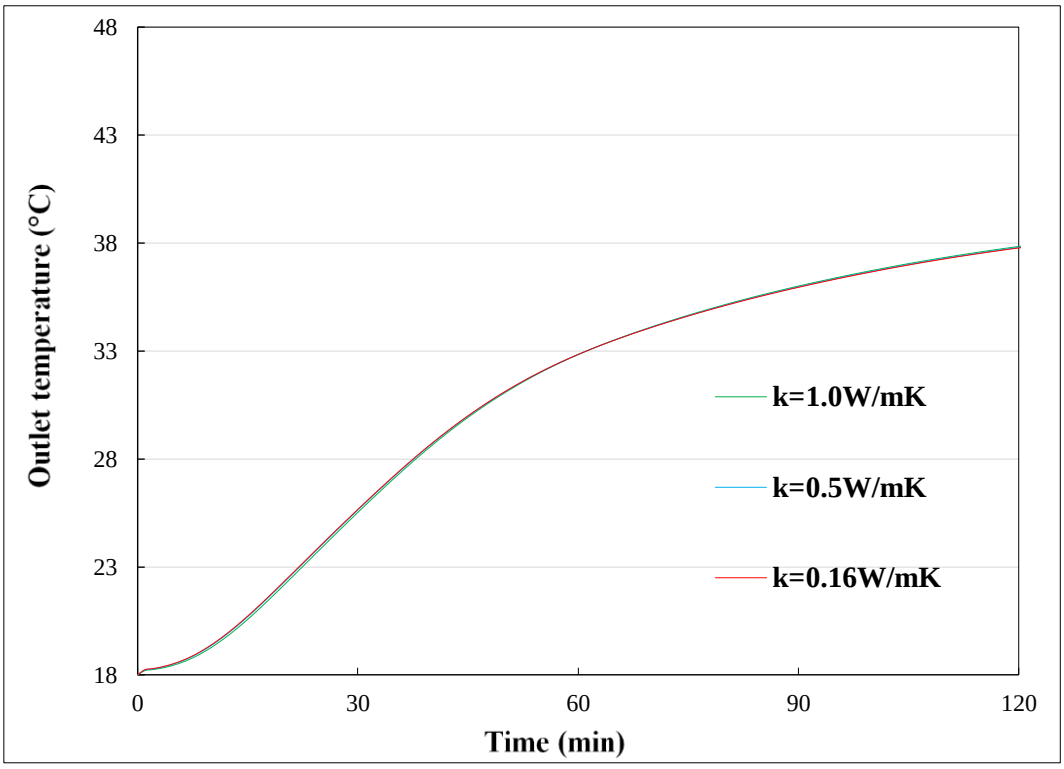

(a)

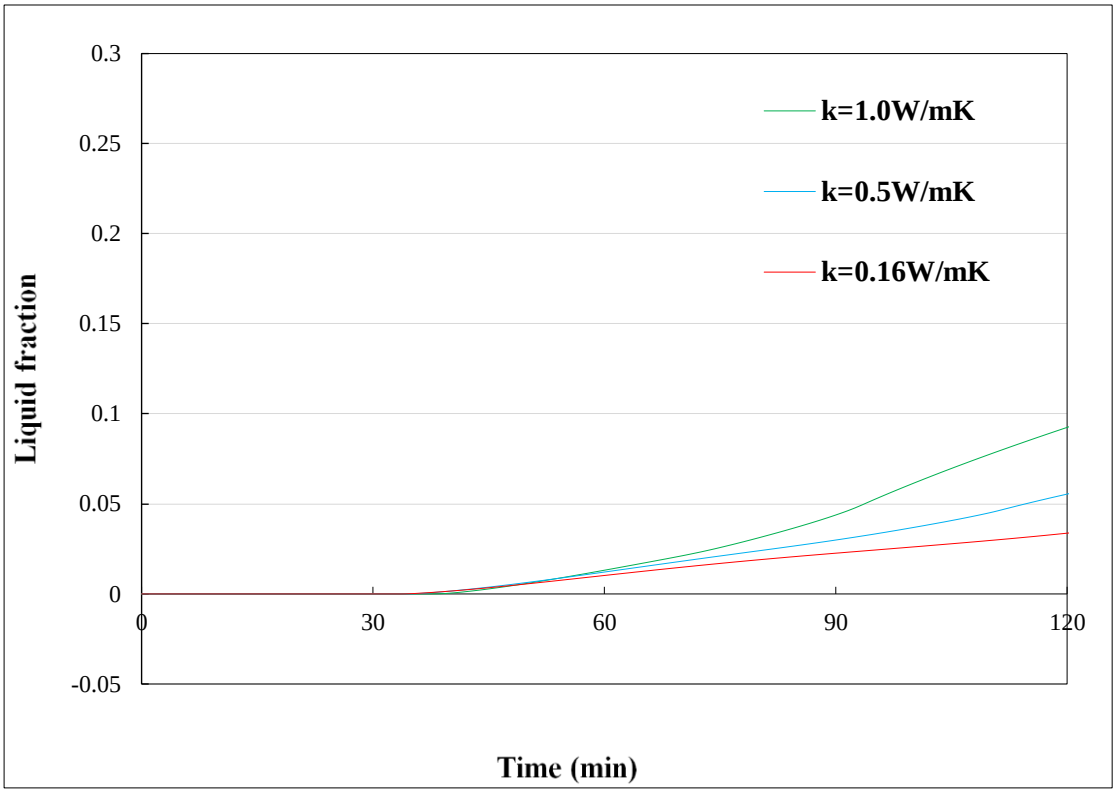
Liquid fraction
0.3
0.25
0.2
0.15
0.1
0.05
0
-0.05
0
30
60
90
120
Time (min)
k=1.0W/mK
k=0.5W/mK
k=0.16W/mK

(b)

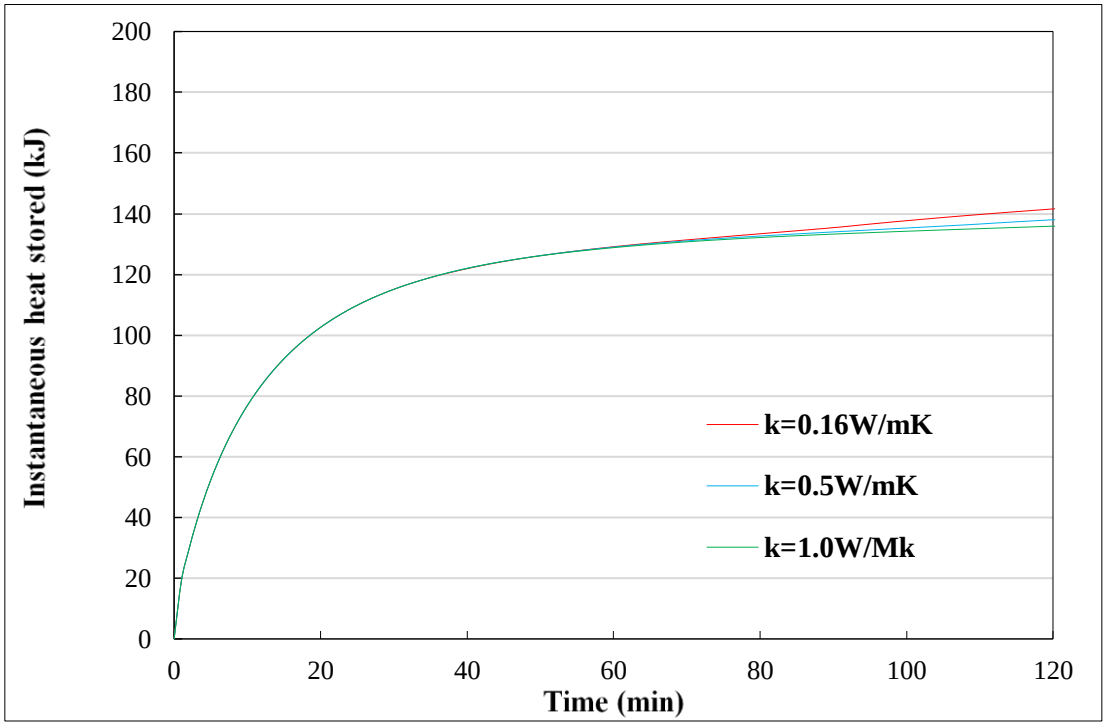
Instantaneous heat stored (kJ)
200
180
160
140
120
100
80
60
40
20
0
0
20
40
60
80
100
120
Time (min)
k=0.16W/mK
k=0.5W/mK
k=1.0W/Mk

(c)

Figure 7-19. Impact of the thermal conductivity of the PCM on (a) outlet temperature and (b) liquid fraction during the charging period

According to Figure 7-19a, it can be seen that the different values of thermal conductivity have negligible effects on the outlet temperature, as the system achieved equally the same outlet temperature of 37.85°C in this 2 hour charging period. Similarly, Figure 7-19b demonstrated that thermal conductivities of 1 and 0.5 W/mK provided liquid fractions of 0.094 and 0.056, respectively. This indicated that increasing the thermal conductivity of a PCM could boost the melting of the PCM wall in order to complete the charging phase in a shorter time period. For instance, in order to achieve a liquid ratio of 0.025, thermal conductivities of 0.16 and 1W/mK spent 70 and 100 mins, respectively. Figure 7-19b shows that the variations in thermal conductivity of the PCM has a limited impact on the liquid faction of the PCM wall for 2 hours of the charging phase. Figure 7-19c also presents that there is a marginal variation in the instantaneous and cumulative heat stored for all the simulation trials with various thermal conductivities. This is because the high surface convection resistance provided by the air (considered to be the heat transfer fluid in this study) plays a key role, although several literatures have stated that the thermal conductivity of a PCM has been seen as a key disadvantage of the latent heat storage system (Jegadheeswaran and Pohekar 2009; Kumaresan et al. 2013). Therefore, it can be concluded that the surface convective heat transfer coefficient and the temperature difference between the plenum air and the PCM wall have a significant importance for the system performance and the melting behaviour of PCM wall, compared to the thermal conductivity of the PCM's back wall. Figure 7-20 shows the variation in thermal conductivity of the PCM regarding outlet temperature and liquid fraction during the solidification process, while maintaining the inlet temperature/plate temperature and airflow rate at 18°C, and 10m^3/hr, separately.

The results of outlet temperature, liquid fraction and instantaneous energy released due to various thermal conductivities (0.16, 0.5, and 1.0W/mK) during the discharging process are presented in Figure 7-20. It can be believed that the influence of different thermal conductivities on the outlet temperature results are marginal, since the building envelope achieved a highly similar reducing trend for various thermal conductivities (Figure 7-20a). However, a lower thermal conductivity could decrease the heat releasing rate and achieve a relatively lower outlet temperature. For instance, Figure 7-20a presents that the thermal conductivities of 0.16 and 1.0W/mK achieved 21.1°C and 22.6, respectively.

Also, the impact of thermal conductivity on the liquid fraction varies due to the results displayed in a similar decreasing trend that can be seen during the discharging process in Figure 7-20b. However, a higher thermal conductivity enables the liquid fraction phenomenon to be completed in a shorter time period. For example, the thermal conductivities of 0.16, 0.5, 1.0W/mK reached the liquid fraction value of 0.13 roughly at 180, 145, and 135 mins, respectively (Figure 7-20b). Such results are expected, due to the fact that PCM-gypsum plasterboard with a higher thermal conductivity enables the stored heat to be released at a higher rate, which takes a short time to complete the solidification behaviour.

Figure 7-20c shows the impact of different thermal conductivities on the instantaneous heat stored during the solidification period. The results are similar with the liquid fraction outcomes. PCM-gypsum plasterboard with a higher thermal conductivity could release the stored heat faster, since the plasterboard is unable to keep the energy for a longer period because of its higher thermal conductivity. For instance, the instantaneous energy stored can be reduced to 60kJ at 75, 90, 110 mins for three different thermal conductivities of 1.0, 0.5, and 0.16W/mK (Figure 7-20c). However, the instantaneous

heat stored needs a longer time to complete, since the instantaneous energy stored was 40kJ at the 420 mins. mark in the discharging process.

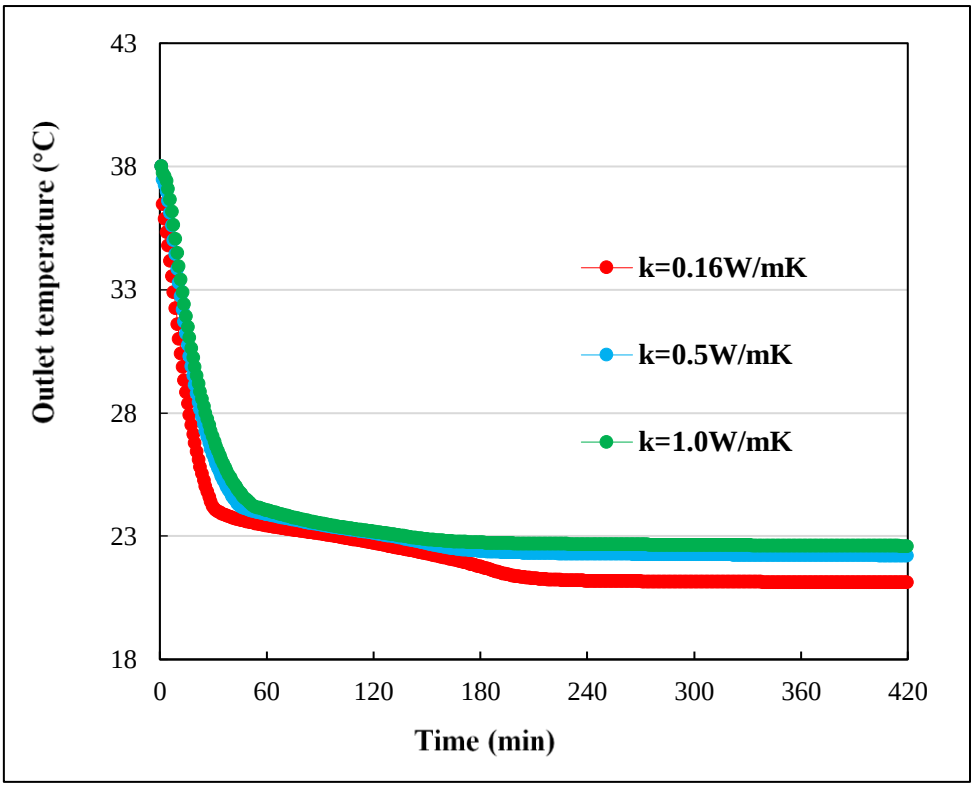

(a)

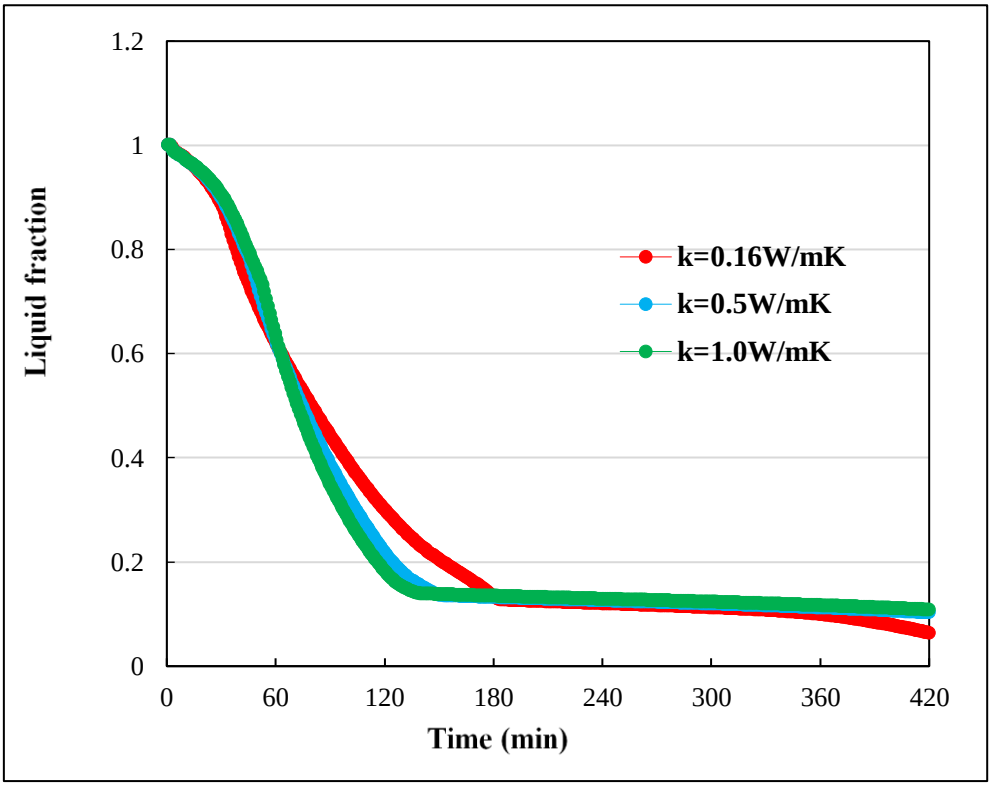
Liquid fraction
1.2
1
0.8
0.6
0.4
0.2
0
0
60
120
180
240
300
360
420
Time (min)
k=0.16W/mK
k=0.5W/mK
k=1.0W/mK

(b)

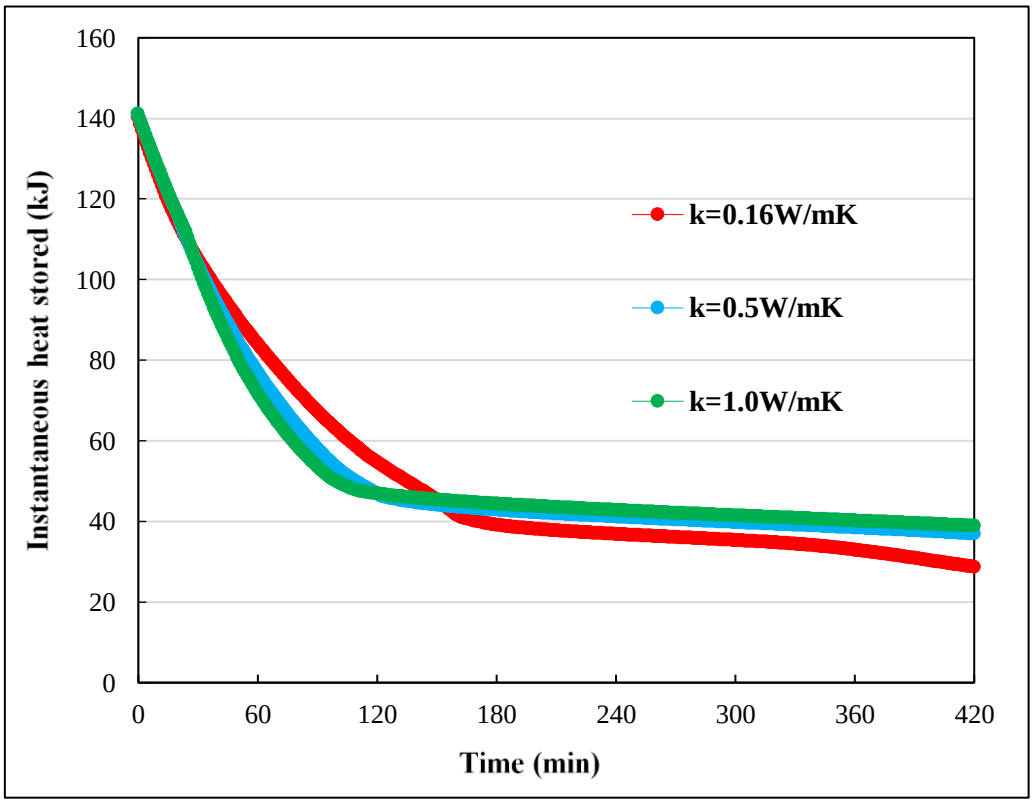
Instantaneous heat stored (kJ)
160
140
120
100
80
60
40
20
0
0
60
120
180
240
300
360
420
Time (min)
k=0.16W/mK
k=0.5W/mK
k=1.0W/mK

(c)

Figure 7-20. Impact of thermal conductivity on (a) outlet temperature and (b) liquid fraction and (c) energy released during the discharging period

Such results in Figure 7-20 can indicate that the PCM-gypsum plasterboard with various thermal conductivities affects the solidification process differently. Relatively higher thermal conductivities can achieve a higher outlet temperature and complete the solidification behaviour within a shorter time, with a higher releasing rate of the heat stored. Hence, it can be indicated that the PCM-gypsum plasterboard introduced with a lower thermal conductivity of PCM could be beneficial by slowly reducing the release of the stored heat. Such indicators are useful for later use, where the outlet temperature and releasing heat will be required for a longer time. Therefore, it can be concluded that various thermal conductivities have limited influence on outlet temperature and moderately affect the releasing rate of the stored energy and the liquid fraction (solidification) competition during the discharging process. Meanwhile, a smaller thermal conductivity has more advantages, especially during the discharging period, according to the results mentioned above. Hence, a thermal conductivity of 0.16W/mK was regarded as the optimal design choice.

Hence, according to the parametric results, the best/optimal parametric can be concluded, as shown in Table 7-3.

Table 7-3. Best case design

Parameters	Values
Airflow rate	$10m^3/hr$
Approach velocity	0.01m/s
Inlet temperature	10°C

Plate temperature	85°C
Plenum width	150mm
Pitch size	20mm
Hole diameter	1mm
Thermal conductivity of PCM	0.16W/mK

7.5 **Performance analysis of the best optimal design for the building envelope**

The optimal value of the main parameters was concluded through the parametric study. It was concluded that the airflow rate had the greatest impact on building envelope performance. The case study was conducted for two different building envelopes with PCM-gypsum plasterboard and gypsum plasterboard. The building envelopes followed the construction and design parameters as shown in Table 7-4. The absorber plate was made of a circular hole with a diameter of 1mm and a pitch size of 20mm. The case study was investigated through ANSYS Fluent software. The default enthalpy method was used to simulate the phase change behaviour during the charging/discharging process. The inlet temperature and plate temperatures were designed at 10 and 85°C. The RNG k-ε model was applied for the heat transfer process through the plate and the plenum. The laminar flow was used for the PCM-gypsum plasterboard melting/solidification process. Also, the residential values for continuity, velocity and turbulence were set at 10^{-6} with 10^{-8} for energy. A time step size of 60s was used during the numerical simulation. During this case study simulation, the wind effect was ignored so that the heat loss to the surroundings through convection would be negligible.

Table 7-4. Design of the case study

Parameters	Values

Height	$10m$
Width	$10m$
Area	$100m^2$
Colour	Black
Absorptivity	0.95
Installation direction	South-facing
Plenum size	$150mm$
Perforation diameter	$1mm$
Pitch size	$20m$
PCM-gypsum plasterboard thickness	$10mm$
Thermal conductivity of PCM	$0.16W/mK$
Inlet temperature	10°C
Approach velocity (m/s)	0.01

According to the design values shown in Table 7-4, the building envelope model was established in ANSYS Fluent software and the relative boundaries/method selections were made accordingly. The case study was simulated for 7 hours of melting (assuming office working hours) and 7 hours of solidification processes. The results were analysed in terms of outlet temperature, HEE and collector efficiency.

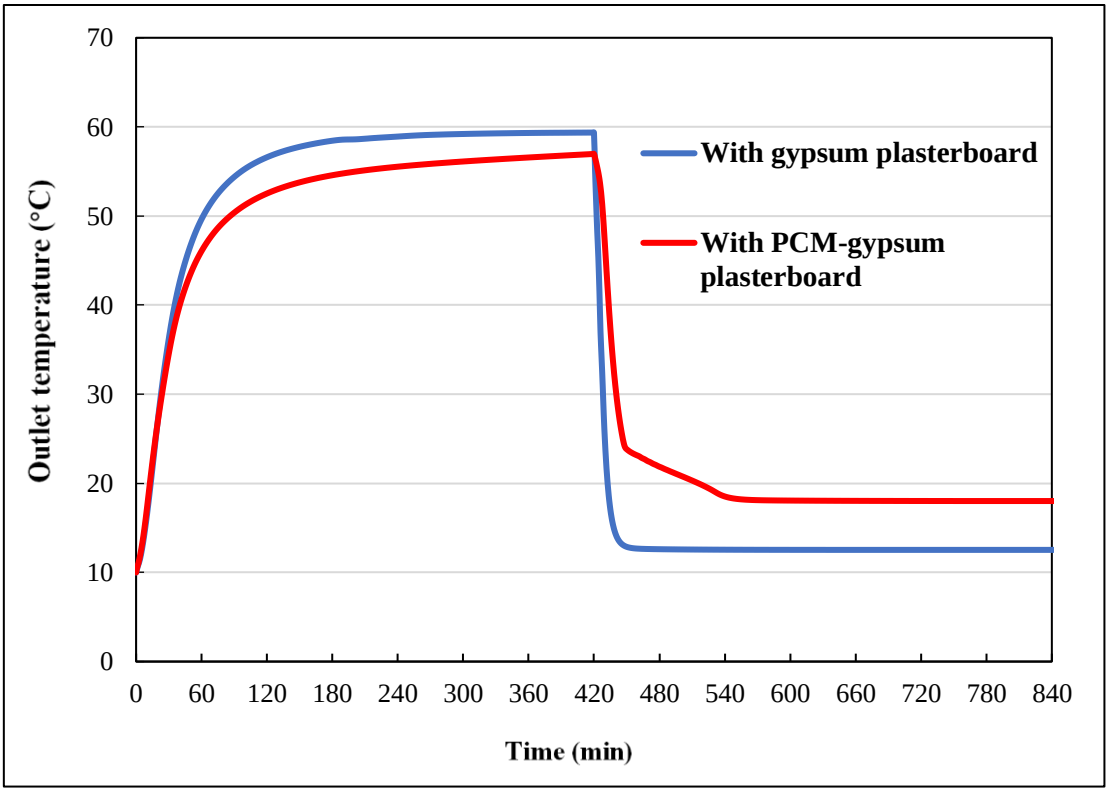

Figure 7-21. Outlet temperature for the building envelope with PCM-gypsum plasterboard and gypsum plasterboard during the charging (0-420min) and discharging (420-840min) periods

Figure 7-21 demonstrates the outlet temperature during the charging and discharging processes for the building envelopes with PCM-gypsum plasterboard and gypsum plasterboard. It can easily be seen that the outlet temperature with the PCM-gypsum plasterboard and the gypsum plasterboard had a rapid increase in the first hour of charging and a slow, steadily increasing trend during the rest of the charging period. The building envelopes with PCM-gypsum plasterboard and gypsum plasterboard achieved outlet temperatures of 56 and 59.4°C, respectively, during the charging period (Figure 7-21). Since the building cases were modelled under same boundary conditions, it can be indicated that the PCM-gypsum plasterboard stored a certain amount of energy which caused the variations in outlet temperature.

During the discharging period within 420-450 mins, the outlet temperature of the building envelopes with PCM-gypsum plasterboard and gypsum plasterboard were 24 and 13°C (Figure 7-21). Meanwhile, the building envelope with the PCM gypsum plasterboard enabled an outlet temperature of 18°C to be delivered, that was 6°C higher than the one provided by the building envelope with gypsum plasterboard. Such results can conclude that the PCM-gypsum plasterboard released the stored energy to deliver a higher outlet temperature during the discharging period. Furthermore, the collector efficiency and heat exchange effectiveness were calculated accordingly for the both building envelopes with PCM-gypsum plasterboard and gypsum plasterboard during the charging period and the results are shown in Figure 7-22.

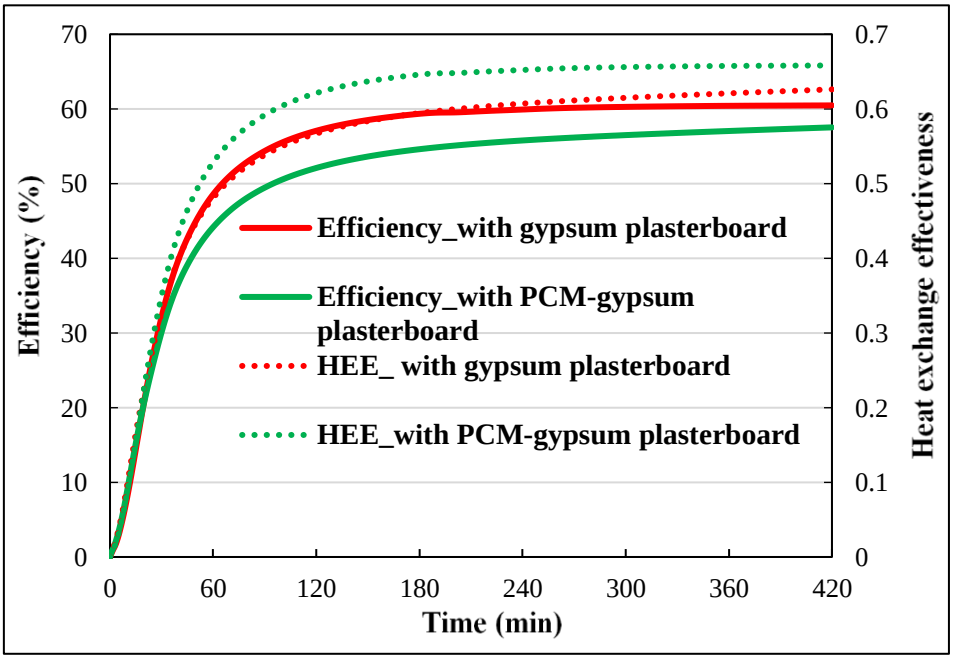

Figure 7-22. Collector efficiency and HEE for the building envelope with PCM-gypsum plasterboard and gypsum plasterboard during the charging period

According to Figure 7-22, it can be stated that the efficiency and the HEE have similar trends to the outlet temperature. The average efficiency and HEE were claimed as 60.5% and 0.63 respectively, for the building envelope with gypsum plasterboard

during the charging period (Figure 7-22). Besides, the building envelope with the PCM-gypsum plasterboard achieved an efficiency of 57.5% and a HEE of 0.66. It was believed that the building envelope with PCM-gypsum plasterboard had lower HEE and efficiency compared to the building envelope with gypsum plasterboard, since the delivered energy was reduced because a certain amount of energy was stored in PCM-gypsum plasterboard for later used during the discharging period. According to the results in Figure 7-21 and Figure 7-22, it can be concluded that the building envelope with the PCM-gypsum plasterboard had major advantages, especially during the discharging period where the sun was not available, because such a building envelope could still provide a higher outlet temperature by using stored energy due to additional PCMs. In addition, while charging, such a building envelope would prevent overcooling problems, especially during the summer hot weather period where preheated air is not required to be delivered. Also, during this discharging process, it would capture the heat loss from the building envelope to reuse in the plenum to preheat the delivered air, especially in the winter.

7.6 **Conclusion**

This chapter illustrated the validation of the numerical modelling with the experimental outcomes through (i) analysing the melting and solidification behaviour using the default enthalpy method and (ii) calculating the overall consistency between the numerical and experimental outlet temperature results. The comparison of the numerical and experimental outlet temperature showed that the maximum consistence error (8.36%) was relatively acceptable and it showed good agreement with the experimental outcomes. Moreover, this validated model was used for the parametric study investigating the effects of various parameters on system performance in terms of outlet temperature, phase change behaviour and heat stored/released during the

charging and discharging periods. Those selected parameters were airflow rate, inlet temperature, plate temperature and thermal conductivity.

The lower (10m^3/hr), medium (30m^3/hr), and higher airflow rates (50m^3/hr) produced outlet temperatures of 44, 39 and 35°C during 2 hours of charging time. In order to achieve 10% melting of the PCM wall, the lowest airflow rate required more than 2 hours. Meanwhile, the higher airflow rate (50m^3/hr) only needed 1.25 hours. The results showed that the building envelope with lower and medium airflow rates achieved higher instantaneous heat stored at 140 and 82kJ, respectively, at 120 minutes of charging. During the discharging process, the lower airflow rate enabled the heat releasing period to be extended for a longer period than the higher airflow rate. It can be found that the airflow rates of 10, 30, and 50m^3/hr had liquid fractions of roughly 0.5, 0.23 and 0.8 respectively, at 240 minutes of discharging time. The variation in airflow rates also affected the heat releasing rate and the highest airflow rate had the highest rate at which the stored energy was released. Hence, the building envelope operating under the lower airflow rate could have the best performance among the various airflow rates.

The different values of inlet temperature are likely to impact slightly on the rate of energy storage and the instantaneous energy stored. For instance, the instantaneous energy stored at 120 minutes was shown as roughly 140kJ for all the inlet temperature trials. Therefore, changing the inlet temperature has a marginal influence on system performance and melting behaviour when the charging time increases. However, during the discharging period, it can be concluded that various inlet temperatures greatly affect the outlet temperature and releasing rate of the stored energy. However, the effect of various inlet temperatures on the charging period is limited. However, the inlet temperature of 18°C has a greater advantage during the discharging process, especially for the releasing rate of stored energy.

The plate temperatures of 40 and 85°C produced outlet temperatures of 30.62°C and 52.30°C, respectively. It could achieve roughly 0.2 and 0.1 of liquid fraction for the PCM-gypsum plasterboard during 2 hours of the charging period by plate temperatures of 85 and 55°C, separately. In addition, the instantaneous heat stored during the time of the charging period on the PCM-gypsum plasterboard would be varied due to the different plate temperatures (simulating solar radiation). For example, the building envelope operating at plate temperatures of 40 and 85°C achieved approximately 68 and 302kJ separately, at the 2 hour mark of the charging duration. Therefore, plate temperature has a great impact on the outlet temperature and charging behaviour of PCM-gypsum plasterboard. That is similar to the effect observed for the variation in the airflow rate. However, the effect of the plate temperature was ignored during the discharging period, where the plate temperature was kept as the ambient air temperature.

The plenum width of 150mm has the greatest liquid fraction and instantaneous energy stored, at 0.093 and 142kJ, respectively. Shrinking the plenum size would greatly and more quickly reduce the outlet temperature. For instance, plenum sizes of 100 and 200mm reduced the outlet temperature to 23 degrees at 100 and 150 mins. However, the impact of plenum size on building envelope performance during charging/discharging is limited. During 2 hours of the charging period, the outlet temperature and HEE reached a relative steadiness after 45 mins. Hence, after 45 mins. of charging, the pitch dimensions of 20mm and 25mm achieved 42^{o}C and 40°C respectively, and the HEE were claimed as 0.65, 0.64, 0.60 separately for three different pitch dimensions (20, 22 and 25mm).

Therefore, increasing the pitch size has a limited impact on outlet temperature and HEE. Increasing the pitch dimension could increase the instantaneous heat stored in the PCM-gypsum plasterboard, as the plenum air temperature increases by increasing the pitch

dimensions. For example, pitch sizes of 20 and 25mm achieved instantaneous energy storage at 140 and 160kJ, respectively. However, during the discharging period, a smaller pitch size would greatly and more quickly reduce the outlet temperature. For example, pitch dimensions of 20 and 25mm achieved outlet temperatures of 21 and 22.60 at 7 hours' discharging period. The impacts of pitch size on the releasing rate of instantaneous energy and liquid fraction are obvious. A smaller pitch is beneficial for building envelope performance.

Hole diameters of 1 and 3mm achieved outlet temperatures of 40.5 and 43°C, respectively. This result could indicate that increasing the hole diameter delivered a lower outlet temperature thereby reduced HEE and collector efficiency. During the discharging process, a smaller hole diameter would greatly and more quickly reduce the outlet temperature among the three different hole sizes. Meanwhile, the diameter of 1mm had the highest releasing rate of instantaneous energy during the discharging period.

In addition, the different values of thermal conductivity have a negligible effect on outlet temperature, as the system achieved equally the same outlet temperature of 37.85°C in this 2 hour charging period under various thermal conductivities of the PCM. Similarly, the thermal conductivities of 1 and 0.5 W/mK provided liquid fractions of 0.094 and 0.056, respectively. Besides, there was a marginal variation in the instantaneous and cumulative heat stored for all the simulation trials with various thermal conductivities. However, it can be indicated that the surface convective heat transfer coefficient and the temperature difference between the plenum air and the PCM wall have a significant importance on system performance and the melting behaviour of the PCM wall, compared to the thermal conductivity of the PCM-gypsum plasterboard.

Overall, the impact of airflow rate, plate temperature (simulation of solar radiation), and pitch size have significant impacts on building envelope performance in terms of HEE and efficiency. However, the impact of inlet temperature, plenum size, hole diameter and thermal conductivity of the PCM have a marginal influence on building envelope performance. Also, the building envelope with PCM-gypsum plasterboard had great advantages compared to the gypsum plasterboard, especially during the discharging process, where the gypsum plasterboard would release the stored energy to deliver a higher outlet temperature for a certain time.

Chapter 8. **Conclusions and recommendations**

8.1 Introduction

This chapter concludes the research findings along with the possible limitations and relative recommendations. It concludes the main research outcomes of this PhD project to provide recommendations for future research on this field. Furthermore, the main points of each chapter are also presented in this conclusion chapter. Lastly, the contribution of this research study in terms of academia and the building industry are also mentioned.

8.2 Fabrication of the building envelope components

The perforated circular holes (1mm diameter) were made for the corrugated metal sheet automatically by a machine in the Coventry University materials laboratory. The MICRONAL® DS 5040X PCM and multi-finish gypsum were mixed homogenously to fabricate the PCM enhanced gypsum plasterboard. In order to finalise the PCM-gypsum plasterboard, different samples were characterised through physical/thermal properties measurements, including thermal conductivity testing, density measurements, compressive strength testing and SEM testing. The characterisation results showed that increasing the PCM proportions reduced the bulk density and compressive strength and increased the thermal conductivity of the PCM-gypsum plasterboard. Due to the purpose of this research (using such a plasterboard to capture limited energy from the plenum), the gypsum plasterboard with 15% of PCM was fabricated to be used in the further experimental study.

8.3 Experimental conclusions

The experimental work was conducted to investigate the performance of the proposed building envelope with PCM-gypsum plasterboard compared to the one with gypsum plasterboard. The results showed that the PCM-gypsum plasterboard stored a certain amount of energy due to the advantages of additional PCM that stored heat during the

charging period and released it during the discharging process. The impact of airflow rate, plenum size and pitch size on building envelope performance were also examined. The (lowest) air temperature rise and HEE averaging 15℃ and 0.5 were caused by the highest airflow rate of 50m^3/hr. Meanwhile, the highest HEE of 0.7 can be claimed for the low airflow rate of 10m^3/hr, which achieved an air temperature rise of 30℃. The lower airflow rate was able to generate a higher outlet temperature and higher energy stored. It achieved a higher outlet temperature and the longest energy releasing time. Hence, the impact of airflow rate on building envelope performance was concluded to be significant.

The plenum size of 250mm gave 35℃ for the charging and 20℃ for the discharging processes within 3 hours after the lighting was off. Meanwhile, the plenum size of 140mm generated a PCM-gypsum plasterboard temperature of 32℃ but was down to 20℃ for the solidification process of the PCM-gypsum plasterboard after 60 mins of lighting-off. The air temperature rises slightly with increased plenum thickness. For example, the plenum thicknesses of 250 and 140mm were able to provide an air temperature rise of 18 and 16℃, respectively. The plenum sizes of 200 and 250mm achieved roughly 71% for collector efficiency, separately. Hence, it was concluded that the influence of plenum size on building envelope performance was limited.

The pitch sizes of 20 and 25mm offered a higher air temperature rise of 20℃ and 25℃. For a constant airflow, the increasing perforation pitch size from 20mm to 25mm brought a 21.6% decrease in HEE. Therefore, the impact of pitch design is partial on building envelope performance. Overall, the experimental study highlighted the airflow rate as the most significant parameter on building envelope performance.

8.4 **Numerical conclusions**

According to the research background of this field, the computational fluid dynamics (CFD) modelling through ANSYS Fluent 19.1 was used for this numerical study. The CFD model was established and the relative boundary conditions were justified, based on the relative assumptions of this numerical investigation. The mesh independence study determined the medium meshing method to be used for the numerical modelling.

In terms of approach velocity, three different approach velocities (0.01, 0.05 and 0.1m/s) introduced the outlet temperatures of 48, 42 and 38°C respectively, during the charging period for the building envelope with gypsum plasterboard. Conversely, the building envelope with the PCM-gypsum plasterboard was able to provide 43, 38, and 35°C respectively, under approach velocities of 0.01, 0.05, and 0.1m/s. The building envelope with the PCM-gypsum plasterboard and the gypsum plasterboard also achieved HEE at 0.46 and 0.56, respectively, under an approach velocity of 0.1m/s. It was concluded that the building envelope with the PCM-gypsum plasterboard produced a lower outlet temperature and HEE due to the additional amount of PCM in the plasterboard that stored the extra heat from the plenum as latent heat.

The impact of the absorber plate temperature was analysed through running the simulation under various plate temperatures at 40, 55 and 70°C. The plate temperatures of 40 and 70°C delivered outlet temperatures of 38 and 67°C, respectively. The plate temperatures of 70°C and 55°C achieved 80 and 63W. Thus, increasing the plate temperature can deliver higher output energy.

The various inlet temperatures would eventually provide the same outlet temperature during the charging period because of the same plate temperature. The inlet temperature variation would not greatly affect the HEE in the case of the PCM-gypsum plasterboard, as the mass of the PCM was kept unchanged.

However, it can be indicated that that the impact of approach velocity and plate temperature (simulating solar radiation) on building envelope performance was significant among these parameters. The approach velocity was used to validate this model through comparing the numerical and experimental results.

8.5 Validation and parametric study conclusions

The comparison between the numerical and experimental outlet temperatures showed that the maximum consistence error (8.36%) was relatively acceptable. It showed good agreement with the experimental outcomes. The validated model through the default enthalpy method in ANSYS Fluent software was used for the parametric study. It investigated the effects of various parameters on system performance in terms of outlet temperature, phase change behaviour and heat stored/released during charging/discharging periods. The parameters investigated were airflow rate, inlet temperature, plate temperature, plenum size, pitch dimension, hole diameter and thermal conductivity.

The results showed that the lower ($10m^3$/hr), medium ($30m^3$/hr), and higher airflow rates ($50m^3$/hr) produced outlet temperatures of 44, 39 and 35°C during 2 hours of charging time. The building envelope with lower and higher airflow rates (10 and $50m^3$/hr) also achieved higher instantaneous heat storage of 140 and 82kJ, respectively, at 120 minutes of charging. The lower airflow rate achieved the optimal envelope performance among the various airflow rates.

The different values of inlet temperature are likely to slightly impact the rate of energy storage and the instantaneous energy stored. For instance, the instantaneous energy stored at 120 minutes was shown as roughly 140kJ for all the inlet temperature trials.

Increasing plate temperature enhanced the melting process of the PCM-gypsum plasterboard. For instance, it produced roughly 0.2 and 0.1 of liquid fraction for the

PCM-gypsum plasterboard during 2 hours of the charging period, by plate temperatures of 85 and 55°C, separately. The building envelope operating at plate temperatures of 40 and 85°C achieved approximately 68 and 302kJ separately, at the 2 hour mark of charging duration. Therefore, plate temperature (simulating solar radiation) has a great impact on the outlet temperature and charging behaviour of PCM-gypsum plasterboard. That was similar to the effects observed for the variations in the airflow rates.

Increasing the plenum depth marginally reduces the outlet temperature and HEE. For example, the plenum sizes of 100 and 200mm provided HEE of 0.68 and 0.62. In order to achieve a liquid fraction of approximately 0.2, the plenum widths of 100, 150 and 200mm consumed 120 mins., 125mins. and 150 mins., respectively. Hence, the plenum size has a marginal impact on building envelope performance.

The impact of pitch size has an increasing trend in terms of outlet temperature and HEE. After 45 mins. of charging, the pitch dimensions of 20 and 25mm achieved 42 and 40°C, respectively, and the HEE were claimed as 0.65, 0.64 and 0.60 separately, for three different pitch dimensions (20, 22 and 25mm). The impact of pitch size on the releasing rate of instantaneous energy and liquid fraction is obvious. However, its effect on outlet temperature during the discharging process is insignificant.

The hole diameters of 1 and 3mm achieved outlet temperatures of 40.5 and 43°C, respectively. The hole diameters of 1 and 3mm also achieved HEE at 0.68 and 0.6. However, during the discharging process, the smaller hole diameter would greatly and more quickly reduce the outlet temperature among the three different hole sizes. Besides, the diameter of 1mm had the highest releasing rate of instantaneous energy during the discharging period. Hence, the hole diameter of 1mm is significantly beneficial for building envelope performance.

In addition, the different values of thermal conductivity have a negligible effect on outlet temperature. The system achieved equally the same outlet temperature of 37.85°C during the charging period under various thermal conductivities of the PCM. Similarly, the thermal conductivities of 1 and 0.5 W/mK provided liquid fractions of 0.094 and 0.056, respectively. Besides, there is a marginal variation in the instantaneous and cumulative heat stored for all the simulation trials with various thermal conductivities.

Overall, the airflow rate, plate temperature (simulating solar radiation) and pitch size have a significant impact on building envelope performance. However, the impact of inlet temperature, plenum size, hole diameter and thermal conductivity of the PCM have a marginal influence on building envelope performance.

8.6 **Limitations and recommendations**

A comprehensive numerical and experimental study has been conducted in this research to analyse a transpired solar collector utilising PCM-gypsum plasterboard. However, there are some limitations and challenges that need to be further addressed for a better building envelope performance. One of the limitations of this research is that the economic and environmental benefits of this buildings were not studied. The potential work can be improved in terms of the numerical and experimental work as summarised in the next section.

8.6.1 ***Experimental work***

One of the main disadvantages of PCM-gypsum plasterboard was its weak compressive strength. Thus, the PCM-gypsum plasterboard should be much more stable and stronger in order to prevent it being destroyed easily during implementation, if it is made through a proper manufacturing process. Also, the proportion of PCM and gypsum can be mixed better using a proper mixer. In addition, thermal conductivity enhancement techniques

are essential to improve the heat transfer between the plenum air and PCM-gypsum plasterboard. Hence, other heat transfer techniques would be a good choice to improve the thermal conductivity, e.g. using aluminum or copper as an additional layer attached to the PCM-gypsum plasterboard.

In terms of the in-lab investigation of building envelope performance, one of the main drawbacks was the ignorance of wind effect. The wind effect should be included in further study as according to the previous studies, it is significantly important in determining the convective heat loss from the absorber plate to the surroundings. Also, the influence of (dynamic/real time) solar radiation could be investigated, as solar radiation is one of the main parameters affecting this building envelope's performance. Last but not least, it would provide reliable results if the experiments were conducted in real weather conditions in an outside environment. This would provide strong results in terms of its implementation in buildings.

8.6.2 *Numerical work*

In the numerical study of this research, the effects of the main parameters on building performance were carried out. The future numerical work should include the impact of parameters such as the hole shape and the absorptivity/emissivity of the absorber plate. Also, the solar radiation should be numerically simulated during the modelling rather than setting the plate temperature as constant. Simulating real life solar radiation behaviour while investigating this building envelope's performance would bring credible and reliable results on how it could be implemented in buildings under real weather conditions. Moreover, the influence of multiple parameters (at one time) on building envelope performance should be studied in future work. In addition, the numerical study should extend its investigation on various melting temperatures due to different PCM types. This would provide useful results on the optimal design in terms of PCM selection and melting temperature, accordingly. It is highly recommended that

the building envelope's performance needs further study for different climate conditions in terms of energy savings and economic and environmental benefits.

Lastly, it is extremely important to run real life trials for this building envelope so that the beneficial data could be developed and applied in a real building envelope to achieve better performance under various types of buildings.

8.7 **Contribution to knowledge**

This research has made contributions to knowledge and theory. The research presented a building envelope introducing TSC technology and PCM enhanced gypsum plasterboard. It provided an integrated design for a TSC and PCM-gypsum plasterboard that was capable of storing extra energy from the plenum for later use when there is no solar radiation occurring. Meanwhile, this thesis delivered knowledge on how to design and fabricate PCM integrated gypsum plasterboard. It showed that the addition of a proportion of PCM provided a lower thermal conductivity for the plasterboard. This research also highlighted that the approach velocity is the most important factor influencing collector efficiency and the storage rate of energy in PCM-gypsum plasterboard. In addition, the building envelope with PCM-gypsum plasterboard was able to provide an outlet temperature roughly 6°C higher than the one with gypsum plasterboard under a longer operation period. It is recommended that integrating a TSC with PCM-gypsum plasterboard for use in building envelope design would be a potential approach to deliver energy savings.

References

Abbassi, F., Dimassi, N. and Dehmani, L. (2014) ‘Energetic study of a Trombe wall system under different Tunisian building configurations’. *Energy and Buildings* 80, 302–308. DOI: 10.1016/j.enbuild.2014.05.036

Abulkhair, H. and Collins, M.R. (2010) ‘Investigation of Wind Heat Loss From Unglazed Transpired Solar Collectors with Trapezoidal Corrugation’. in *Proceedings of the 5th Annual Green Energy Conference.* held June 2010 at Waterloo, Ontario, Canada.

Agathokleous, R. et al. (2019) ‘Building façade integrated solar thermal collectors for air heating: experimentation, modelling and applications’. *Applied Energy* 239, 658-679. DOI: 10.1016/j.apenergy.2019.01.020

Ahmed, Abdullahi et al. (2018) ‘Experimental evaluation of passive cooling using phase change materials (PCM) for reducing overheating in public building’. *E3S Web Conf.* 32, 1001. DOI: 10.1051/e3sconf/20183201001

Ahmed, M. M. S. et al. (2016) ‘Double Skin Façade : The state of art on building energy efficiency’. *JOCET* 4 (1), 84-89. DOI: 10.7763/JOCET.2016.V4.258

Akeiber, H. et al. (2016a) ‘A review on phase change material (PCM) for sustainable passive cooling in building envelopes’. *Renewable and Sustainable Energy Reviews* 60, 1470–1497.DOI: 10.1016/j.rser.2016.03.036

Akeiber, H. et al. (2016b) ‘A review on phase change material (PCM) for sustainable passive cooling in building envelopes’. *Renewable and Sustainable Energy Reviews* 60, 1470–1497. DOI: 10.1016/j.rser.2016.03.036

Al-Maghalseh, M. M. (2017) ‘Investigate the natural convection heat transfer in a PCM thermal storage system using ANSYS/FLUENT’. *Jordan Journal of Mechanical and Industrial Engineering* 11(4), 217–223

Al-Saadi, S. N. and Zhai, Z. (2013) 'Modeling phase change materials embedded in building enclosure: A review' *Renewable and Sustainable Energy Reviews* 21, 659–673. DOI: 10.1016/j.rser.2013.01.024

Aldersgate GroupC.F.T.U.O.S.P. (2018) *Increasing investment for commercial energy efficiency* [online]. available from: <http://www.aldersgategroup.org.uk/asset/1012> [21April 2021]

Allen, A. (2011) *Sustainable Building Envelope Centre (SBEC)* [online]. available from: <https://www.tatasteelconstruction.com/en_GB/tata-steel-case-studies/commercial/Sustainable-Building-Envelope-Centre> [8 June 2017]

Amirante, R. et al. (2017) 'Overview on recent developments in energy storage: Mechanical, electrochemical and hydrogen technologies'. *Energy Conversion and Management* 132, 372–387. DOI: 10.1016/j.enconman.2016.11.046

Anderson Materials Evaluation (no date) *Differential Scanning Calorimetry (DSC) Thermal Analysis*, *Anderson Materials Evaluation, Inc* [online]. available from: <http://www.andersonmaterials.com/dsc.html/> [13 December 2018]

Anderson, T. N. et al. (2009) 'Performance of a building integrated photovoltaic/thermal (BIPVT) solar collector'. *Solar Energy*, 83(4), 445–455. DOI: 10.1016/j.solener.2008.08.013

Anon. (no date a) *Elipse Blc.* [online]. available from <http://solarwall.com/media/download_gallery/cases/ElipseBLCLatvia_Y09_SolarWallCaseStudy.pdf> [21 April 2021]

Anon. (no date b) *Erlangen City Hall* [online]. available from <http://solarwall.com/media/download_gallery/cases/ErlangenCityHall_Y05_SolarWallCaseStudy.pdf> [31 May 2017]

Anon. (no date c) *Case Studies of Transpired Solar Collector* [online]. available from <http://solarwall.com/en/case-studies/search-and-filter-cases.php?lang=EN> [7 June

2017]

Anon. (no date d) *Commercial: Jaguar / Land Rover Academy* [online]. available from <http://solarwall.com/media/download_gallery/cases/JaguarLandRover_Y09_SolarWallCaseStudy.pdf.> [21 April 2021]

Anon. (no date e) *Commercial: Sainsbury / Prologis* [online]. available from <http://solarwall.com/media/download_gallery/cases/SainsburyPrologis_Y08_SolarWallCaseStudy.pdf.> [21 April 2021]

Anon. (no date f) *Commercial: Toyota Car Dealership (Oviedo Spain)* [online]. available from <http://solarwall.com/media/download_gallery/cases/ToyotaDealershipOviedo_Y10_SolarDuctCaseStudyv2.pdf> [31 May 2017]

Anon. (no date g) *Institutional: Flin Flon General Hospital* [online]. available from: <http://solarwall.com/media/download_gallery/cases/FlinFlonHospital_Y09_SolarWallCaseStudy.pdf> [21 April 2021]

Anon. (no date h) *Institutional: Peel Regional Paramedic Service Station* [online]. available from: <http://solarwall.com/media/download_gallery/cases/PeelRegionalParamedicsServiceStation_Y16_SolarWallCaseStudyv2.pdf> [31 May 2017]

Anon. (no date i) *Institutional: Sherbrooke University Hospital* [online]. Available from <http://solarwall.com/media/download_gallery/cases/SherbrookeUniversity_SolarWallCaseStudy_Y14.pdf> [31 May 2017]

Anon. (no date j) *Windsor Essex Community Housing Corp* [online]. available from <http://solarwall.com/media/download_gallery/cases/Windsor_Essex_Community_Housing_Testimonial_SolarWallCaseStudy.pdf.> [21 April 2021]

Anon. (1997) *Various Applications, Germany: Metallbau Eisenach and Erlangen City*

Hall [online]. available from: <http://solarwall.com/media/download_gallery/cases/GermanCaseStudies_Y06_SolarWallCases.pdf.> [21 April 2021]

Anon. (2004) *Centre commercial Leclerc de Valréas* [online]. available from http://solarwall.com/media/download_gallery/cases/french/Casapplication-SolarWall-CentreCommercialLeclercDeValreas_Y11.pdf [31 May 2017]

Anon. (2007) *Industrial: Krause Plan Poland, Europe's Largest SolarWall Installation* [online]. available from <http://solarwall.com/media/download_gallery/cases/KrausePoland_Y07_SolarWallCaseStudyv2.pdf> [31 May 2017]

Anon, (2007) *Industrial: Toyota Motor Manufacturing France* [online]. available from <http://solarwall.com/media/download_gallery/cases/ToyotaFrance_SolarWallCaseStudy_Y11.pdf> [31 May 2017]

Anon. (2008) *Beijing Olympic Village* [online]. available from <http://www.asiabusinesscouncil.org/docs/BEE/GBCS/GBCS_OlympicVillage.pdf> [21 April 2021]

Anon. (2008) *Commercial: Auchan Miskolk* [online]. available from http://solarwall.com/media/download_gallery/cases/Auchan_SolarWallCaseStudy_Y09.pdf [31 May 2017]

Anon. (2011) *New COOL-PHASE system from Monodraught solves overheating problem for Notre Dame School* [online]. available from https://news.cision.com/monodraught-limited/r/new-cool-phase-pcm-system-from-monodraught-solves-overheating-problem-for-notre-dame-school,c9207955 [21 April 2021]

Anon. (2012) *COOL-PHASE® system is specified for 'Problem Room' at Sheffield Hallam University* [online]. available from https://news.cision.com/monodraught-

limited/r/monodraught-s-cool-phase-system-is-specified-for--problem-room--at-sheffield-hallam-university,c9272744 [21 April 2021]

Anon. (2012) *Industrial: Cicame Énergie Inc* [online]. available from <http://solarwall.com/media/download_gallery/cases/CicameEnergieInc_SolarWallCaseStudy_Y12.pdf> [31 May 2017]

Anon. (2013) *Commercial: Marks and Spencer* [online]. available from <http://solarwall.com/media/download_gallery/cases/Marks&Spencer_Y13_SolarWallCaseStudy.pdf> [31 May 2017]

Anon. (2013) *Swalec Smart Energy Centre* [online]. available from < https://www.tatasteeleurope.com/ts/construction/case-studies/swalec-smart-energy-centre> [21 April 2021]

Anon. (2019) *Designing Buildings Wiki: Wall types* [online]. available from https://www.designingbuildings.co.uk/wiki/Wall_types [10 November 2019]

Antony Aroul Raj, V. and Velraj, R. (2011) 'Heat transfer and pressure drop studies on a PCM-heat exchanger module for free cooling applications'. *International Journal of Thermal Sciences* 50(8), 1573–1582. DOI: 10.1016/j.ijthermalsci.2011.01.025

Arulanandam, S. J., Hollands, K. G. T. and Brundrett, E. (1999) 'A CFD heat transfer analysis of the transpired solar collector under no-wind conditions'. *Solar Energy* 67(1–3), 93–100. DOI: 10.1016/S0038-092X(00)00042-6

Ascione, F. et al. (2019) 'Energy refurbishment of a University building in cold Italian backcountry. Part 2: Sensitivity studies and optimization'. *Energy Procedia* 159, 10-15. DOI: 10.1016/j.egypro.2018.12.010

Asimakopoulou, E. K., Kolaitis, D. I. and Founti, M. A. (2015) 'Fire safety aspects of PCM-enhanced gypsum plasterboards: An experimental and numerical investigation'. *Fire Safety Journal* 72, 50-58. DOI: 10.1016/j.firesaf.2015.02.004

Asman, G. E. et al. (2019) 'Critical components of Environmentally Sustainable

Buildings Design Practices of office buildings in Ghana'. *Journal of Building Engineering*, 26. DOI: 10.1016/j.jobe.2019.100925.

Athienitis, A. K. et al. (1997) 'Investigation of the thermal performance of a passive solar test-room with wall latent heat storage'. *Building and Environment* 32(5), 405–410. DOI: 10.1016/S0360-1323(97)00009-7

Athienitis, A. K. et al. (2011) 'A prototype photovoltaic/thermal system integrated with transpired collector'. *Solar Energy* 85(1), 139–153. DOI: 10.1016/j.solener.2010.10.008

ATP Instrumentation Ltd. (no date) *How To Measure Light | Using Your Light Meter Correctly* [online]. available from <https://www.atp-instrumentation.co.uk/blog/how-to-measure-light-levels/ > [28 January 2018]

Badache, M. et al. (2012) 'Experimental and two-dimensional numerical simulation of an unglazed transpired solar air collector'. *Energy Procedia* 30, 19–28. DOI: 10.1016/j.egypro.2012.11.004

Badache, M. et al. (2013) 'Experimental and numerical simulation of a two-dimensional unglazed transpired solar air collector'. *Solar Energy* 93, 209–219. DOI: 10.1016/j.solener.2013.02.036

Badache, M. et al. (2014) 'An experimental investigation of a two-dimensional prototype of a transparent transpired collector'. *Energy and Buildings* 68, 232–241. DOI: 10.1016/j.enbuild.2013.09.010

Badache, M., Hallé, S. and Rousse, D. (2012) 'A full 3 4 factorial experimental design for efficiency optimization of an unglazed transpired solar collector prototype'. *Solar Energy* 86(9), 2802–2810. DOI: 10.1016/j.solener.2012.06.020

Badescu, V. et al. (2019a) 'Regularizing the operation of unglazed transpired collectors by incorporating phase change materials'. *Energy Conversion and Management* 184, 681–708. DOI: 10.1016/j.enconman.2019.01.049

Badescu, V. et al. (2019b) ‘Regularizing the operation of unglazed transpired collectors by incorporating phase change materials’. *Energy Conversion and Management* 184. DOI: 10.1016/j.enconman.2019.01.049

Bajare, D., Kazjonovs, J. and Korjakins, A. (2011) ‘The thermal characteristics of gypsum boards with phase change materials (PCM)’. *Environment. Technology. Resources. Proceedings of the 8th International Scientific and Practical Conference* 2, 132–138 [online]. available from: <http://zdb.ru.lv/conferences/3/VTR8_II_132.pdf> [21 April 2021]

Bake, M. et al. (2019) ‘A systematic review on parametric dependencies of transpired solar collector performance’, *International Journal of Energy Research* 43 (1), 86-112. DOI: 10.1002/er.4200

Bake, M. et al. (2020) ‘Comparative Assessment on the Use of Energy Storage in the Building Envelopes’. in *Low Carbon Energy Supply Technologies and Systems*. 1st edn. ed. by Atul Sharma, Amritanshu Shukla, R. S. Boca Raton: CRC press, 36. DOI: 10.1201/9780429353192

Balaras, C. A. *et al.* (2000) ‘Potential for energy conservation in apartment buildings’. *Energy and Buildings* 31(2), 143–154. DOI: 10.1016/S0378-7788(99)00028-6

Bandara, W., Amarasekara, B. and Rupasinghe, C. (2018) ‘Assessment of the possibility of unglazed transpired type solar collector to be used for drying purposes: A comparative assessment of efficiency of unglazed transpired type solar collector with glazed type solar collector’. in *Procedia Engineering* 212, 1295–1302. DOI: 10.1016/j.proeng.2018.01.167

Bhamare, D. K., Rathod, M. K. and Banerjee, J. (2020) ‘Numerical model for evaluating thermal performance of residential building roof integrated with inclined phase change material (PCM) layer’. *Journal of Building Engineering*, 28. DOI: 10.1016/j.jobe.2019.101018

Bigaila, E. et al. (2015) ‘A study of a BIPV/T collector prototype for building façade applications’. *Energy Procedia* 78, 1931–1936. DOI: 10.1016/j.egypro.2015.11.374

Biswas, K. et al. (2014) ‘Combined experimental and numerical evaluation of a prototype nano-PCM enhanced wallboard’. *Applied Energy* 131, 517–529. DOI: 10.1016/j.apenergy.2014.02.047

Bojic, M., Yik, F. and Sat, P. (2002) ‘Energy performance of windows in high-rise residential buildings in Hong Kong’. *Energy and Buildings* 34(1), 71–82. DOI: 10.1016/S0378-7788(01)00079-2

Bokor, B. et al. (2017) ‘Theoretical and experimental analysis on the passive cooling effect of transpired solar collectors’. *Energy and Buildings* 156, 109–120. DOI: 10.1016/j.enbuild.2017.09.063

Borreguero, A. M. et al. (2010) ‘Improvement of the thermal behaviour of gypsum blocks by the incorporation of microcapsules containing PCMS obtained by suspension polymerization with an optimal core/coating mass ratio’. *Applied Thermal Engineering* 30(10), 1164–1169. DOI: 10.1016/j.applthermaleng.2010.01.032

Borreguero, A. M. et al. (2011) ‘Thermal testing and numerical simulation of gypsum wallboards incorporated with different PCMs content’. *Applied Energy* 88(3), 930–937. DOI: 10.1016/j.apenergy.2010.08.014

Borreguero, A. M., Garrido, I. et al. (2014) ‘Development of smart gypsum composites by incorporating thermoregulating microcapsules’. *Energy and Buildings* 76, 631–639. DOI: 10.1016/j.enbuild.2014.03.005

Borreguero, A. M., Serrano, A. et al. (2014) ‘Polymeric-SiO2-PCMs for improving the thermal properties of gypsum applied in energy efficient buildings’. *Energy Conversion and Management* 87, 138–144. DOI: 10.1016/j.enconman.2014.07.027

Boudali Errebai, F., Chikh, S. and Derradji, L. (2018) ‘Experimental and numerical investigation for improving the thermal performance of a microencapsulated phase

change material plasterboard'. *Energy Conversion and Management* 174, 309-321. DOI: 10.1016/j.enconman.2018.08.052

Brown, C. et al. (2014) 'Transpired solar collector installations in Wales and England'. in *Energy Procedia* 48, 18–27. DOI: 10.1016/j.egypro.2014.02.004

Buker, M. S. and Riffat, S. B. (2015) 'Building integrated solar thermal collectors - A review'. *Renewable and Sustainable Energy Reviews* 51, 327–346. DOI: 10.1016/j.rser.2015.06.009

Bunea, M. *et al.* (2015) 'Mathematical modelling of unglazed solar collectors under extreme operating conditions'. *Solar Energy* 118, 547–561. DOI: 10.1016/j.solener.2015.06.012

Butala, V. and Stritih, U. (2009) 'Experimental investigation of PCM cold storage'. *Energy and Buildings* 41(3), 354–359. DOI: 10.1016/j.enbuild.2008.10.008

Butcher, M. F. et al. (2009) *Northern Arizona University*, *New Directions for Student Services* [online]. available from: https://onlinelibrary.wiley.com/doi/abs/10.1002/ss.327. DOI: 10.1002/ss.327

Cabeza, L. F. et al. (2007) 'Use of microencapsulated PCM in concrete walls for energy savings'. *Energy and Buildings* 39(2), 113–119. DOI: 10.1016/j.enbuild.2006.03.030

Cabeza, L. F. et al. (2011) 'Materials used as PCM in thermal energy storage in buildings: A review'. *Renewable and Sustainable Energy Reviews* 15 (3), 1675-1695. DOI: 10.1016/j.rser.2010.11.018

Castell, A. and Farid, M. M. (2014) 'Experimental validation of a methodology to assess PCM effectiveness in cooling building envelopes passively'. *Energy and Buildings*, 81, 59–71. DOI: 10.1016/j.enbuild.2014.06.011

Chan, A. L. S. (2011) ‘Energy and environmental performance of building façades integrated with phase change material in subtropical Hong Kong’. *Energy and Buildings* 43(10), 2947–2955. DOI: 10.1016/j.enbuild.2011.07.021

Chan, H.-Y., Riffat, S.B. and Zhu, J. (2010) ‘Review of passive solar heating and cooling technologies’. *Renewable and Sustainable Energy Reviews* 14(2), 781–789. DOI: 10.1016/j.rser.2009.10.030

Chan, H.-Y., Riffat, S.B. and Zhu, J. (2011) ‘Experimental Performance of Unglazed Transpired Solar Collector for Air Heating’. *Proceedings of World Renewable Energy Congress 2011*. held 8-13 May 2011 at Linkőping, Sweden

Chan, H.-Y., Riffat, S.B. and Zhu, J. (2010) ‘Review of passive solar heating and cooling technologies’. *Renewable and Sustainable Energy Reviews* 14, pp. 781–789. DOI: 10.1016/j.rser.2009.10.030

Chan, H. -Y., Zhu, J. and Riffat, S. (2013) ‘Heat transfer analysis of the transpired solar facade’. *Energy Procedia* 42, 123–132. DOI: 10.1016/j.egypro.2013.11.012

Charvát, P. et al. (2019) ‘Solar air collector with the solar absorber plate containing a PCM – Environmental chamber experiments and computer simulations’. *Renewable Energy* 143, 731–740. DOI: 10.1016/j.renene.2019.05.049

Chauhan, A. et al. (2018) ‘Energy storage by PCM for building applications’. in *Handbook of Energy Systems in Green Buildings*. ed. by Wang, R. and Zhai, X. New York: Springer, 995–1023. DOI: 10.1007/978-3-662-49120-1_41

Chen, Q. (1995) ‘Comparison of different k -ε models for indoor air flow coputations'. *Numerical Heat Transfer, Part B: Fundamentals* 28(3), 353–369. DOI: 10.1080/10407799508928838

Cheung, C. K., Fuller, R. J. and Luther, M. B. (2005) ‘Energy-efficient envelope design for high-rise apartments’. *Energy and Buildings* 37(1), 37–48. DOI: 10.1016/j.enbuild.2004.05.002

Chialastri, A. and Isaacson, M. (2017) ‘Performance and optimization of a BIPV/T solar air collector for building fenestration applications’. *Energy and Buildings* 150, 200–210. DOI: 10.1016/j.enbuild.2017.05.064

Chwieduk, D. A. (2013) ‘Dynamics of external wall structures with a PCM (phase change materials) in high latitude countries’. *Energy* 59, 301–313. DOI: 10.1016/j.energy.2013.06.066

Ciampi, M, Leccese, F. and Tuoni, G. (2003) ‘Ventilated facades energy performance in summer cooling of buildings’. *Solar Energy* 75, 491–502. DOI: 10.1016/j.solener.2003.09.010

Ciampi, M., Leccese, F. and Tuoni, G. (2003) ‘Ventilated facades energy performance in summer cooling of buildings’. *Solar Energy* 75(6), 491–502. DOI: 10.1016/j.solener.2003.09.010

Collins, M. R. and Abulkhair, H. (2014) ‘An evaluation of heat transfer and effectiveness for unglazed transpired solar air heaters’. *Solar Energy* 99, 231–245. DOI: 10.1016/j.solener.2013.11.012

Comodi, G. et al. (2017) ‘Storing energy for cooling demand management in tropical climates: A techno-economic comparison between different energy storage technologies’. *Energy* 121, 676–694. DOI: 10.1016/j.energy.2017.01.038

Reigger, C. (2008)*Transpired Solar Collector Walls: use solar, save green* [online]. available from: <http://rci-online.org/wp-content/uploads/2008-12-riegger.pdf> [21 April 2021]

Creswell, J. W. (2014) *Research design : qualitative, quantitative, and mixed methods approaches*. 4th edn. Thousand Oaks, CA: Sage

Croitoru, C. et al. (2016) ‘Thermal Evaluation of an Innovative Type of Unglazed Solar

Collector for Air Preheating'. *Energy Procedia* 85, 149–155. DOI: 10.1016/j.egypro.2015.12.285

Croitoru, C. V. et al. (2016) 'Thermodynamic investigation on an innovative unglazed transpired solar collector'. *Solar Energy* 131, 21–29. DOI: 10.1016/j.solener.2016.02.029

Cui, Y. et al. (2017) 'A review on phase change material application in building'. *Advances in Mechanical Engineering* 9(6), 1-15. DOI: 10.1177/1687814017700828

Darkwa, J. and Su, O. (2013) 'Thermal modelling and simulation of composite high conductivity laminated microencapsulated phase change material'. *JP Journal of Heat and Mass Transfer*, 7(2), 113–128

Van Decker, G. W. E., Hollands, K. G. T. and Brunger, A. P. (2001) 'Heat-exchange relations for unglazed transpirred solar collectors with circular holes on a square or triangular pitch'. *Solar Energy*, 71(1), 33–46. DOI: 10.1016/S0038-092X(01)00014-7.

Delisle, V. and Kummert, M. (2014) 'A novel approach to compare building-integrated photovoltaics/thermal air collectors to side-by-side PV modules and solar thermal collectors'. *Solar Energy* 100, 50–65. DOI: 10.1016/j.solener.2013.09.040

Densley Tingley, D., Hathway, A. and Davison, B. (2015) 'An environmental impact comparison of external wall insulation types'. *Building and Environment* 85, 182–189. DOI: 10.1016/j.buildenv.2014.11.021

Department for Business, Energy and Industrial Strategy. (2018) *Helping Businesses To Improve the Way They Use Energy: Call for Evidence* [online]. available from: <https://www.gov.uk/government/consultations/helping-businesses-to-improve-the-way-they-use-energy-call-for-evidence> [21 April 2021].

Diarce, G. et al. (2014) 'A comparative study of the CFD modeling of a ventilated

active facade including phase change materials'. *Applied Energy* 126, 307–317. DOI: 10.1016/j.apenergy.2014.03.080

Duffie, J. A. and Beckman, W. A. (2013) 'Flat-Plate Collectors'. in *Solar Engineering of Thermal Processes*. ed. by Duffie, J. A. and Beckman, W. A. Hoboken, NJ, USA: John Wiley & Sons, Inc., 236–321

Durakovic, B. and Torlak, M. (2016) 'Experimental and numerical study of a PCM window model as a thermal energy storage unit'. *International Journal of Low-Carbon Technologies* 12(3), 270-280. DOI: 10.1093/ijlct/ctw024

Dymond, C. and Kutscher, C. (1997) 'Development of a flow distribution and design model for transpired solar collectors'. *Solar Energy*, 60(5), 291–300. DOI: 10.1016/S0038-092X(96)00157-0

Eames, P. et al. (2014) 'The Future Role of Thermal Energy Storage in the UK Energy System : An Assessment of the Technical Feasibility and Factors Influencing Adoption Research Report'. *Ukerc* [online]. available from: < https://ukerc.rl.ac.uk/UCAT/PUBLICATIONS/The_future_role_of_thermal_energy_storage_in_the_uk_energy_system.pdf> DOI: UKERC/RR/ED/2014/001

Elarga, H. et al. (2016) 'Thermal and electrical performance of an integrated PV-PCM system in double skin facades: A numerical study'. *Solar Energy* 136, 112–124. DOI: 10.1016/j.solener.2016.06.074

Ellobody, E., Feng, R. and Young, B. (2014) 'Introduction', in *Finite Element Analysis and Design of Metal Structures*. ed. by Ellobody, E., Feng, R., and Young, B. Boston: Butterworth-Heinemann, 1–14. DOI: https://doi.org/10.1016/B978-0-12-416561-8.00001-9.

EPSRC (2019) *Visualising our Portfolio* [online]. available from: <https://epsrc.ukri.org/research/ourportfolio/vop/ > [10 November 2019]

Erenturk, S. and Erenturk, K. (2018a) 'Comparisons of novel modeling techniques to

analyze thermal performance of unglazed transpired solar collectors'. *Measurement: Journal of the International Measurement Confederation* 116, 412–421. DOI: 10.1016/j.measurement.2017.11.033

Erenturk, S. and Erenturk, K. (2018b) 'Comparisons of novel modeling techniques to analyze thermal performance of unglazed transpired solar collectors'. *Measurement: Journal of the International Measurement Confederation* 116, 412-421. DOI: 10.1016/j.measurement.2017.11.033

Eryener, D., Hollick, J. and Kuscu, H. (2017a) 'Thermal performance of a transpired solar collector updraft tower'. *Energy Conversion and Management* 142, 286–295. DOI: 10.1016/j.enconman.2017.03.052

Eryener, D., Hollick, J. and Kuscu, H. (2017b) 'Thermal performance of a transpired solar collector updraft tower'. *Energy Conversion and Management* 142, 286–295. DOI: 10.1016/j.enconman.2017.03.052

Eryener, D. and Kuscu, H. (2018) 'Hybrid transpired solar collector updraft tower'. *Solar Energy* 159, 561–571. DOI: 10.1016/j.solener.2017.11.035

Farid, M. M. et al. (2004) 'A review on phase change energy storage: Materials and applications'. *Energy Conversion and Management* 45, 1597–1615. DOI: 10.1016/j.enconman.2003.09.015

Fleck, B. A., Meier, R. M. and Matovic, M. D. (2002) 'A Field Study of the Wind Effects on the Performance of an Unglazed Transpired Solar Collector'. *Solar Energy*, 73(3), 209–216

Fořt, J. et al. (2017) 'Effect of the mode and dynamics of thermal processes on DSC-acquired phase-change temperature and latent heat of different kinds of PCM'. *Materiali in Tehnologije* 51(6), 919–924. DOI: 10.17222/mit.2017.026

Frank, E. and Budig, C. (2006) 'Experimental and Theoretical Investigation of Unglazed Transpired Air Collectors in a Multicomponent Solar Thermal System'

Proceedings of EuroSun 2006 81, 62-75. held 27-29 June 2006 at Glasgow, UK.

Franklin, Allan and Perovic, S. (2019) 'Experiment in Physics'. *Stanford Encyclopedia of Philosophy Archive* Winter 2019 [online].. available from: <https://plato.stanford.edu/archives/win2019/entries/physics-experiment/> [21 April 2021]

Frigione, M., Lettieri, M. and Sarcinella, A. (2019) 'Phase change materials for energy efficiency in buildings and their use in mortars'. *Materials* 12(8) 1260. DOI: 10.3390/ma12081260

Gagliano, A., Nocera, F. and Aneli, S. (2016) 'Thermodynamic analysis of ventilated fa??ades under different wind conditions in summer period'. *Energy and Buildings* 122, 131–139. DOI: 10.1016/j.enbuild.2016.04.035

Gantenbein, P. and Rindt, C. (2012) *Collection of experimental data on the behavior of TCM/PCM-materials to bench-mark numerical codes Report A3.2 of the Working Group on Numerical Modelling Compact Thermal Energy Storage: Material Development for System Integration 2 Collection of experime* [online]. available from <http://task42.iea-shc.org/Data/Sites/1/publications/T4224-A3.2--Collection-of-experimental-data-on-the-behavior-of-TCM-and-PCM-materials-to-benchmark-numerical-codes.pdf.> [21 April 2021]

Gao, L. et al. (2013) 'Experimental study of a building-integrated solar air heating system in cold climate of China'. *Energy and Buildings* 65, 359–367. DOI: 10.1016/j.enbuild.2013.06.014

Gao, L., Bai, H. and Mao, S. (2014) 'Potential application of glazed transpired collectors to space heating in cold climates'. *Energy Conversion and Management* 77, 690–699. DOI: 10.1016/j.enconman.2013.10.030

Gao, M. et al. (2020) 'A study on thermal performance of a novel glazed transpired solar collector with perforating corrugated plate'. *Journal of Cleaner Production*

257(10). DOI: 10.1016/j.jclepro.2020.120443

Gärtner, J. A., Massa Gray, F. and Auer, T. (2020) 'Assessment of the impact of HVAC system configuration and control zoning on thermal comfort and energy efficiency in flexible office spaces'. *Energy and Buildings* 212. DOI: 10.1016/j.enbuild.2020.109785

Genevès, C. et al. (no date) *Review of Unglazed Transpired Collectors (UTCs)* [online]. available from < http://t3e.info/pdf/Publications/Preprint/2012_UTC-Literature%20Review-PREPRINT_2012_09_14.pdf> [21 April 2021]

Ghaffarianhoseini, A. et al. (2016) 'Exploring the advantages and challenges of double-skin facades (DSFs)'. *Renewable and Sustainable Energy Reviews* 60, 1052–1065. DOI: 10.1016/j.rser.2016.01.130

Gholampour, M. and Ameri, M. (2016) 'Energy and exergy analyses of Photovoltaic/Thermal flat transpired collectors: Experimental and theoretical study'. *Applied Energy* 164, 837–856.DOI: 10.1016/j.apenergy.2015.12.042

Giovannelli, A. and Bashir, M. A. (2017a) 'Charge and discharge analyses of a PCM storage system integrated in a high-temperature solar receiver'. *Energies* 10(12), 1–13. DOI: 10.3390/en10121943

Giovannelli, A. and Bashir, M. A. (2017b) 'Charge and discharge analyses of a PCM storage system integrated in a high-temperature solar receiver'. *Energies* 10(12). DOI: 10.3390/en10121943

Gnanachelvam, S., Ariyanayagam, A. and Mahendran, M. (2019) 'Fire resistance of light gauge steel framed wall systems lined with PCM-plasterboards'. *Fire Safety Journal* 108. DOI: 10.1016/j.firesaf.2019.102838

Goia, F., Time, B. and Gustavsen, A. (2015) 'Impact of opaque building envelope configuration on the heating and cooling energy need of a single family house in cold climates'. *Energy Procedia* 78, 2626–2631. DOI: 10.1016/j.egypro.2015.11.328

Gov.UK (2018) *The Clean Growth Strategy* [online] available from <https://assets.publishing.service.gov.uk/government/uploads/system/uploads/attachment_data/file/700496/clean-growth-strategy-correction-april-2018.pdf> [21 April 2021]

Gowreesunker, B. L., Tassou, S. A. and Kolokotroni, M. (2012) 'Improved simulation of phase change processes in applications where conduction is the dominant heat transfer mode'. *Energy and Buildings* 47, 353–359. DOI: 10.1016/j.enbuild.2011.12.008

Gowreesunker, B. L., Tassou, S. A. and Kolokotroni, M. (2013) 'Coupled TRNSYS-CFD simulations evaluating the performance of PCM plate heat exchangers in an airport terminal building displacement conditioning system'. *Building and Environment* 65, 132–145. DOI: 10.1016/j.buildenv.2013.04.003

De Gracia, A. et al. (2013) 'Numerical study on the thermal performance of a ventilated facade with PCM'. *Applied Thermal Engineering* 61(2), 372–380. DOI: 10.1016/j.applthermaleng.2013.07.035

De Gracia, A. and Cabeza, L. F. (2015) 'Phase change materials and thermal energy storage for buildings'. *Energy and Buildings* 103, 414–419. DOI: 10.1016/j.enbuild.2015.06.007

Hachem-Vermette, C. (2018) 'Multistory building envelope: Creative design and enhanced performance'. *Solar Energy* 159, 710–721. DOI: 10.1016/j.solener.2017.11.012

Hafer, M. et al. (2018) 'Occupant engagement leads to substantial energy savings for plug loads'. in *2017 IEEE Conference on Technologies for Sustainability, SusTech 2017*. held 12-14 November 2017 at Phoenix AZ USA. DOI: 10.1109/SusTech.2017.8333475

Hall, R. and Allen, A. (2015) 'A New Tool for Assessing the performance of Transpired

Solar Collectors Used for Solar Ventilation Pre-heating'. in *Energy Procedia* 70, 57–64. DOI: 10.1016/j.egypro.2015.02.097

Han, W., Jiao, H. and Fox, D. (2018) 'Scanning electron microscopy'. *Springer Tracts in Modern Physics* 272, 35–68. DOI: 10.1007/978-981-13-0454-5_2

Abulkhair, H. and Collins, M.R. (2010) 'Investigation of Wind Heat Loss From Unglazed Transpired Solar Collectors with Trapezoidal Corrugation'. in *Proceedings of the 5th Annual Green Energy Conference.* held June 2010 at Waterloo, Ontario, Canada.

Hed, G. and Bellander, R. (2006) 'Mathematical modelling of PCM air heat exchanger'. *Energy and Buildings*. 38(2), 82–89. DOI: 10.1016/j.enbuild.2005.04.002

Heim, D. and Clarke, J. A. (2004) 'Numerical modelling and thermal simulation of PCM-gypsum composites with ESP-r'. *Energy and Buildings* 36(8), 795–805. DOI: 10.1016/j.enbuild.2004.01.004

Huang, X. et al. (2019) 'Thermal properties and applications of microencapsulated PCM for thermal energy storage : A review'. *Applied Thermal Engineering* 147, 841–855. DOI: 10.1016/j.applthermaleng.2018.11.007

Hussain, S. et al. (2018) 'Numerical Modeling for Engineering Analysis and Designing of Optimum Support Systems for Headrace Tunnel'. *Advances in Civil Engineering* 2018. DOI: 10.1155/2018/7159873

Iribar-Solaberrieta, E. et al. (2015) 'Energy performance of the opaque ventilated facade'. *Energy Procedia* 78, 55–60. DOI: 10.1016/j.egypro.2015.11.114

Iten, M., Liu, S. and Shukla, A. (2016) 'A review on the air-PCM-TES application for free cooling and heating in the buildings'. *Renewable and Sustainable Energy Reviews* 61, 175-186. DOI: 10.1016/j.rser.2016.03.007

Izquierdo-Barrientos, M. A. et al. (2012) 'A numerical study of external building walls

containing phase change materials (PCM)'. *Applied Thermal Engineering* 47, 73–85. DOI: 10.1016/j.applthermaleng.2012.02.038

Jaber, S. and Ajib, S. (2011) 'Optimum design of Trombe wall system in mediterranean region'. *Solar Energy* 85, 1891–1898 DOI: 10.1016/j.solener.2011.04.025

Jacob, R. and Bruno, F. (2015) 'Review on shell materials used in the encapsulation of phase change materials for high temperature thermal energy storage'. *Renewable and Sustainable Energy Reviews* 48, 79–87. DOI: 10.1016/j.rser.2015.03.038.

Janusevicius, K. et al. (2016) 'Validation of Unglazed Transpired Solar Collector Assisted Air Source Heat Pump Simulation Model'. in *Energy Procedia* 95, 167–174. DOI: 10.1016/j.egypro.2016.09.039

Jaworski, M. and Abeid, S. (2011) 'Thermal conductivity of gypsum with incorporated phase change material (PCM) for building applications'. *Journal of Power Technologies* 91(2), 49–53.

Jegadheeswaran, S. and Pohekar, S. D. (2009) 'Performance enhancement in latent heat thermal storage system: A review'. *Renewable and Sustainable Energy Reviews* 13(9), 2225-2244. DOI: 10.1016/j.rser.2009.06.024

Jenkins, C. et al. (2019) 'Effective management of plug loads in commercial buildings with occupant engagement and centralized controls'. *Energy and Buildings* 201, 194-201. DOI: 10.1016/j.enbuild.2019.06.030

Jeong, S. G. et al. (2017) 'Energy performance evaluation of heat-storage gypsum board with hybrid SSPCM composite'. *Journal of Industrial and Engineering Chemistry* 51, 237–243. DOI: 10.1016/j.jiec.2017.03.007

Ji, R. et al. (2016) 'Simulating the effects of anchors on the thermal performance of building insulation systems'. *Energy and Buildings* 140, 501-507. DOI: 10.1016/j.enbuild.2016.12.036

Jin, X. et al. (2014) 'Effects of PCM state on its phase change performance and the

thermal performance of building walls'. *Building and Environment* 81, 334–339. DOI: 10.1016/j.buildenv.2014.07.012

Jin, X., Medina, M. A. and Zhang, X. (2013) 'On the importance of the location of PCMs in building walls for enhanced thermal performance'. *Applied Energy* 106, 72–78. DOI: 10.1016/j.apenergy.2012.12.079

Kalnas, S. E. and Jelle, B. P. (2015) 'Phase change materials and products for building applications: A state-of-the-art review and future research opportunities'. *Energy and Buildings* 94, 150–176. DOI: 10.1016/j.enbuild.2015.02.023

Kalogirou, S. A. (2004) 'Solar thermal collectors and applications'. *Progress in Energy and Combustion Science* 30(3) 231–295. DOI: 10.1016/j.pecs.2004.02.001

Kant, K., Shukla, A. and Sharma, A. (2018) 'Heating Ventilation and Air-Conditioning Systems for Energy-Efficient Buildings'. in *Sustainability through Energy-Efficient Buildings* [online]. ed. by Shukla, S. and Sharma, A. Boca Raton, FL, USA: CRC Press, 165–180. available from <https://www.taylorfrancis.com/books/e/9781351658454/chapters/10.1201/9781315159065-11> [21 April 2021]

Karaipekli, A. and Sari, A. (2016) 'Development and thermal performance of pumice/organic PCM/gypsum composite plasters for thermal energy storage in buildings'. *Solar Energy Materials and Solar Cells* 149, 19–28. DOI: 10.1016/j.solmat.2015.12.034

Karthikeyan, S. et al. (2014) 'Parametric studies on packed bed storage unit filled with PCM encapsulated spherical containers for low temperature solar air heating applications'. *Energy Conversion and Management* 78, 74–80. DOI: 10.1016/j.enconman.2013.10.042

Kim, S. H. et al. (2020) 'Numerical modeling and experimental validation of a phase change material-based compact cascade cooling system for enhanced thermal

management'. *Applied Thermal Engineering* 164. DOI: 10.1016/j.applthermaleng.2019.114470

Koller, M., Walter, H. and Hameter, M. (2016) 'Transient numerical simulation of the melting and solidification behavior of NaNo 3 using awire matrix for enhancing the heat transfer'. *Energies*, 9(3), 205. DOI: 10.3390/en9030205

Kong, X. et al. (2014) 'Numerical study on the thermal performance of building wall and roof incorporating phase change material panel for passive cooling application'. *Energy and Buildings* 81, 404–415. DOI: 10.1016/j.enbuild.2014.06.044

Konuklu, Y. et al. (2015) 'Review on using microencapsulated phase change materials (PCM) in building applications'. *Energy and Buildings* 106, 134–155. DOI: 10.1016/j.enbuild.2015.07.019

Kośny, J. (2015) *PCM-Enhanced Building Components*. New York, USA: Springer International Publishing.DOI: 10.1007/978-3-319-14286-9

Kośny, J. et al. (2012) 'Field thermal performance of naturally ventilated solar roof with PCM heat sink'. *Solar Energy* 86(9), 2504–2514. DOI: 10.1016/j.solener.2012.05.020

Kozubal, E. et al. (2008) 'Evaluating the Performance and Economics of Transpired Solar Collectors for Commercial Applications'. in *Office of Scientific and Technical Information Technical Reports*. Golden, CO, USA: National Renewable Energy Laboratory, 193–208

Kumaresan, V. et al. (2013) 'Role of PCM based nanofluids for energy efficient cool thermal storage system'. *International Journal of Refrigeration* 36(6), 1641-1647. DOI: 10.1016/j.ijrefrig.2013.04.010

Kutscher, C. F. (1994) 'Heat exchange effectiveness and pressure drop for air flow through perforated plates with and without crosswind'. *Journal of Heat Transfer* 116(2), 391-399. DOI: 10.1115/1.2911411Kutscher, C. F., Christensen, C. B. and

Barker, G. M. (1993) ‘Unglazed Transpired Solar Collectors: Heat Loss Theory’. *Journal of Solar Energy Engineering* 115(3), 182. DOI: 10.1115/1.2930047

Kuznik, F. and Virgone, J. (2009a) ‘Experimental assessment of a phase change material for wall building use’. *Applied Energy* 86(10), 2038–2046. DOI: 10.1016/j.apenergy.2009.01.004

Kuznik, F. and Virgone, J. (2009b) ‘Experimental assessment of a phase change material for wall building use’. *Applied Energy* 86(10), 2038–2046. DOI: 10.1016/j.apenergy.2009.01.004

Kyriaki, E., Drosou, V. and Papadopoulos, A. M. (2015) ‘Solar Thermal Systems for Low Energy Hotel Buildings: State of The Art, Perspectives and Challenges’. *Energy Procedia* 78, 1968–1973. DOI: 10.1016/j.egypro.2015.11.385

Lachheb, M. et al. (2017) ‘Thermal behavior of a hybrid PCM/plaster: A numerical and experimental investigation’. *Applied Thermal Engineering* 111, 49–59. DOI: 10.1016/j.applthermaleng.2016.09.083

Lamberg, P., Lehtiniemi, R. and Henell, A. M. (2004) ‘Numerical and experimental investigation of melting and freezing processes in phase change material storage’. *International Journal of Thermal Sciences* 43(3), 277–287. DOI: 10.1016/j.ijthermalsci.2003.07.001

Lappa, M. (2004) ‘Growth of semiconductors: the floating zone technique’. in *Fluids, Materials and Microgravity*. ed. by Lappa, M. Oxford: Elsevier, 195–344. DOI: https://doi.org/10.1016/B978-008044508-3/50005-0

Lathia, R. and Mistry, J. (2016) ‘Process of designing efficient, emission free HVAC systems with its components for 1000 seats auditorium’ *Pacific Science Review A: Natural Science and Engineering* 18(2), 109–122. DOI: 10.1016/j.psra.2016.09.010

LCRI (2015) *SOLCER House* [online]. available from <https://www.cardiff.ac.uk/research/explore/find-a-project/view/solcer-house> [21

April 2021]

Leal Filho, W. et al. (2019) ‘A comparative study of approaches towards energy efficiency and renewable energy use at higher education institutions’. *Journal of Cleaner Production* 237. DOI: 10.1016/j.jclepro.2019.117728

Lee, K. O., Medina, Mario A, et al. (2015) ‘Assessing the integration of a thin phase change material (PCM) layer in a residential building wall for heat transfer reduction and management’. *Applied Energy* 137, 699–706. DOI: 10.1016/j.apenergy.2014.09.003

Lee, K. O., Medina, M. A. et al. (2015) ‘Assessing the integration of a thin phase change material (PCM) layer in a residential building wall for heat transfer reduction and management’. *Applied Energy* 137, 699–706. DOI: 10.1016/j.apenergy.2014.09.003

Lei, J., Yang, J. and Yang, E.-H. (2016a) ‘Energy performance of building envelopes integrated with phase change materials for cooling load reduction in tropical Singapore’. *Applied Energy* 162, 207–217. DOI: 10.1016/j.apenergy.2015.10.031

Lei, J., Yang, J. and Yang, E.-H. (2016b) ‘Energy performance of building envelopes integrated with phase change materials for cooling load reduction in tropical Singapore’. *Applied Energy* 162, 207–217. DOI: 10.1016/j.apenergy.2015.10.031

Leon, M. A. and Kumar, S. (2007a) ‘Mathematical modeling and thermal performance analysis of unglazed transpired solar collectors’. *Solar Energy* 81(1), 62–75. DOI: 10.1016/j.solener.2006.06.017

Leon, M. A. and Kumar, S. (2007b) ‘Mathematical modeling and thermal performance analysis of unglazed transpired solar collectors’. *Solar Energy* 81(1),62–75. DOI: 10.1016/j.solener.2006.06.017

Leon, M. A. and Kumar, S. (2007c) ‘Mathematical modeling and thermal performance analysis of unglazed transpired solar collectors’. *Solar Energy* 81(1), 62-75. DOI: 10.1016/j.solener.2006.06.017

Li, B. et al. (2014) ‘Mathematical modeling and experimental verification of vacuum glazed transpired solar collector with slit-like perforations’. *Renewable Energy* 69, 43–49. DOI: 10.1016/j.renene.2014.02.054

Li, C. et al. (2019) ‘Novel hybrid microencapsulated phase change materials incorporated wallboard for year-long year energy storage in buildings’. *Energy Conversion and Management* 183, 791-802. DOI: 10.1016/j.enconman.2019.01.036

Li, C., Yu, H. and Song, Y. (2019) ‘Experimental investigation of thermal performance of microencapsulated PCM-contained wallboard by two measurement modes’. *Energy and Buildings*, 184, 34–43. DOI: 10.1016/j.enbuild.2018.11.032

Li, D. et al. (2015) ‘Numerical analysis on thermal performance of roof contained PCM of a single residential building’. *Energy Conversion and Management* 100, 147–156. doi: 10.1016/j.enconman.2015.05.014

Li, S. and Karava, P. (2012) ‘Numerical Study of Convective Heat Transfer for Flat Unglazed Transpired Solar Collectors’. in *Proceedings of the International High Performance Buildings Conference.* held 24-28 May 2012 at West Lafayette, IN, USA [online] available from <https://docs.lib.purdue.edu/ihpbc/75/> [21 April 2021]

Li, S. et al. (2013) ‘Airflow and thermal analysis of flat and corrugated unglazed transpired solar collectors’. *Solar Energy* 91, 297–315. DOI: 10.1016/j.solener.2013.01.028

Li, S. et al. (2014) ‘Energy modeling of photovoltaic thermal systems with corrugated unglazed transpired solar collectors - Part 1: Model development and validation’. *Solar Energy* 102, 282–296. DOI: 10.1016/j.solener.2013.12.040

Li, S. and Karava, P. (2014) ‘Energy modeling of photovoltaic thermal systems with corrugated unglazed transpired solar collectors – Part 2: Performance analysis’. *Solar Energy*, 102, 297–307. DOI: http://dx.doi.org/10.1016/j.solener.2013.12.041

Li, X. et al. (2020) ‘A new energy saving ventilation system assisted by transpired solar

air collectors for primary and secondary school classrooms in winter'. *Building and Environment*, 177. DOI: 10.1016/j.buildenv.2020.106895

Li, X., Li, C. and Li, B. (2016) 'Net heat gain assessment on a glazed transpired solar air collector with slit-like perforations'. *Applied Thermal Engineering* 99, 1–10. DOI: 10.1016/j.applthermaleng.2015.12.069

Lin, Y. et al. (2018) 'Review on thermal conductivity enhancement , thermal properties and applications of phase change materials in thermal energy storage'. *Renewable and Sustainable Energy Reviews*. 82(3), 2730–2742. DOI: 10.1016/j.rser.2017.10.002

Ling, H. et al. (2019) 'Effect of thermophysical properties correlation of phase change material on numerical modelling of agricultural building'. *Applied Thermal Engineering* 157. DOI: 10.1016/j.applthermaleng.2019.03.150

Ling, T.-C. and Poon, C.-S. (2013) 'Use of phase change materials for thermal energy storage in concrete: An overview'. *Construction and Building Materials* 46, 55–62. DOI: 10.1016/j.conbuildmat.2013.04.031

Lizana, J. et al. (2017) 'Advances in thermal energy storage materials and their applications towards zero energy buildings: A critical review'. *Applied Energy* 203, 219-239. DOI: 10.1016/j.apenergy.2017.06.008

Lushnikova, N. and Dvorkin, L. (2016) 'Sustainability of gypsum products as a construction material'. in *Sustainability of Construction Materials*. 2nd edn. ed. by Khatib, J.M. Cambridge, UK: Woodhead Publishing, 643–681. DOI: https://doi.org/10.1016/B978-0-08-100370-1.00025-1

Ma, D. and Xue, Y. (2013) 'Solar Energy and Residential Building Integration Technology and Application'. *International Journal of Clean Coal and Energy* 2(2B), 8–12. DOI: 10.4236/ijcce.2013.22B002

Ma, H. et al. (2016) 'Application of low cost active and passive energy saving technologies in an ultra-low energy consumption building'. *Energy Procedia* 88, 807–

813. DOI: 10.1016/j.egypro.2016.06.132

Mahlia, T. M. I. et al. (2014) ‘A review of available methods and development on energy storage; technology update’. *Renewable and Sustainable Energy Reviews* 33, 532–545. DOI: 10.1016/j.rser.2014.01.068

Marin, P. et al. (2016) ‘Energy savings due to the use of PCM for relocatable lightweight buildings passive heating and cooling in different weather conditions’ *Energy and Buildings* 129, 274–283. DOI: 10.1016/j.enbuild.2016.08.007

Markarian, E. and Fazelpour, F. (2019) ‘Multi-objective optimization of energy performance of a building considering different configurations and types of PCM’. *Solar Energy* 191, 481-496 DOI: 10.1016/j.solener.2019.09.003

Mehrban, N. and Bowen, J. (2017) ‘Monitoring biomineralization of biomaterials in vivo’. in *Monitoring and Evaluation of Biomaterials and their Performance In Vivo*. ed. by Narayan, R. J. Cambridge, UK: Woodhead Publishing, 81–110. DOI: https://doi.org/10.1016/B978-0-08-100603-0.00005-5

Memon, S. A. (2014) ‘Phase change materials integrated in building walls: A state of the art review’. *Renewable and Sustainable Energy Reviews* 31, 870–906. DOI: 10.1016/j.rser.2013.12.042

Mi, X. et al. (2016) ‘Energy and economic analysis of building integrated with PCM in different cities of China’. *Applied Energy* 175, 324–336. DOI: 10.1016/j.apenergy.2016.05.032

Migoya, D. C. E. and Crespo, A. (2011) *Comparison of turbulence models for the computational fluid dynamics simulation of wind turbine wakes in the atmospheric boundary layer* [online]. available from <https://core.ac.uk/download/pdf/19730457.pdf> [24 June 2019]

Mija, A. et al. (2017) ‘Humins as promising material for producing sustainable carbohydrate-derived building materials’. *Construction and Building Materials* 139,

594–601. DOI: 10.1016/j.conbuildmat.2016.11.019

Misevičiūtė, V. and Rudzinskas, L. (2014) ‘Simulation of ventilation system with unglazed solar collector and air heat pump’. in *Proceedings of the 9th International Conference ‘Environmental Engineering’*. [online]. held 22-23 May 2014 at Vilnius, Lithuania. available from <http://enviro2014.vgtu.lt/Articles/6/274_Miseviciute.pdf> [21 April 2021] DOI: 10.3846/enviro.2014.274

Modin, H. (2014) *Adaptive building envelopes, Chalmers University of Technology* [online]. available from < file:///C:/Users/NORMAL~1/AppData/Local/Temp/214574.pdf> [21 April 2021]

Moon, B. E. and Kim, H. T. (2019) ‘Evaluation of thermal performance through development of a PCM-based thermal storage control system integrated unglazed transpired collector in experimental pig barn’. *Solar Energy* 194, 856-870. DOI: 10.1016/j.solener.2019.11.009

Mosaffa, A. H. et al. (2014) ‘Energy and exergy evaluation of a multiple-PCM thermal storage unit for free cooling applications’. *Renewable Energy* 68. 452–458. DOI: 10.1016/j.renene.2014.02.025

Muruganantham, K., Horwath, P., Ludlam, D. and McDonald, T. (2010) ‘Experimental Investigation of a Bio-Based Phase Change Material to Improve Building Energy Performance’. in *Proceedings of ASME 2010 4th International Conference on Energy Sustainability*, 979–984. held 17-22 May 2010 at Phoenix Arizona, USA. DOI: 10.1115/ES2010-90035

Navarro, L. et al. (2016) ‘Thermal energy storage in building integrated thermal systems: A review. Part 1. active storage systems’, *Renewable Energy*, 88, 526–547. DOI: 10.1016/j.renene.2015.11.040

Nghana, B. and Tariku, F. (2016) ‘Phase change material’s (PCM) impacts on the energy performance and thermal comfort of buildings in a mild climate’. *Building and*

Environment 99, 221–238. DOI: 10.1016/j.buildenv.2016.01.023

Ogden, R. et al. (2011) 'Transpired solar collectors for ventilation air heating'. *Proceedings of the ICE - Energy* 164(3), 101–110. DOI: 10.1680/ener.2011.164.3.101

Olenets, M., Piotrowski, J. Z. and Stroy, A. (2015) 'Heat transfer and air movement in the ventilated air gap of passive solar heating systems with regulation of the heat supply'. *Energy and Buildings* 103, 198–205. DOI: 10.1016/j.enbuild.2015.05.051

Oliver, A. (2012) 'Thermal characterization of gypsum boards with PCM included: Thermal energy storage in buildings through latent heat'. *Energy and Buildings* 48, 1–7. DOI: 10.1016/j.enbuild.2012.01.026

Omrany, H. et al. (2016) 'Application of passive wall systems for improving the energy effciency in buildings: A comprehensive review'. *Renewable and Sustainable Energy Reviews* 62, 1252–1269. DOI: 10.1016/j.rser.2016.04.010

Oral, G. K., Yener, A. K. and Bayazit, N. T. (2004) 'Building envelope design with the objective to ensure thermal, visual and acoustic comfort conditions'. *Building and Environment* 39(3), 281–287. DOI: 10.1016/S0360-1323(03)00141-0

Osterman, E., Butala, V. and Stritih, U. (2015) 'PCM thermal storage system for "free" heating and cooling of buildings'. *Energy and Buildings*, 106, 125–133. DOI: 10.1016/j.enbuild.2015.04.012

Schossiga P., Henninga, H.M., Gschwandera, S. and Haussmannb, T. (2005) 'Micro-encapsulated phase-change materials integrated into construction materials'. *Solar Energy Materials and Solar Cells* 89(2–3), 10

Panchabikesan, K. et al. (2019) 'Influence of PCM thermal conductivity and HTF velocity during solidification of PCM through the free cooling concept – A parametric study'. *Journal of Energy Storage* 21, 48–57. DOI: 10.1016/j.est.2018.11.005

Panwar, N. L., Kaushik, S. C. and Kothari, S. (2011) 'Role of renewable energy sources in environmental protection: A review'. *Renewable and Sustainable Energy Reviews*

15(3), 1513-1524. DOI: 10.1016/j.rser.2010.11.037

Papadopoulos, A. M. (2005) ‘State of the art in thermal insulation materials and aims for future developments’. *Energy and Buildings* 37(1), 77–86. DOI: 10.1016/j.enbuild.2004.05.006

Park, B. and Krarti, M. (2016) ‘Energy performance analysis of variable reflectivity envelope systems for commercial buildings’. *Energy and Buildings* 124, 88–98. DOI: 10.1016/j.enbuild.2016.04.070

Pearson, C. (2011) *A BSRIA Guide: Thermal Imaging Of Building Fabric* [online]. available from < file:///C:/Users/NORMAL~1/AppData/Local/Temp/Thermal%20Imaging%20of%20 Building%20Fabric%20Sample.pdf> [21 April 2021]

Peci, F. et al. (2020) ‘Experimental study of a modular Unglazed transpired collector Façade for building refurbishment’. *Solar Energy* 201, 247-258. DOI: 10.1016/j.solener.2020.02.103

Peng, J., Lu, L. and Yang, H. (2013) ‘An experimental study of the thermal performance of a novel photovoltaic double-skin facade in Hong Kong’. *Solar Energy* 97, 293–304. DOI: 10.1016/j.solener.2013.08.031

Pérez-Lombard, L., Ortiz, J. and Pout, C. (2008) ‘A review on buildings energy consumption information’. *Energy and Buildings* 40(3), 394–398. DOI: 10.1016/j.enbuild.2007.03.007

Perisoglou, E. and Dixon, D. (2015) ‘Experimental Monitoring of Different Dimensions of Transpired Solar Collectors’. in *Energy Procedia* 70, 111–120. DOI: 10.1016/j.egypro.2015.02.105

Petrone, G., and Cammarata, G. (2012) *Simulation of PCM Melting Process in a Differentially Heated Enclosure* [online]. available from < https://www.comsol.com/paper/download/151829/petrone_paper.pdf> [21 April 2021]

Poirazis, H. (2004) *Double Skin Façades for Office Buildings Literature Review* [online]. available from < https://www.ebd.lth.se/fileadmin/energi_byggnadsdesign/images/Publikationer/Bok-EBD-R3-G5_alt_2_Harris.pdf > [21 April 2021]

Ponshanmugakumar, A. et al. (2017) 'Thermal Energy analysis using TRNSYS in PCM Storage Tank'. *International Journal on Future Revolution in Computer Science & Communication Engineering* 3(11), 1–5 [online]. available from <http://www.ijfrcsce.org>

Poole, M. R. et al. (2018) 'Performance of a coupled transpired solar collector—phase change material-based thermal energy storage system'. *Energy and Buildings* 161, 72–79.DOI: 10.1016/j.enbuild.2017.12.027

du Prel, J.B. et al. (2009) 'Confidence interval or p-value?'. *Deutsches Arzteblatt international* 106(19), 335-339. DOI: 10.3238/arztebl.2009.0335

Rad, H. M. and Ameri, M. (2016) 'Energy and exergy study of unglazed transpired collector-2stage'. *Solar Energy* 132, 570–586. DOI: 10.1016/j.solener.2016.03.045

Rathore, P. K. S. and Shukla, S. K. (2020) 'An experimental evaluation of thermal behavior of the building envelope using macroencapsulated PCM for energy savings'. *Renewable Energy* 149, 1300-1330. DOI: 10.1016/j.renene.2019.10.130

Reddy, J.N and Gartling, D. K. (2010) *The Finite Element Method in Heat Transfer and Fluid Dynamics*. 3rd edn. Boca Raton, FL, USA: CRC press

Renewable Energy Association (2015) *Energy Storage in the UK An Overview* [online]. available from <https://www.r-e-a.net/wp-content/uploads/2019/10/Energy-Storage-FINAL6.pdf> [21 April 2021]Residovic, C. (2017) 'The New NABERS Indoor Environment tool - The Next Frontier for Australian Buildings'. in *Procedia Engineering* 180, 303–310. DOI: 10.1016/j.proeng.2017.04.189

Saadatian, O. et al. (2012) 'Trombe walls: A review of opportunities and challenges in

research and development'. *Renewable and Sustainable Energy Reviews* 16(8), 6340–6351. DOI: 10.1016/j.rser.2012.06.032

Sadineni, S. B., Madala, S. and Boehm, R. F. (2011) 'Passive building energy savings: A review of building envelope components'. *Renewable and Sustainable Energy Reviews* 15, 3617–3631. DOI: 10.1016/j.rser.2011.07.014

Safijahanshahi, E. and Salmanzadeh, M. (2019a) 'Performance simulation of combined heat pump with unglazed transpired solar collector'. *Solar Energy* 108, 575–593. DOI: 10.1016/j.solener.2019.01.038

Safijahanshahi, E. and Salmanzadeh, M. (2019b) 'Performance simulation of combined heat pump with unglazed transpired solar collector'. *Solar Energy* 180, 575-593. DOI: 10.1016/j.solener.2019.01.038

Salunkhe, P. B. and Shembekar, P. S. (2012) 'A review on effect of phase change material encapsulation on the thermal performance of a system'. *Renewable and Sustainable Energy Reviews* 16(8), 5603–5616. DOI: 10.1016/j.rser.2012.05.037

Saman, W. Y. et al. (2004) 'Roof Integrated Unglazed Transpired Solar Air Heater'. *Solar Energy* 76(1-3), 61-69

Sarbu, I. and Sebarchievici, C. (2017) ' Thermal Energy Storage'. in *Solar Heating and Cooling Systems*. ed. by Sarbu, I. and Sebarchievici, C. Cambridge, MA, USA: Academic Press, 99–138. DOI: https://doi.org/10.1016/B978-0-12-811662-3.00004-9

Sayadi, S. et al. (2019) 'Exergy-based control strategies for the efficient operation of building energy systems'. *Journal of Cleaner Production* 241. DOI: 10.1016/j.jclepro.2019.118277

Schossiga P., Henninga, H.M., Gschwandera, S. and Haussmannb, T. (2005) 'Micro-encapsulated phase-change materials integrated into construction materials'. *Solar Energy Materials and Solar Cells* 89(2–3), 10

Serrano, S. et al. (2015) 'Composite gypsum containing fatty-ester PCM to be used as

constructive system: Thermophysical characterization of two shape-stabilized formulations'. *Energy and Buildings* 86, 190–193. DOI: 10.1016/j.enbuild.2014.10.015

Serrano, S. et al. (2016) 'Use of multi-layered PCM gypsums to improve fire response. Physical, thermal and mechanical characterization'. *Energy and Buildings* 127, 1–9. DOI: 10.1016/j.enbuild.2016.05.056

Sewalk, S., Liston, K. S. and Maher, M. D. (2009) 'Transpired Solar Air Collectors : An Energy Efficient Technology for Commercial Buildings'. *The Journal of Sustainable Real Estate* 5(1), 183-205

Sharifi, N. P., Shaikh, A. A. N. and Sakulich, A. R. (2017) 'Application of phase change materials in gypsum boards to meet building energy conservation goals'. *Energy and Buildings* 138, 455-467. DOI: 10.1016/j.enbuild.2016.12.046

Sharma, A. et al. (2009) 'Review on thermal energy storage with phase change materials and applications'. *Renewable and Sustainable Energy Reviews* 13(2), 318–345. DOI: 10.1016/j.rser.2007.10.005

Shi, X. et al. (2014) 'Experimental assessment of position of macro encapsulated phase change material in concrete walls on indoor temperatures and humidity levels'. *Energy and Buildings* 71, 80–87. DOI: 10.1016/j.enbuild.2013.12.001

Shukla, A. et al. (2012) 'A state of art review on the performance of transpired solar collector'. *Renewable & Sustainable Energy Reviews* 16(6), 3975–3985. DOI: 10.1016/j.rser.2012.02.029

Shukla, N., Fallahi, A. and Kosny, J. (2012) 'Performance characterization of PCM impregnated gypsum board for building applications'. in *Energy Procedia* 30, 370–379. DOI: 10.1016/j.egypro.2012.11.044

Singh, S. P. and Bhat, V. (2018) 'Performance evaluation of dual phase change material gypsum board for the reduction of temperature swings in a building prototype in composite climate'. *Energy and Buildings* 159, 191-200. DOI:

10.1016/j.enbuild.2017.10.097

Soares, N. et al. (2014) ‘Multi-dimensional optimization of the incorporation of PCM-drywalls in lightweight steel-framed residential buildings in different climates’. *Energy and Buildings* 70, 411–421. DOI: 10.1016/j.enbuild.2013.11.072

Souayfane, F., Fardoun, F. and Biwole, P. H. (2016) ‘Phase change materials (PCM) for cooling applications in buildings: A review’. *Energy and Buildings* 129, 396–431. DOI: 10.1016/j.enbuild.2016.04.006

Sozer, H. (2010) ‘Improving energy efficiency through the design of the building envelope’. *Building and Environment*. 45(12), 2581–2593. DOI: 10.1016/j.buildenv.2010.05.004

Srinivas Shastri, S. and Allen, R. (1998) ‘Method of lines and enthalpy method for solving moving boundary problems’. *International Communications in Heat and Mass Transfer* 25(4), 531–540. DOI: 10.1016/s0735-1933(98)00040-2

Srinivasaraonaik, B. et al. (2020) ‘Studies on the mechanical properties and thermal behavior of microencapsulated eutectic mixture in gypsum composite board for thermal regulation in the buildings’. *Journal of Building Engineering* 31. DOI: 10.1016/j.jobe.2020.101400

Stamenic, L., Smiley, E. and Karim, K. (2004) ‘Low light conditions modelling for building integrated photovoltaic (BIPV) systems’. *Solar Energy* 77(1), 37–45. DOI: 10.1016/j.solener.2004.03.016

Stojanović, B., Hallberg, D. and Akander, J. (2010) ‘A steady state thermal duct model derived by fin-theory approach and applied on an unglazed solar collector’. *Solar Energy* 84(10), 1838–1851. DOI: 10.1016/j.solener.2010.06.016

Straube, J. (2006) *BSD-007: Historical Development of the Building Enclosure, Building Science Ciorporation* [online]. available from <https://www.buildingscience.com/documents/digests/bsd-007-historical-

development-of-the-building-enclosure> [10 November 2019]

Summers, D.N.; Mitchell, J.W.; Klein, S.A.; Beckman, W. A. (1996) 'Thermal simulation and economic assessment of unglazed transpired collector systems'. in *Proceedings of the American Solar Energy Society conference*. held 13-18 April 1996 at Asheville, NC, USA. [online] available from <https://digital.library.unt.edu/ark:/67531/metadc687671/m2/1/high_res_d/395455.pdf> [21 April 2021]

Sun, W. et al. (2011) 'Performance of PV-Trombe wall in winter correlated with south facade design'. *Applied Energy* 88(1), 224–231. DOI: 10.1016/j.apenergy.2010.06.002

Tajdaran, S. et al. (2016) 'CFD modeling of transpired solar collectors and characterisation of multi-scale airflow and heat transfer mechanisms'. *Solar Energy* 131, 149–164. DOI: 10.1016/j.solener.2016.02.042

Tajdaran, S. et al. (2020) 'Geometrical optimisation of Transpired Solar Collectors using design of experiments and computational fluid dynamics'. *Solar Energy* 197, 527–537. DOI: 10.1016/j.solener.2020.01.018

Tanner, K. (2018) 'Experimental research'. in *Research Methods: Information, Systems, and Contexts*. 2nd edn. ed. by Williamson, K. and Johanson, G.. Cambridge, MA, USA and Kidlington, OX, UK, 337-356. DOI: 10.1016/B978-0-08-102220-7.00014-5.

Tay, N. H. S., Belusko, M. and Bruno, F. (2012) 'Experimental investigation of tubes in a phase change thermal energy storage system'. *Applied Energy* 90(1), 288–297. DOI: 10.1016/j.apenergy.2011.05.026

Tettey, U. Y. A., Dodoo, A. and Gustavsson, L. (2016) 'Primary energy implications of different design strategies for an apartment building'. *Energy* 104, 132–148. DOI: 10.1016/j.energy.2016.03.071

Thambidurai, M. et al. (2015) 'Review on phase change material based free cooling of

buildings-The way toward sustainability'. *Journal of Energy Storage* 4, 74–88. DOI: 10.1016/j.est.2015.09.003

Thiele, A. M., Sant, G. and Pilon, L. (2015) 'Diurnal thermal analysis of microencapsulated PCM-concrete composite walls'. *Energy Conversion and Management* 93, 215–227. DOI: 10.1016/j.enconman.2014.12.078

Tian, M. et al. (2018) 'A study on incorporation of transpired solar collector in a novel multifunctional PV/Thermal/Daylighting (PV/T/D) panel'. *Solar Energy* 165, 90–99. DOI: 10.1016/j.solener.2018.03.009

Tian, Z. (2006) *Numerical modelling of turbulent gas-particle flow and Its applications*. Unpublished PhD Thesis. Melborne: RMIT University.

Tillman, D. A., Duong, D. N. B. and Harding, N. S. (2012) 'Modeling and Fuel Blending'. in *Solid Fuel Blending*. ed. by Tillman, D. A., Duong, D. N. B., and Harding, N. S. Boston: Butterworth-Heinemann, 271–293. DOI: https://doi.org/10.1016/B978-0-12-380932-2.00007-6

Toppi, T. and Mazzarella, L. (2013) 'Gypsum based composite materials with micro-encapsulated PCM: Experimental correlations for thermal properties estimation on the basis of the composition'. *Energy and Buildings* 57, 227–236. DOI: 10.1016/j.enbuild.2012.11.009

Torlak, M., Teskeredzic, A. and Delalic, N. (2013) 'Modeling and Simulation of Heat Storage in Phase-Change Materials Based on Computational Fluid Dynamics'. *Proceedings of the 17th International Research/Expert Conference: Trends in the Development of Machinery and Associated Technology*. held 10-11 September 2013 at Istanbul, Turkey, 405–408 [online]. available from < https://www.tmt.unze.ba/zbornik/TMT2013/102-TMT13-060.pdf> [21 April 2021]

Tyagi, V. V. et al. (2012) 'Review on solar air heating system with and without thermal energy storage system'. *Renewable and Sustainable Energy Reviews* 16(4), 2289–2303.

DOI: 10.1016/j.rser.2011.12.005

United Nations Environment Programme (2007) *Buildings and Climate Change: Status, Challenges and Opportunities* [online]. available from <https://wedocs.unep.org/bitstream/handle/20.500.11822/7783/-Buildings%20and%20Climate%20Change%20-%20Status,%20Challenges%20and%20Opportunities-20073934.pdf?sequence=3&isAllowed=y> [21 April 2021]Uqaili, M. A. and Harijan, K. (2012) *Energy, environment and sustainable development*, *Energy, Environment and Sustainable Development*. New York, USA: Springer. DOI: 10.1007/978-3-7091-0109-4.

Vanegas, M. (2014) *Moondraught Cool-phase® helps Ford Retail car showrooms go green* [online]. available from: <https://www.prweb.com/releases/2014/04/prweb11796422.htm> [21 April 2021]

Vasan, N. and Stathopoulos, T. (2014) 'Experimental study of wind effects on unglazed transpired collectors'. *Solar Energy* 101, 138–149. DOI: 10.1016/j.solener.2013.11.037

Vaziri, R., Ilkan, M. and Egelioglu, F. (2015) 'Experimental performance of perforated glazed solar air heaters and unglazed transpired solar air heater'. *Solar Energy* 119, 251–260. DOI: 10.1016/j.solener.2015.06.043

Venegas, T. et al. (2018) 'Effect of the insulation level on the thermal response of a PCM-modified envelope of a dwelling in Chile'. *Applied Thermal Engineering* 141, 79-89. DOI: 10.1016/j.applthermaleng.2018.05.083

Vogt, W. P. (2012) *When to Use What Research Design*. New York: Guilford Publications

Walker, I.S and Sherman, M. H. (2001) *Heat Recovery in Building Envelopes* [online]. available from <

https://www.aivc.org/sites/default/files/members_area/medias/pdf/Conf/2003/2003017-Walker.pdf> [21 April 2021]

Wang, D. et al. (2019) ‘Experimental study on heating characteristics and parameter optimization of transpired solar collectors’. *Applied Energy* 238, 534-546. DOI: 10.1016/j.apenergy.2019.01.004

Wang, X. et al. (2017) ‘A simplified method for evaluating thermal performance of unglazed transpired solar collectors under steady state’. *Applied Thermal Engineering* 117, 185–192. DOI: 10.1016/j.applthermaleng.2017.01.053

Wang, Y., Kuckelkorn, J. and Liu, Y. (2017) ‘A state of art review on methodologies for control strategies in low energy buildings in the period from 2006 to 2016’. *Energy and Buildings* 78, 1102–1116. DOI: 10.1016/j.enbuild.2017.04.066

Wang, Y., Shukla, A. and Liu, S. (2017) ‘A state of art review on methodologies for heat transfer and energy flow characteristics of the active building envelopes’. *Renewable and Sustainable Energy Reviews* 78, 1102–1116. DOI: 10.1016/j.rser.2017.05.015

Wright, L. (2012) *Deeside Leisure Centre* [online]. available from: <https://blog.tatasteelconstruction.com/deeside-leisure-centre/> [31 May 2017]

Wu, S. et al. (2018) ‘A review of ground-source heat pump systems with heat pipes for energy efficiency in buildings’. *Energy Procedia* 152, 413–418. DOI: 10.1016/j.egypro.2018.09.167

Xie, Jingchao et al. (2018) ‘Experimental and numerical study of thermal performance of the PCM wall with solar radiation’. *Construction and Building Materials* 177, 443–456. DOI: 10.1016/j.conbuildmat.2018.05.123

Xie, J. et al. (2018) ‘Experimental and numerical study of thermal performance of the PCM wall with solar radiation’. *Construction and Building Materials* 177, 443-456. DOI: 10.1016/j.conbuildmat.2018.05.123

Xu, J., Wang, R. Z. and Li, Y. (2014) ‘A review of available technologies for seasonal thermal energy storage’. *Solar Energy* 103, 610–638. DOI: 10.1016/j.solener.2013.06.006

Yakhot, V. et al. (1992) ‘Development of turbulence models for shear flows by a double expansion technique’. *Physics of Fluids A Fluid Dynamic* 43(7). DOI: 10.1063/1.858424

Yang, T. and Athienitis, A. K. (2015) ‘Experimental investigation of a two-inlet air-based building integrated photovoltaic/thermal (BIPV/T) system’. *Applied Energy* 159, 70–79. DOI: 10.1016/j.apenergy.2015.08.048

Yang, T. and Athienitis, A. K. (2016) ‘A review of research and developments of building-integrated photovoltaic/thermal (BIPV/T) systems’. *Renewable and Sustainable Energy Reviews* 66, 886–912. DOI: 10.1016/j.rser.2016.07.011

Yang, Y. et al. (2020) ‘Study of a novel ceramsite-based shape-stabilized composite phase change material (PCM) for energy conservation in buildings’. *Construction and Building Materials* 256. DOI: 10.1016/j.conbuildmat.2020.118479

Younes, C., Shdid, C. A. and Bitsuamlak, G. (2011) ‘Air infiltration through building envelopes: A review’. *Journal of Building Physics*, 35(3), 267–302. DOI: 10.1177/1744259111423085

Young, B. A. et al. (2018) ‘Reduced-scale experiments to evaluate performance of composite building envelopes containing phase change materials’. *Construction and Building Materials* 162, 584-595. DOI: 10.1016/j.conbuildmat.2017.11.160

Youssef, W., Ge, Y. T. and Tassou, S. A. (2018) ‘CFD modelling development and experimental validation of a phase change material (PCM) heat exchanger with spiral-wired tubes’. *Energy Conversion and Management* 157, 498–510. DOI: 10.1016/j.enconman.2017.12.036

Yu, G. et al. (2017) ‘Experimental verification of state space model and thermal

performance analysis for active solar walls'. *Solar Energy* 142, 109–122. DOI: 10.1016/j.solener.2016.12.021

Zeng, C., Shukla, A. and Liu, S. (2017) 'Adaptability research on phase change materials based technologies in China'. *Renewable and Sustainable Energy Reviews* 73, 14

Zhang, D., Fung, A. and Siddiqui, O. (2007) 'Numerical Studies of Integrated Concrete With a Solid-Solid Phase Change Material'. in *Proceedings of the 2nd Canadian Solar Buildings Conference*. held 10-14 June 2007 at Calgary, Canada [online] available from <
http://citeseerx.ist.psu.edu/viewdoc/download?doi=10.1.1.666.5827&rep=rep1&type=pdf> [21 April 2021]

Zhang, T. et al. (2016) 'A glazed transpired solar wall system for improving indoor environment of rural buildings in northeast China'. *Building and Environment* 98, 158–179. DOI: 10.1016/j.buildenv.2016.01.011

Zhang, Y. et al. (2008) 'Thermal storage and nonlinear heat-transfer characteristics of PCM wallboard'. *Energy and Buildings*, 40(9), 1771–1779. DOI: 10.1016/j.enbuild.2008.03.005

Zhang, Z. (2007) *Modeling of airflow and contaminant transport in enclosed environments*. Unpublished PhD. Purdue University: West Lafayette, Indiana

Zhou, D. and Zhao, C. Y. (2011) 'Experimental investigations on heat transfer in phase change materials (PCMs) embedded in porous materials'. in *Applied Thermal Engineering* 31, 970–977. DOI: 10.1016/j.applthermaleng.2010.11.022

Zhou, D., Zhao, C. Y. and Tian, Y. (2012) 'Review on thermal energy storage with phase change materials (PCMs) in building applications'. *Applied Energy* 92, 593–605.DOI: 10.1016/j.apenergy.2011.08.025

Zhou, G. et al. (2007) 'An assessment of mixed type PCM-gypsum and shape-stabilized

PCM plates in a building for passive solar heating'. *Solar Energy* 81(11), 1351–1360. DOI: 10.1016/j.solener.2007.01.014

Zhou, G. et al. (2008) 'Thermal analysis of a direct-gain room with shape-stabilized PCM plates'. *Renewable Energy* 33(6), 1228–1236. DOI: 10.1016/j.renene.2007.06.024

Zhu, L. and Yang, Y. (2019) 'Numerical study on the thermal performance of pipe-embedded PCM building envelope in the heating season'. in *Energy Procedia* 158, 2663-2670. DOI: 10.1016/j.egypro.2019.02.019